FLEXIBLE CASE-GRAIN INTERACTION IN BALLISTIC WEAPON SYSTEMS - STRUCTURAL TEST VEHICLE EVALUATIONS

Samuel W. Jang, et al

Aerojet Solid Propulsion Company

Prepared for:

Air Force Rocket Propulsion Laboratory

October 1975

AFRPL-TR-75-7

FLEXIBLE CASE-GRAIN INTERACTION IN BALLISTIC WEAPON SYSTEMS

Special Report for Period 1 May 1972 to 31 December 1973

Structural Test Vehicle Evaluations

Samuel W. Jang and Kenneth W. Bills, Jr.
Aerojet Solid Propulsion Company
P.O. Box 13400
Sacramento, California 95813

Harold Leeming
Harold Leeming, Ph.D. and Associates
P.O. Box 79
Redlands, California 92373

October 1975

Prepared for

AIR FORCE ROCKET PROPULSION LABORATORY
DIRECTOR OF SCIENCE AND TECHNOLOGY
AIR FORCE SYSTEMS COMMAND
EDWARDS, CALIFORNIA 93523

When U. S. Government drawings, specifications, or other data are used for any purpose other than a definitely related Government procurement operation, the Government thereby incurs no responsibility nor any obligation whatsoever, and the fact that the Government may have formulated, furnished, or in any way supplied the said drawings, specifications, or other data, is not to be regarded by implication or otherwise, or in any manner licensing the holder or any other person or corporation, or conveying any rights or permission to manufacture, use or sell any patented invention that may in any way be related thereto.

FOREWORD

This report was submitted by Aerojet Solid Propulsion Company, P. O. Box 13400, Sacramento, California, 95813, under Contract No. F04611-72-C-0055, Job Order No. 305910 JU with the Air Force Rocket Propulsion Laboratory, Edwards, California, 93523. The report summarizes a portion of the technical efforts conducted under this contract during the period from May 1972 to December 1973.

The efforts reported herein represent the combined efforts of the Aerojet Solid Propulsion Company and Harold Leeming, Ph.D., and Associates (HL&A), with consulting assistance from Konigsberg Instruments, Inc.

The key technical personnel on this program were: Mr. Kenneth W. Bills, Jr., Project Engineer at ASPC, who coordinated the overall program· Mr. Samuel W. Jang, ASPC, and Dr. Harold Leeming, HL&A, who were responsible for the technical aspects of the program; and Messrs. Robert D. Steele and Albert B. Curtis who performed the experimental tests.

This report has been reviewed by the Information Office/DOZ and is releasable to the National Technical Information Service (NTIS). At NTIS it will be available to the general public, including foreign nations.

Durwood I. Thrasher
Project Engineer

Charles E. Payne, Major, USAF
Chief, Surveillance and Mechanical
Behavior Section

FOR THE COMMANDER

Charles R. Cooke, Chief
Solid Rocket Division

Unclassified

SECURITY CLASSIFICATION OF THIS PAGE *(When Data Entered)*

REPORT DOCUMENTATION PAGE

READ INSTRUCTIONS BEFORE COMPLETING FORM

1. REPORT NUMBER: AFRPL-TR-75-7	2. GOVT ACCESSION NO.
3. RECIPIENT'S CATALOG NUMBER	
4. TITLE *(and Subtitle)*: Flexible Case-Grain Interaction in Ballistic Weapon Systems - Structural Test Vehicle Evaluations	5. TYPE OF REPORT & PERIOD COVERED: Special Technical Report, May 1972 to December 1973
	6. PERFORMING ORG. REPORT NUMBER: 1953-26SR-3
7. AUTHOR(s): Samuel W. Jang, Kenneth W. Bills, Jr., Harold Leeming	8. CONTRACT OR GRANT NUMBER(s): F04611-72-C-0055
9. PERFORMING ORGANIZATION NAME AND ADDRESS: Aerojet Solid Propulsion Company, P. O. Box 13400, Sacramento, California, 95813	10. PROGRAM ELEMENT, PROJECT, TASK AREA & WORK UNIT NUMBERS: AFSC Project 3059, Task 10
11. CONTROLLING OFFICE NAME AND ADDRESS: Air Force Rocket Propulsion Laboratory, Edwards, California, 93523	12. REPORT DATE: October 1975
	13. NUMBER OF PAGES: 225
14. MONITORING AGENCY NAME & ADDRESS *(if different from Controlling Office)*	15. SECURITY CLASS. *(of this report)*: Unclassified
	15a. DECLASSIFICATION/DOWNGRADING SCHEDULE

16. DISTRIBUTION STATEMENT *(of this Report)*

Approved for Public Release; Distribution Unlimited

17. DISTRIBUTION STATEMENT *(of the abstract entered in Block 20, if different from Report)*

18. SUPPLEMENTARY NOTES

19. KEY WORDS *(Continue on reverse side if necessary and identify by block number)*

Structural Test Vehicles
Instrumentation
Solid Propellant
Transducers
Normal Stress Gages
Failure Event Gages
Shear Stress Gages

20. ABSTRACT *(Continue on reverse side if necessary and identify by block number)*

Five series of Structural Test Vehicle studies were conducted to verify that several types of embedded stress transducers and their installation methods could be successfully used with the fiberglass chamber of the Minuteman III, Third Stage motor.

The results showed that the transducers could be installed with lead-wires brought out through the case wall without causing fluid leakage paths

DD FORM 1 JAN 73 1473 EDITION OF 1 NOV 65 IS OBSOLETE

Unclassified

SECURITY CLASSIFICATION OF THIS PAGE *(When Data Entered)*

20. Abstract (Cont.)

or degrading the case structure. Potting of normal stress transducers in an inert trowellable insulation was shown to yield the same stress measurements as potting them in propellant. "Ruggedized" shear transducers were shown to function successfully up to the point of propellant/liner interface failure in shear. Successful performance of elastomeric failure event gages in the detection of bondline shear failure was demonstrated.

TABLE OF CONTENTS

TABLE OF CONTENTS (CONT.)

TABLE OF CONTENTS (CONT.)

TABLE OF CONTENTS (CONT.)

LIST OF FIGURES

LIST OF FIGURES (CONT.)

LIST OF FIGURES (CONT.)

LIST OF FIGURES (CONT.)

LIST OF TABLES

SECTION 1

INTRODUCTION

This report presents some key data that were required in the early part of the Flexible Case-Grain Interaction Program. A number of program delays have caused the results to become outdated, while new test data have shown that these early measurements may contain some inaccuracies.

The following sub-sections give the objectives for this work, statements of the problems requiring STV evaluations, and a summary of some of the difficulties subsequently obtained while using the normal stress gages. A final sub-section briefly outlines the text of the STV report.

A. OBJECTIVES

Five special studies were performed using the fiberglass structural test vehicles (STV's). These studies were conducted to verify that several types of embedded stress transducers and their installation methods could be successfully used without affecting the integrity of the grain or fiberglass chamber of the Minuteman III, Third Stage motor. This latter requirement reflects the fact that these STV studies constitute just one task of the "Flexible Case-Grain Interaction Program".

The overall program involves a heavily instrumented third stage motor that was designed as a full-scale structural test vehicle. The original purpose of this instrumented motor was to provide an experimental assessment of existing structural analysis techniques in the prediction of

grain stresses and strains under various conditions of handling and use. Unfortunately, this objective had to be changed due to unexpected problems in the use of the transducers. A description of the STV evaluations conducted, and a brief discussion of how the gage problems impact the STV data re presented below.

B. PROBLEMS REQUIRING STV EVALUATIONS

The required instrumentation in the full-scale motor led to a number of problems; particularly, at the propellant-insulation bondline. Here, a large number of gages (about 56) with a much larger number of leadwires (about 185 wires) were required to gain the desired data. These leadwires could have been bonded to the insulation surface and brought out through fore and aft bosses. But, that approach probably would have affected the bondline integrity of the grain; especially, where a large number of the wires would come together. The problem was solved by bringing the leadwires out through the case wall. Such an approach had been demonstrated on other motors, but its acceptability to the Minuteman motor required further evaluation. That became one of the tasks requiring STV testing (see STV No. 1, below).

In addition, a number of technical problems had been solved on paper or in the laboratory. But, before they could be applied in the full-scale motor, these solutions had to be demonstrated and evaluated under motor use conditions. The structural test vehicles provided the testing medium for these evaluations and demonstrations.

The original plan was to use only four STV's, but a fifth was added to complete some testing requirements overlooked in the earlier STV testing. The five STV's and the problems they were designed to address are described below.

1. STV No. 1 - Bonding and Case Failure Tests

Task Statement:

> Conduct bonding and case failure tests with normal stress gages and thermocouples to define the best technique for through-the-case wall installation.

This task involved two separate evaluations. First, there was the problem of drilling holes through the fiberglass case as mentioned above.

Second, the flexibility of the case produces problems of differential deformations with respect to the rigid metal normal stress gages. The solution to this problem involved the use of an elastomeric adhesive, whose adequacy had to be verified in an STV.

2. STV No. 2 - Evaluation of Gage Potting and Calibration Methods

Task Statement:

> Pre-pot and calibrate normal stress gages and shear gages, then test under hydrostatic and differential pressures while measuring viscoelastic responses of the propellant. Also, compare the performances of gages using the pre-potting procedure with those post-potted in propellant (the conventional method).

This task involved protecting the instrumented case during motor firing. Wherever gage leadwires were brought through the case wall there existed the possibility of case burn-through. To protect against this contingency, all of the gages were to be embedded within rubber insulation material. This was accomplished partly by potting the gages and partly by embedding the gages within the V-45 insulation layer.

This task also required a performance evaluation of a new small diameter (0.1 in. diaphragm) normal stress gage. This gage was required for making measurements in high stress gradient areas. Previous to this program the normal stress gages used 0.25 in. diaphragms.

3. STV No. 3 - Failure Detection Using Shear and Failure Event Gages

Task Statement:

> Verify shear gage and failure event gage performances up to failure of the grain/insulation bond.

Because of the very large bondline areas in the Minuteman III motor, it was essential that as many of the gages as possible be able to detect local failures. This required the use of a new rugged version of the shear cube (developed by Harold Leeming, Ph.D., and Associates). All previous designs were far too fragile for this treatment.

To give an additional failure detection capability at a low price, ASPC designed an elastomeric failure event gage. This gage is a simple device designed to detect passage of a crack or bondline separation. The gage was made of a conductive rubber, failure of the gage being determined by the loss of electrical conductivity.

4. STV No. 4 - Investigation of Stress-Free Temperature Change

Task Statement:

> Stress-free temperature monitoring during motor storage and test at 80°F.

The behavior of the solid propellant itself is known to cause a number of analytical difficulties. One of these difficulties, changes in the stress-free temperature, is especially important to the use of stress gages in solid propellant grains. STV tests of this parameter were intended only to illustrate the problem for ANB-3066 propellant.

This background will be of value in later evaluations of future test data from a second full-scale motor prepared on this program. That motor is expected to show significant changes in its stress-free temperature.

5. STV No. 5 - Re-test of STV No. 3

Task Statement:

> Calibrate normal stress and shear gages using hydrostatic and differential pressure tests. Conduct failure detection tests using shear and failure event gages.

C. LATER OBSERVATIONS SHOWING STRESS GAGE PERFORMANCE ANOMALIES

Numerous anomalies have been observed while monitoring stress gages in the full-scale motor. These gave large effects and they occurred in almost every aspect of stress gage installation and measurement. Because of their general occurrence in the full-scale motor, it is likely that the same, or similar, anomalies were present while conducting the STV tests. The following paragraphs briefly indicate the major problems encountered.

1. Effects of the Fundamental Premise of the Program

The overall program was conceived on the premise that the stress gages were proven devices and fully qualified for use in full-scale motors. In actuality that premise was incorrect, but the acceptance of it caused everyone associated with the program to follow a rather casual approach to gage measurements. A number of preventable errors in the data acquisition are attributed to this assumption.

2. Measurement Accuracies

After a revision to the overall program, techniques were adopted by ASPC to give gage output signal measurement accuracies that are nearly an order of magnitude better than those previously used in the industry for solid propellant stress instrumentation. (The present data measurements are limited to $\pm$ 0.1 mv or $\pm$ 1.5% of reading, whichever is larger). Unfortunately, the early, less accurate measurement methods were used in conducting the STV tests.

3. Transducer Stability

The stability of the gages in aging was found to be compromised by corrosion of the junctions to the stainless steel leadwires. After two years aging, one gage was found to have changed by 30 mv output (equivalent to about 38 psi stress). Potentially, this leadwire corrosion could lead to any electrical change up to infinite resistance (infinite "apparent" stress). Since the same gage designs were used in the STV tests, it is expected that some of the leadwire corrosion was also present when these studies were conducted.

4. Thermal Effects

It has been said that these devices make better temperature sensors than stress transducers. This is demonstrated on observing that the resistance of the semi-conductor strain gages (the transducer sensing element) change in resistance by about 1Ω/°F. But an imbalance between paired semi-conductors of only ± 0.05Ω represents the limit of our measurement accuracy.

The large temperature sensitivity of the semi-conductor gages prevents using the stress transducers under thermal gradients. This is because one of the semi-conductors is externally mounted and the other internally mounted to the diaphragm. In these positions the two gages cannot be equally heated, or cooled, when placed in a thermal gradient.

Another thermal effect of interest is the occurrence of self-heating in the semi-conductor gages. The flow of a current across these gages (which act like resistors of about 500Ω at room temperature) causes them to be heated. One measurement showed a temperature increase of about 25°F on the semi-conductor. The significance of this effect is that the gage slowly heats the surrounding material and theoretically never reaches equilibrium. As the surrounding material gradually warms up, so does the semi-conductor which causes the gage output voltage to change. For accuracy, we have found it practical to establish upper and lower limits to the gage heating times.

5. High Rate Pressurization Effects

While conducting some simple gage evaluations it was noted that they showed marked dependence upon the rates of pressure loading. Recent measurements (at 7.5°F) gave as much as a 10% difference in output between a high rate of loading (about 75 psi/sec) behavior and a constant pressure "calibration".

Additional effects include large hysteresis loops on unloading plus a residual output signal at zero load that only slowly recovers to its original value.

The mechanisms causing these effects have not been defined, but some suspected mechanisms are:

(1) Pressure heating of the surrounding material giving an imbalance in the semi-conductor gages

(2) A viscoelastic interaction between the transducer diaphragm and the surrounding material.

(3) A possible viscoelastic reaction of the epoxy adhesive that bonds the semi-conductor gages to the transducer diaphragm.

This latter point is not at all understood, but available data strongly suggest that it could be happening

6. Overall View of Stress Transducers

In spite of the negative impressions given above, stress transducers are considered to be conceptually practical devices. But, they do need further development prior to their generalized applications as experimental stress analysis tools for solid propellant grains.

D. ORGANIZATION OF REPORT

The report was organized on simple lines as follows:

Section 2, Summary and Conclusions, briefly states the principal results of the program.

Section 3, Motor Case Design and Proof Testing, provides descriptions of the motor cases, their internal insulation and hydrotesting.

Section 4, Improved Shear Gage Development provides a review of the design and testing of the improved high-stress shear gages.

Sections 5 to 9, STV No. 1 to STV No. 5, describe in separate sections the experimental and analytical efforts conducted on these test motors. The information gained from each study is described.

SECTION 2

SUMMARY AND CONCLUSIONS

The structural test vehicle (STV) evaluations described in this report were designed to verify that the selected types of embedded stress transducers and their installations would work properly within a Third Stage Minuteman III motor and would not impair the structural integrity of either the motor case or the propellant grain. To this end a series of small fiberglass STV's were made and tested. The results of the tests are summarized below:

A. STV NO. 1

This STV gave experience in the use of the new installation techniques. Several useful procedures and special tooling were developed as a result of these studies.

The planned gage installations required that 0.060-in. diameter holes be drilled through the motor case. Prior experience on the Polaris A-3 program had demonstrated that a typical fiberglass case was not significantly weakened by small holes of this size. The tests on STV-1 provided the added demonstration that the holes would not cause case degradation leading to fissuring of the surrounding insulation with gas leaking through the holes in the fiberglass case.

B. STV NO. 2

A novel technique of "pre-potting" the normal stress gages within an inert insulation material (IBT-115) was devised for the full scale motor program. The tests on this STV showed that:

1. Pre-potting of these transducers may be satisfactory for preliminary calibrations and compensation purposes. Nevertheless, final calibrations and compensations should be made after the gage is mounted in place.

2. To minimize material property differences the potting or prepotting material should be the live propellant or an inert version of it.

3. Over the limited temperature range of 30° to 110°F the IBT-115 pre-potted gages and the propellant post-potted gages gave essentially the same "measured" stress data, within expected errors.

4. Both types of gage potting are sensitive to improper preparation errors, such as voids occurring within the potting near the gage diaphragm. Careful procedures plus X-ray examinations of <u>all</u> potting procedures should be instituted.

The shear gage performances under differential (shear) tests within the STV were very similar to those observed during the calibration within the shear test fixture. However, apparent gage calibration factors were approximately 14% higher in the STV than those determined in the shear fixture, assuming a uniform shear stress along the length of the STV. This effect was attributed partly to voids or microvoids within the grain that produced a more compressible propellant than expected. This condition would produce the higher gage outputs (higher apparent gage calibration factors) which were observed.

C. STV NO. 3

The 77°F test series performed on STV No. 3 was designed to evaluate the performances of the shear and elastomeric failure gages under realistic combinations of pressure and shear loads up to failure of the propellant-liner-insulation bond. A premature failure of the bond at a shear stress of 32 psi, without a superimposed hydrostatic pressure, led to a decision to make an additional STV (No. 5) to repeat the complete sequence of failure tests.

The STV No. 3 test data showed that the new ruggedized shear gages operated satisfactorily up to bond failure. But, the earliest types of elastomeric shear gages proved to be too delicate. Later experience indicated that eight of ten of these gages would break during grain casting. On the other hand, two of the failure event gages debonded rather than breaking during the differential pressure tests. Clearly, more development work was required before re-evaluating the event gages in STV No. 5.

D. STV NO. 4

This STV was similar in design to the other STV's and contained two normal stress gages and two shear gages. One purpose of this STV was to determine changes in the stress-free reference temperature which would occur in ANB-3066 propellant during long term storage at 77°F. The normal stress data for STV No. 4 decayed from approximately 5 psi at the start of storage at 77°F to 0 psi then, seemingly, became compressive after 33 to 46 weeks. This behavior is attributed to changes in both the stress-free temperature of the propellant grain and the zero-stress calibration of the normal stress gages. The relative contributions of these two effects could not be estimated from the available data.

Another test performed on STV No. 4 was a week-long differential pressure test to ascertain whether plastic deformation was obtained with the propellant. Monitoring of the grain displacements after removal of the pressure showed that a creep of approximately 0.020-in. remained 30 days after the end of the test. This small plastic deformation is possibly insignificant.

E. STV NO. 5

This STV was designed to evaluate the performances of the shear gages and bondline failure event gages under realistic combinations of hydrostatic and differential pressure (shear) stresses. The shear stress data from the STV gave similar gage sensitivities to those measured in the calibration shear fixture. However, precise agreement was not achieved. Observed defects in the gage installation techniques, excessive liner material surrounding the gages, and significant voids close to the gages, plus an estimated 5 vol. % level of casting voids in the grain, are considered to be factors which contribute to the apparent changes in gage sensitivities.

A significant aspect of the STV No. 5 data was the verification that shear stress gages which exhibit a large sensitivity to hydrostatic pressure will produce spurious outputs under combined shear and pressure loads. Three of the shear gages showed an excessive response under hydrostatic pressure. One of these gages, SH-39, had been tested under combined hydrostatic pressure and shear during its calibration and had been rejected for use in a full-scale motor because of excessive response to hydrostatic pressure. Its behavior in STV No. 5 confirmed that this decision was warranted.

The STV failure tests performed with a hydrostatic pressure component of 600 psi were successfully carried out; failure occurred at a gage-measured shear stress of 22 psi. All the shear gages gave good indications of the initiation of grain failure. All four of the failure event gages also gave clear indications of the initiation of bond failure during the test.

The performance of the improved failure event gages in STV No. 5 was very encouraging and suggested that they should be satisfactory in the full scale motor applications.

SECTION 3

MOTOR CASE DESIGN AND PROOF TESTING

A. DESIGN

The STV cases were designed and fabricated to the drawing shown in Figures 1 and 2. The case consisted of a 6 inch I.D. fiberglass cylinder, which was made of an Epon 828 resin and Dow DER-330 glass matrix, helically wrapped at a 26.5 degree angle. The wall thickness of the case was 0.25 in. and the length was 16.5 in. The ends of the cases were machined to match tapered end rings that were bonded to them. The closures for the STV cases were steel caps fitted with O-rings and held in place by retaining rings. The simplicity of the design and ease of fabrication provided a very economical structural test vehicle.

STV No. 1 was different in that a 4-in. length of the mid-section was turned-down to give a wall thickness of 0.10 in.

B. HYDROTEST OF THE STV CASES

The primary objective of these tests was to verify that the STV cases and the bonded, steel end rings exceeded a minimum strength; namely, that required to support 1400 psig internal pressure.

An additional effort for STV No. 1 required the measurement of axial and hoop strains in the case as the motor was pressurized. This test was performed on the case prior to machining the motor sidewall. The plan was to determine the case thickness that would yield more than 1% hoop strain at 1800 psig internal pressure.

The testing sequence was the following:

a. Assemble STV, closures, O-rings, and pressurization system to the schematic shown in Figure 3. Bond tapered steel rings to the ends of the fiberglass case using Chemlok 305 adhesive in the bond interface.

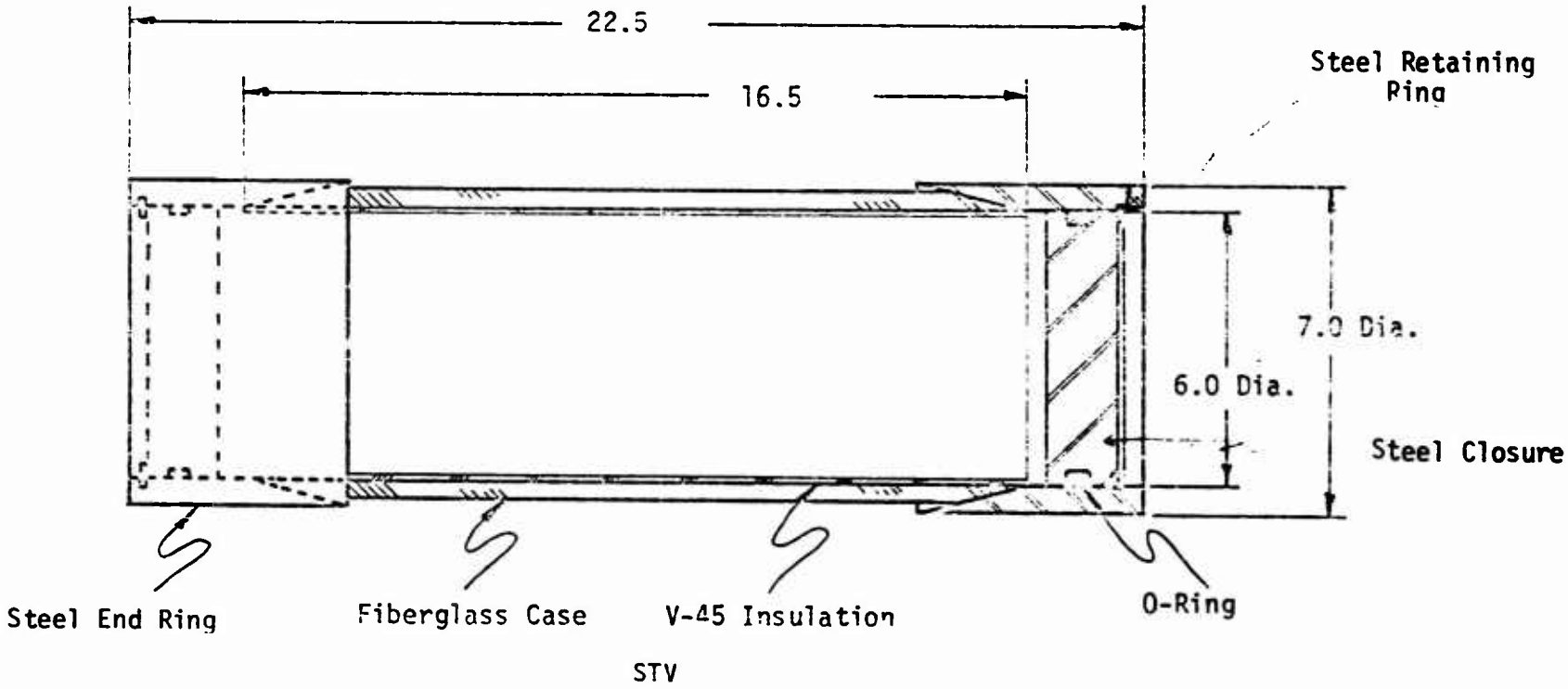

Figure 1. Design of the Structural Test Vehicle

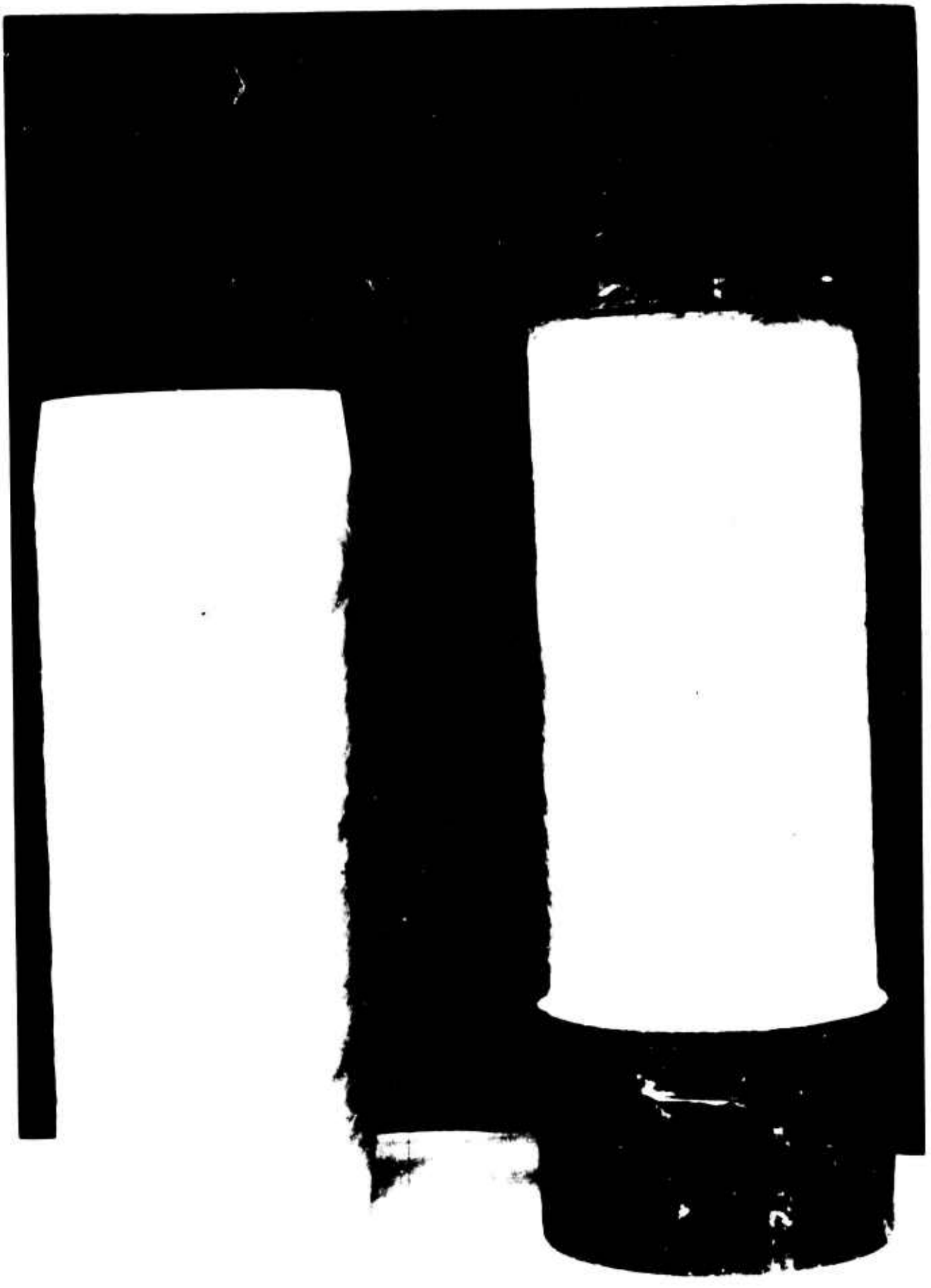

Figure 2. Photograph of the Fiberglass Case Used in the STV's
(End tapers and steel end-rings are shown)

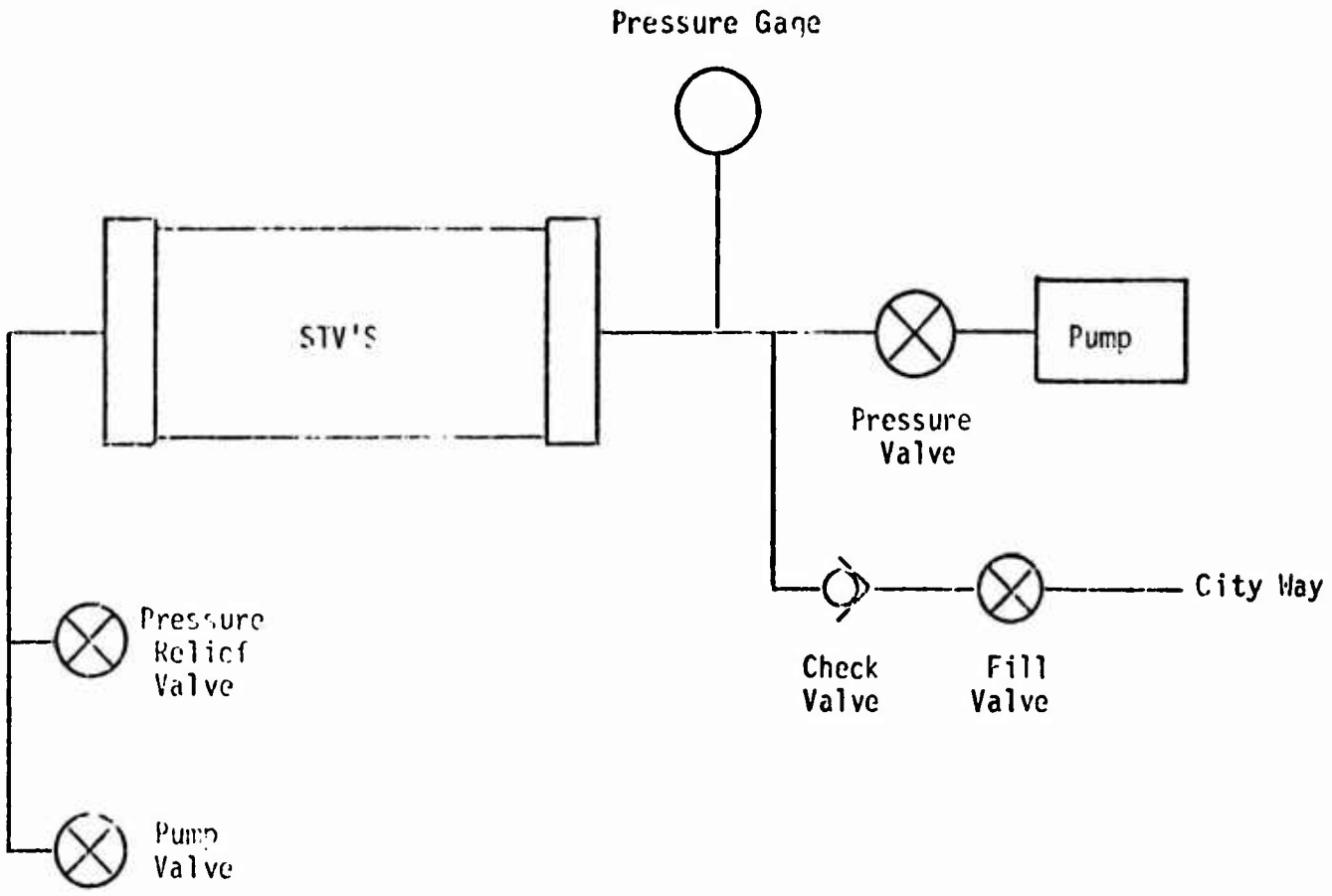

Figure 3. Hydrotest Setup for STV Testing

b. For STV No. 1, only: Bond BLH-PA-7 strain gages on to the case outer surface, at its midlength, using SR-4 post-yield cement.

c. Fill STV with water and bleed out air.

d. Perform visual leak test.

e. Verify that the STV is at 0 psig; then for STV No. 1, only, zero the case strain gages.

f. Pressurize STV to 100 psig and check for leaks, return to 0 psig.

g. Pressurize STV to 1400 psig, hold for 60 seconds and return to 0 psig.

h. Vent STV system and drain water.

i. Visually check STV for any structural damage and verify bond line integrity between STV and ring on tapered portion.

j. After the testing is complete, dry STV with a clean dry cloth.

All of the STV's were hydrotested according to this plan. Post-test damage assessments of the cases and end-joints showed them to have no apparent water leaks or other damage effects.

The measured axial and hoop strains versus applied internal pressure are given in Figure 4 for STV No. 1. From these data it was determined that a case thickness of 0.10 in. would yield about 1% hoop strain at 1800 psig internal pressure.

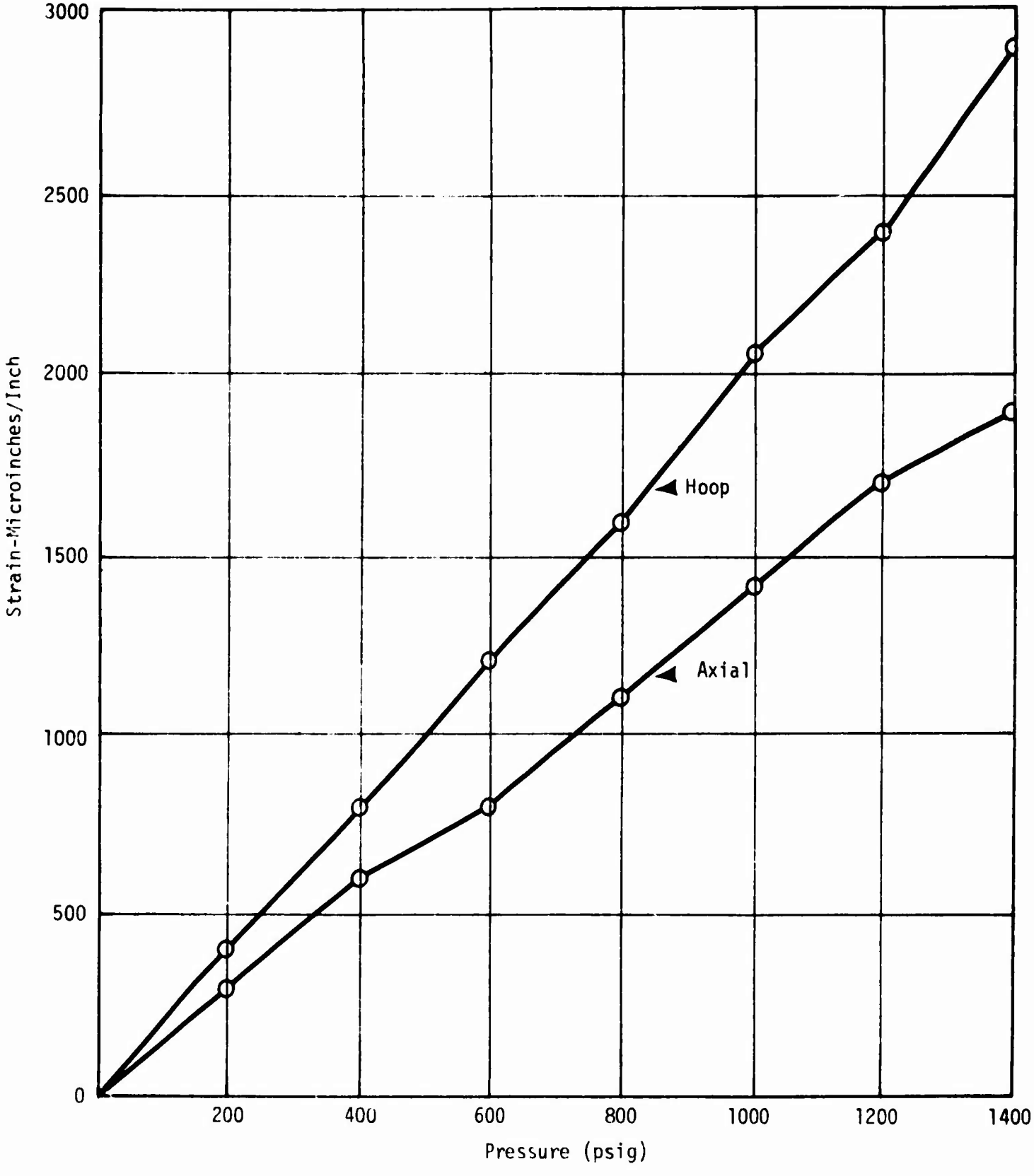

Figure 4. Flexibility Measurements of STV No. 1 During Hydrotest

SECTION 4

IMPROVED SHEAR GAGE DEVELOPMENT

A. SHEAR GAGE DESIGN

Shear gages available at the start of this program were delicate devices designed principally for measuring low shear stresses (1 to 2 psi). They were not suitable for measurement of the large bond shear stresses that will occur during the high rate testing of the full-scale motor.

Improved shear gages were designed around the Kulite "Ruggedized" semi-conductor strain gages. These devices consisted of semi-conductor elements embedded within a matrix of epoxy-glass as shown in Figure 5. The effect of the epoxy-glass matrix is two-fold:

1. It attenuates the strain applied to the semi-conductor element, and

2. It reduces the apparent sensitivity of the gage element.

Another modification introduced at this stage was the use of V-45 insulation material for the body of the shear gage. It was believed that the V-45 rubber would exhibit a linear and almost elastic response up to much larger stresses than would be possible in an inert or live propellant material. For this reason it was expected that the V-45 shear gage employing the Kulite ruggedized semi-conductor strain gages would remain intact and would not fail before the propellant-insulation adhesive bond in the motor.

A test specimen was designed to verify the performance of the new shear gages up to failure of a propellant-insulation bond.

B. SHEAR GAGE FAILURE TEST SPECIMEN

Figure 6 shows the test specimen adopted for testing the improved shear gages. The configuration provides simultaneous compression and shear to the 1/2-in. thick V-45 rubber sheet containing the shear gage.

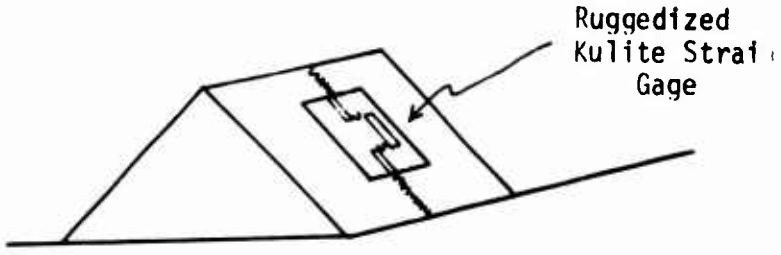

Shear Gage
(V-45 Rubber Triangle
with Kulite Gages Attached)

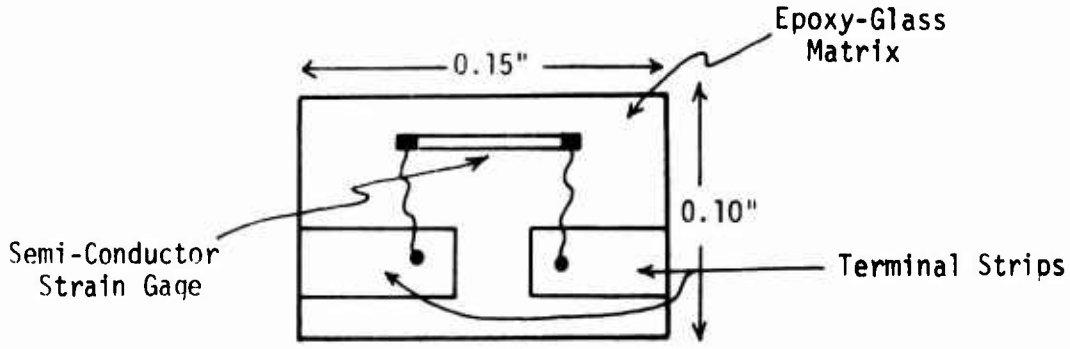

Kulite Ruggedized Strain Gage

Figure 5. Shear Gage Made from Kulite Ruggedized Strain Gage

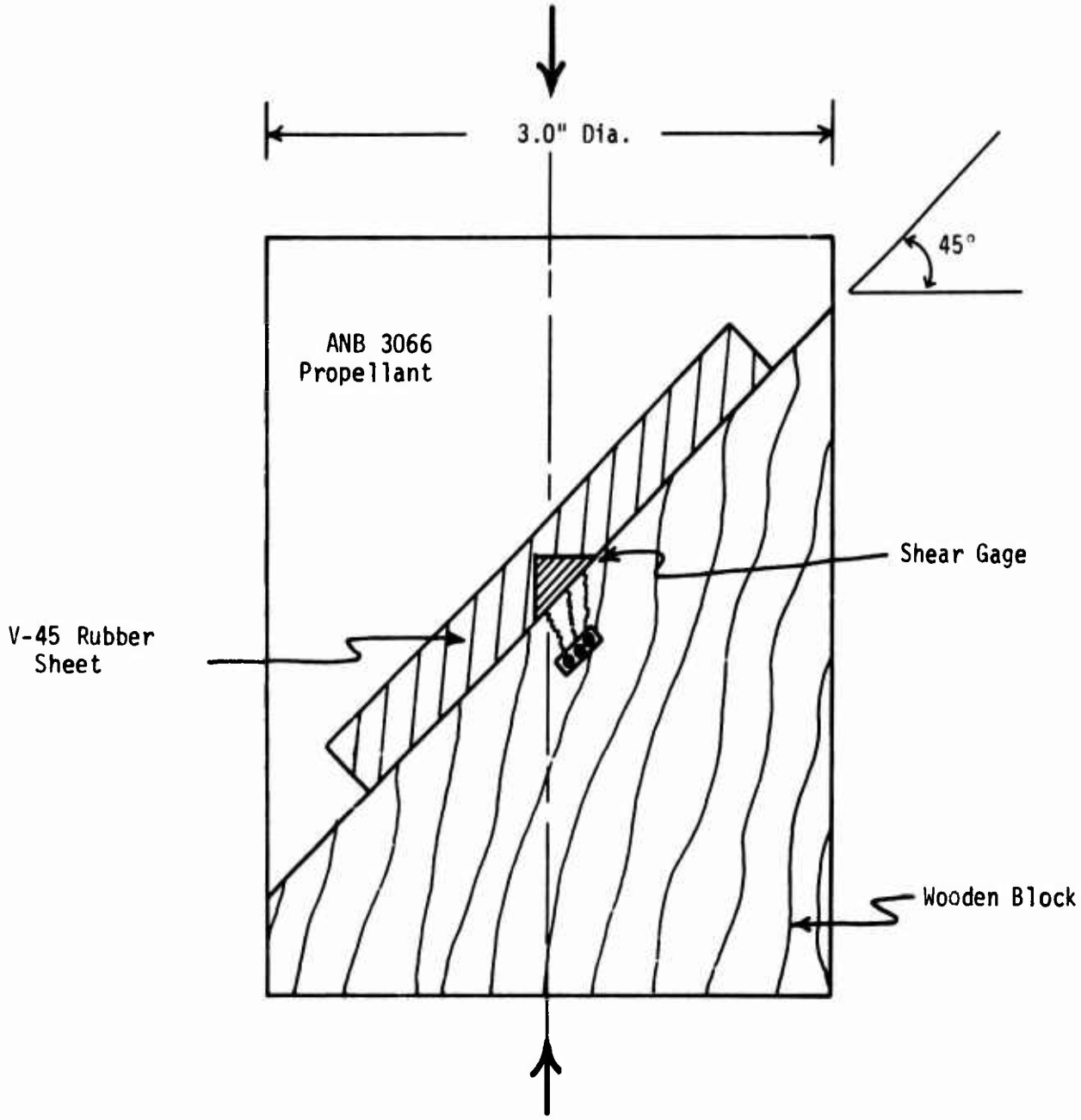

Figure 6. Shear and Compression Test Specimen

The lower part of the specimen was made of wood and the V-45 rubber was bonded to it with an epoxy adhesive. The intent of the specimen was to simulate the type of combined compression and shear stresses which would be obtained close to the knuckle region during a pressure test of a full-scale motor.

The 45° angle configuration provides equal compressive and shear stresses at the gage location. Although this does not duplicate the full-scale motor stress distribution it was believed to be sufficiently close for the resulting test data to be meaningful. Two test specimens were made with the ANB-3066, third stage Minuteman propellant cast onto the V-45 rubber surface and cured for the required period.

C. FAILURE TEST DATA FROM SHEAR GAGES

Prior to this testing, the two shear gage specimens were wired into bridge circuits. Two different circuits were used to account for the output ranges that would be preferred when using the gage for failure test measurements and for measuring small stresses. These are shown in Figures 7a and 7b. The only difference between them is the value of the feed resistor used to supply the bridges. The small strain type of circuit employs a 3.5K ohm feed resistor whereas the large strain (failure) gage circuit uses a 13K ohm value feed resistor.

The two specimens were tested in combined compression and shear using a constant crosshead speed to certain values of the shear stress; then holding the crosshead fixed, the stress and the gage readings were allowed to relax. Several steps (of about 10 psi each) of increasing stress magnitude were used until the specimens failed.

Shear specimen No. 1, with the "failure stress" circuit failed at 89 psi while specimen No. 2, containing the "small stress" circuit, failed at 60 psi. The failures involved propellant unbonding from the insulation layer containing the gage. Also, shear gage No. 2 was still working after the failure of the specimen whereas the shear gage in specimen No. 1 was not (open circuit).

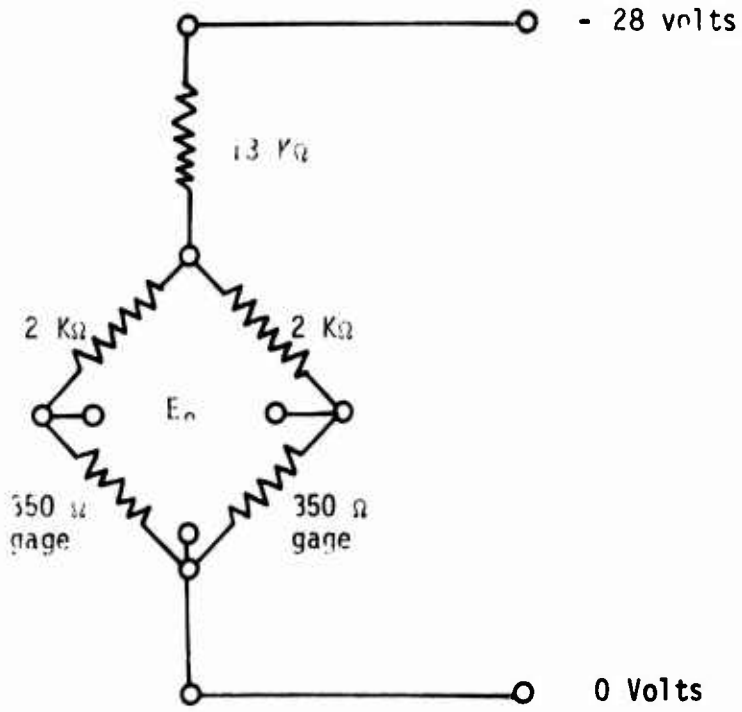

Figure 7-a Failure Shear Gage Circuit - Specimen No. 1

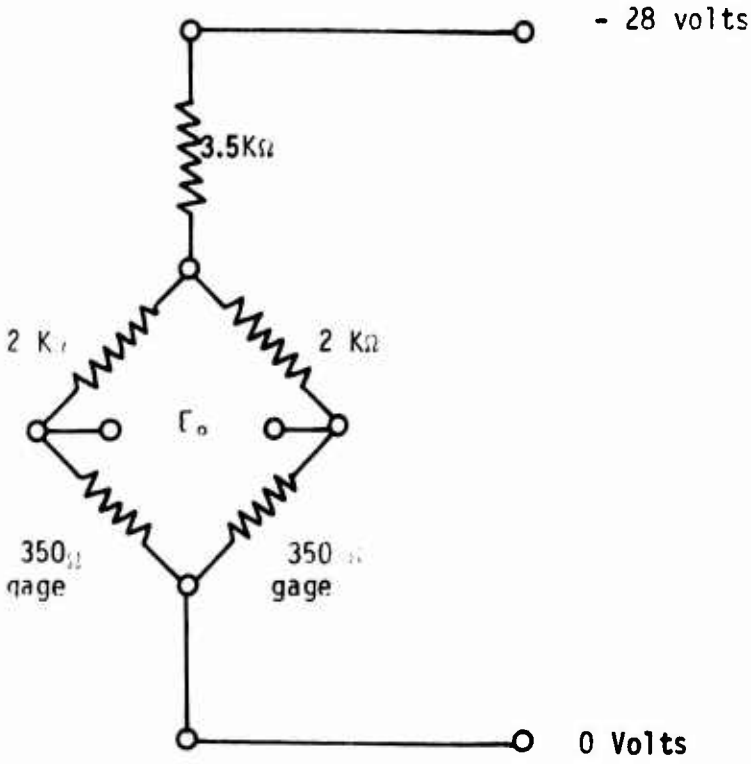

Figure 7-b Small Stress Shear Gage Circuit - Specimen No. 2

The response data obtained from these two compression-shear tests are given in Figures 8 and 9. The gage response is a reasonably linear function of applied shear stress up to approximately 50 psi but becomes appreciably more nonlinear at higher stress levels. The specimens were loaded by ramp-loading steps followed by relaxation periods. Although some hysteresis was obtained at low stress levels there is little non-linearity in response. At the larger stress levels the gage response during relaxation did not follow the loading curve showing distinct hysteresis effects. When the loading was continued at the end of the relaxation the response slope was almost identical to the earlier loading slope but displaced vertically. The overall envelope of the gage output versus shear stress therefore appears non-linear whereas it would probably have been much closer to a straight line under a continuous loading type of test. Note that specimen No. 2 with fewer loading and unloading sequences exhibits a more linear response than specimen No. 1.

It was concluded from these preliminary tests that the new (modified) shear gages would measure the propellant shear stresses to more than 60 psi at 70°F. This was believed adequate for much of the testing planned for the third-stage Minuteman motor.

A further conclusion is that the V-45 shear gages are slightly rate sensitive. A short series of tests showed that the gage response varied between 8.125 mv/psi at a strain rate of 20 in./in./min. and 9.30 mv/psi at 0.02 in./in./min.

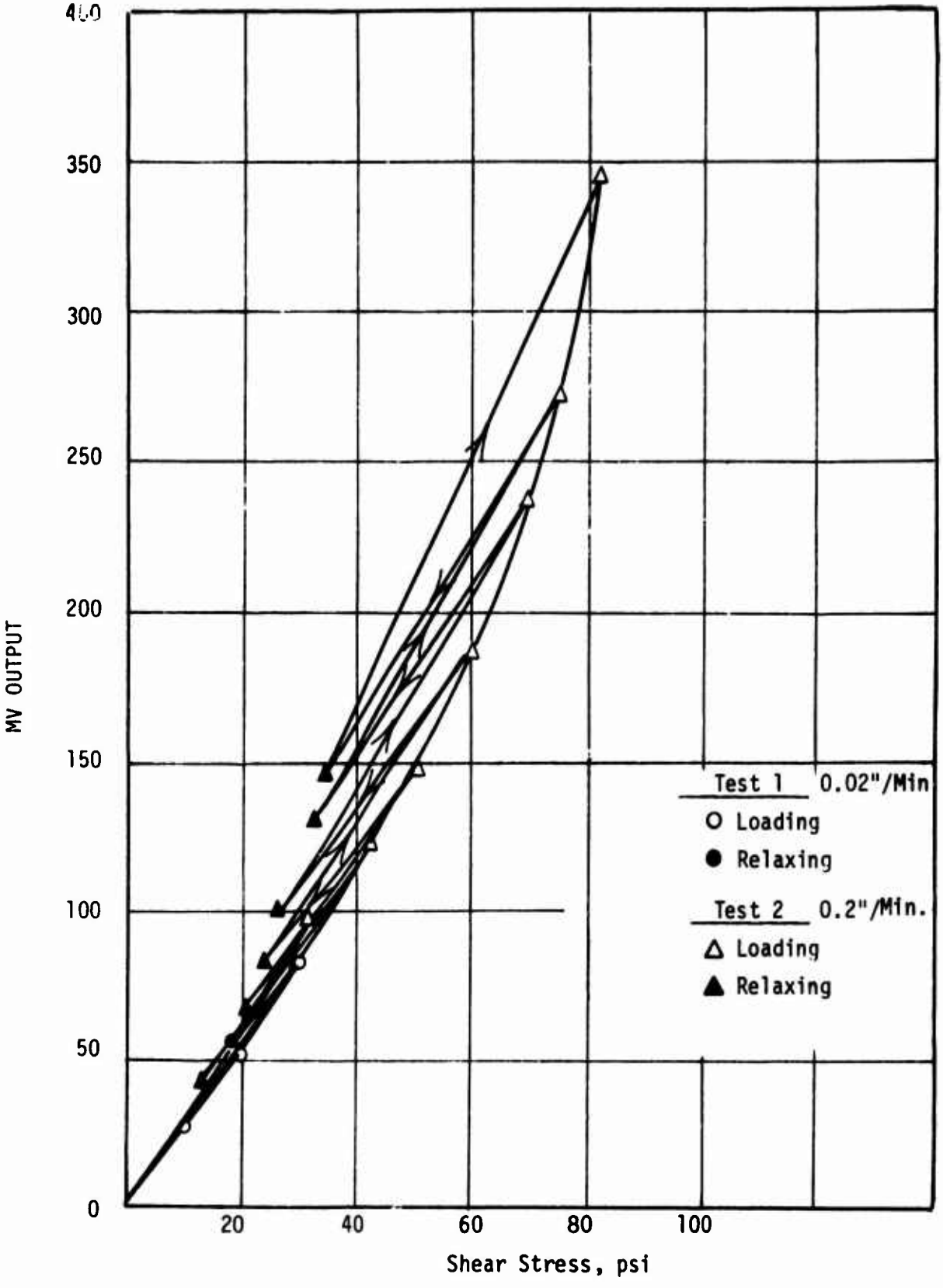

Figure 8. Failure Test of Shear Gage No. 1
Combined Shear and Compression

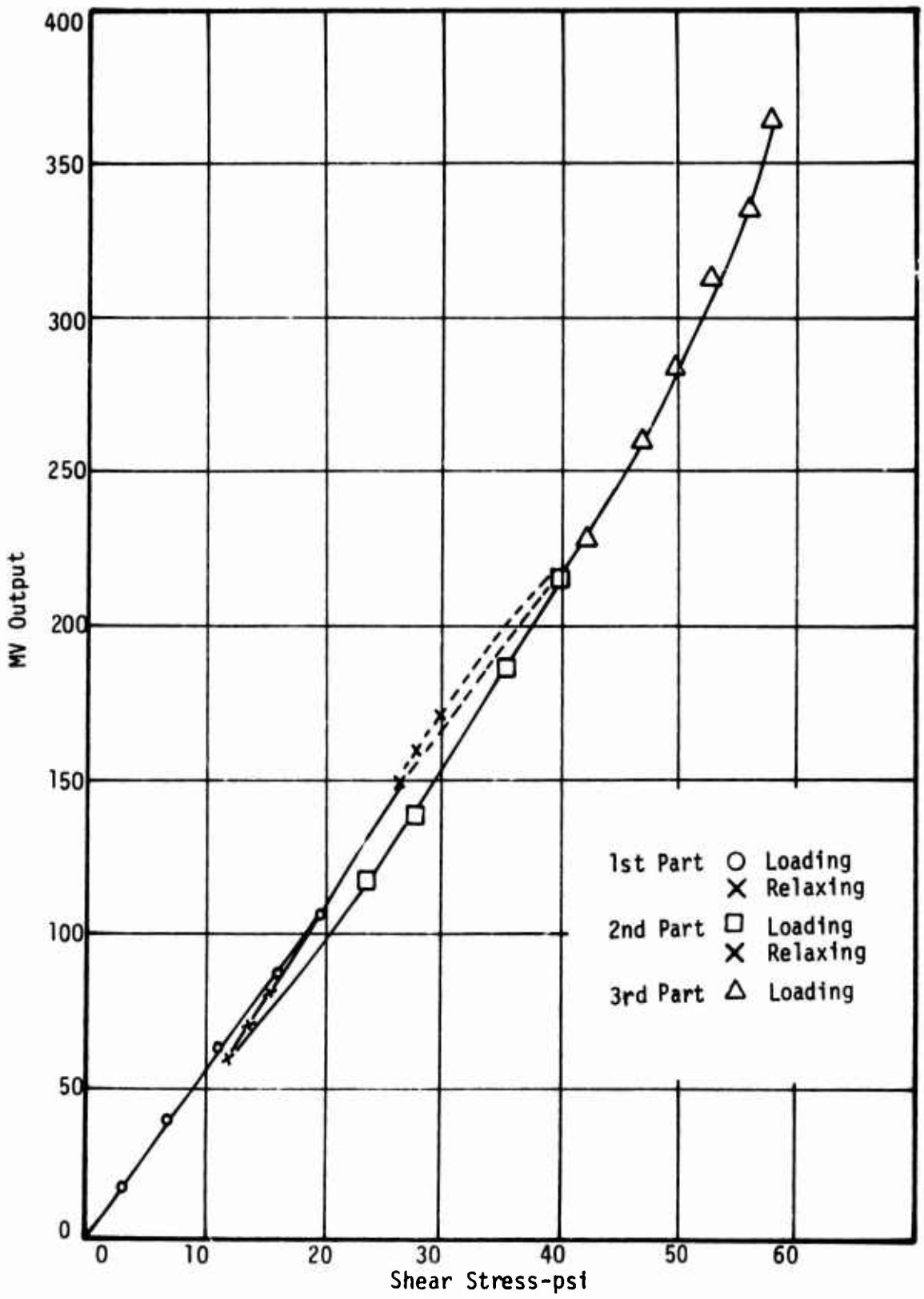

Figure 9. Failure Test of Shear Gage No. 2 in Combined Shear and Compression

SECTION 5

STV NO. 1 - BONDING AND CASE FAILURE TESTS

A. TEST OBJECTIVES

A primary objective was the investigation of special techniques to bond normal stress and shear gages directly to the motor case or to the internal rubber insulation. A slightly flexible adhesive was used because a too-rigid adhesive would cause transducer-case bond failures when the flexible case expanded upon internal pressurization.

A second objective was a study of the effect of drilling holes through the motor case wall to provide exits for the instrumentation leadwires. Prior experience on the Polaris A-3 program (1) had demonstrated the practicality of this concept on full-scale motors. Hole sizes from 0.090 to 0.249 in. were employed in that program and the largest holes reduced case strength only 10%. The maximum hole size planned for the Flexible Case-Grain Interaction program was only 0.060 in. so negligible effects on case strength were expected. However, the possibility of local case degradation leading to fissuring of the insulation and gas leaking were real problem areas requiring evaluation.

The possibility of firing motors containing gages led to the third objective which was the development of procedures for thermally protecting the gages and the holes in the case wall. The proposed technique was to seat the gages as deeply as possible into the V-45 rubber insulation, then cover them with a thick layer of an insulating adhesive, i.e., potting material. The practicality of this concept was tested on STV No. 1. Figure 10 shows the gage "potting" concept and installation in the motor case.

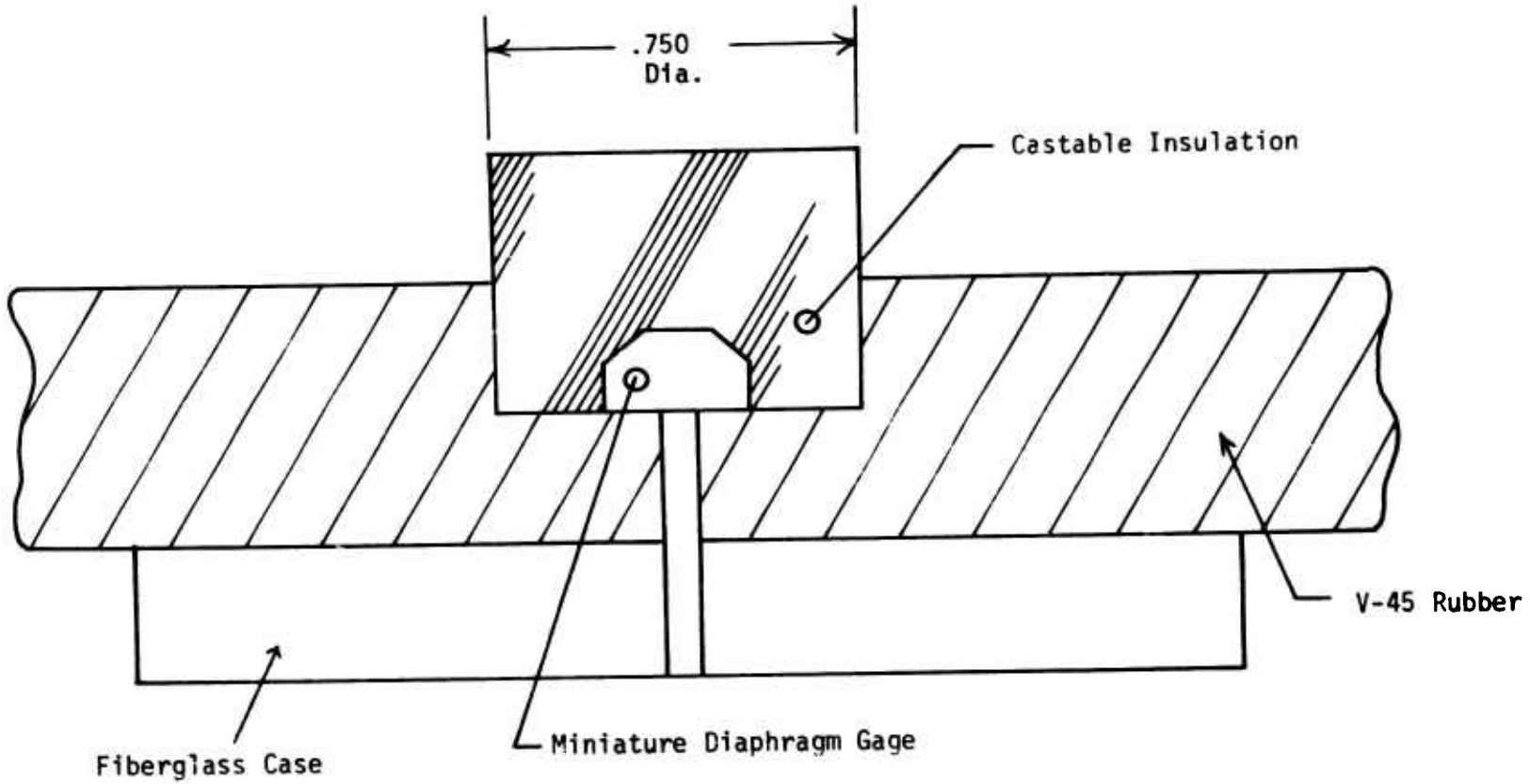

Figure 10. Typical Normal Stress Gage Installation

B. CASE MACHINING

A 4-inch long section in the middle of the fiberglass case of STV No. 1 was machined to reduce the wall thickness to 0.10 in. This modification reduced the rigidity of the case so that it would fail with a hoop strain greater than 1.0% at a pressure of 1800 psig.

This chamber modification permitted evaluations of the failure behaviors of the flexible adhesive, the potting material around the gages, and the 0.060 in. holes drilled through the case wall.

C. SELECTION OF THE FLEXIBLE ADHESIVE

The adhesive was selected to meet the requirements of the overall Flexible Case Program which were:

1. Flexibility, required because of the bonding interface between the rigid gages, the fiberglass case, and the rubbery insulation. Many elastomeric adhesives could have been chosen to meet this requirement.

2. Bonding to the V-45 insulation, a requirement that could be met by many epoxy and urethane adhesives.

3. Insulation properties approximately equal to those for the V-45 rubber. This requirement was imposed because the second full-scale motor was to be fired at some future date.

4. Previous Applications in Solid Rocket Motors

IBT-115, a trowelable insulation material, was found to satisfy these requirements. This material was specifically developed by the Aerojet Solid Propulsion Company for the internal insulation of large solid rocket motors (2).

The viscosity of the IBT-115 trowelable insulation in its uncured state allowed it to be poured and worked in a manner to encapsulate the transducers, while they were being held in restricted molds. The Shore A hardness of the cured V-45 insulation material is approximately 68 to 70, which is close to that of the cured trowelable insulation IBT-115; namely, 66 to 70. The relaxation moduli of the two materials are significantly different; the V-45 modulus being about six (6) times the IBT-115 at 10 minutes. On the other hand, the IBT-115 has relaxation properties close to those for the ANB-3066 propellant.

D. MILLING OF THE INTERNAL RUBBER INSULATION

The procedures employed in STV No. 1 were designed to simulate as closely as possible the operations to be used on the full-scale motors 1 and 2. The major difference was that the small inside diameter in the STV prevented machining of the insulation inside the STV. To simulate the embedment procedures that were to be used on the full scale motors, a section of an old Minuteman III case was used to develop the machining techniques (Figure 11).

The basic tool for this drilling was a modified 3/4 in. diameter end mill with a pilot guide welded to its center, Figure 12. The tool is driven by a high speed air drill. The pilot guide is inserted into a 0.060 in. diameter hole, previously drilled through the case. The guide automatically centers the cutting edge of the end mill making a 3/4 in. diameter recess in the insulation (this accommodates the seating of the normal and shear stress gages). An excluded length was designed into the tool to provide a positive "stop". This stop prevented the end mill from cutting into the case wall (just one cut of this kind could make the case unacceptable for pressurization testing).

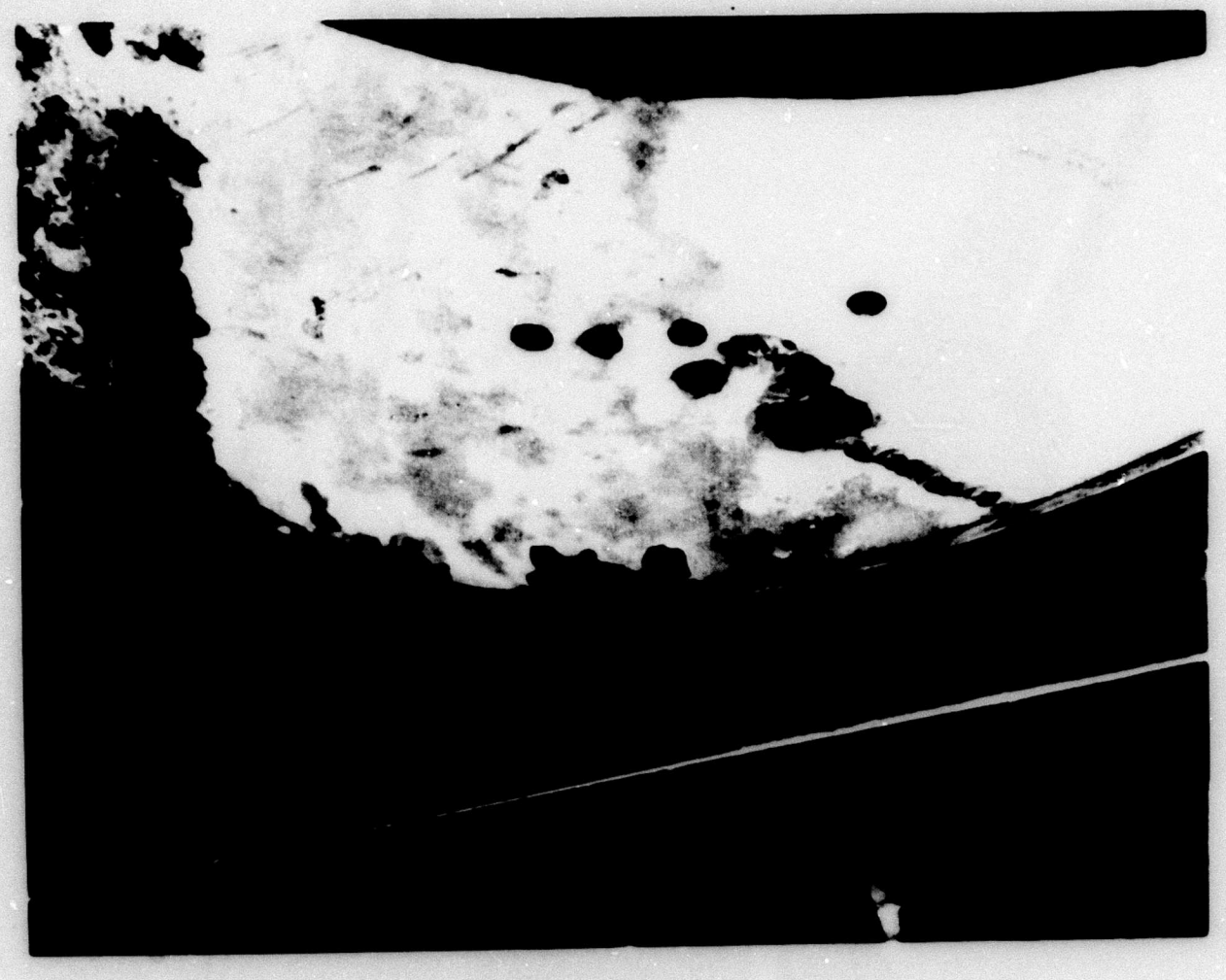

Figure 11. Holes Made While Developing Drilling Techniques
(Made in the insulation of a section of a Minuteman III,
Stage III motor case)

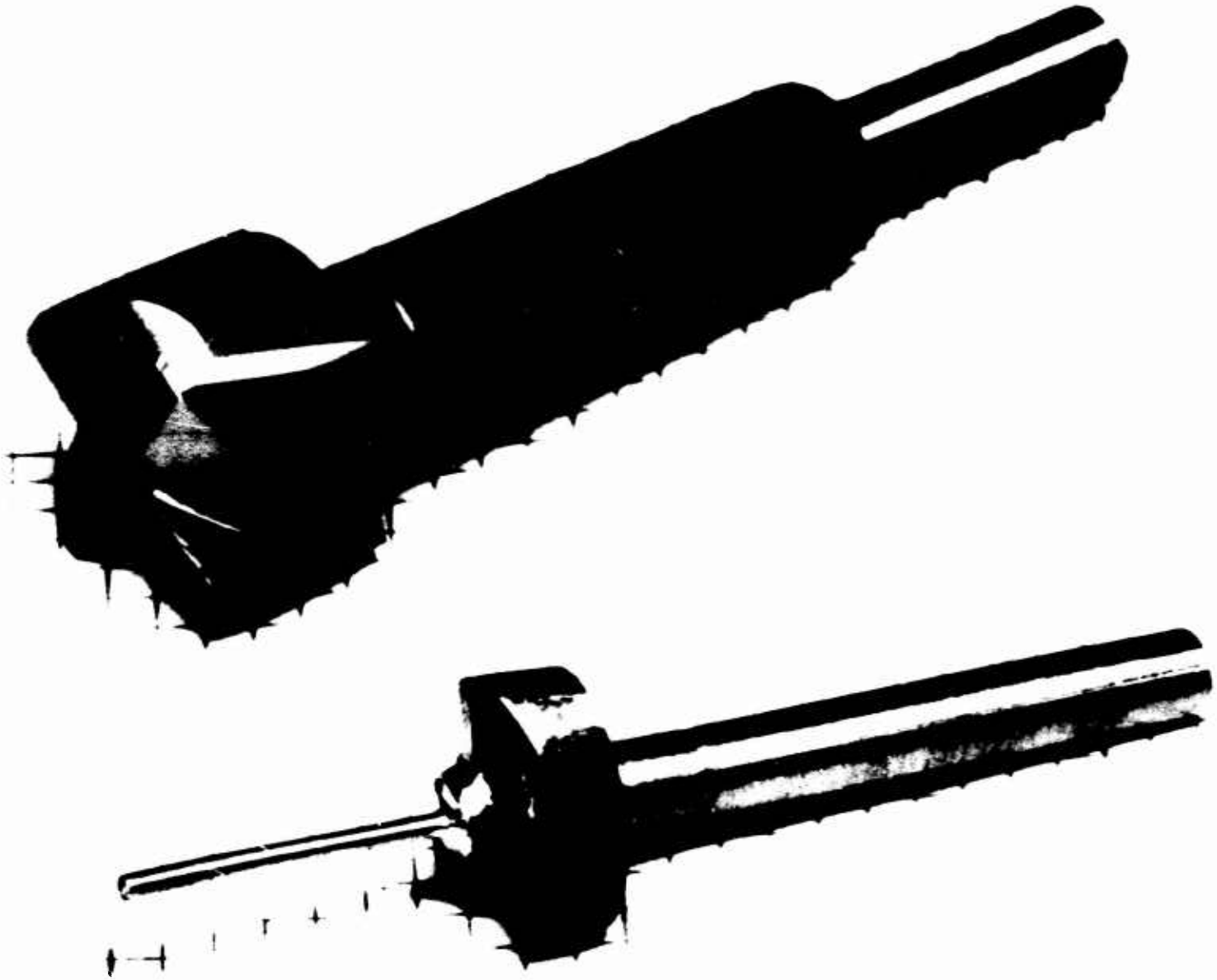

Figure 12. Modified 3/4 In. Dia End Mill

E. INSULATION LAY-UP AND DUMMY GAGE INSTALLATION

Because the end mill could not be used inside the STV, it was necessary to form the recess holes during insulation lay-up. This was accomplished using 1 in. diameter metal plugs bonded to the case at six different locations; the insulation was installed around the metal discs.

The internal insulation lay-up followed standard preparation procedures for the Minuteman III, Stage III motor, except for the prime coat. The interral surface of the case was coated with thin layers of Chemlok 203 primer and Chemlok 220 and HF 1127 adhesives. Then a 10-in. long by 0.25 in. thick layer of V-45 rubber insulation was bonded and cured in the mid-section of the case around the six metal plugs.

After the insulation was cured the metal plugs were removed. Holes of 0.055 in. were then drilled through the case at the center of each recessed hole. The dummy potted gages were 3/4 in. diameter, 1/4 inch high, and had a metal stem 0.050 in. in diameter (see Figure 13). The clearance between the 1.0 inch diameter recessed holes and the potted dummy gages was large enough to allow air bubbles and excess adhesive to be squeezed out. Teflon tapes were used to hold the dummy gages in place during cure, which required 4 hours at 175°F.

The dummy gages were, in reality, steel thumb tacks, which were dimensionally close to the normal stress gage. The stem (0.050 in. dia.) of the thumb tack is an excellent substitute for the tubing (0.055 in. dia.) that surrounds the leadwires of both the normal and shear stress gages.

After cure of the adhesive, the tapes were removed and the dummy gage installations inspected. All of them appeared to be satisfactory.

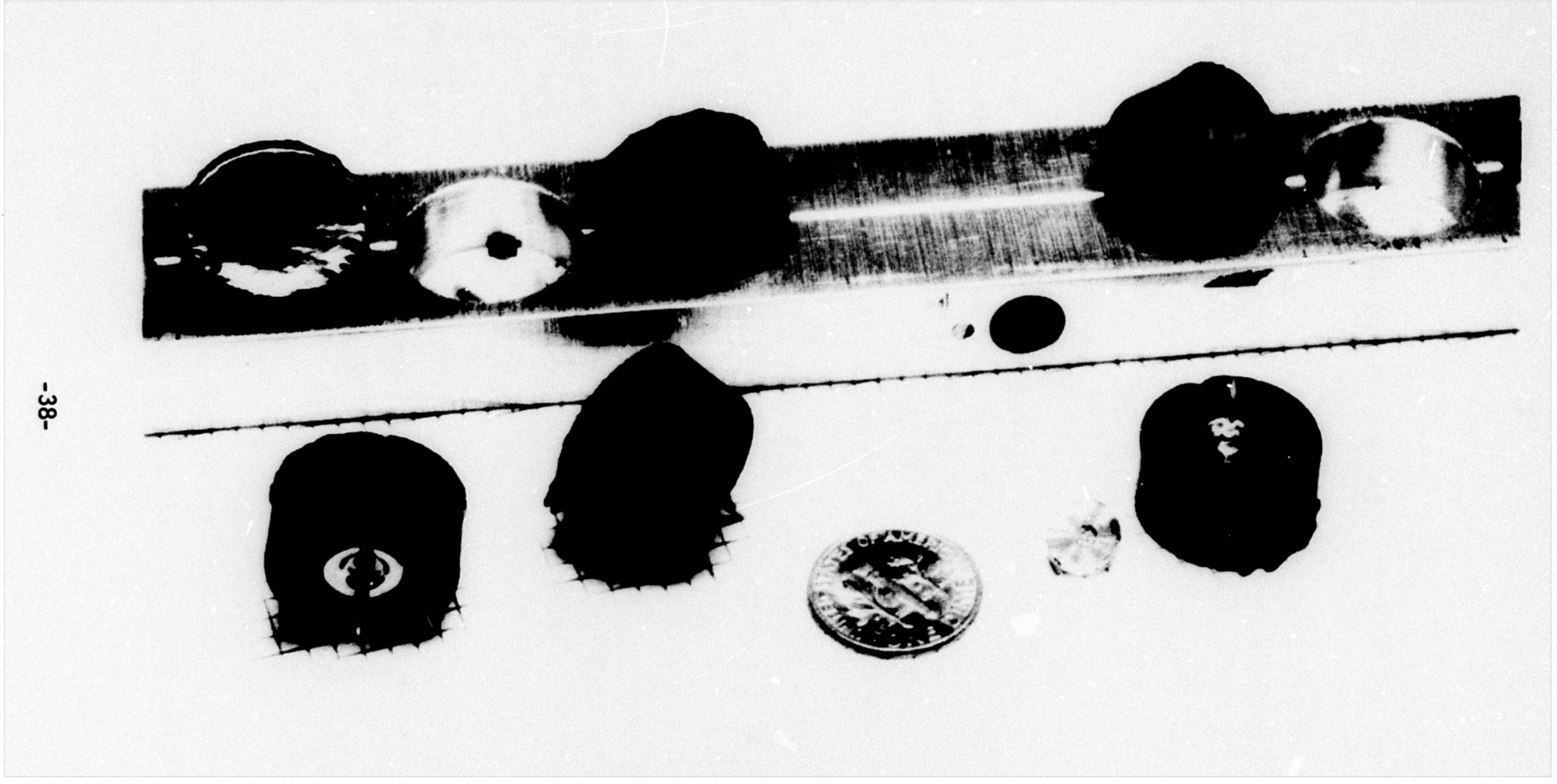

Figure 13. Dummy Normal Stress Gages Used in STV No. 1

F. PRESSURIZATION TO FAILURE

Upon final cure of the adhesive, the end closures and retaining rings were installed in preparation for the burst test. The hydraulic pressurization and instrumentation set-ups are shown in Figure 14. A pressure source, consisting of a high pressure water pump, valve, pressure gage, and regulator, was employed. In addition, a strain gage indicator was used to monitor case hoop strains during the test, while an X-Y plotter provided a recording of the hoop strain versus the internal pressure.

G. TEST RESULTS

The data from the burst test are shown in Figure 16. Following the burst test, STV No. 1 was sectioned as shown in Figure 15, then visually inspected with the following results:

1. Bonding procedures were adequate, with no case leakage evident up to the 1790 psig failure pressure, Figure 16.

2. The case hoop strain exceeded the value predicted from the hydroproof pressure tests (1.27% observed versus 1% predicted at 1800 psig). This softening may have been caused by the slight damage produced in earlier pressure testing.

3. The gage-to-case and gage-to-insulation bonds successfully withstood the differential strains developed on pressurization (1.27% hoop strain, Figure 16).

4. Holes drilled through the chamber produced no significant reduction in case strength. There was no case delamination around <u>any</u> of the six holes, although severe delamination did occur at a number of sites away from the holes but within the thin mid-section of the case.

5. No moisture leakage was observed at any of the holes, showing that the gage potting and insulation did not fissure during the testing. These results clearly demonstrated the adequacy of the new adhesive and gage installation procedures. Accordingly, they were accepted for use in the full-scale motors.

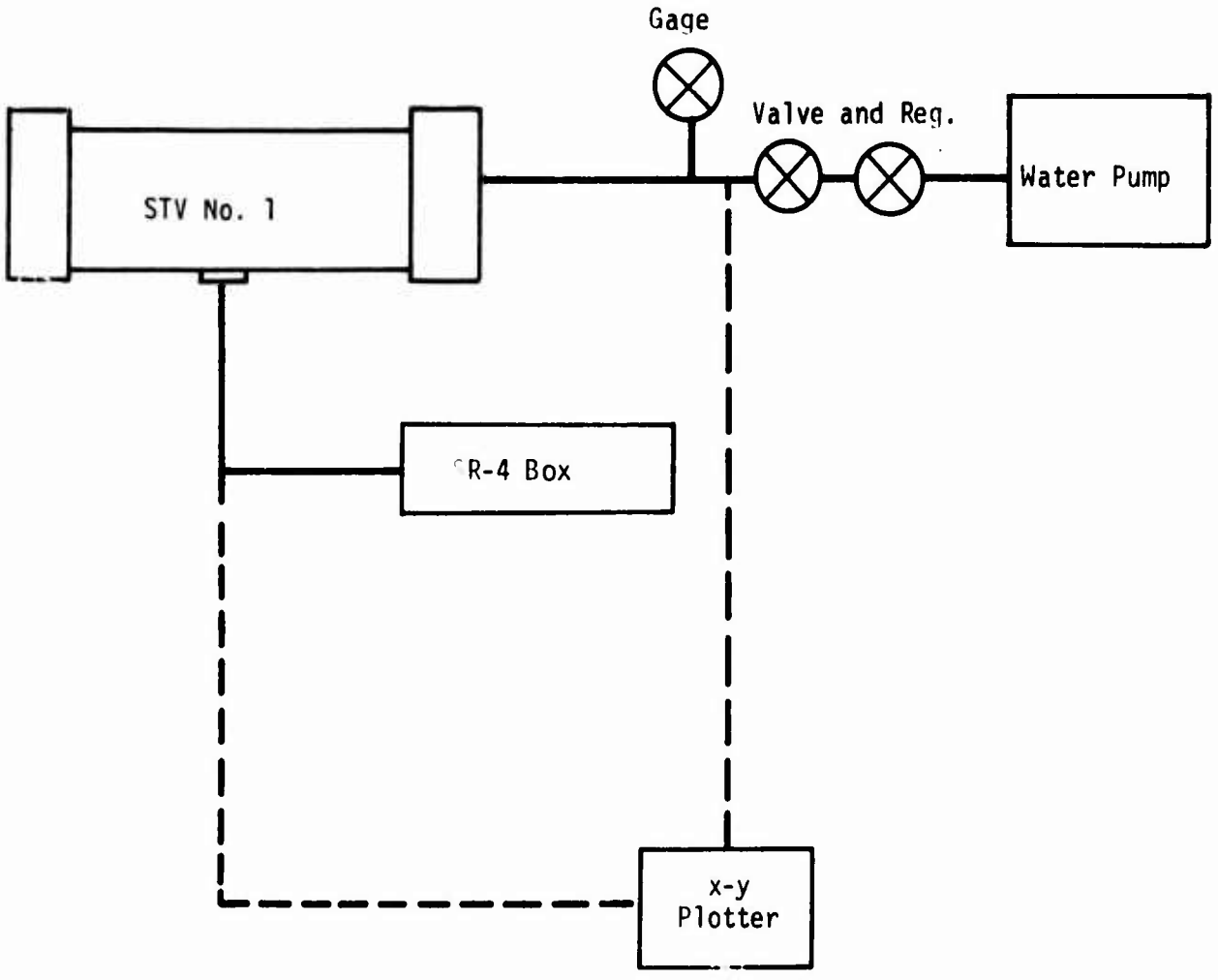

Figure 14. Pressurization and Instrumentation Setups for STV-1

Figure 15. Sections of STV No. 1 After Failure Testing

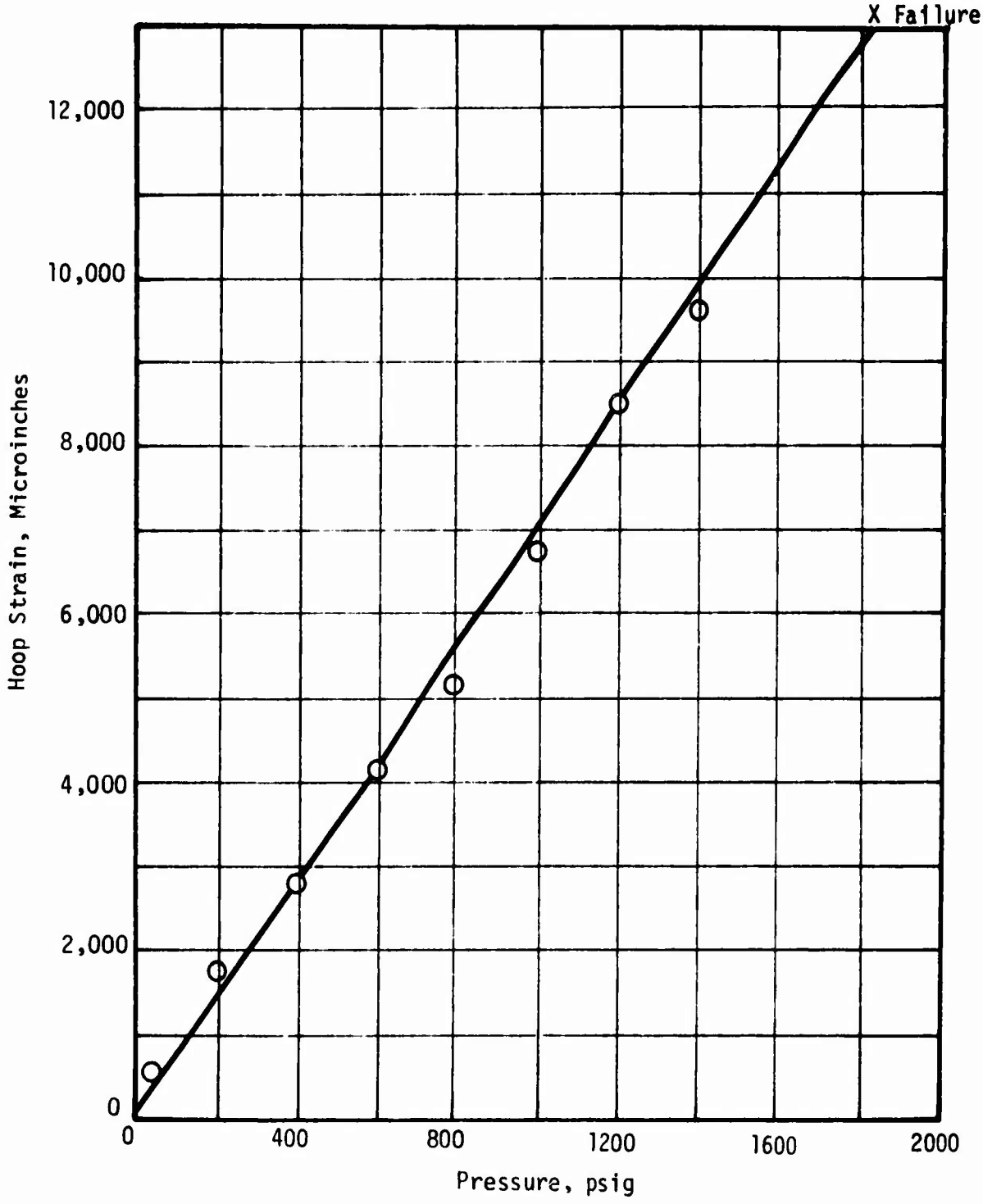

Figure 16. Hoop Strain Versus Internal Pressure During Test to Failure of STV No. 1

SECTION 6

STV NO. 2 - EVALUATION OF GAGE POTTING AND CALIBRATION METHODS

A. TEST OBJECTIVES

The planning at the beginning of the overall program led to a concept of pre-potting of the gages into an inert insulation material. This pre-potting was intended to provide electrical safeguards for the grain (physically isolate the propellant from possible electrical shorts) plus simplifications in the gage calibration and temperature compensation procedures. The calibration procedure, hopefully, would be simplified by external (outside of the motor) calibrations of the gages assuming the pre-potting would take into account gage-grain interactions. It was hoped that the temperature compensation would be improved since most of the gage-grain interaction would be included because of interactions with the large mass of potting material.

STV No. 2 was designed to evaluate these new concepts. Specifically STV No. 2 was intended to accomplish the following:

1. To demonstrate that pre-potting, external calibration and improved thermal compensation of the normal stress gages were satisfactory and sound techniques.

2. To compare the pre-potting, external gage calibration and thermal compensation techniques with the LPC approach of installing the gage in the motor, potting it in propellant, and then calibrating it in-situ.

3. To demonstrate the validity of the shear gage calibration in a simple external shear fixture by means of differential pressure tests in an STV.

4. To demonstrate the performance of the normal and shear gages under thermal and pressurization loading environments.

The results of the experimental tests on STV No. 2 in relation to these objectives are discussed below.

B. STRESS TRANSDUCERS

Both normal and shear stress transducers were used in these evaluations. The normal stress transducer is a conventional diaphragm-type pressure gage that has been modified to minimize the propellant-gage interaction. It was originally developed for solid propellant testing by Leeming and Konigsberg (References 3, 4 and 5). Further details on the design, fabrication, calibration, and thermal compensation of these gages are given in Appendix A. Also, the calibration data for the gages used in STV No. 2 and the voltage measurements taken from the motor tests are given in Appendix C.

The shear gages were also developed by Leeming (3, 4 and 5). They consist of two semi-conductor strain gages bonded to a triangular shaped piece of elastomeric material and mounted at 90° to each other and at 45° to the plane of the shear that is being measured. Because of large grain-gage interactions these transducers are considered to be less accurate than the normal stress gages. Details of the design, fabrication, calibration and thermal compensation of the shear gages are given in Appendix B, while the experimental test data are provided in Appendix C.

C. GAGE PRE-POTTING CONCEPT

The proposal planning efforts for this program led to the new concept of gage pre-potting. Previously the normal stress gages were mounted on the case wall, then they were potted in a cup of propellant as shown in Figure 17. After propellant cure, the gages were calibrated through internal pressurization of the motor case. Temperature compensation of the gages was performed prior to delivery by the vendor (Konigsberg Instruments, Inc.).

The new potting concept resulted from the intention to embed the gages within the insulation for thermal protection during motor firing. Since the insulation is inert it was possible to pre-pot the gages before calibration and temperature compensation by the vendor.

The entire gage affects the local grain stresses while the grain modifies the performance of the gage diaphragm. This latter effect is considered to be of the greatest importance. The "zone of influence" for this interaction is shown schematically in Figure 18 (see References 3, 4 and 5). The size of this zone is directly related to the dimensions of the gage diaphragm. As shown in Appendix A, the gage diaphragm is only 0.10 in. in diameter. Since a major portion of the zone of influence occurs within two radii of the edge of the diaphragm we have a region with a total diameter of about 0.30 in. Thus, much of the zone of influence for the diaphragm falls within the diameter of the base of the gage, 0.310 in. diameter.

The finally selected prepotting design considerably exceeds the gage base with an overall diameter of 0.75 in. and a height of 0.375 in. This enlarged prepotting region also takes into account the discontinuity effects arising at the edge of the metal disc. These produce their own zone of influence effects which, for this gage design, are considered almost negligible.

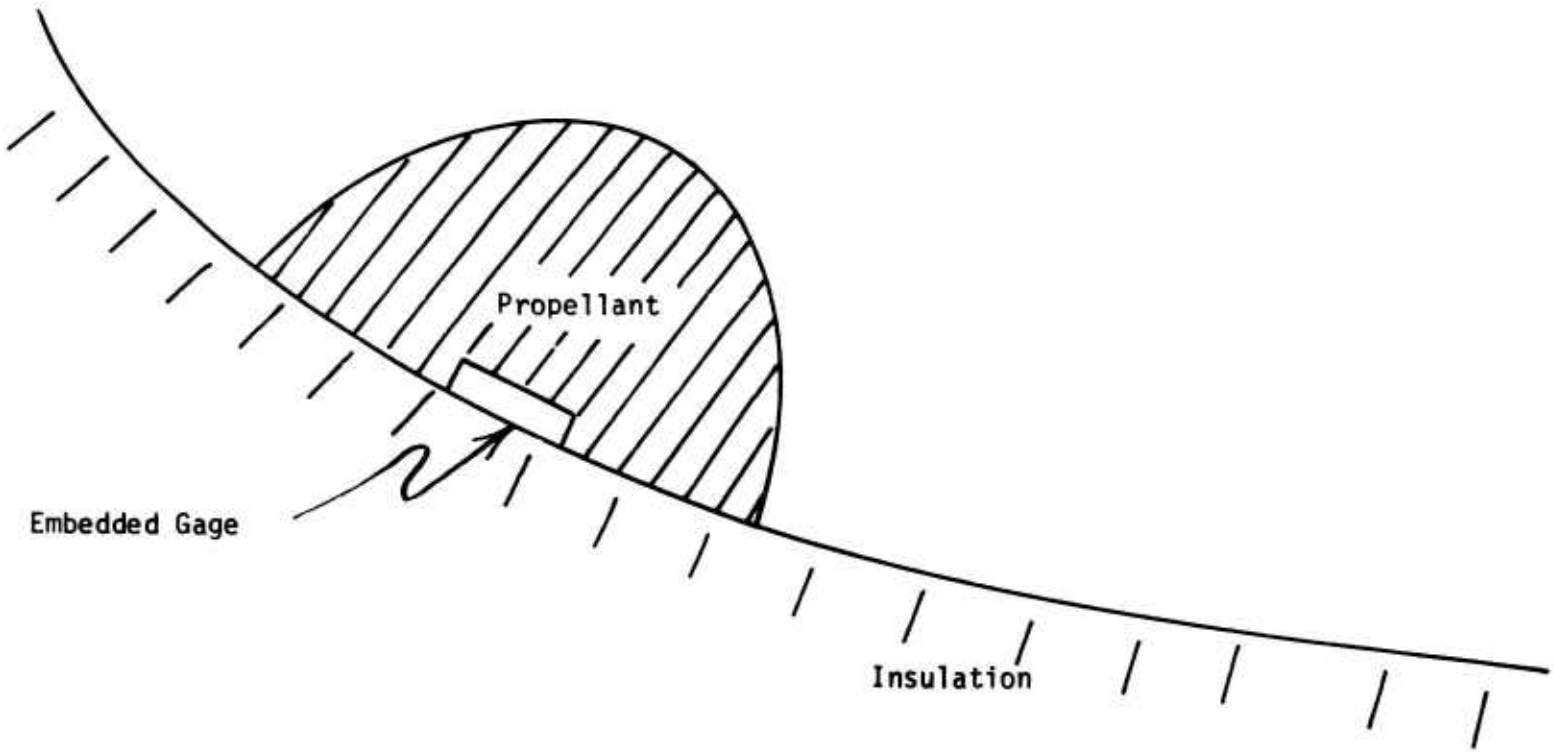

Figure 17. Previous Gage Embedment Procedure

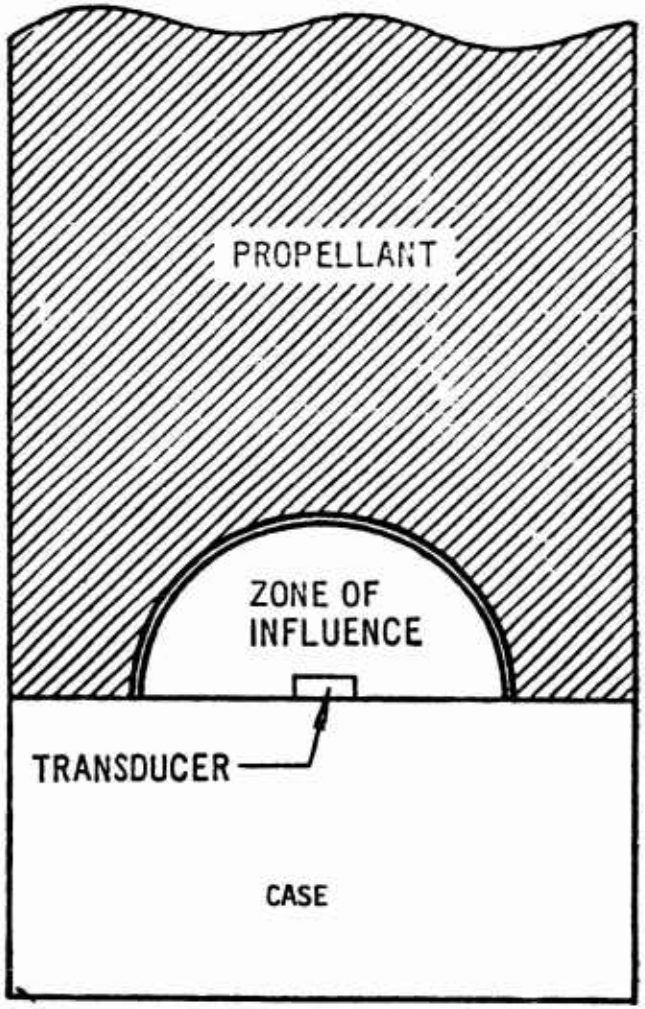

Figure 18. Zone of Influence of Gage at Propellant/Case Interface

D. DESCRIPTION OF GAGE INSTALLATIONS

The configuration of STV No. 2 is shown schematically in Figure 19. The internal surface of the case was lined with a thin layer of V-45 rubber to prevent water seepage during hydrotest. Then a 10-in. long by 0.25 in. thick layer of V-45 insulation was bonded to the mid-section of the case and vulcanized in place. At locations where the gages were to be embedded in the insulation, metal plugs (1-in. diameter cylinders and 0.5 in. by 1-inch long rectangles) were placed during installation layup and then removed following insulation cure. Holes having a diameter of 0.060 in. were drilled through the case wall into these thinly-insulated areas to permit exit of the gage lead wires from the interior of the case.

Four 150 psi normal stress gages were bonded into the insulation next to the case. Two of these gages were procured from the manufacturer (Konigsberg Instruments, Inc.), encapsulated in a trowelable insulation and temperature compensated prior to delivery to ASPC, and then bonded into the motor. The second pair of gages (both unencapsulated) were bonded into the case insulation and then covered with a cup of ANB-3066 propellant about 1-in. high and 1.0 to 1.5 in. diameter and cured 12 days at 110°F. Two shear gages were also installed in the locations shown in Figure 19. The completed gage installations are shown photographically in Figure 20.

Lead wires from the gages were connected to terminal strips mounted on the case exterior, Figure 21. Bridge completion circuits were mounted on a control panel, which was connected to the STV when required for motor testing. A digital voltmeter was used to monitor the gage output while a 28 volt power supply was used to power the bridge circuit.

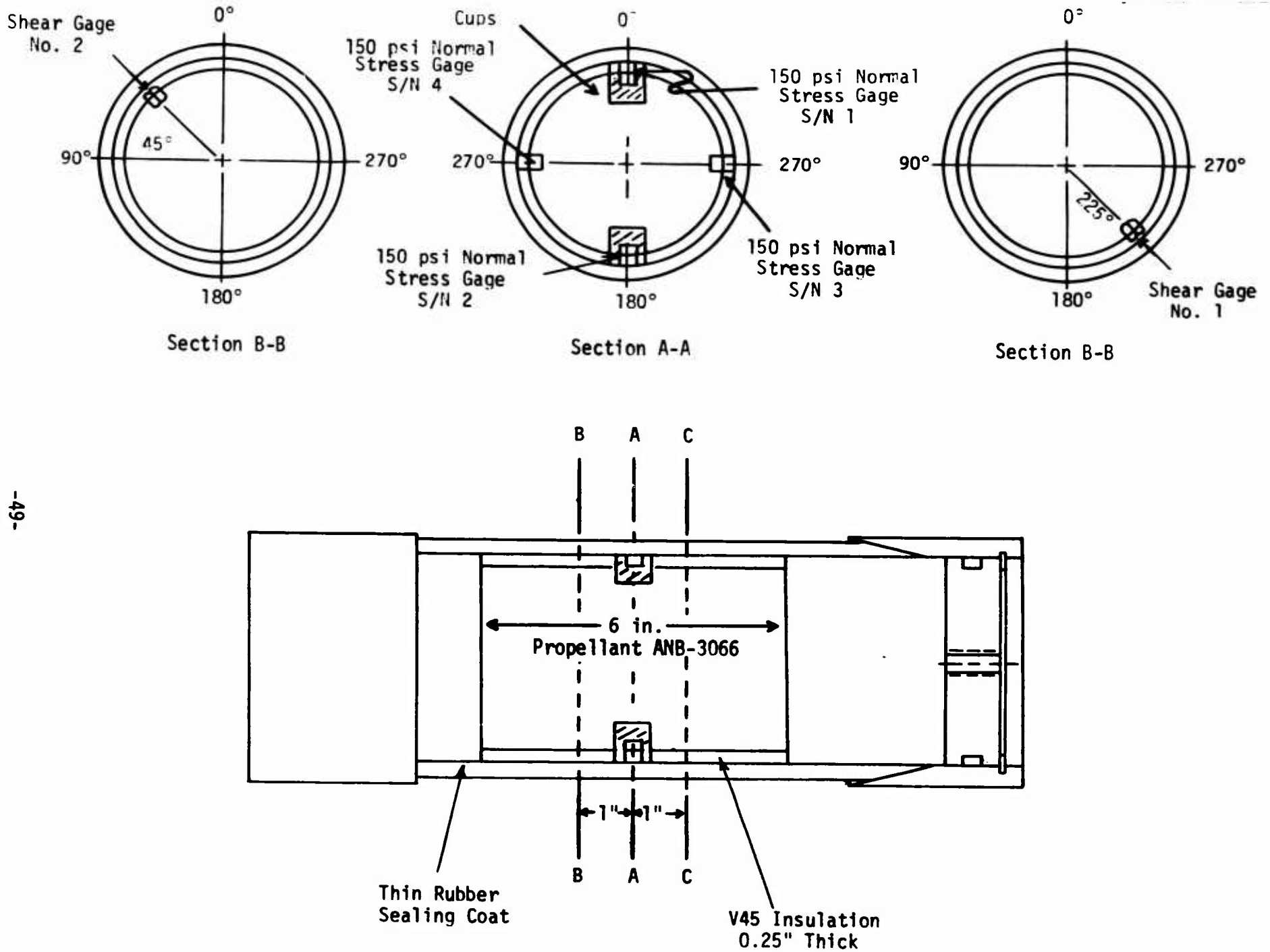

Figure 19. STV-2 Configuration

Figure 20. Photograph of Gage Installations in STV No. 2

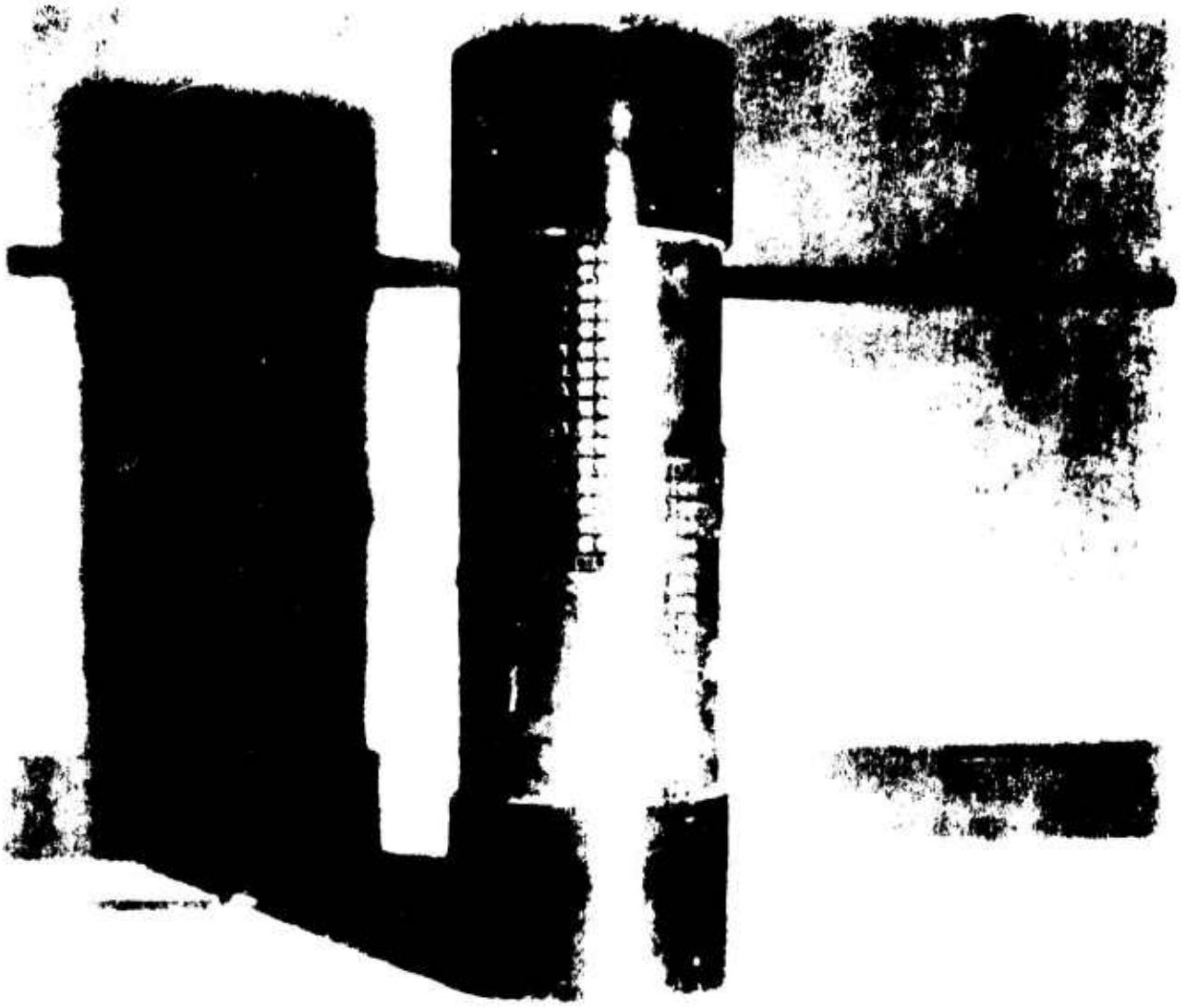

Figure 21. Photograph of STV No. 2 After Grain Casting

The series of tests performed on this STV required casting a non-perforated propellant grain. Following calibration and compensation of the propellant-encased 150 psi gages, the interior of the STV was cleaned, lined and prepared for propellant casting. When STV No. 2 was originally cast the grain was found to be approximately 10 in. long instead of the specified length of 6 in. After preliminary hydrostatic and differential pressure tests it was found that unbonds existed towards the ends of the grain. Because the grain had been cast overlength it was possible to machine it to its correct size and eliminate the unbonds. The hydrostatic and differential step pressure tests were then performed as described below.

E. TEST PROCEDURES

The first measurements on STV No. 2 were pressure calibrations of the propellant-potted gages at 30°, 80° and 130°F. These were performed prior to grain casting and repeated again after the grain was cast and cured. The test results and assessments are provided in Appendix C.

The second test series was designed to obtain comparative grain thermal stress data from gages installed using the two methods of gage potting. These measurements were made at 30°, 70° and 110°F. These data are discussed below.

The third set of measurements involved differential pressure tests conducted at 77°F. These tests were designed to provide accurate calibrations of the shear cubes. The test results are presented below.

F. COMPARISONS OF NORMAL STRESS MEASUREMENTS DURING GRAIN THERMAL TESTING

After the grain was cast, cured, and machined to 6-in. long, the STV was conditioned to three test temperatures (110°, 70° and 30°F) and the gage data were analyzed to determine the thermal stresses at the

mid-plane of the grain. Gage N2-2 did not provide data because of a wiring failure during the test, while gages N2-1, N3-1 and N3-2 evinced non-linear behaviors during the pressure calibration tests (Appendix C). These effects are attributed to the presence of casting bubbles at the gages.

The measured gage output voltages and the corresponding values of the gage stresses based on the in-situ calibrations of the gages before grain casting are presented in Table 1.* Comparison of data from gages pre-potted in IBT-115 and those potted in-situ in ANB-3066 propellant shows good agreement, except at 110°F. Here the propellant-potted gages ranged from +0.17 to +1.12 psi while the IBT-115 pre-potted gages ranged from -0.41 to -1.16 psi. This difference can be explained only by assuming zero-stress calibration errors for this test temperature.

The fair correlations (except at 110°F) between the two methods of gage potting are better illustrated by the mean and range data given below:

	30°F		70°F		110°F	
	Propellant	IBT	Propellant	IBT	Propellant	IBT
Mean, psi	15.6	15.5	4.77	4.52	0.65	-0.81
Range, psi	3.1	1.6	1.17	0.65	0.95	0.75

Although the conclusions are consistent with the data, it is believed that the limited test data, plus aging or other changes in the gages and associated electrical circuits leave a number of uncertainties. Hence, it is possible that future evaluations might reverse the conclusions made here.

---

* The data were reduced using the equation $\sigma = (V-a)/b$

where σ is the normal stress, psi
V is the measured output voltage, mv
a is the zero stress output (mv) at the test temperature
b is the gage sensitivity (mv/psi) at the test temperature

The values of a and b were obtained by interpolation from the data listed in Table C-1 of Appendix C.

TABLE 1

NORMAL STRESS MEASUREMENTS IN STV NO. 2

AT THREE TEMPERATURES

Gage No.	Potting and Pre-Potting	Gage MV Output			Gage Stress, psi		
		30°F	70°F	110°F	30°F	70°F	110°F
N1-1	Propellant	-10.33	-3.54	-0.07	15.6	4.76	0.17
N1-2		-10.62	-4.38	-0.17	17.2	4.72	0.66
N2-1*	Propellant	- 9.48	-3.35	-0.43	14.1	4.21	1.12
N2-2**			-4.20		-	5.38	-
N3-1*	IBT-115	-11.71	-3.71	-0.99	15.0	4.07	-0.67
N3-2*		-11.67	-4.87	-1.09	14.8	4.70	-1.16
N4-1	IBT-115	-11.62	-3.27	-0.40	16.4	4.59	-0.41
N4-2		-13.11	-3.96	+ .77	15.9	4.72	-1.00

* Gages questioned because of unusual performances during calibration and STV testing.

** Gage malfunctioned electrically.

G. CALIBRATION BEHAVIOR OF THE RUGGEDIZED SHEAR GAGES

The differential pressure tests were designed for calibration of the shear cubes, and were performed at a temperature of 77°F. The STV was fitted so that nitrogen pressure could be applied to either or both ends of the grain to create a differential (shear) load across the grain (Figure 22). The initial efforts involved a 10 psig pressure step applied to one end of the grain while the responses of the gages were monitored for two minutes. Then the pressure was released and the gage response again monitored for another two minutes (originally a 10 minute dwell time was used, but it was found that little change occurred after two minutes and therefore the shorter time was used for all of the testing). The same procedure was followed with a 10 psi pressure applied to the opposite end of the grain. This test sequence was repeated using 20 and 30 psi pressure steps applied to alternate ends of the grain. Table 2 describes the testing sequence.

To avoid the possibility of premature shear failure of the grain, the maximum differential pressure was limited to 30 psi giving a mean shear stress of 7.5 psi.

The gage output data from the 77°F tests are presented against the differential pressure in Figures 23 and 24. The linearity of the gage response is evident in the data, and there is no detectable change in slope through the origin with gage SH-2. A slight change in slope is evident with gage SH-1, although it is not significant and a mean value may be used.

The calculated gage sensitivities for SH-1 and SH-2 at 5.43 mv/psi shear and 6.88 mv/psi shear respectively are higher than those measured in the shear specimen, i.e., 4.74 mv/psi and 6.09 mv/psi, respectively. These differences in gage sensitivity (14.5 and 13.0%, respectively) are not large; and it is believed that they result from a systematic error of some kind.

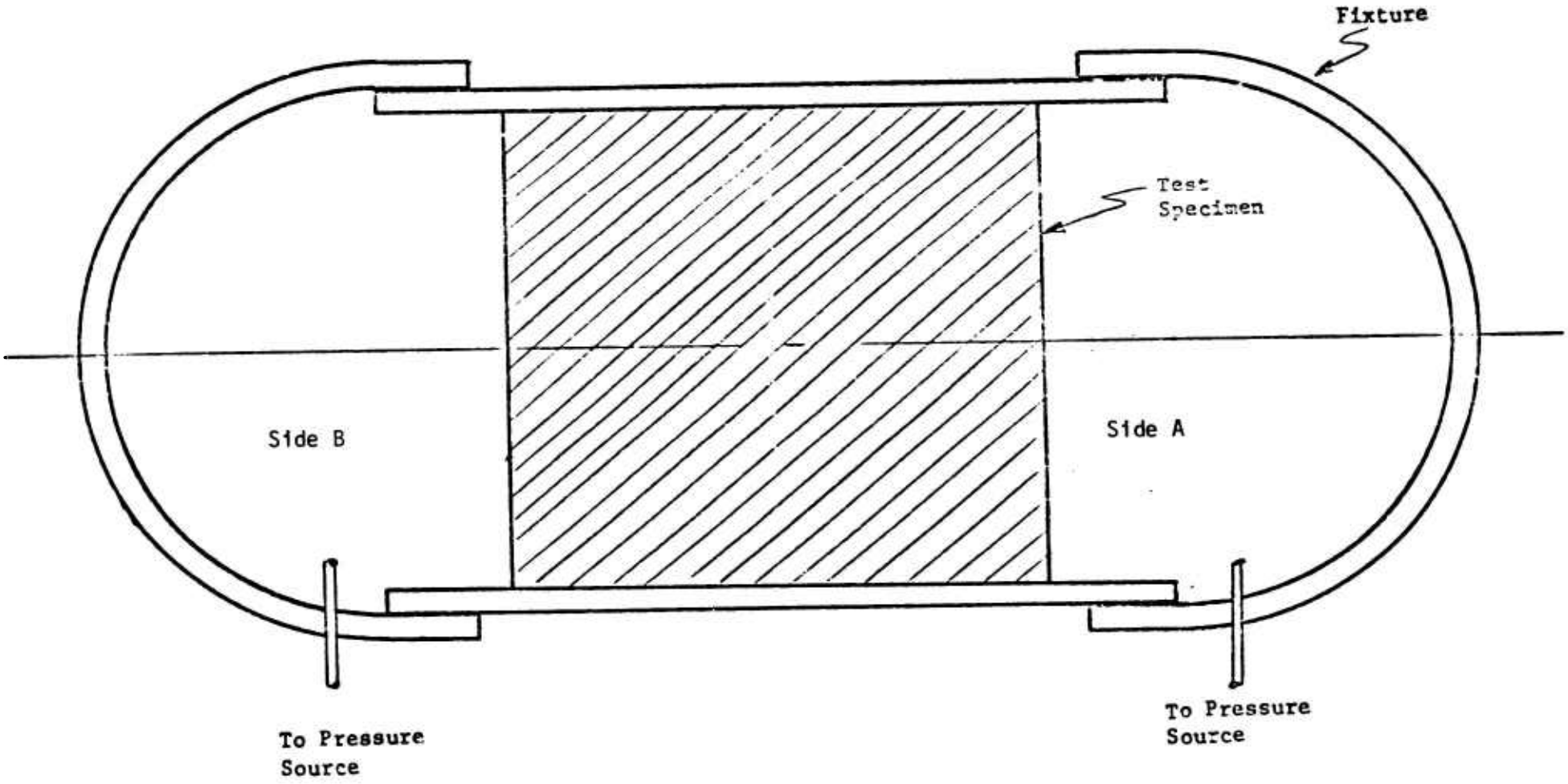

Figure 22. Schematic Arrangement of Pressurization Shear Test Device

TABLE 2

TESTING SEQUENCE FOR DIFFERENTIAL PRESSURE TESTS

(Two Minutes Dwell Time at Each Step)

Step No.	Side A	Side B
1	0	0
2	10	0
3	0	0
4	0	10
5	0	0
6	20	0
7	0	0
8	0	20
9	0	0
10	30	0
11	0	30
12	0	0

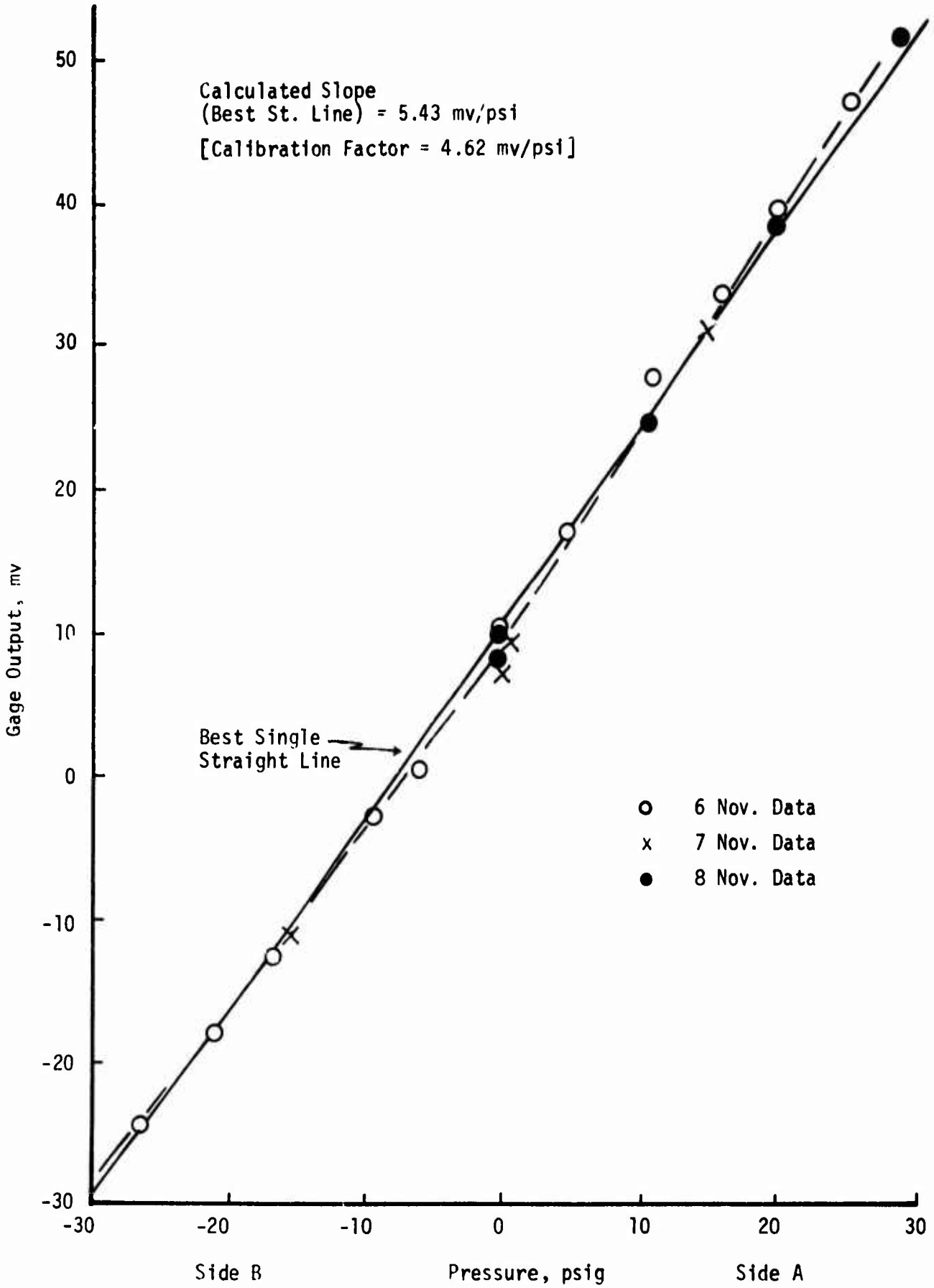

Figure 23. STV No. 2 Gage SH-1 Response to Differential Pressure Across the Propellant Grain

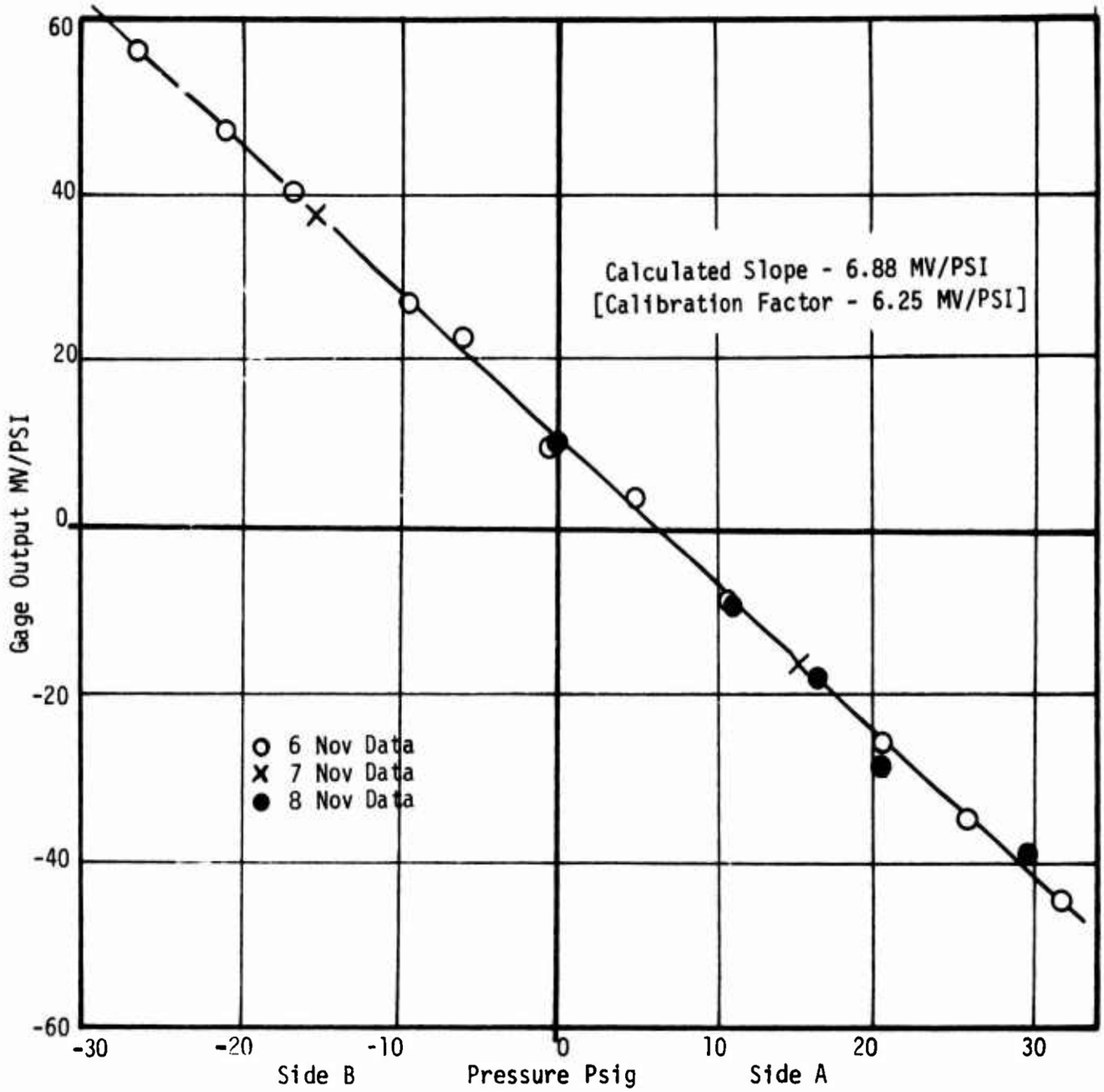

Figure 24. STV No. 2. Gage SH-2 Response to Differential Pressure Across the Propellant Grain

A larger than expected pressure attenuation by the grain would produce such an effect. As stated previously this attenuation is believed to be real, and to arise from the presence of entrapped gases in the grain. These may occur either as casting voids or as microvoids.

H. THERMAL DATA FROM NEW SHEAR GAGES

The calculated thermal shear stresses derived from Gages SH-1 and SH-2 are shown in Figure 25. The data appear consistent with the normal stress data presented in Table 3. The output of gages SH-1 and SH-2 obtained during the thermal conditioning tests performed on STV No. 2 are given in Appendix C along with their gage sensitivities.

I. CONCLUSIONS

On the basis of the STV No. 2 normal stress gage test data it was concluded that it was reasonable to go ahead with the use of pre-potted normal stress gages in the full-scale motors.

The results of the hydrostatic pressure and thermal step tests on STV No. 2 may be summarized as follows:

1. External potting of the normal stress gages appears to be satisfactory for preliminary calibration and compensation purposes. However, a final calibration and compensation must be made in-situ.

2. To minimize material property differences, it is recommended that the potting or pre-potting be done with the live propellant or an inert version of it.

3. Thermal zero load gage readings must be obtained with the potted gage bonded in place in the motor.

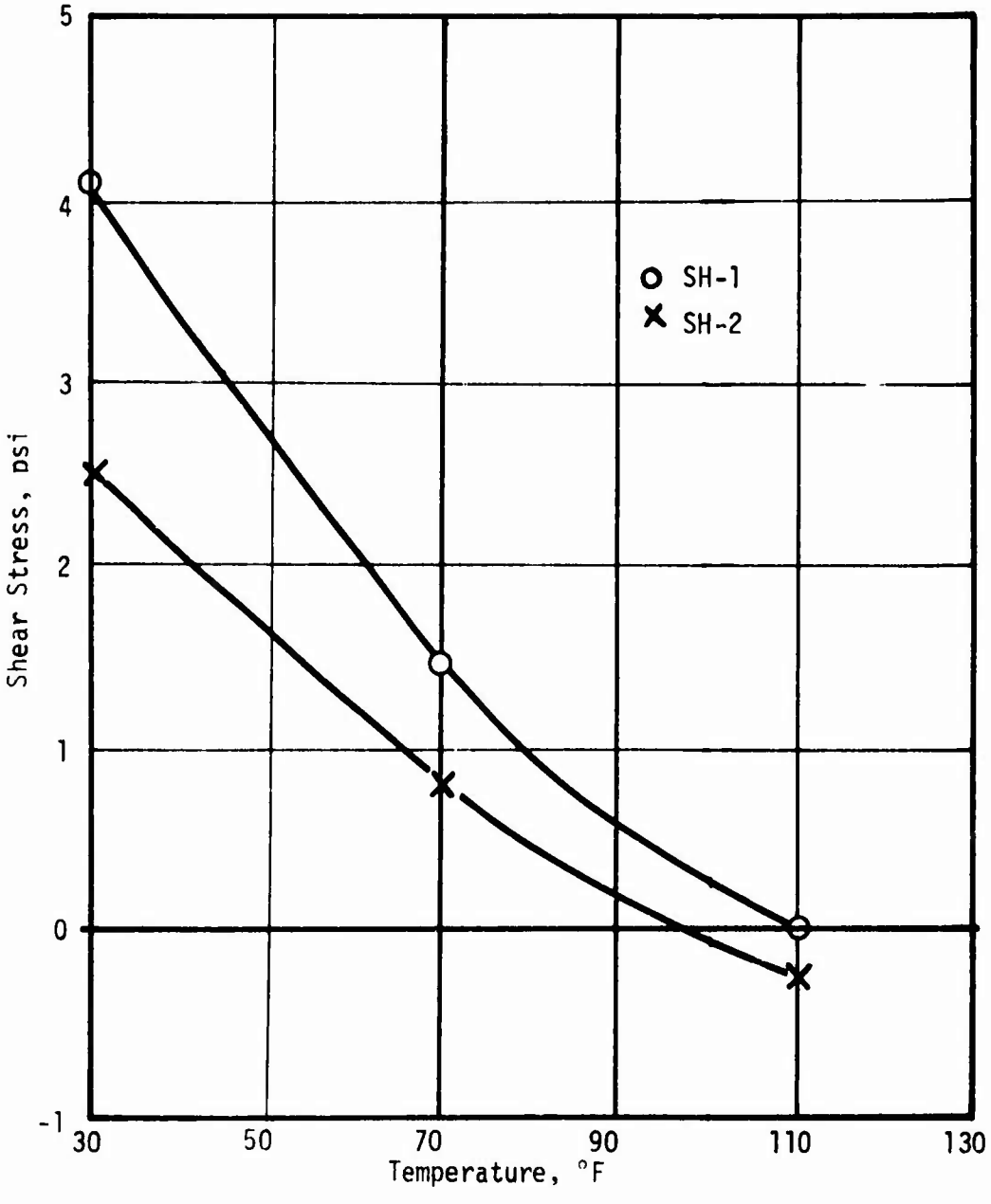

Figure 25. Thermal Shear Stresses in STV No. 2 Measured by Gages SH-1 and SH-2

TABLE 3

SHEAR STRESS MEASUREMENTS IN STV NO. 2

AT THREE TEMPERATURES

Gage No.	Gage MV Output			Gage Stress, psi		
	30°F	70°F	110°F	30°F	70°F	110°F
SH-1	17.48	4.13	-4.15	4.10	1.46	-0.01
SH-2	19.25	6.45	-3.69	2.49	0.80	-0.27

4. Over the limited temperature range of 30° to 110°F the IBT-115 pre-potted gages and the propellant potted gages gave essentially the same data, within expected errors.

5. Both the potting and the pre-potting are sensitive to improper potting, e.g., voids near the gages or unbonds at the gage location.

Calibration differences of up to 15% were observed between STV-2 and laboratory specimen testing of the shear gages. However, this was attributed to pressure attenuation by the grain, which could be accounted for in subsequent testing, and therefore the gages were judged acceptable for use.

SECTION 7

STV NO. 3 - FAILURE DETECTION USING SHEAR AND FAILURE GAGES

A. INTRODUCTION

STV No. 3 was designed and tested to demonstrate that the new high range shear gages could withstand greater stress levels than the low-range gages used in earlier work. The new shear gages are required to measure the large shears that occur on full-scale motor firing, particularly at points where bond failures are likely to occur. Evaluation and calibration of these gages under pressure loads representative of those in the Minuteman III, Stage III motor was essential to achieve the overall goals of the full-scale motor program.

Failure event gages developed at ASPC were also investigated under representative motor conditions and tested to establish their suitability for use in the full-scale motors. These gages, which exhibit a rise in electrical resistance just prior to grain failure, were intended for placement across planes where cracking or failure are considered probable. Again, completion of this effort was a prerequisite for initiation of work on the full-scale motors and attainment of program objectives. Two shear gages and eight failure gages were installed in STV-3, as shown in Figure 26. A solid propellant, end burner type of grain was cast and cured, the gages calibrated, and an investigation of gage performance under realistic pressure and shear loads was carried out until failure of the propellant/liner bond.

B. TEST OBJECTIVES

The major objectives of this task were (a) confirmation of the performance of high range shear cubes under the high shear and normal

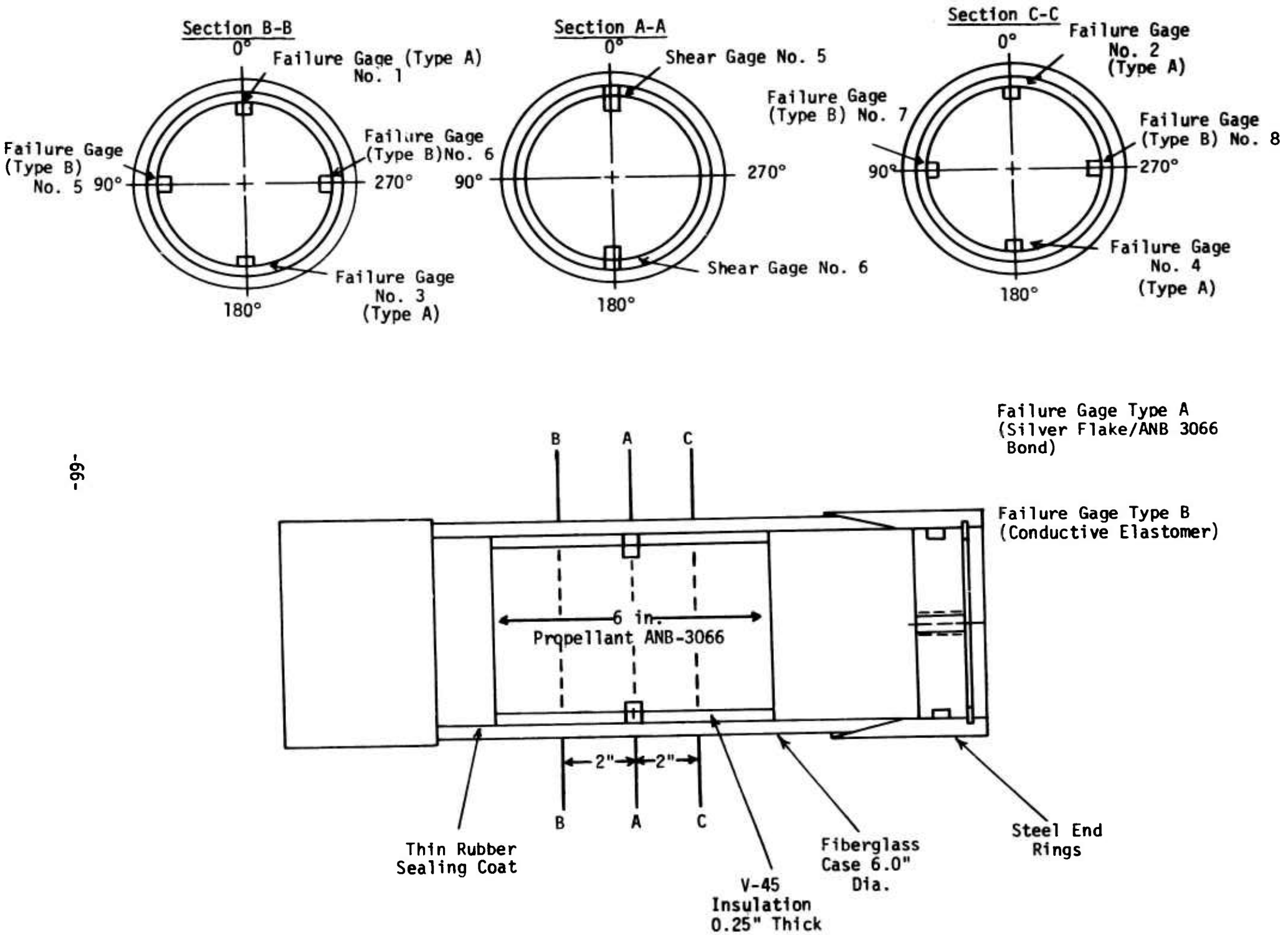
Section B-B
0°
Failure Gage (Type A) No. 1
Failure Gage (Type B) No. 5
90°
270°
Failure Gage (Type B) No. 6
180°
Failure Gage No. 3 (Type A)
Section A-A
0°
Shear Gage No. 5
90°
270°
Shear Gage No. 6
180°
Section C-C
0°
Failure Gage No. 2 (Type A)
Failure Gage (Type B) No. 7
Failure Gage (Type B) No. 8
90°
270°
Failure Gage No. 4 (Type A)
180°
Failure Gage Type A (Silver Flake/ANB 3066 Bond)
Failure Gage Type B (Conductive Elastomer)
B
A
C
6 in.
Propellant ANB-3066
2"
2"
B
A
C
Thin Rubber Sealing Coat
V-45 Insulation 0.25" Thick
Fiberglass Case 6.0" Dia.
Steel End Rings

stresses expected to occur in the full-scale Minuteman III, Stage III motor under rapid pressurization conditions, and (b) a demonstration of the performance of ASPC failure gages under representative full-scale motor conditions.

C. DESCRIPTION OF TEST ITEMS AND APPARATUS

STV-3 was fabricated with an 8-inch long layer of 0.25 inch thick V-45 insulation vulcanized in place of the mid-section of the case. Once again, dummy gage inserts of Teflon, or Teflon-coated metal were located in the insulation layer during lay-up and left in place during vulcanization. After cure the dummy gage inserts were removed and the real gages installed. Small (0.060-inch diameter) holes were drilled through the case wall for the gage lead wires and the gage installed. Two shear gages, SH-5 and SH-6, were located at the axial midpoint and eight failure gages were mounted 1-in. from the ends of the grain and spaced at 90° intervals around the periphery.

Two types of failure gage were evaluated in STV No. 3:

Type A - A failure event gage made with ANB-3066 binder filled with silver flakes, and

Type B - A failure event gage made with a commercially produced conductive rubber.

The gages were bonded in place in the insulation layer using the IBT-115 adhesive selected from STV-1 studies. Following gage installation, the interior of the STV was coated with liner material and a 6-inch long ANB-3066 grain cast and cured. During the test set-up, the eight failure gages installed were checked to verify their continuity and resistance after casting the grain. The four failure gages using ANB-3066 binder filled with silver flakes and two of the four failure gages using commercial conductive elastomers failed during the cast and cure operation.

D. LABORATORY EVALUATION OF FAILURE EVENT GAGES

The principal requirements of the failure event gages were:

1. A tensile modulus of elasticity of approximately 450 psi.

2. Good bonding capability to ANB-3066 propellant.

3. Rapid break characteristics after a propellant crack or unbond propagates into gage locality.

4. Little disturbance to bond line integrity.

Prior to installation in STV No. 3 the two types of failure event gages were tested in the laboratory.

The objective was to determine the gage's elongation, loading and ruggedness characteristics. The ASPC design failure event gage was made of binder filled with conductive silver and is shown in Figure 27. The gage, which is 1/4" x 1", was cut from pre-molded .030-inch thick sheet and wire terminations were bonded to the gage with a similar material. The failure gage strips were then bent into a configuration resembling an inverted "Tee" or trouser leg, such that when placed perpendicular to the direction of separation growth, the leg portion of the inverted tee (embedded in the propellant) would shear off.

The second type of failure event gage tested was the Technit Products model made with a commercial conductive elastomer (Consil G). Its configuration is shown in Figure 28.

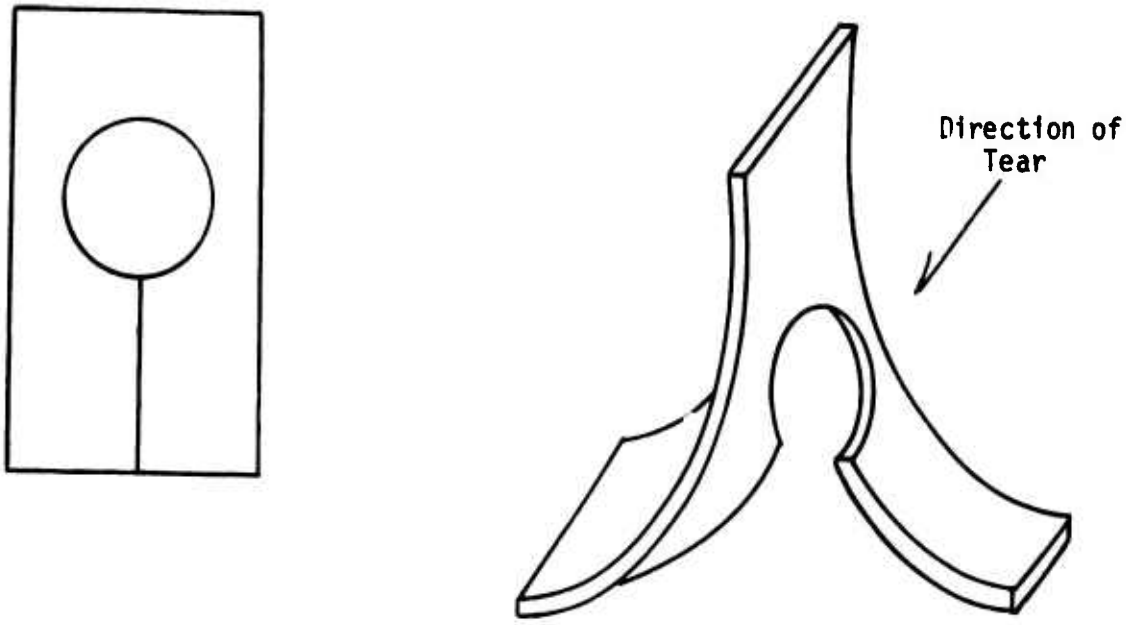

Figure 27. ASPC Failure Gage Schematic

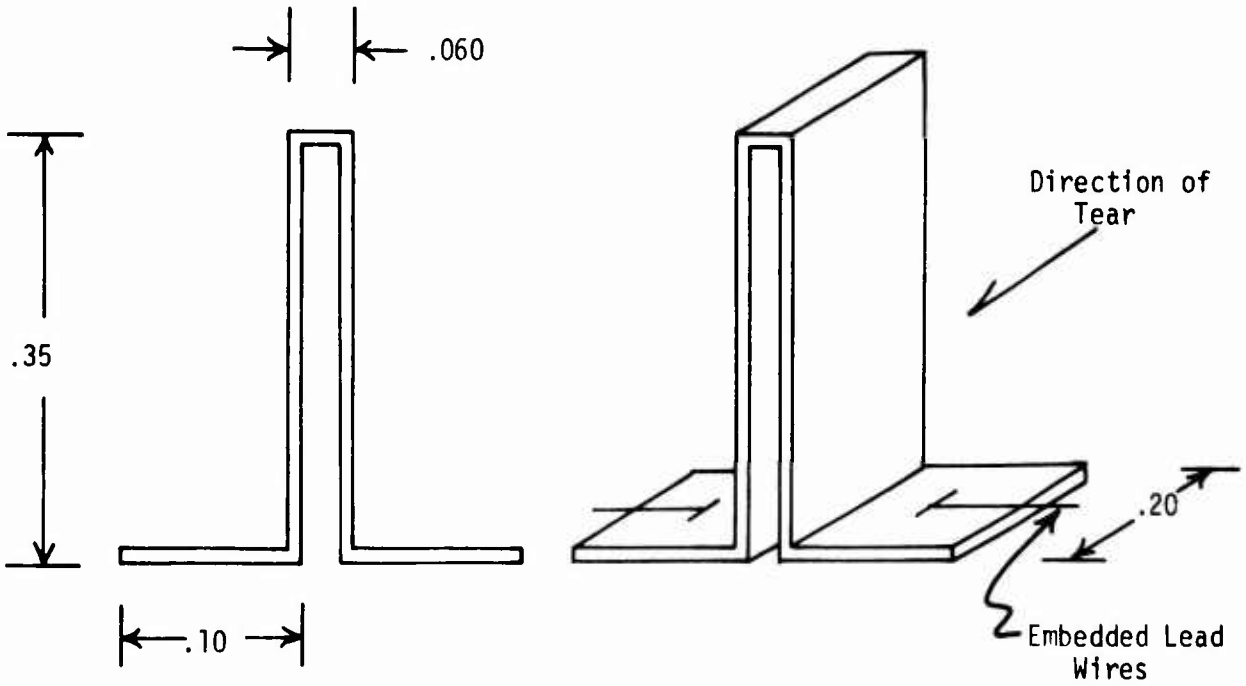

Figure 28. Technit Products Failure Event Gage

Made of a Silicone Elastomer

The failure event gages were bonded to the bottom plate of a compression shear fixture with IBT-115 trowelable insulation, then lined with liner material and ANB-3066 propellant was cast around them. The test set-up used is shown in Figure 29. Test results indicated that the ASPC gages performed more consistently than the Technit gages. However, when the Technit gage was encapsulated properly it performed as well as the ASPC gage. Both types of gages failed in the 15 to 25% elongation range.

E. STV NO. 3 TEST PROCEDURES AND CONDITIONS

Following propellant cure, the motor was disassembled from the casting equipment and chamber closures attached. Shear gages were connected to their bridge completion panel circuits and the failure gages monitored for continuity.

After conditioning to 80°F, the STV was connected by high pressure hoses to a high pressure nitrogen source. Valves in the pressure test set-up permitted establishment of a pressure differential across the grain.

STV No. 3 was then subjected to the differential step pressure test. Initially the pressure on one face of the grain was maintained at zero psi while the pressure applied to the other face was rapidly increased to 10 psi and held constant for 10 minutes. The pressure was then rapidly returned to 0 psi and again held for 10 minutes. A 10 psi pressure step was applied to the second face of the STV and held for 10 minutes before being returned to 0 psi. The shear gages were monitored continuously during this testing.

This alternating pressure step - zero pressure cycle was repeated for pressures of 50 and 100 psi, 150 and 200 psi, at which pressure the propellant-liner-insulation bond failed.

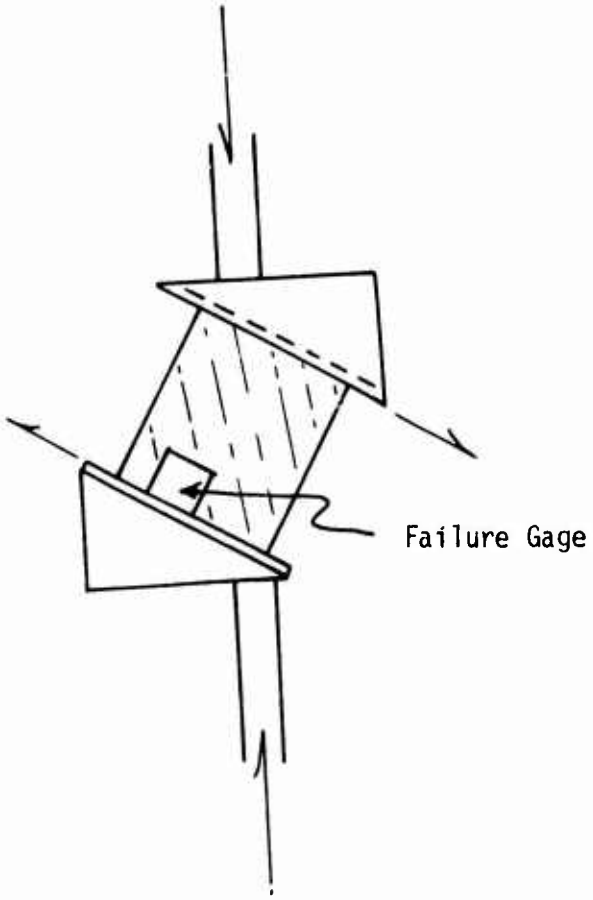

Figure 29. Test Fixture for Simultaneous Testing in Compression and Shear

F. TEST RESULTS

The experimental data obtained from the two shear gages during the test are shown in Figure 30 where it will be noted that the gages performed satisfactorily up to the point of failure at approximately 32 psi. Gage No. SH-5 began to give erratic readings when a pressure of 150 psi was applied to face B. This is equivalent to a shear stress of 20 psi. Shear Gage SH-6 continued to give readings up to a pressure of 200 psi applied to face B. At this point the bond between the case insulation and the grain failed and shear gage SH-6, after indicating a large reading, went back to reading a small value approximating its zero reading.

Only two failure event gages (Type B) were monitored during these tests. No significant changes in the readings of these devices were measured during the tests.

STV No. 3 failed at a shear stress of 32 psi before the planned pressurization to failure test. This "premature" failure was produced by cumulative damage at the interfacial bond which was not taken into account in selecting the loading schedule.

Because the complete series of differential pressure tests was not completed and in view of the poor performance of the failure event gages, it was decided to repeat the failure tests in a new STV. Details of the new STV (STV No. 5) and associated testing are given in Section 9.

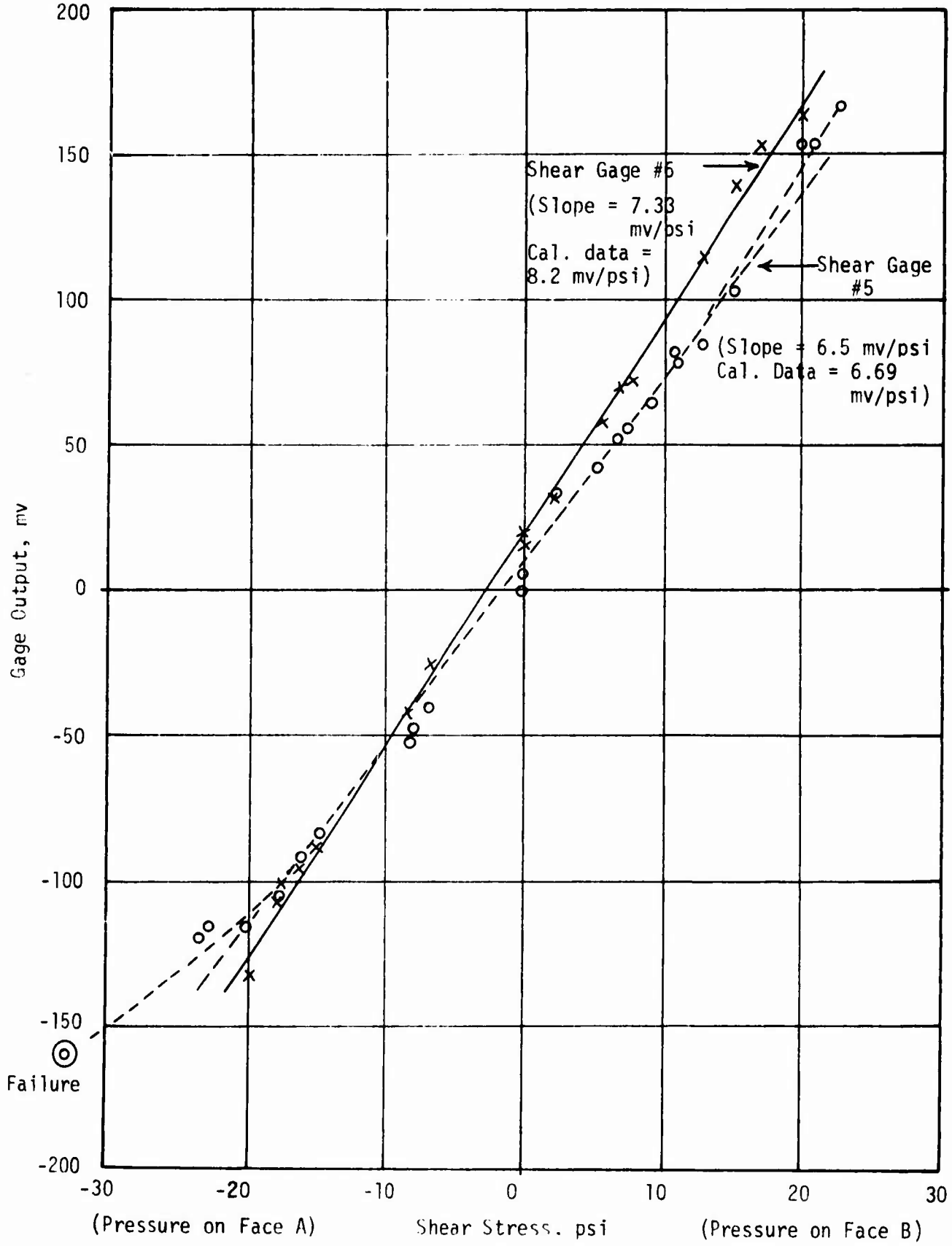

Figure 30. STV No. 3 Failure Test Results from Shear Gages

SECTION 8

STV NO. 4 - INVESTIGATION OF STRESS-FREE TEMPERATURE CHANGES

A. INTRODUCTION

For the purposes of stress analyses composite propellants are always treated as elastic materials. The elasticity assumption, linear or non-linear, with or without time effects, implies that the material has a permanent recollection of some reference configuration to which it will return whenever it is stress-free. For propellants cured at atmospheric pressure with little or no cure shrinkage, this stress-free configuration is essentially the cured shape. However, there is considerable experimental evidence demonstrating that propellant behavior is not elastic, but may in fact be closer to a plastic type behavior. Experimental results from a recently completed program (6) have shown that very large shifts in the stress-free temperature can be achieved in grains stored at temperatures other than that where it is cured. These changes may be attributed to the following:

1. Chemical re-arrangements in the polymeric binder of the propellant due to chain scission and chain formation after cure.

2. Plastic flow in the propellant.

3. Volume change due to loss of volatiles on storage.

ANB-3066 has been shown to exhibit significant permanent set even during storage at ambient temperature. Data obtained to date indicate that the stress-free temperature of the Minuteman System after long-term storage at ambient conditions will approach ambient temperature

within one year. Thus, stress analyses based on the stress-free temperature being identical with the cure temperature would be greatly in error. This downward shifting of the stress-free temperature during ambient temperature storage is beneficial for the motor as long as it remains at ambient conditions. However, if for some reason the motor is subsequently returned to storage at temperatures above the cure temperature where the allowables are low and the grain thought to be under low stresses, then failure could possibly result. For these reasons, it is important to establish the stress-free temperature shifts that can occur on storage.

B. TEST OBJECTIVES

The objectives of the STV No. 4 test series were defined as follows:

1. To provide a direct determination of a change in the stress-free temperature of a grain during long-term storage at 77°F.

2. To evaluate a change in the stress-free temperature resulting from plastic deformation of the propellant.

3. To monitor the effects of loss of volatile materials from the propellant on the stress-free temperature.

C. DESCRIPTION OF STV NO. 4

The configuration of STV No. 4 is shown schematically in Figure 31. Two "150 psi" normal stress gages pre-potted in IBT-115, were embedded in the insulation at the mid-length of the grain, while two of the new ruggedized shear gages were embedded at a distance of 2 inches either side of the grain center. The calibration data for the gages used in STV No. 4 are given in Appendix E. (As discussed later, one of the normal stress gages had been erroneously identified).

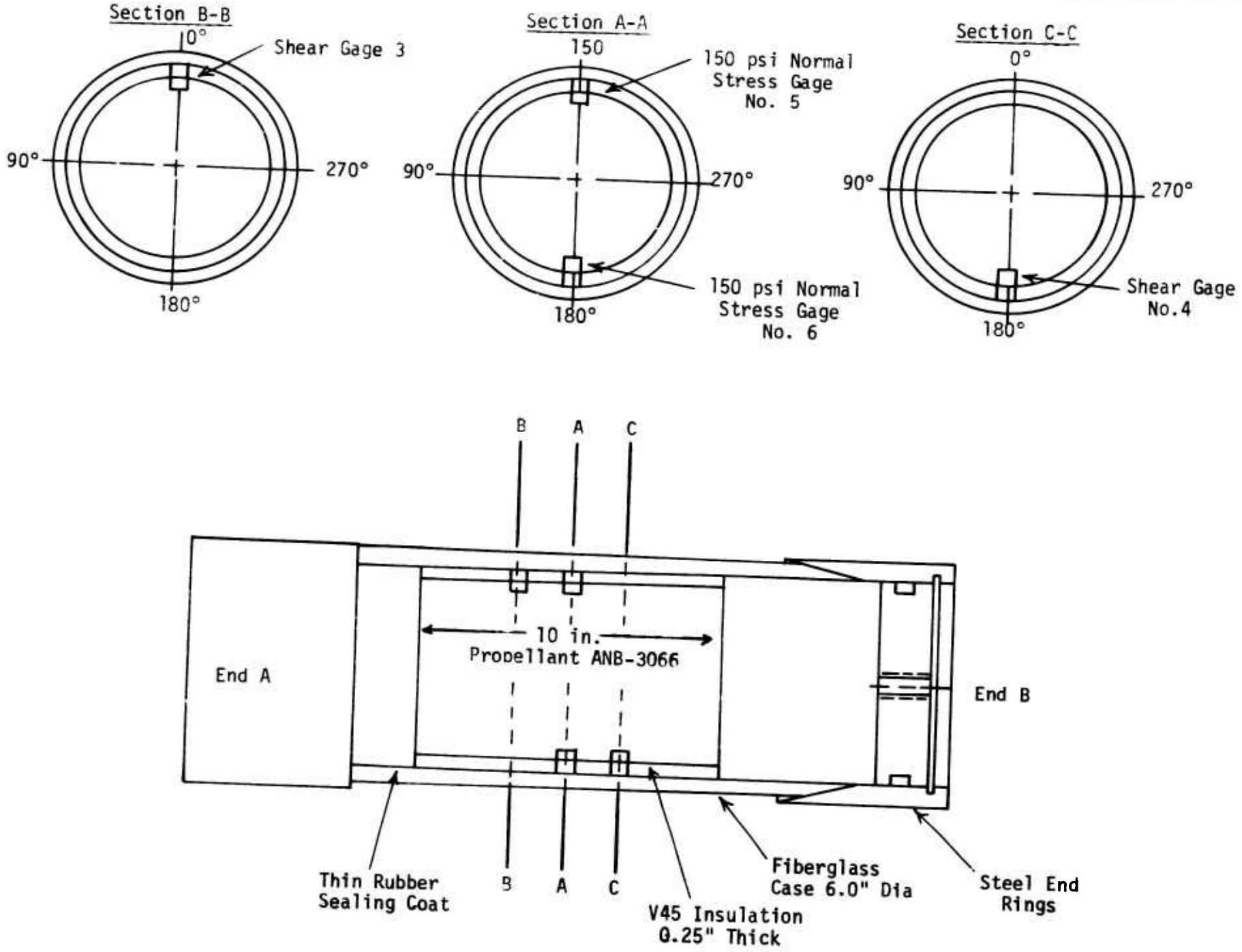

Figure 31. STV-4 Configuration

After installation of the normal and shear gages using IBT-115 as an adhesive the interior of the STV case was coated with liner and the 10" long ANB-3066 propellant grain was cast. The STV was then placed in a 110°F conditioning chamber for propellant cure. The bridge completion networks for the gages were connected to the STV when it was placed in the 110°F conditioning chamber. The gage readings were monitored during cure and during the subsequent cooldown of the STV to 77°F.

At this time a linear potentiometer was mounted to End B of the STV to provide measures of the deflection of the end of the grain.

D. TEST PROCEDURES

Upon completion of cure and cooldown, and installation of the linear potentiometer, testing proceeded as shown below:

1. The motor was placed in the 77°F conditioning box for a period of 12 months. The gages were monitored periodically during this time.

2. At the end of the aging period a differential pressure of 67.5 psi was applied to end B of the grain and maintained for one week. The pressure was then released and the gage reading monitored for a period of three months to observe the recovery of the grain.

3. After the three months recovery from the differential pressure test, flowing nitrogen gas was passed over both ends of the grain for a period of one month and the gage readings were monitored. This test was designed to determine the effects of removing any volatile materials from the propellant grain.

E. EXPERIMENTAL RESULTS

Only the normal stress data from gage N-5 are presented in this report. At an early stage in the testing it was found that N-6 was in fact a 450 psi gage with the same serial number as the 150 psi gage which should have been used in this STV. As a result the precise sensitivity of this gage and its zero stress readings as a function of temperature were not known. The gage calibrations and tabulated data for the tests conducted on STV No. 4 are given in Appendix E.

1. Storage Test

The data measured during the 52 week aging of the STV at 77°F are presented in Figures 32 and 33. The data of Figure 32 show a gradual loss in normal stress from a value of approximately 5 psi, at the beginning of the aging period, to apparent negative (compressive) values after 33 to 46 weeks. The initial stress level of 5 psi is in reasonable agreement with a theoretical value of 4.5 psi (assuming a propellant modulus of 180 psi after 10^3 min. at 77°F).

The fall away of the gage stress is consistent with the concept of a changing stress-free temperature of the grain. This behavior contradicts those predictions which assume the bond stress to be proportional to the relaxation modulus of the propellant as it ages. In this propellant the relaxation modulus increases as the propellant ages. In fact, during the first year this hardening more than offsets the modulus decay during relaxation. Thus, after one year of propellant age-hardening and stress relaxation at 77°F the relaxation modulus should be a little larger than its unaged value at 10^3 min.

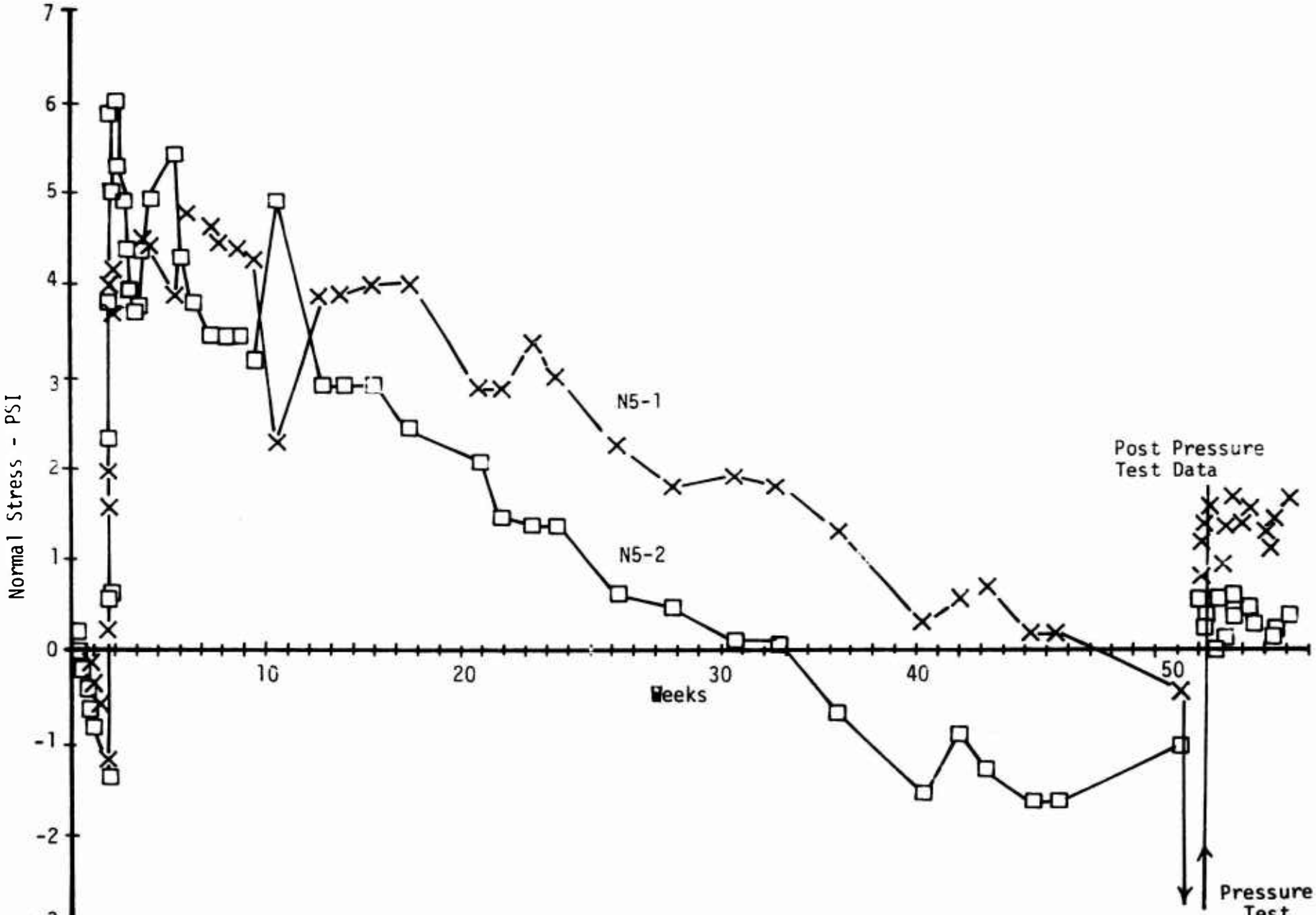

Figure 32. STV No. 4 - Normal Stress Gage Behavior on Storage at 77°F for one year

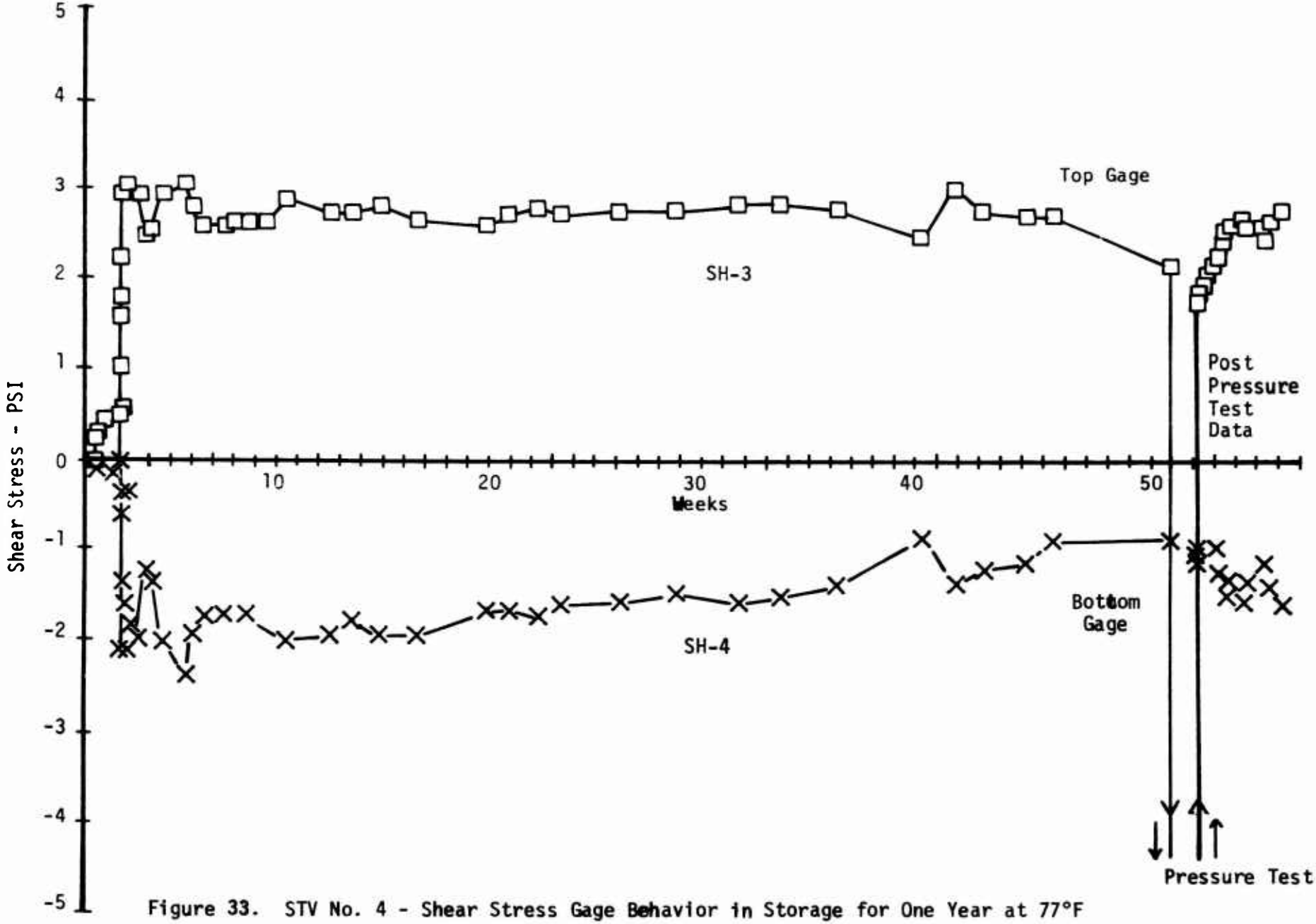

Figure 33. STV No. 4 - Shear Stress Gage Behavior in Storage for One Year at 77°F

Unfortunately, the decay in the gage stresses may also be attributed to changes in the gage calibrations. From later observations, we know that both the "zero" and gage sensitivity parameters changed with time. But, the zero stress output seemed to change the most. In this case, there may have been a gradual change in the zero over the one year storage period. The decay of the gages into "apparent" compressive stress readings certainly is consistent with changes in the gage zeroes.

The overall impression of the test data is that there were changes in both the stress-free temperature and the gage zero stress calibrations. Unfortunately, there is no way to separate the relative contributions of the two effects using the data collected here.

The shear gage data from SH-3 and SH-4 do not tell such a dramatic story (Figure 33). Gage SH-3 which was towards the upper end of the grain during the storage period shows virtually no change in reading with storage time. Gage SH-4 towards the bottom of the grain during storage shows some loss in shear stress from about 2 psi at the beginning of the storage period to approximately 1 psi after 50 weeks of storage. Both shear gages gave initial stress measurements that were higher than the theoretical ones by about 1 psi; 3 psi for gage SH-3 and 2 psi for gage SH-4.

2. Differential Pressure Test

The results of the differential pressure test on STV No. 4 are presented in Figures 34 through 36. Figure 34 shows the data from the normal stress gage N-5 during the application of the 67.5 psi step pressure (on end B) and after the step pressure had been removed. It will be noted that the normal stress at the gage location is approximately

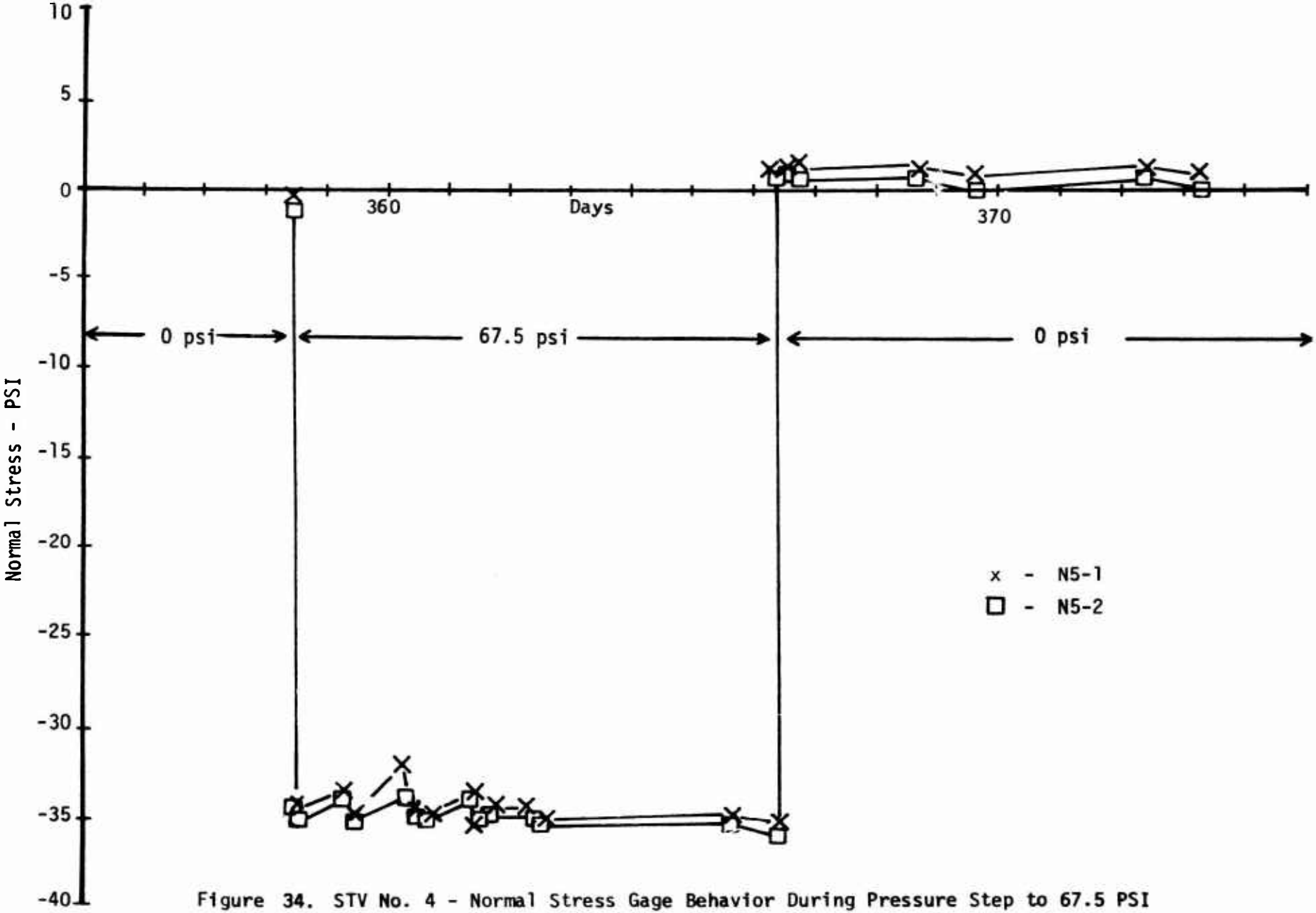

Figure 34. STV No. 4 - Normal Stress Gage Behavior During Pressure Step to 67.5 PSI

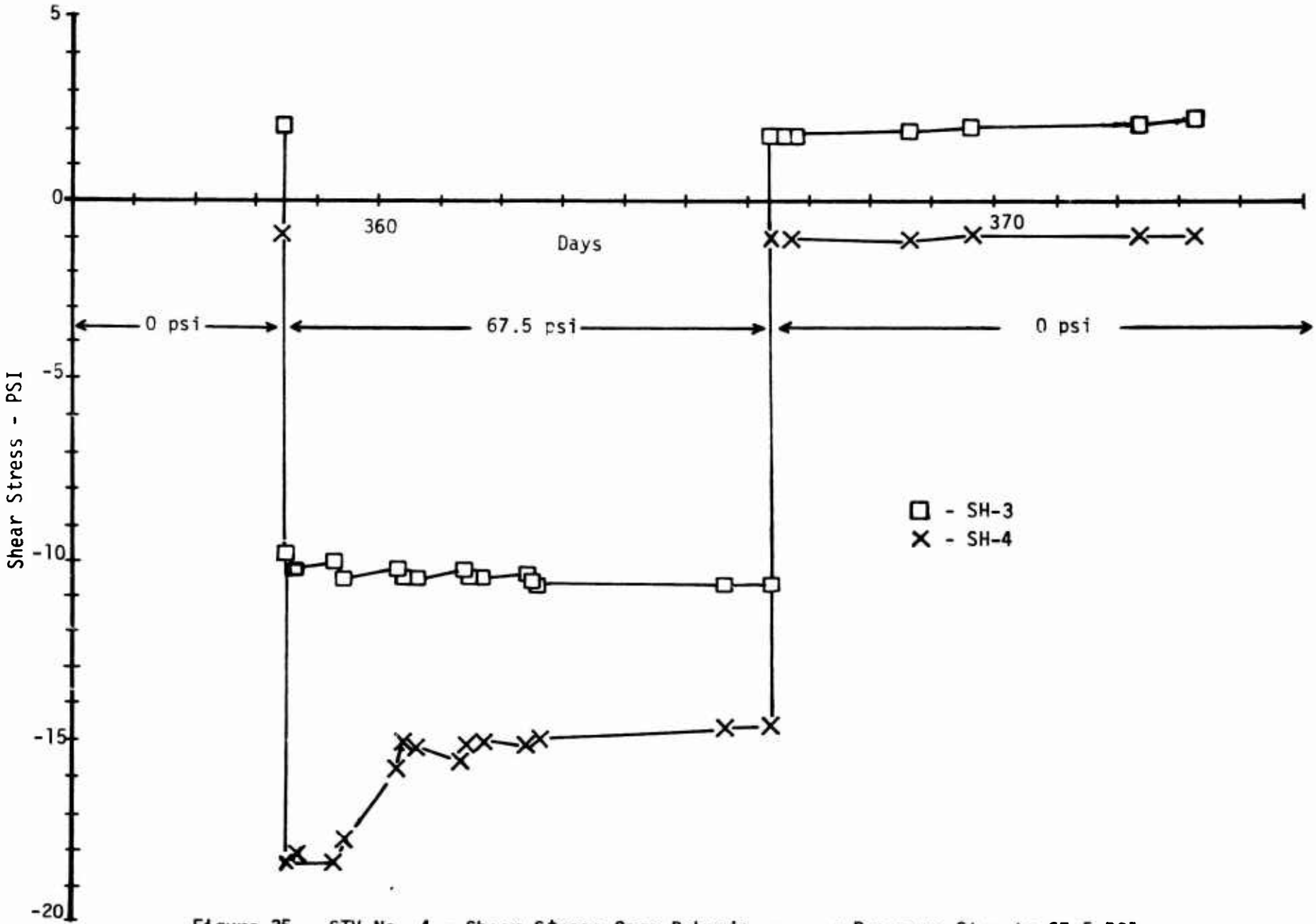

Figure 35. STV No. 4 - Shear Stress Gage Behavio[illegible] Pressure Step to 67.5 PSI

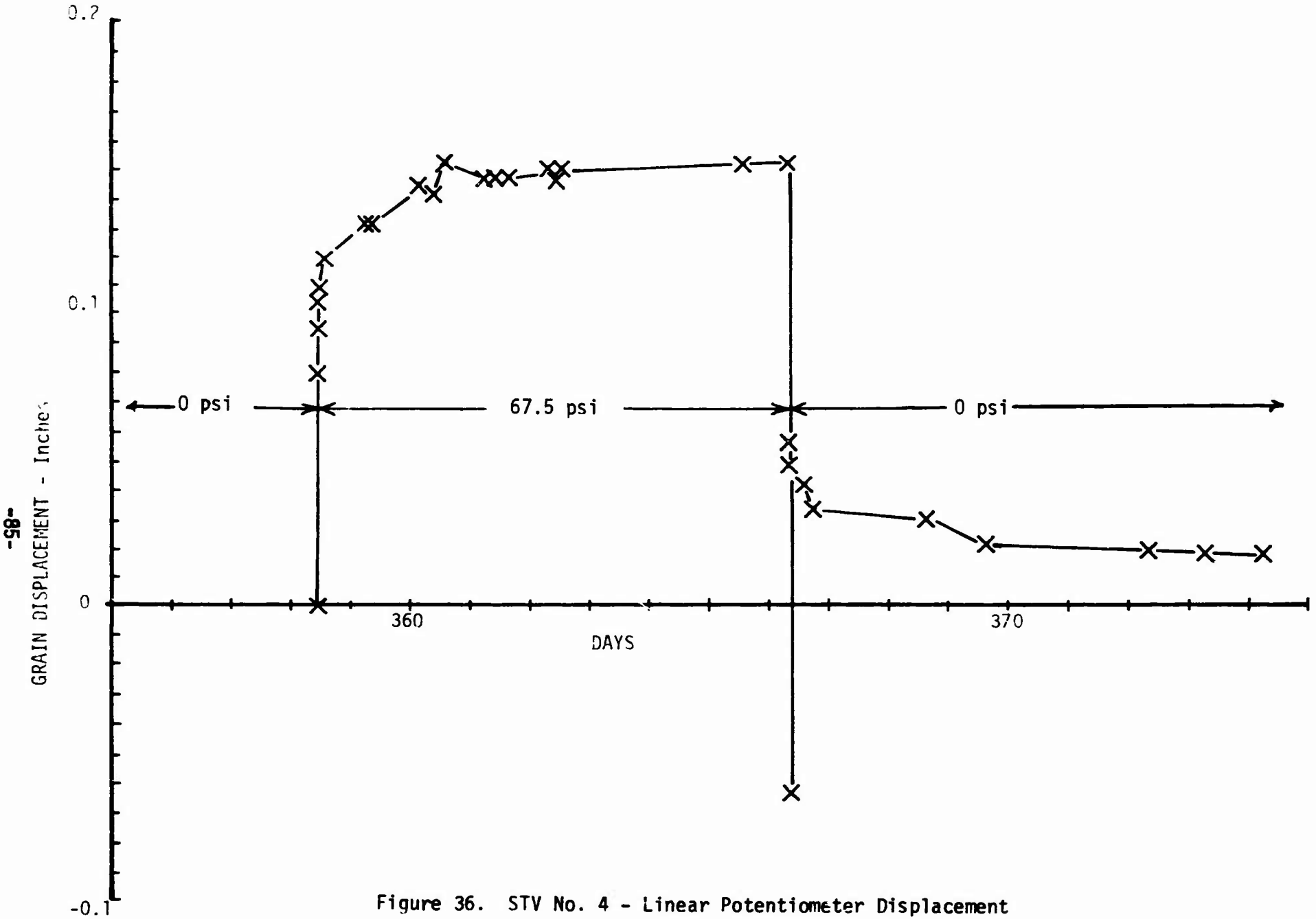

Figure 36. STV No. 4 - Linear Potentiometer Displacement During Pressure Step to 67.5 psi

35 psi (analysis gives a value of 30 psi) and that the gage returns from an initial reading of -1 psi at the beginning of the test to a value of +1 psi after the removal of the step pressure.

Figure 35 shows the response of shear gages SH-3 and SH-4. Gage SH-3, which is farthest removed from the pressurized end (End B) of the grain, shows an instantaneous response from +2 psi shear to -10 psi shear* when the differential pressure is applied, followed by a gradual creep of approximately 1 psi during the time that the pressure is maintained. When the pressure is removed the gage response quickly reverts to its pre-test reading of approximately +2 psi shear.

Gage SH-4, which is closest to the applied pressure, shows a high initial shear stress change from -1 to -18.5 psi upon the application of the step pressure. However, during the subsequent one and a half days time period this shear stress relaxes to a value of -15 psi. This is probably due to relaxation effects in the propellant grain. Upon the removal of the step pressure gage SH-3 rapidly reverts to a reading of approximately -1.5 psi shear** which is very close to its pre-test reading.

The displacement of the end of the grain was obtained during the time of the pressure step application and its removal and they are plotted in Figure 36. When the pressure was applied a rapid displacement of the end of the grain of approximately 0.12" occurred and creep was observed to occur thereafter until at the end of the pressurization period the grain deflection had increased to 0.15". Upon removal of the step pressure an almost immediate grain displacement of 0.1" occurred back towards its original configuration followed by a slow recovery for

---

* This makes a total change of 12 psi shear, which is to be compared to an analytical prediction of 10 psi.

** Thus, a total change of 13.5 psi shear was obtained. This is close to that for SH-3 and significantly larger than the predicted value of 10.5 psi.

the next ten days. At the end of this time the grain was still approximately .02" displaced and showed no further recovery during the next 20 days. It would seem, therefore, that the propellant did undergo a small plastic deformation in this room temperature test.

The observed changes in the grain stresses and in its plastic flow are considered to be small and, possibly, insignificant.

3. Nitrogen Purge Test

The final test to which STV No. 4 was subjected was a continuous wash with dry nitrogen gas (at both ends) for a period of one month at 77°F. The resulting test data are presented in Figure 37. An examination of this figure suggests that little change in gage reading occurs as a result of the dry nitrogen purge. However, shear gage SH-4 did change its reading from -1 psi at the beginning of the test to a value of -2 psi at the end of the test. This appears to be the only change of significance in the gage readings during the test*.

It is concluded, therefore, as a result of the dry nitrogen purge test that any loss of volatiles produced by the purge were not sufficient to cause significant changes in the grain stresses of STV No. 4.

F. CONCLUSIONS

Large changes occurred in the grain stress readings upon storage of the grain for one year at 77°F. The observed stress decay is attributed to changes in both the stress-free temperature of the propellant grain and the zero stress calibrations of the gages.

---

* Large differences in the readings of gage N5-1 are seen on comparing the data of Figure 37 to those at the end of aging (Figure 32) and at the end of the pressure differential test (Figure 34). These differences are attributed to changes in the gage zero stress calibration.

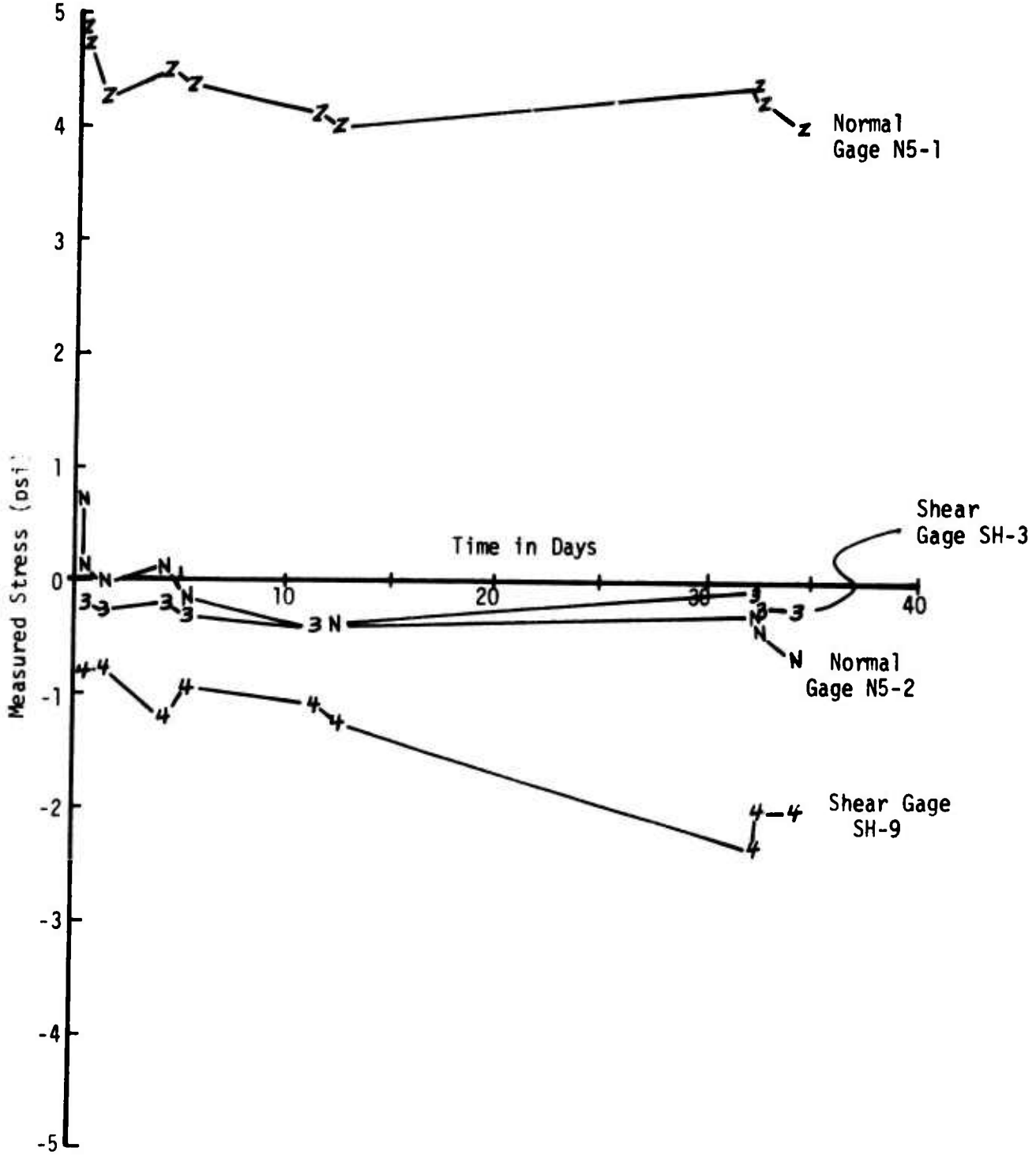

Figure 37. STV No. 4 - Nitrogen Purge Test Data

Small, possibly insignificant, changes in the grain shape and grain shear stresses were obtained from the plastic flow tests.

Any changes caused by the loss of grain volatiles were too small to measure.

SECTION 9

STV NO. 5 - RE-TEST OF STV NO. 3

A. INTRODUCTION

STV No. 5 was built to complete some of the tasks not accomplished with STV's No. 2 and No. 3. Differential pressure tests at moderate stress levels and at three temperatures were not completed on STV No. 2, and on STV No. 3 the differential pressure tests at high superimposed hydrostatic stress levels were not completed because of the unexpected failure of the propellant grain-liner bond. The new STV contained seven shear gages, four failure event gages and one normal stress gage so that an investigation of gage performance under realistic pressure and shear levels up to and including failure of the propellant liner bond could be carried out.

Unfortunately, this grain was defective due to a number of casting voids in the bulk of the grain and adjacent to the gages. The stress gage measurements were strongly affected by these voids, so the test results are not of value for engineering purposes. But, the results should be of considerable value to those experimentalists who may be faced with similar gage problems in the future.

Tests of the failure event gages were not affected by these voids, however, and good results were obtained. They show the concept to be a practical one.

B. TEST OBJECTIVES

The original objectives of STV No. 5 may be listed as follows:

1. To investigate the performance of shear and failure event gages under differential pressure and combined differential and hydrostatic pressures up to the failure of the propellant liner bond.

2. To provide an assessment of the accuracy of the laboratory calibration technique for the shear gages.

3. To investigate the performance of shear gages embedded at different depths within the V-45 insulation layer.

C. DESCRIPTION OF TEST ITEMS

STV No. 5 was fabricated in accordance with Figure 38. Four conductive elastomeric failure gages made by Technical Wire Products using the design shown in Figure 38 were installed in the STV. Two failure event gages were installed 2.5" from each end of the 11 in. long propellant grain (the grain was one inch longer than originally planned). Seven shear gages were installed, three at the mid-point of the grain and two each 2.5" from each end of the propellant grain. One normal stress gage was installed 2.5" from end B of the grain.

Shear gages Nos. 39, 100 and 102 were installed on top of the 0.30" thick V45 insulation. Shear gages Nos. 64 and 103 were installed halfway into the insulation and shear gages Nos. 66 and 103 were almost completely buried in the 0.30" insulation layer.

STV No. 5 had three pairs of shear gages installed: one set at the axial mid-point of the grain, and the others located at 3-inches from the mid-point. When the grain was subjected to differential pressure the mid-plane gages were approximately the same distance from the pressurized end, whichever end was pressurized, whereas the gages situated

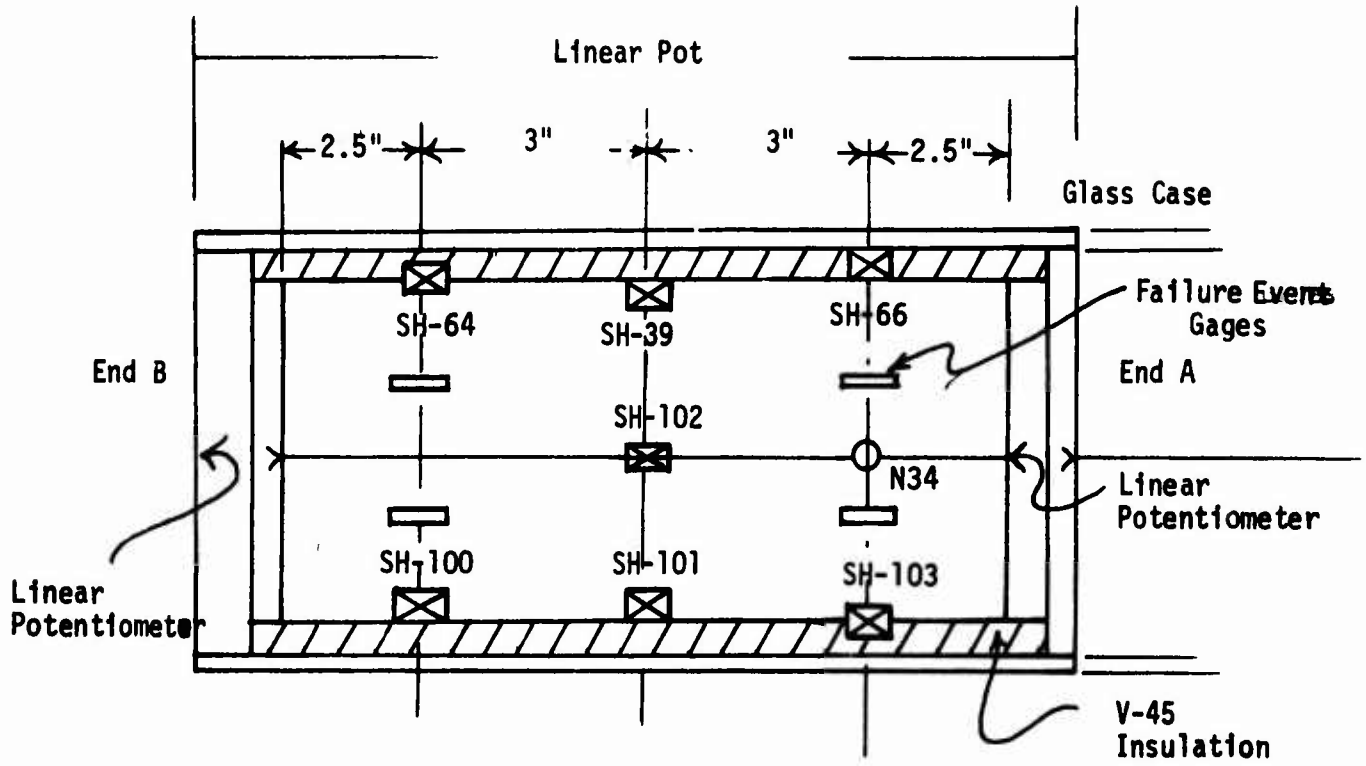

[The failure event gages and the normal stress gage were placed on the back side of the STV as drawn here.]

Figure 38. Sketch of Gage Placements in STV No. 5

off the mid-plane were either close to the pressurized end or remote from it. Because of this gage placement, when a differential pressure is applied to the ends of the grain, the shear gage will experience the same shear stress but different hydrostatic pressures. The performance of the gage in two different combinations of shear and pressure stresses may therefore be investigated.

D. OBSERVED PREPARATION DEFECTS

The gage placements were visually evaluated after the testing was completed and bond system failure had occurred. After this failure the grain was easily pushed out of the chamber and the gage sites conveniently examined. A number of casting voids were found both in the bulk of the propellant grain and the propellant adjacent to the liner, as well as in the liner. Also, thick layers of the low modulus liner material were found near some of the transducers. Those defects that could have had some effect upon transducer performances are illustrated in the sketch of Figure 39.

The suspect gages are:

SH - 39
SH - 66
SH - 101
SH - 103
N - 34

Shear gages SH-66 had been placed in the grain at a slight angle and was not completely embedded, as planned. Evidently, this was corrected using IBT-115 insulation, which produced the tapered shape observed in the grain. For this reason we added the shear transducer SH-66 to the suspect list.

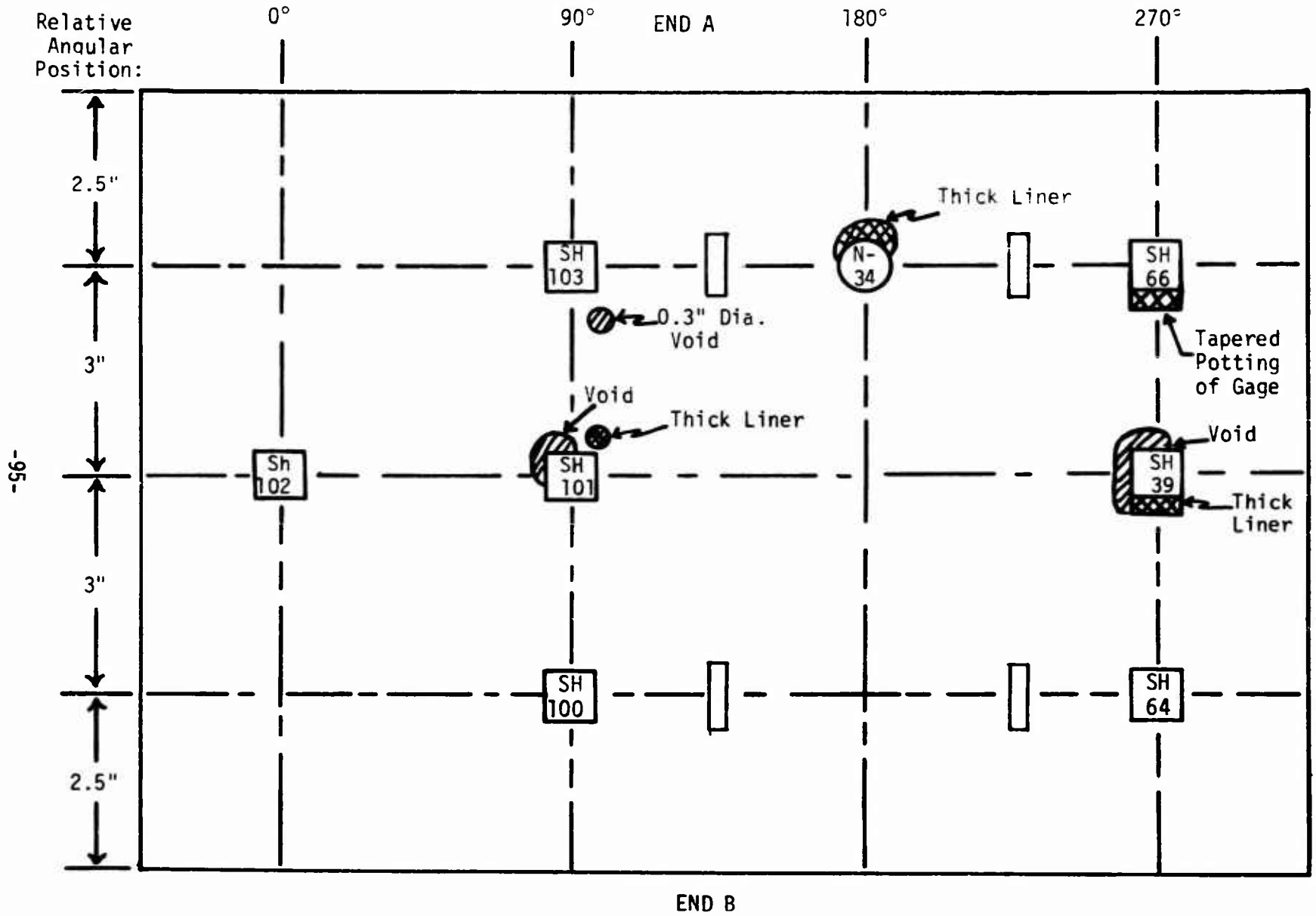

Figure 39. Sketch of Defects Located Around the Stress Gages

Since the bulk of the propellant also contained casting voids (estimated to be 5 volume %), all of the stress gages would have been affected somewhat.

E. TEST PROCEDURES

Two types of pressure tests were conducted on STV No. 5. Hydrostatic pressure tests (i.e., both ends of the grain pressurized simultaneously) were performed and differential pressure tests (i.e., tests in which one end of the grain was subject to a different pressure than the other end) were also performed. The test procedure adopted was to condition the STV to a certain temperature (the first test temperature was 80°F), then perform the hydrostatic step pressure tests. Ten psi steps were used to a maximum pressure of 50 psi and back down to zero psi.

At the conclusion of the hydrostatic step pressure test the differential pressure tests were performed. The test set-up used was identical to that employed with STV No. 2. A 5 psi step pressure was applied initially to one end of the grain and the response of the gages was monitored for two minutes. The pressure was then released and the gage response monitored for an additional two minutes. The 5 psi pressure step was then applied to the opposite end of the grain and the response of the gages was monitored for another two minutes. The pressure was then returned to zero while the gage response was monitored for two more minutes. This test sequence was repeated using 10, 15, and 20 psi pressure steps applied to alternate ends of the grain.

For the second differential pressure test sequence a hydrostatic pressure of 10 psi was applied initially to the STV and the gage readings were allowed to equilibrate. Five psi differential pressure steps were then applied alternately to the ends of the grain while maintaining the

10 psi pressure on the other end. This test sequence was identical with the first differential pressure test except that a superposed 10 psi hydrostatic pressure was maintained in addition to the differential pressures. For the remainder of this test series, identical test sequences were followed using hydrostatic superimposed pressure levels of 20, 50 and 200 psi while increasing at 10 psi increments in turn for each end. Table 4 shows the details of this series of differential pressure tests.

Upon completion of the hydrostatic test series and the differential pressure test series, the temperature was changed to 114°F and the whole test sequence was repeated. The entire test sequence was also repeated at 44°F.

The final test sequence performed on STV No. 5 was the failure test. In this case the STV was conditioned to 77°F, a hydrostatic pressure of 600 psi was applied to the STV and the gage readings were allowed to equilibrate. Differential pressures were then applied to alternate ends of the grain; the differential pressure being increased 10 psi at each step (the first step being 10 psi) until failure occurred at a differential pressure of approximately 160 psi. The grain failed at the propellant-liner-insulation bond and the whole grain was pushed out of the case.

F. EXPERIMENTAL TEST RESULTS

The experimental test data obtained with STV No. 5 are discussed next. Only selected, typical test data are presented in the text, the majority of the STV No. 5 data being given in Appendix F. The various parts of the experimental test program are discussed below.

TABLE 4

DIFFERENTIAL PRESSURE TESTS FOR STV NO. 5

Step	Test (1)		Test (2)		Test (3)		Test (4)		Test (5)	
	End A	End B	End A	End B	End A	End B	End A	End B	End A	End B
	0	0	0	0	0	0	0	0	0	0
1	5	0	10	10	20	20	50	50	200	200
2	0	0	15	10	30	20	60	50	210	200
3	0	5	10	10	20	20	50	50	200	200
4	0	0	10	15	20	30	50	60	200	210
5	10	0	10	10	20	20	50	50	200	200
6	0	0	20	10	40	20	70	50	220	200
7	0	10	10	10	20	20	50	50	200	200
8	0	0	10	20	20	40	50	70	200	220
9	15	0	10	10	20	20	50	50	200	200
10	0	0	25	10	30	20	60	50	210	200
11	0	15	10	10	20	20	50	50	200	200
12	0	0	10	25	20	30	50	60	200	210
13	20	0	10	10	20	20	50	50	200	200
14	0	0	30	10	0	0	0	0	0	0
15	0	20	10	10						
16	0	0	10	30						
17	15	0	10	10						
18	0	0	25	10						
19	0	15	10	10						
20	0	0	10	25						
21	10	0	10	10						
22	0	0	20	10						
23	0	10	10	10						
24	0	0	10	20						
25	5	0	10	10						
26	0	0	15	10						
27	0	5	10	10						
28	0	0	10	15						
29			10	10						

1. Hydrostatic Pressure Test Results

Figure 40 shows the output from normal stress gage N-34 resulting from the application of hydrostatic pressure steps to STV No. 5. The data measured at three temperatures, 114, 80, and 44°F are shown in this figure. The gage response versus hydrostatic pressure is a linear relationship whose slope is always less than that measured during the calibration of the gage without the grain in place (Table 5). This reduction in gage response is too great to be accounted for by any reasonable degree of hydrostatic stress attenuation in a void-free grain. But the grain had numerous internal casting voids (estimated to total more than 5 volume %), and there was a casting void adjacent to the gage (Figure 39). The marked sensitivity to temperature of the gage responses is attributed to the voids which permit a marked attenuation of the hydrostatic pressure.

Figure 41 illustrates the results of moderate pressure level testing, up to 50 psi, upon the output of the shear gages at 114°F. With two exceptions, the gages show only a small change in output under hydrostatic pressure loads. Theoretically a shear gage should exhibit no response to a hydrostatic pressure load, but because of inherent small defects in the gages, liner, and the surrounding propellant, some gage effects are often obtained.

In the case of shear gages SH-39 and SH-100, the output under hydrostatic pressure loads is extremely high. It must be expected, therefore, that these gages would show considerably different results depending on which end of the STV is pressurized during a differential pressure test, even if the shear stress were constant over the grain length.

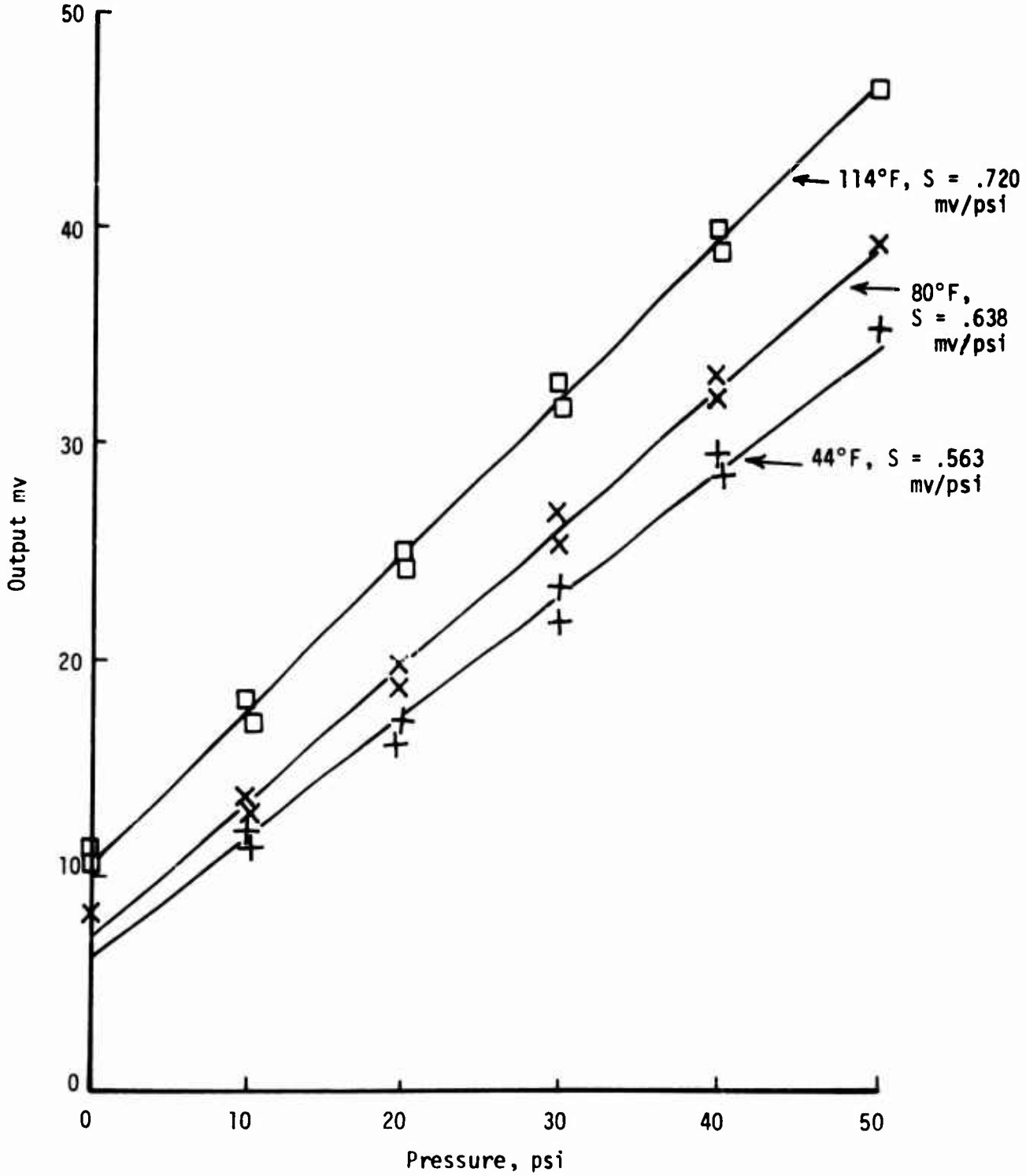

Figure 40. Hydrostatic Pressure Test Data from Normal Gage N-34 In STV No. 5

TABLE 5

COMPARISON OF NORMAL STRESS GAGE (N-34) SENSITIVITY
CALIBRATION WITH MEASURED GAGE RESPONSE
IN THE GRAIN OF STV NO. 5

	Gage Response, MV/psi		
	44°F	80°F	114°F
Calibration	0.813	0.810*	0.816*
Response in Grain	0.563	0.638	0.720

*by Extrapolation and Interpolation from data obtained at 44°, 72°, and 106°F.

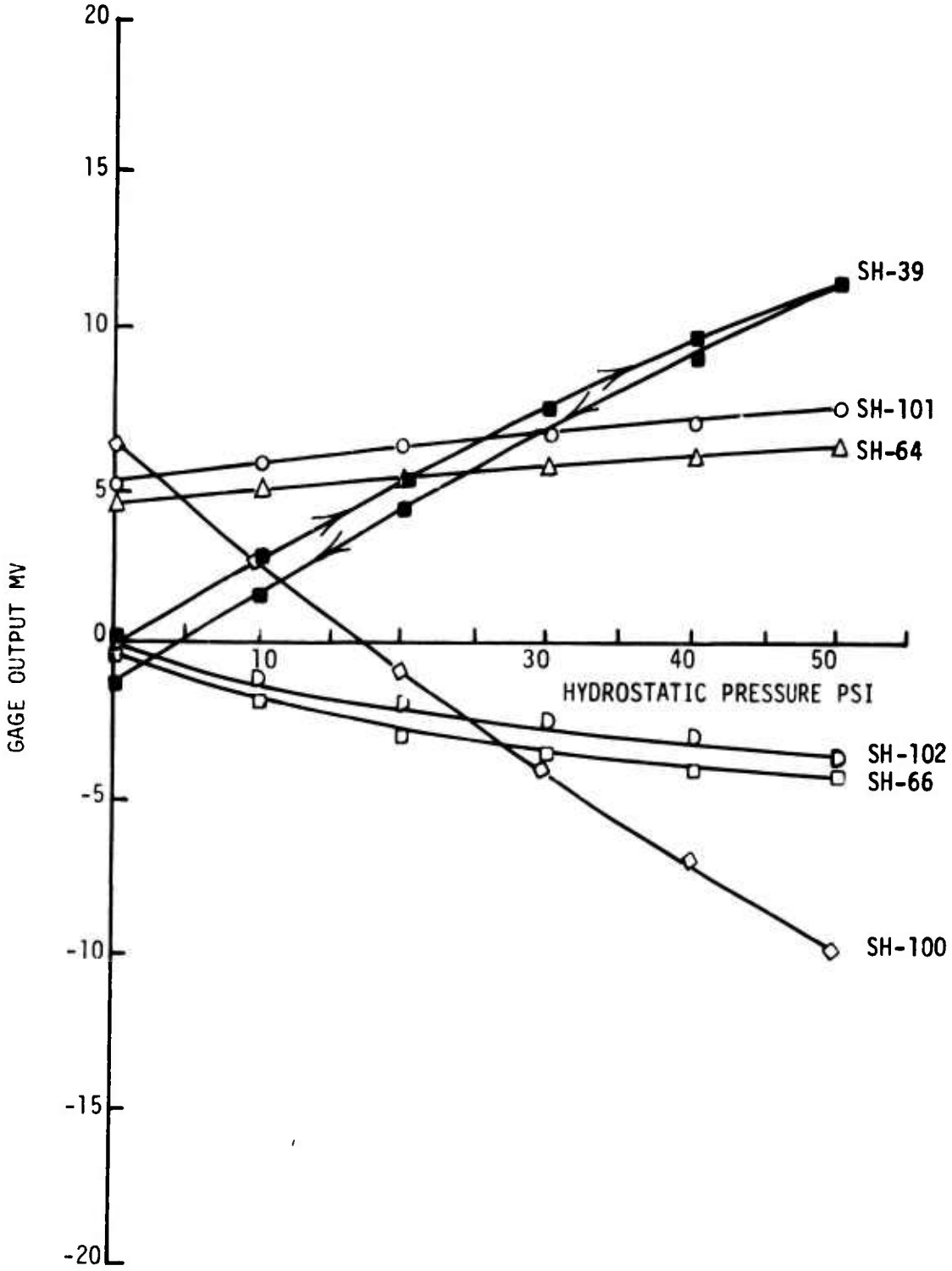

Figure 41. Effects of Low Hydrostatic Pressure on Shear Gages in STV No. 5 at 114°F

Figures 42 through 44 show more details of the effects of hydrostatic pressure on the shear gage responses. In these figures the responses of the shear gages are shown plotted against the hydrostatic pressure up to 200 psi. The results of all the hydrostatic pressure tests at the three temperatures are shown. It should be evident that the responses of the shear gages to hydrostatic pressure are markedly non-linear. This non-linearity is attributed primarily to the voids at the gages or in the grain near to them.

2. Differential Step Pressure Test Results

The output from the shear gages in STV No. 5 are plotted as a function of differential pressure in Figures 45 through 48. They are arranged in groups, the first group comprising the 114°F test data. The 80°F group and the 44°F group of differential pressure test data are given in Appendix F. The slopes of these response data are summarized in Table 6.

Each group shows one figure in which the data from the shear gages at the middle of the grain (i.e., gages SH-39, SH-101, and SH-102) are plotted against differential pressure. In the case of the 114°F tests Figure 45 shows this plot. The next figure, Figure 46, shows the same data for the gages located towards the end of the STV grain; i.e., gages SH-64, SH-66 and gage SH-100. Both these initial figures show the test data for the case of zero hydrostatic pressure applied to the STV. Thus, there is zero pressure applied to one end of the grain at all times.

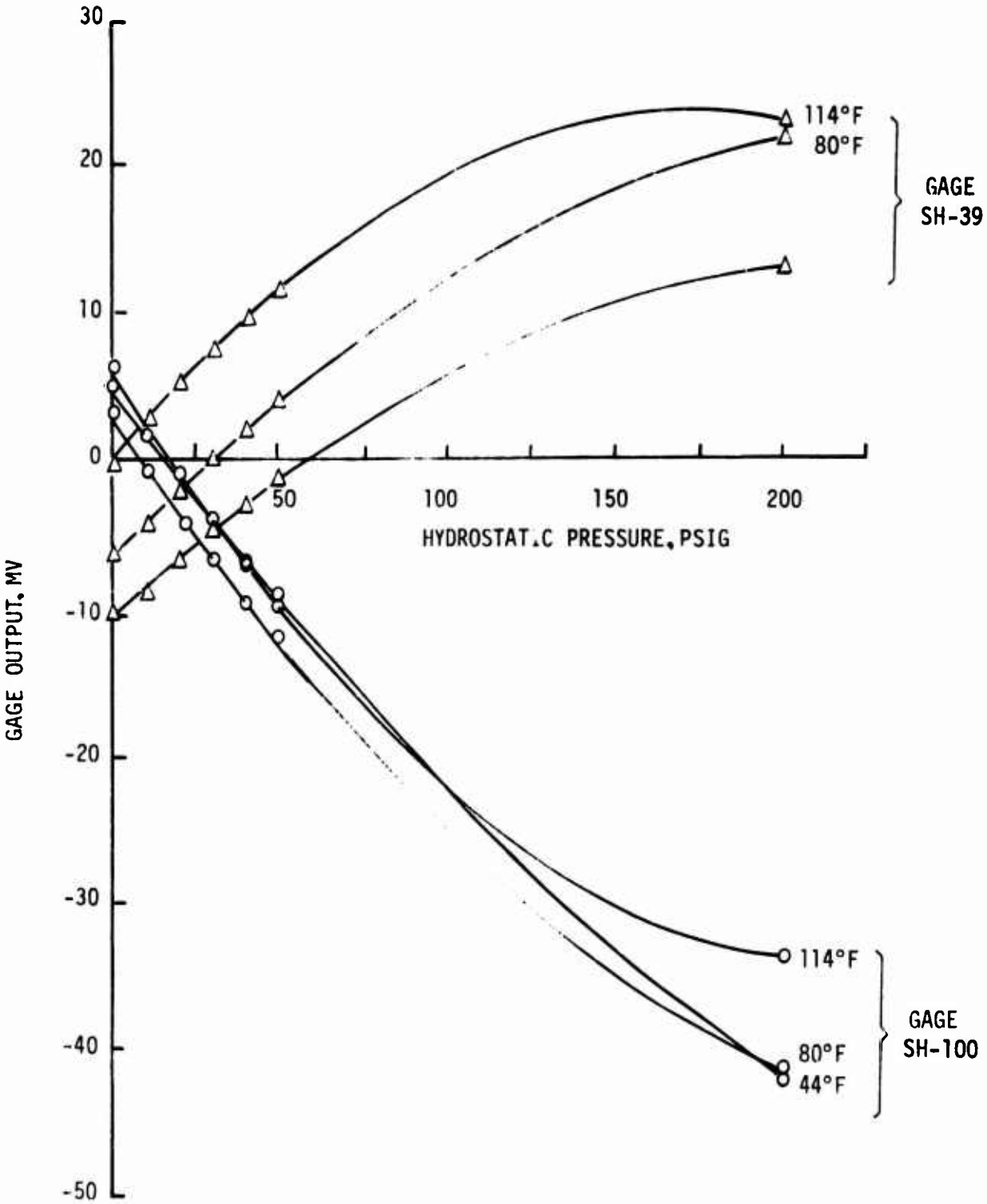

Figure 42. Shear Gages SH-39 and SH-100 Output versus Hydrostatic Pressure

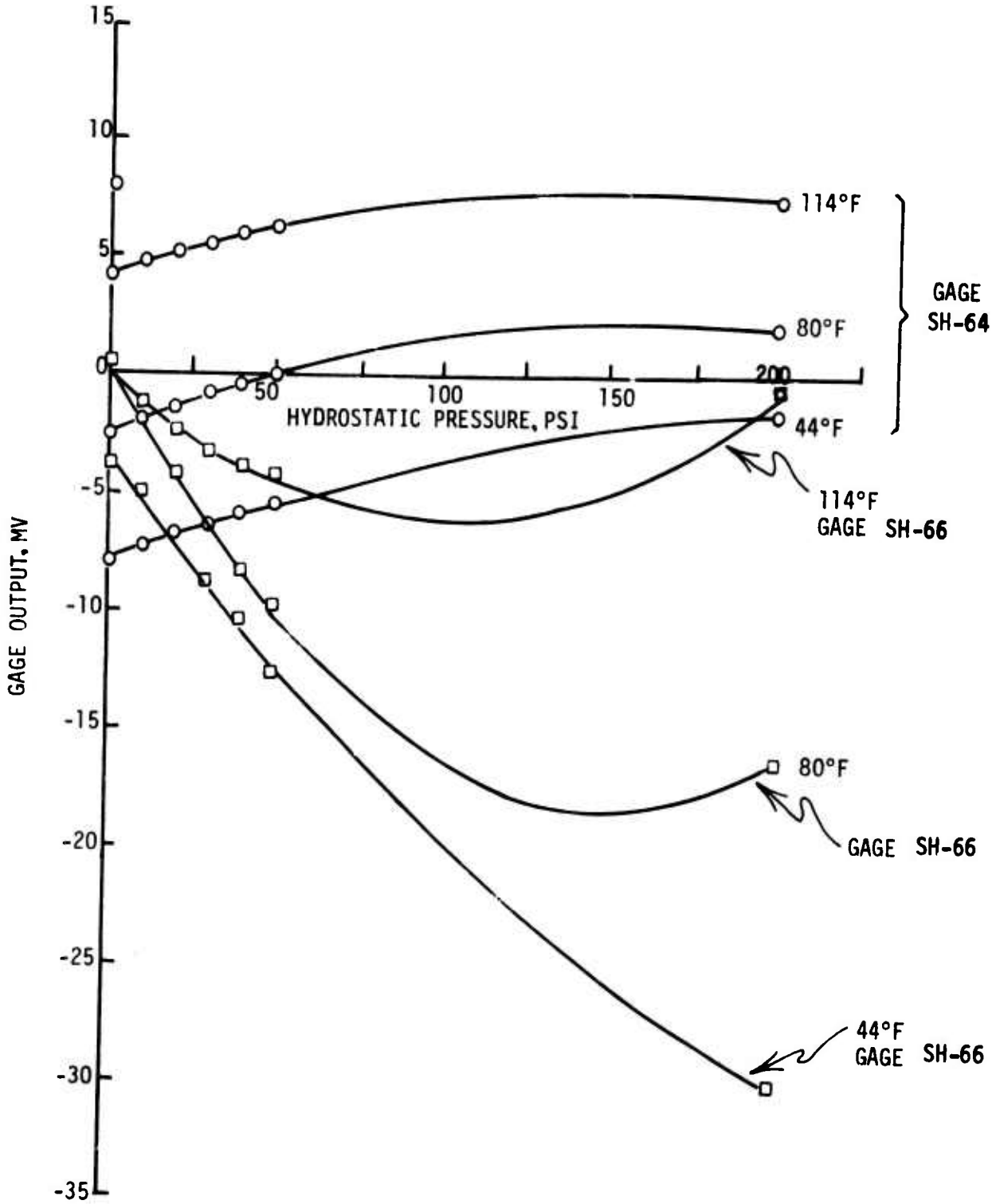

Figure 43. Shear Gages SH-64 and SH-66 Output Versus Hydrotstatic Pressure

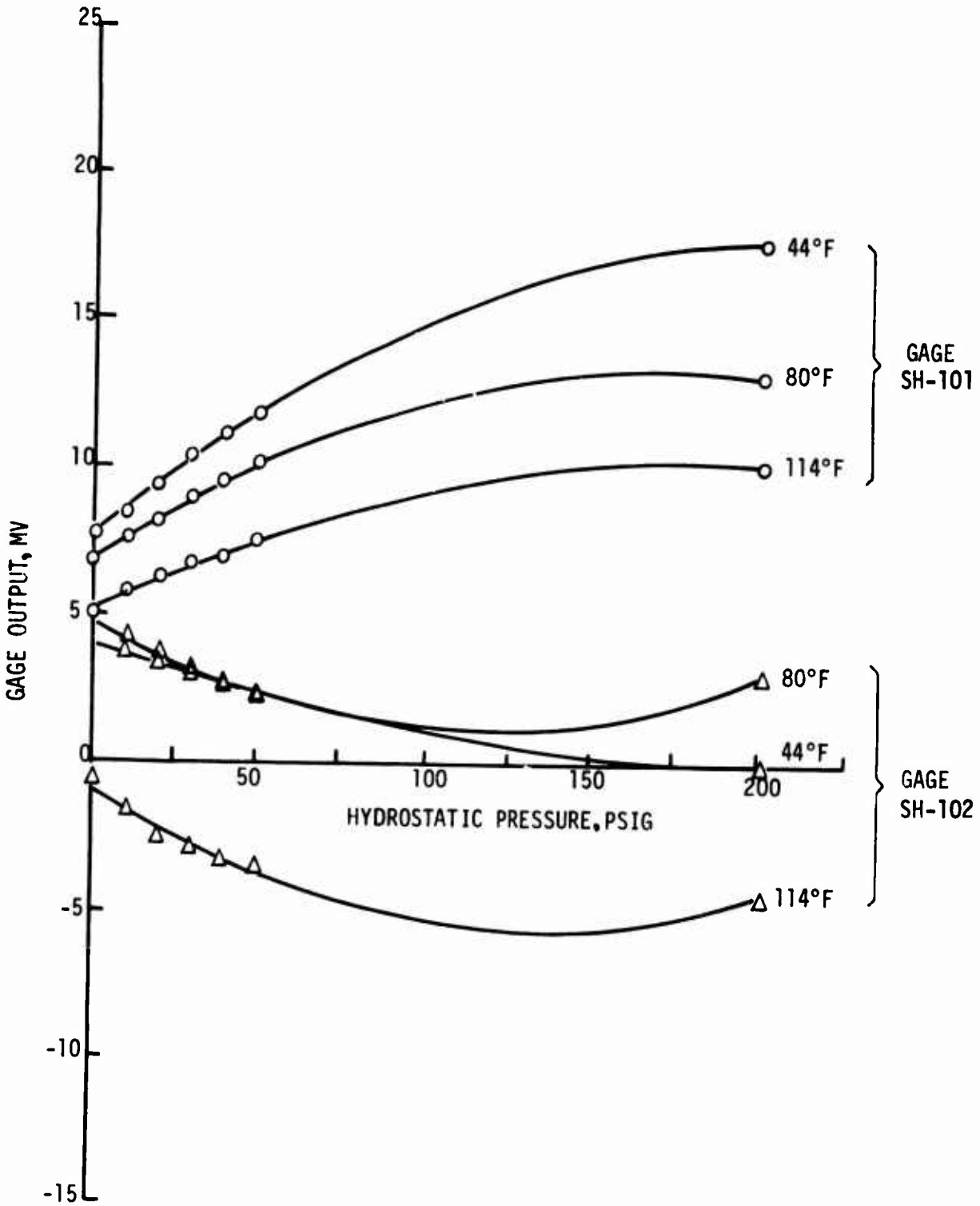

Figure 44. Shear Gages SH-101 and SH-102 Output Versus Hydrostatic Pressure

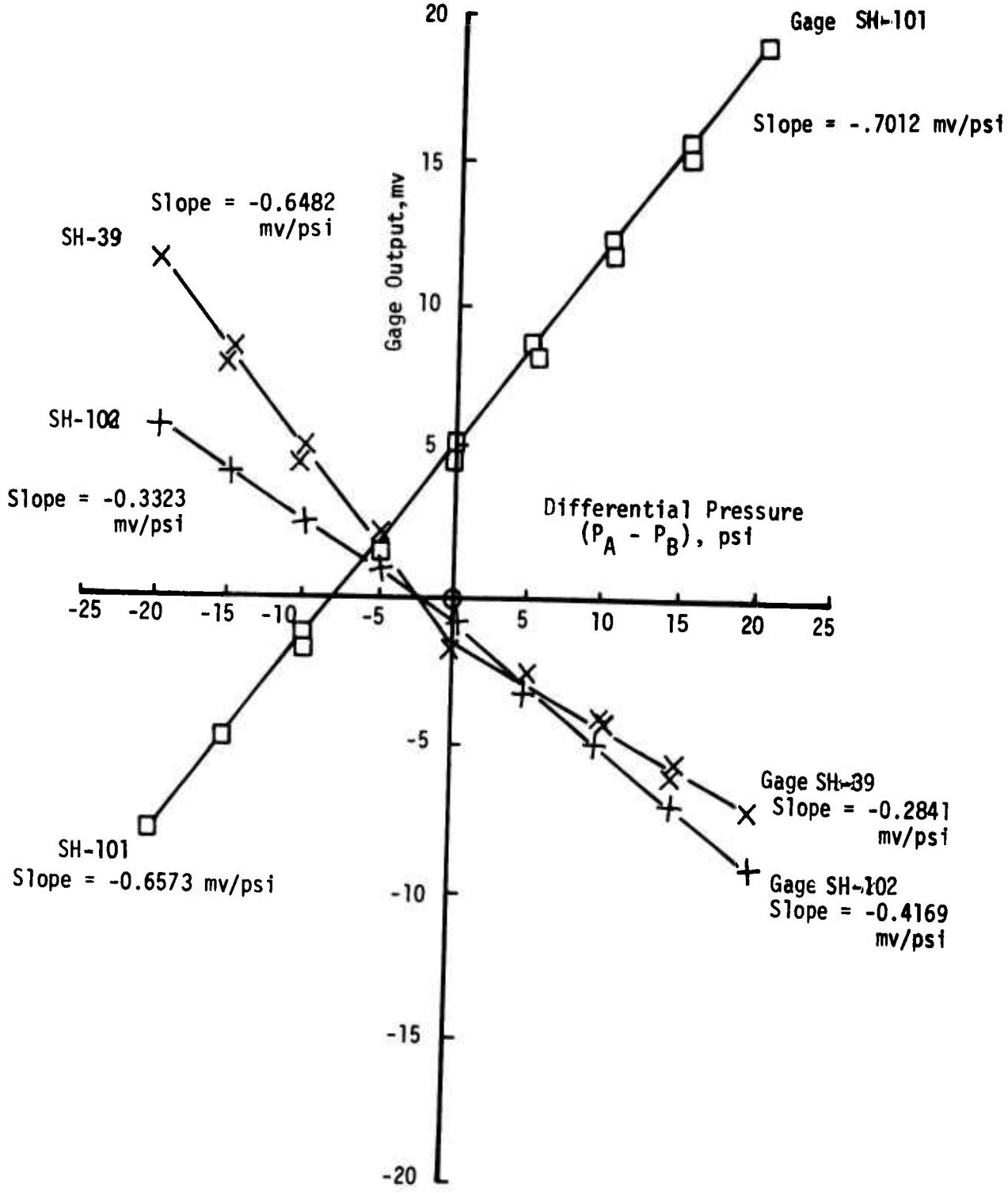

Figure 45. Gages SH-39, SH-101 and SH-102 at Midpoint of STV No. 5 Output vs Differential Pressure;

$T = 114°F$, $P_H = 0$

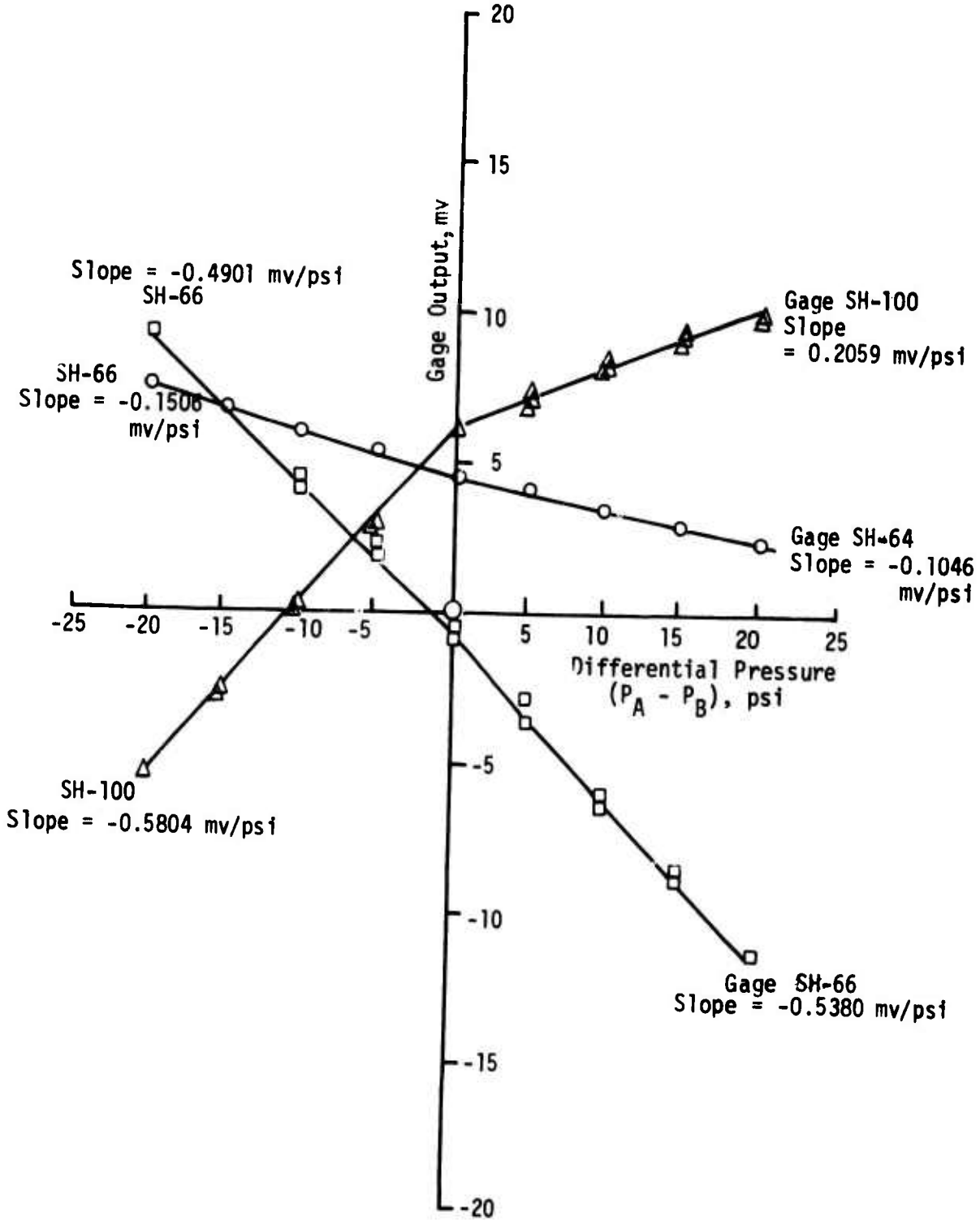

Figure 46. Gages SH-64, SH-66 and SH-100 Near Ends of STV No. 5 Output Versus Differential Pressure
T = 114°F, p_H = 0

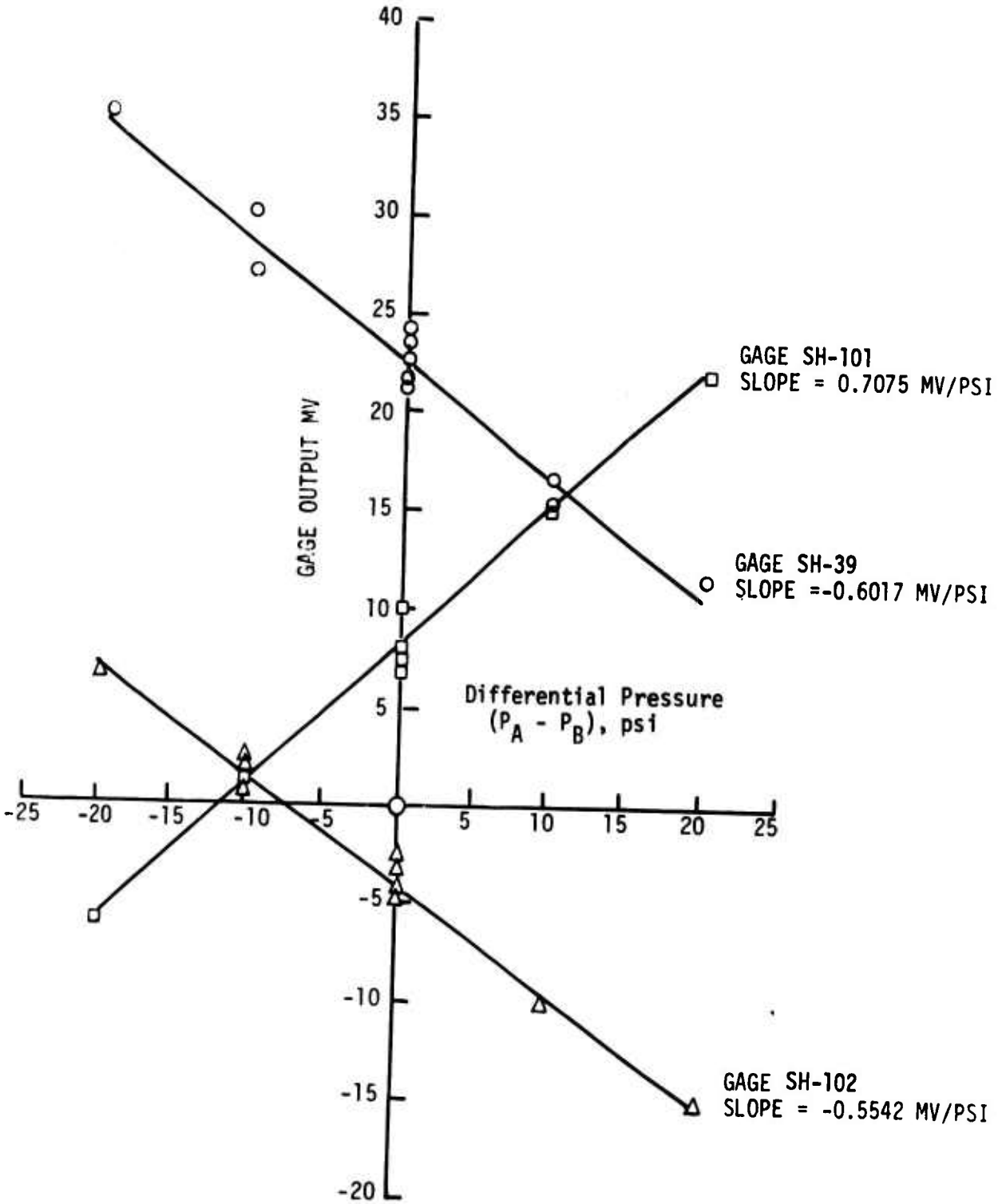

Figure 47. Gages SH-39, SH-101 and SH-102 Output versus Differential Pressure;
T = 114°F, P_H = 200 psi

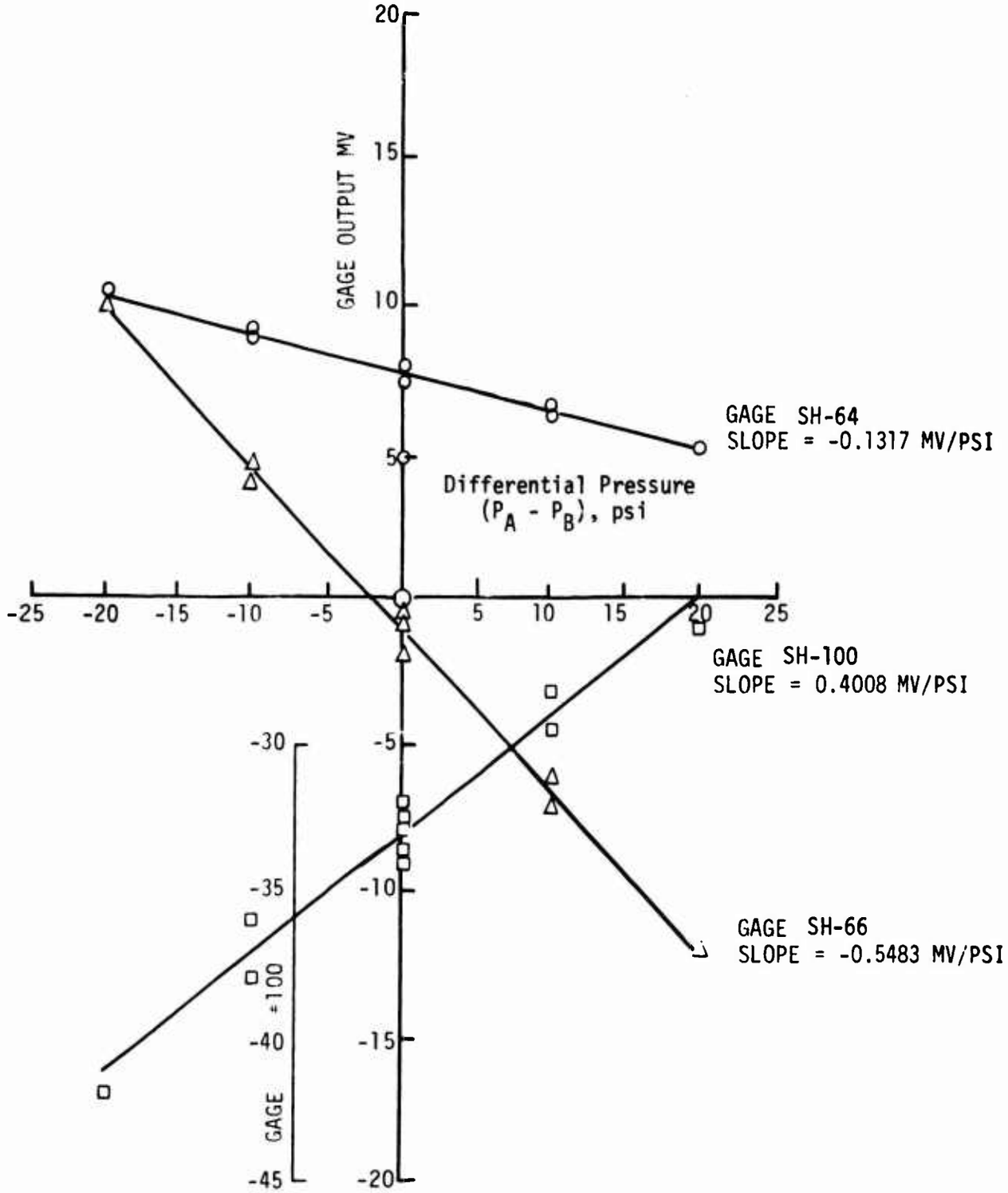

Figure 48. Gages SH-64, SH-66 and SH-100 Output versus Differential Pressure; T = 114°F, P_H = 200 psi

TABLE 6

COMPARISON OF GAGE RESPONSE DATA DURING
DIFFERENTIAL PRESSURE TESTING

Gage	Base Hydrostatic Pressure, psi	Slopes of Gage Responses, MV/psi					
		44°F		80°F		114°F	
		Differential Press.		Differential Press.		Differential Press.	
		On Side A	On Side B	On Side A	On Side B	On Side A	On Side B
SH-39	0	0.222	0.419	0.290	0.466	0.284	0.648
SH-64	0	0.065	0.127	0.060	0.150	0.105	0.151
SH-66	0	0.391	0.210	0.535	0.290	0.538	0.490
SH-100	0	0.115	0.403	0.135	0.455	0.206	0.580
SH-101	0	0.480	0.418	0.557	0.515	0.701	0.657
SH-102	0	0.271	0.277	0.327	0.268	0.417	0.332
SH-39	200	0.328*		0.435*		0.602*	
SH-64	200	0.094		0.107		0.132	
SH-66	200	0.318		0.479		0.548	
SH-100	200	0.168		0.239		0.401	
SH-101	200	0.361		0.516		0.708	
SH-102	200	0.253		0.357		0.554	

* The slopes were identical for differential pressure on side A and on side B.

The next two figures in the first group, i.e., Figures 47 and 48 show similar plots but for the case where a mean hydrostatic pressure of 200 psi is applied to the grain. Thus, Figure 47 shows the data from the shear gages at the middle of the grain at a temperature of 114°F plotted versus differential pressure and Figure 48 shows the gage output for the end shear gages versus differential pressure.

An examination of Figure 45 shows that the centrally located shear gages SH-101, SH-102 and SH-39 exhibit almost linear plots of output as a function of applied differential pressure. However, closer examination of these curves shows that the slope of the gage output versus differential pressure applied to the end A of the grain is generally slightly different from the slope of the output of the gage versus differential pressure applied at end B. This effect is small in shear gage SH-101, slightly larger in shear gage SH-102 and is the most pronounced in the case of shear gage SH-39.

Plots presented earlier of the effect of hydrostatic pressure on shear gage output showed that in many instances the change in gage reading was reduced significantly at the higher hydrostatic pressure levels. For this reason it is interesting to examine the data of Figures 47 and 48 and Table 6 which show the shear gage output (for those gages located in the middle and ends of the grain, respectively) when a 200 psi hydrostatic pressure is applied to the grain. A comparison of Figures 45 and 47 shows that in spite of more data scatter at the higher pressure levels, the changes in slope obtained with zero hydrostatic pressure are not obtained with the 200 psi hydrostatic pressure applied to the grain. This is particularly noticeable in the case of gage SH-39 which showed such a marked change in slope depending on which end of the STV was pressurized. A similar comparison between the data in Figures 46 and 48 also shows that the change in slope has

been virtually eliminated at the 200 psi applied hydrostatic pressure level. Even gage SH-100 does not appear to exhibit a noticeable change in slope with the change of the ends, for the differential pressurization, although the hydrostatic pressure test data suggested that this gage would still exhibit a significant hydrostatic pressure effect at 200 psi.

The output of the normal gage under differential pressure loading for the 114°F temperature is shown in Figure 49. It will be noted that the gage output versus pressure is significantly different depending upon which end of the grain is pressurized, as would be expected. Also shown in Figure 49 is the response of the normal stress to hydrostatic pressure. The slope of the normal stress measurement to hydrostatic pressure at 114°F is 0.724 mv/psi. When a differential pressure is applied to the end nearest the normal gage the measured slope is 0.645 mv/psi. When the pressure is applied at the end of the grain remote from the gage, the gage response is only 0.10 mv/psi. These slopes are to be compared to a gage calibration sensitivity at 114°F of 0.813 mv/psi. From this it can be seen that under hydrostatic pressure, the normal stress gage sees only 89% of the hydrostatic pressure applied to the STV. Clearly the propellant itself is carrying some of the hydrostatic pressure load. The pressure measured by the gage when only the closest end is pressurized is equal to 79.3% of the pressure on that end, whereas when the end remote from the gage is pressurized the pressure on the gage is only 12.3% of the pressure on the end of the grain.

Figure 50 shows the gage response to the differential pressure at a temperature of 80°F. The data are similar to that shown in Figure 49 but the gage output for the same applied pressure is much smaller at the lower temperature: compare the slope of 0.418 mv/psi at 80°F with the slope of 0.645 mv/psi at 114°F.

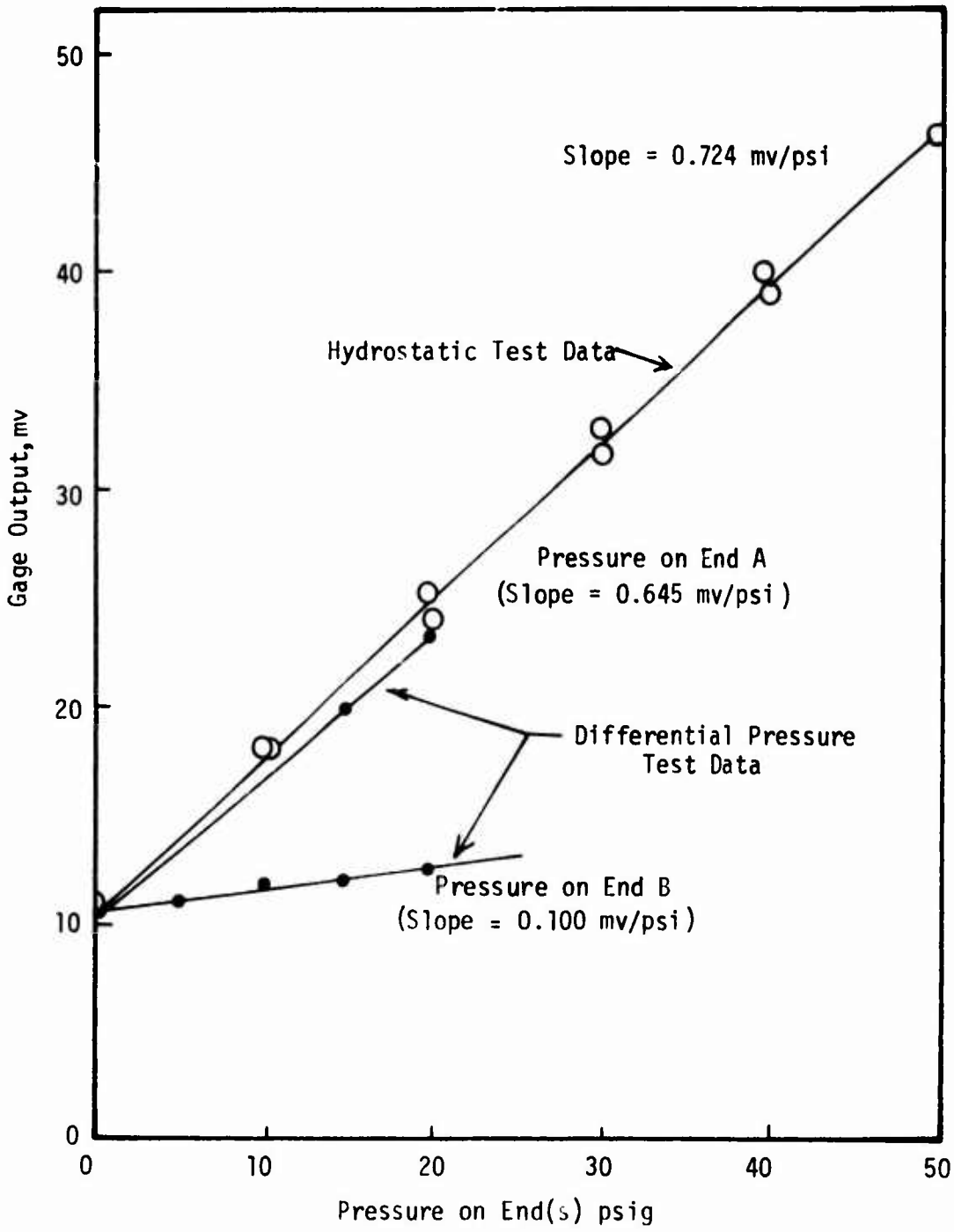

Figure 49. STV No. 5 Normal Gage Output Versus Hydrostatic and Differential Pressure (P_H=0); T = 114°F

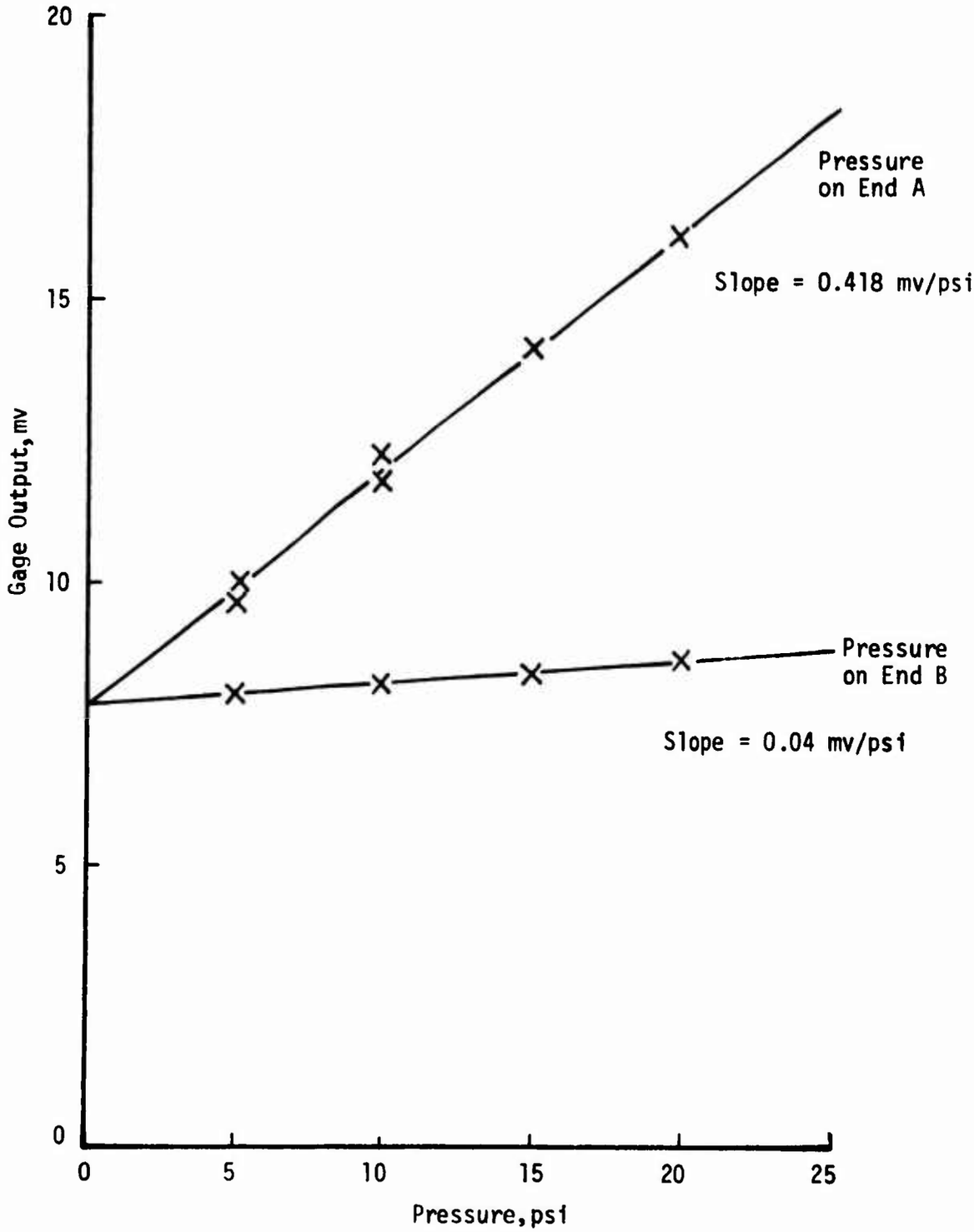

Figure 50. STV No. 5 Normal Stress Gage Response Versus Differential Pressure (P_H = 0): T = 80°F

3. Thermal Data from STV No. 5

Figures 51 and 52 show the thermal stresses measured at the three test temperatures by the normal and shear gages in STV No. 5. It will be noted that the shear gages (SH-39, 101, 102) located at the middle of the STV show essentially no thermal shear stress as the temperature is lowered (Figure 52). This was, of course, expected since no shear stress should be generated at the middle of a symmetrical grain. The large compressive stress at 114°F and zero stress at 44°F indicated by data from the normal stress gage shows that this gage must have changed its characteristics.

The behaviors of the shear gages (SH-64, 66, and 100) at the grain ends are given in Figure 52. These gages should behave similarly except for the sign of the stress readings. Gages SH-64 and SH-66 are observed to follow the predicted behavior, the stresses differing at 44° and 80°F up to a maximum of 50%. The magnitudes of the observed stresses from shear gages SH-100 follow those for SH-64 except at 44°F. However the signs of the shear stresses from gage SH-100 appear to be in error, in that they are opposite to those for shear gage SH-64.

4. STV No. 5 Failure Test Data

As was mentioned earlier, STV No. 5 was failure tested while subject to a mean hydrostatic pressure of 600 psi. Increasing differential pressures were applied to the STV until the propellant-insulation bond failed. The differential pressure steps were applied to each end of the grain alternately, the pressure difference being maintained for approximately five minutes at each step. At the end of the five-minute period the pressure was reduced to 600 psi and the hydrostatic condition maintained for a further five-minute period before applying the next pressure differential to the other end of the grain.

The results of the tests from shear gages are shown in Figures 53 through 55, with further data given in Appendix F. For each gage, the output in millivolts is plotted against the differential pressure up to the point of failure. It will be noted that the plots of gage output versus differential pressure are linear although some scatter in the measured data are apparent. This indicates that any effects of hydrostatic pressure on the gage readings were suppressed by the application of the 600 psi superimposed hydrostatic pressure.

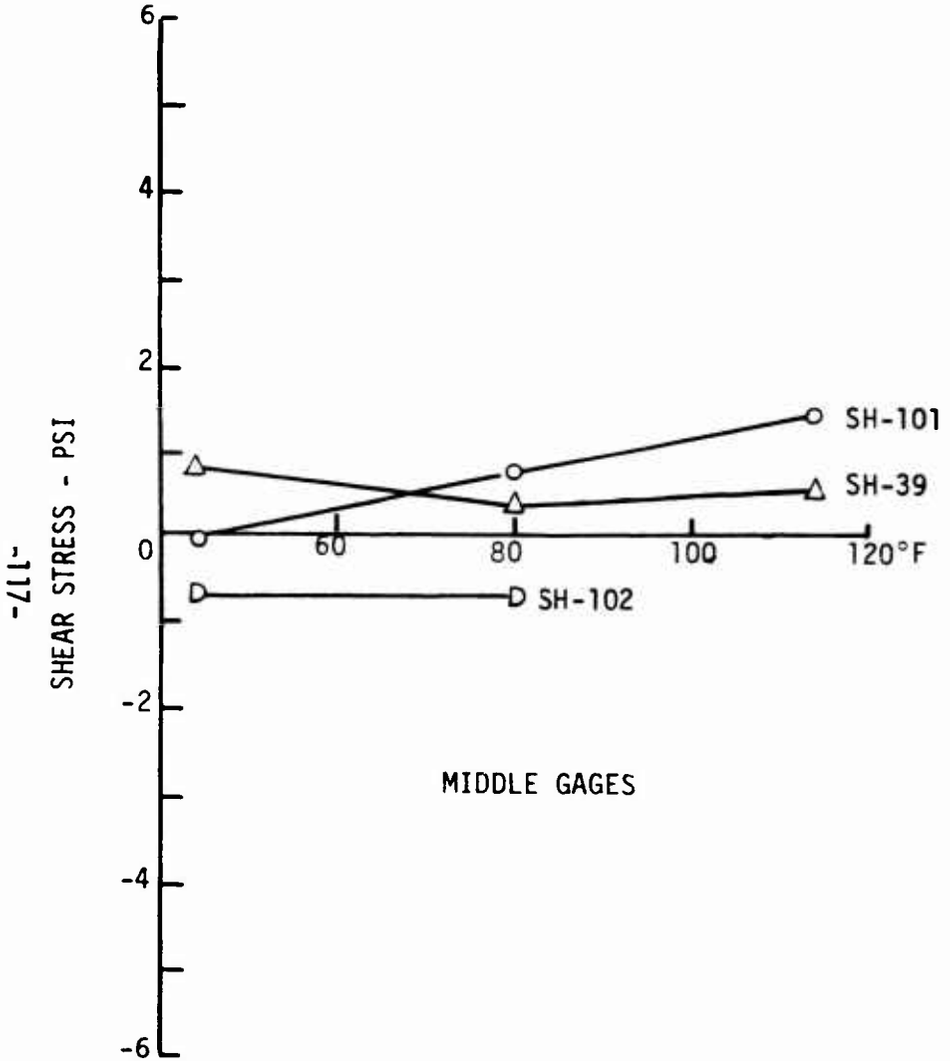

Figure 51. Thermal Shear Stress Versus Temperature for Mid-Plane Shear Gages in STV No. 5

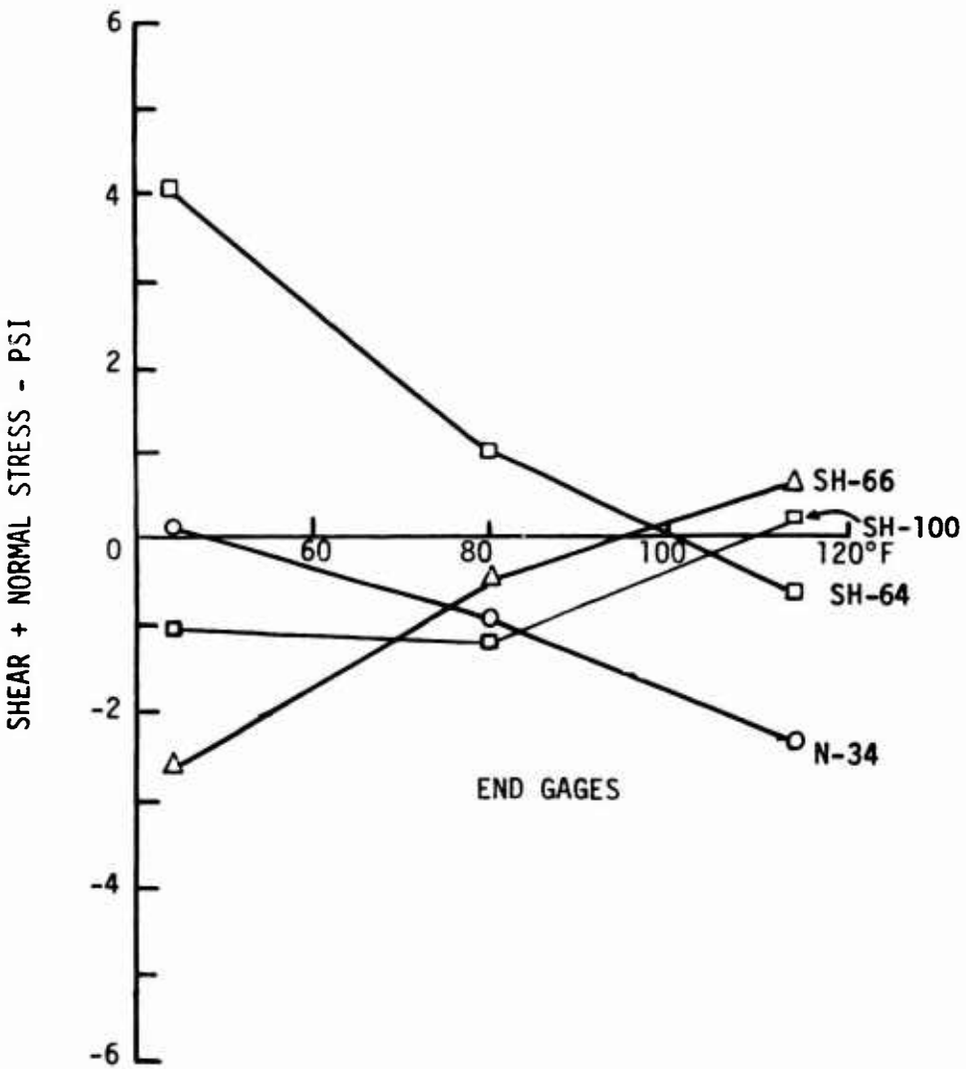

Figure 52. Thermal Normal and Shear Stresses vs. Temperature for End Gages in STV No. 5

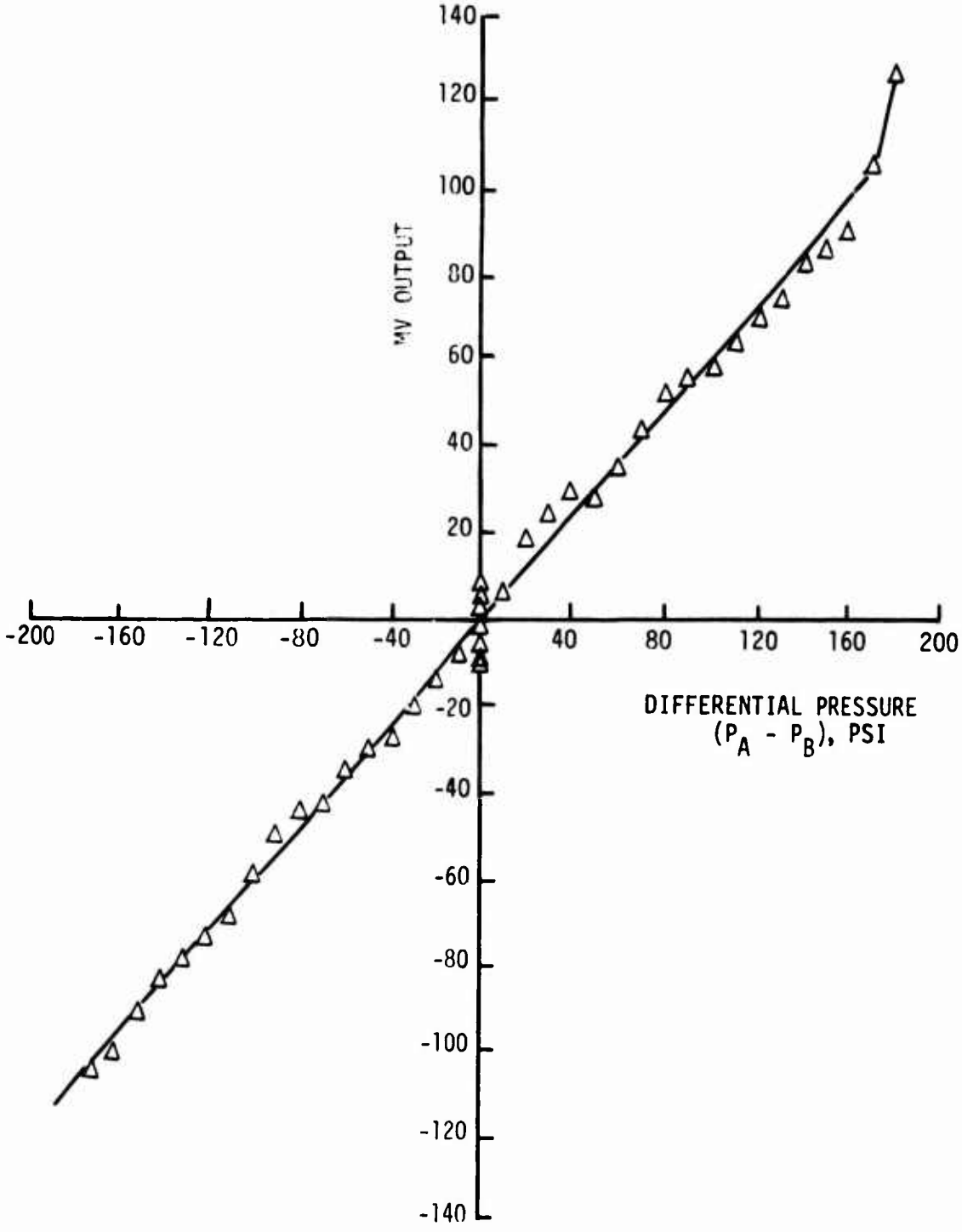

Figure 53. STV No. 5. Failure Test. Shear Gage SH-39 Output vs. Differential Pressure

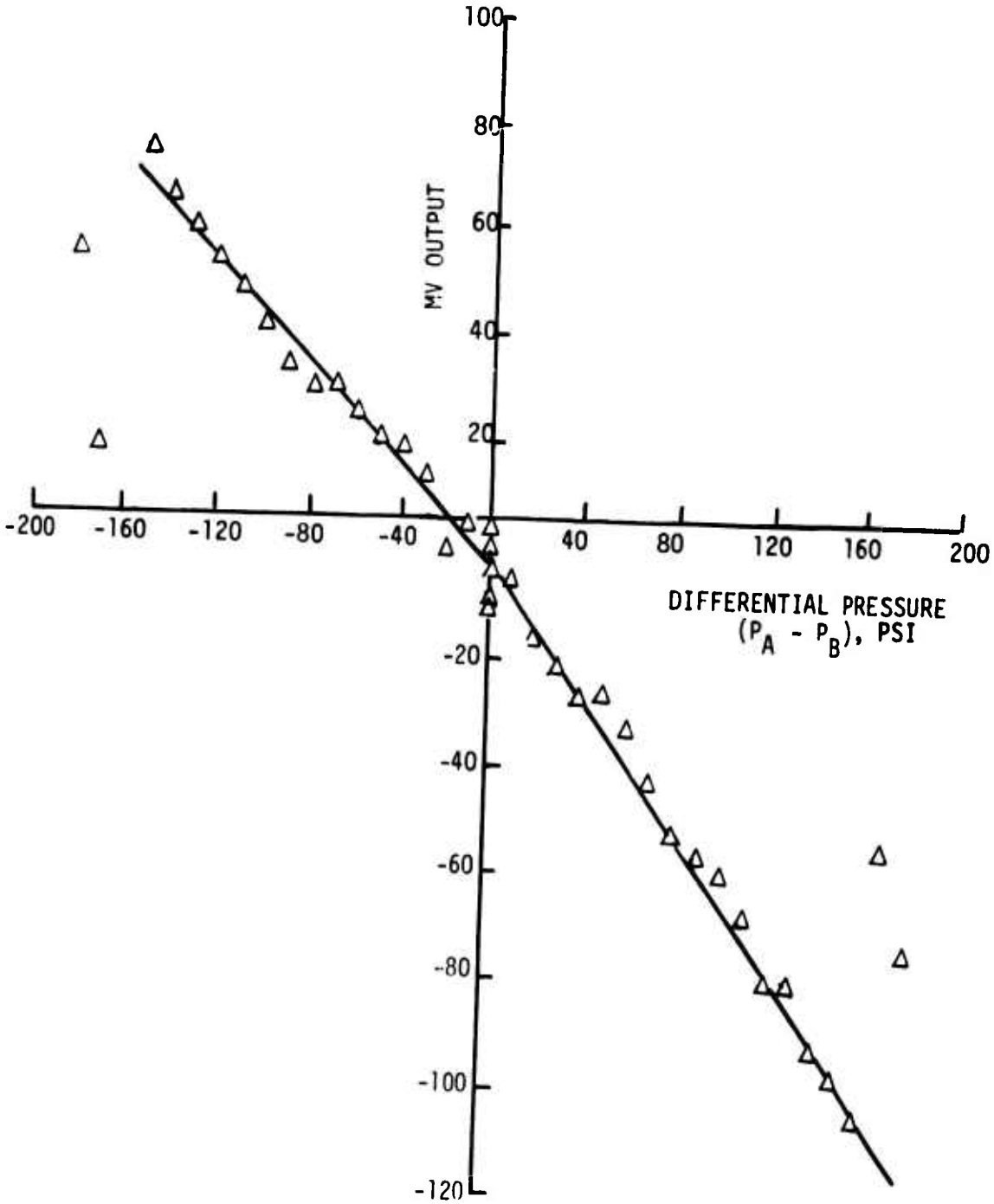

Figure 54. STV No. 5. Failure Test. Shear Gage SH-101 Output versus Differential Pressure

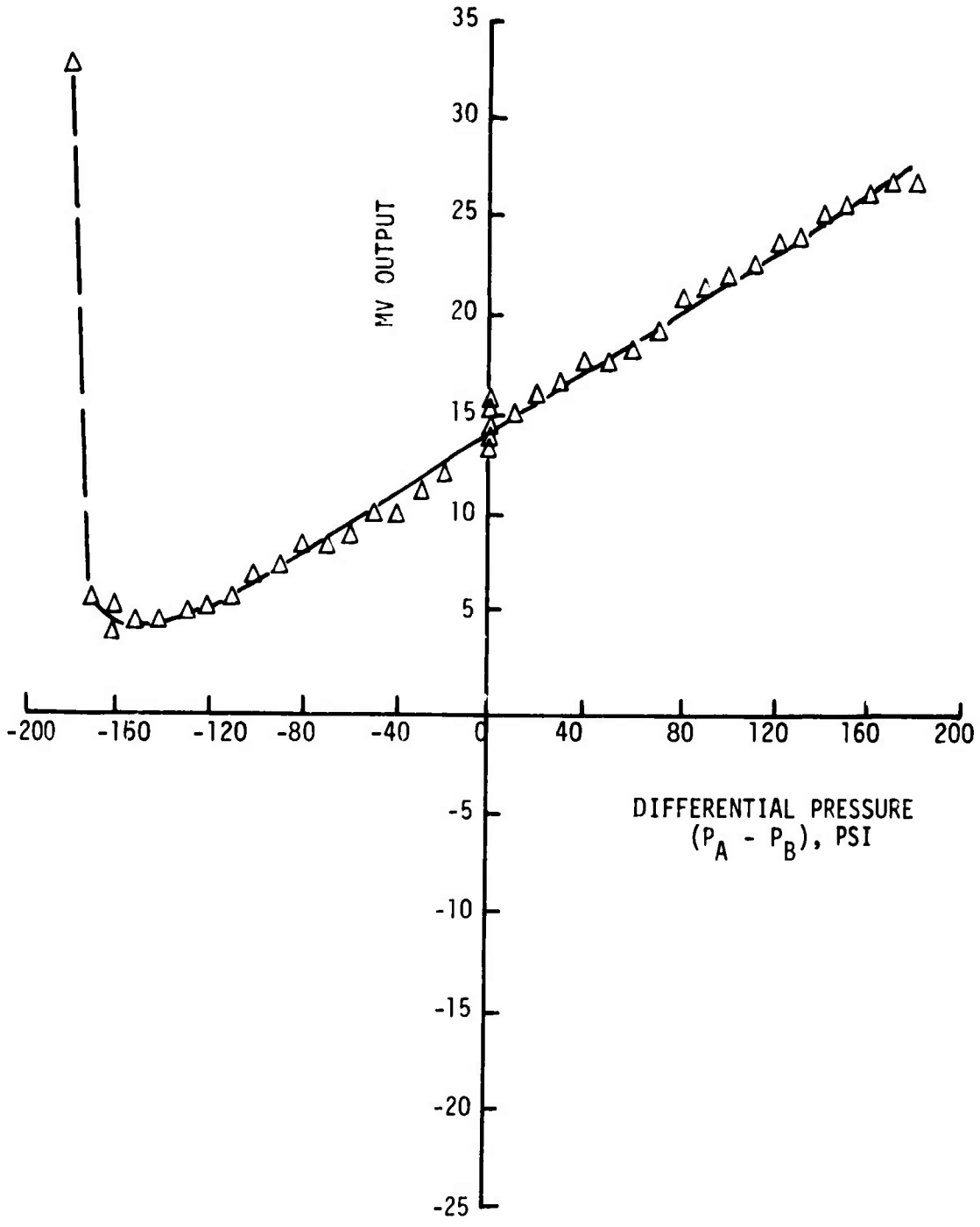

Figure 55. STV No. 5. Failure Test. Shear Gage SH-102 Output vs. Differential Pressure

The onset of failure is clearly evident in the data from these shear gages. Thus shear gage SH-101, for instance, clearly shows that failure occurred initially at a differential pressure of 150 psi applied at the end B. Shear gage SH-102 also clearly defines that failure initiated at some differential pressure level between 130 and 160 psi. In fact, all the shear gages gave proper indications of motor failure and all the gages functioned consistently up to and including the point of failure of the propellant-liner bond. The failure shear stress equivalent to the 160 psi differential pressure is only 22 psi. This is much less than the shear stress value of 32 psi obtained on the earlier STV No. 3 failure test. The earlier STV was, however, tested to failure much more rapidly than STV No. 5 so that the damage accumulation on it was much less than on STV No. 5.

Of particular interest in STV No. 5 was the behavior of the failure event gages during these failure tests. Four failure event gages were installed in the STV. Nos. 1 and 3 were at end A of the grain and failure gages 2 and 4 were close to end B. The first gage to give an indication of failure was failure gage No. 4 which became discontinuous when a differential pressure of 160 psi was applied to end B of the STV. Failure gage No. 3 became discontinuous when the differential pressure was 170 psi applied to end B, while failure gage No. 1 did not become discontinuous until this pressure equalled 180 psi (applied to the same end). Failure Gage No. 2 also appeared to behave erratically at this time, showing the onset of failure at that location.

It is clear therefore that the new improved type of failure event gage gave a clear indication when failure of the bond occurred. However, it seems possible that the shear gages will give an indication of the onset of failure prior to the actual separation.

Figure 56 shows the pressure measured by the 150 psi normal stress gage during the failure test. The gage performed well in spite of the fact that the test began at 600 psi hydrostatic pressure, i.e., 4 times the maximum range of the gage. It continued to read the STV pressure up to grain failure at 775 psi at the gage. Also, the gage was still functioning after the failure test was finished. The large attenuation experienced when pressurizing side B is attributed primarily to grain voids.

Figures 57 and 58 show the deflections of the ends of the grain as measured by linear potentiometers. The initiation of failure at End B is clearly shown in Figure 58 at a pressure of 160 psi.

G. CONCLUSIONS

The most significant information resulting from the STV No. 5 test data is the fact that the shear gages can produce a spurious output signal if they have a significant response to hydrostatic pressure. Fortunately, this fact was appreciated early in the program and the shear gages intended for use in the full-scale motors were subjected to a combined shear plus hydrostatic pressure test (at 200 psi). Gage SH-39 in fact was rejected for use in the first full-scale motor because of excessive response to hydrostatic pressure. The STV No. 5 data confirms the wisdom of this decision.

The attenuation of hydrostatic pressures superimposed upon the grain can be significantly increased by the casting voids. The effect is to increase grain shear stresses and to modify gage responses from those expected using void-free structural analyses. Also, the effects are highly temperature dependent.

The shear stress and failure event gages seemed to perform well in defining initiations of failures at the bondline.

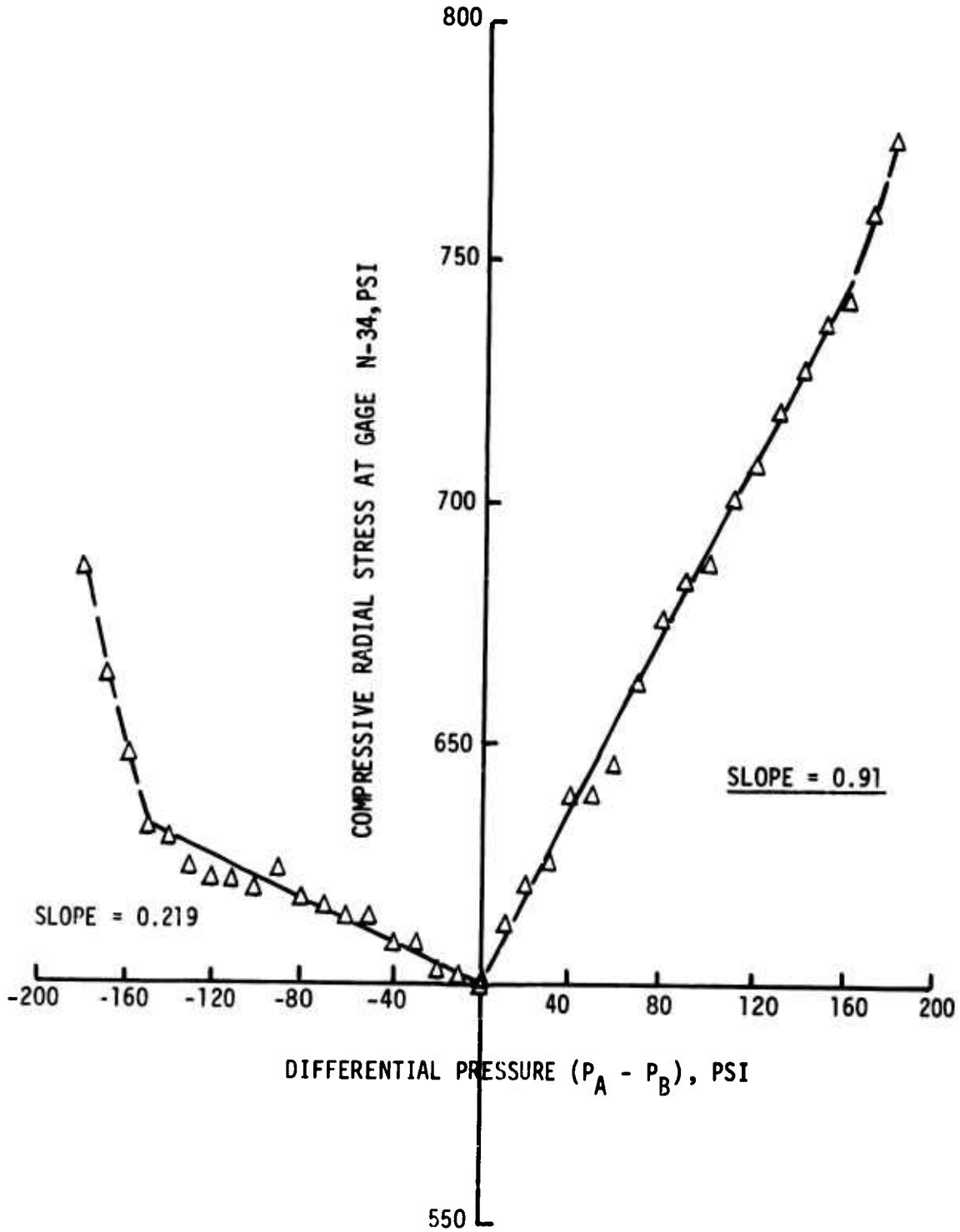

Figure 56. STV No. 5. Failure Test. Normal Gage N-34 Stress vs. Differential Pressure

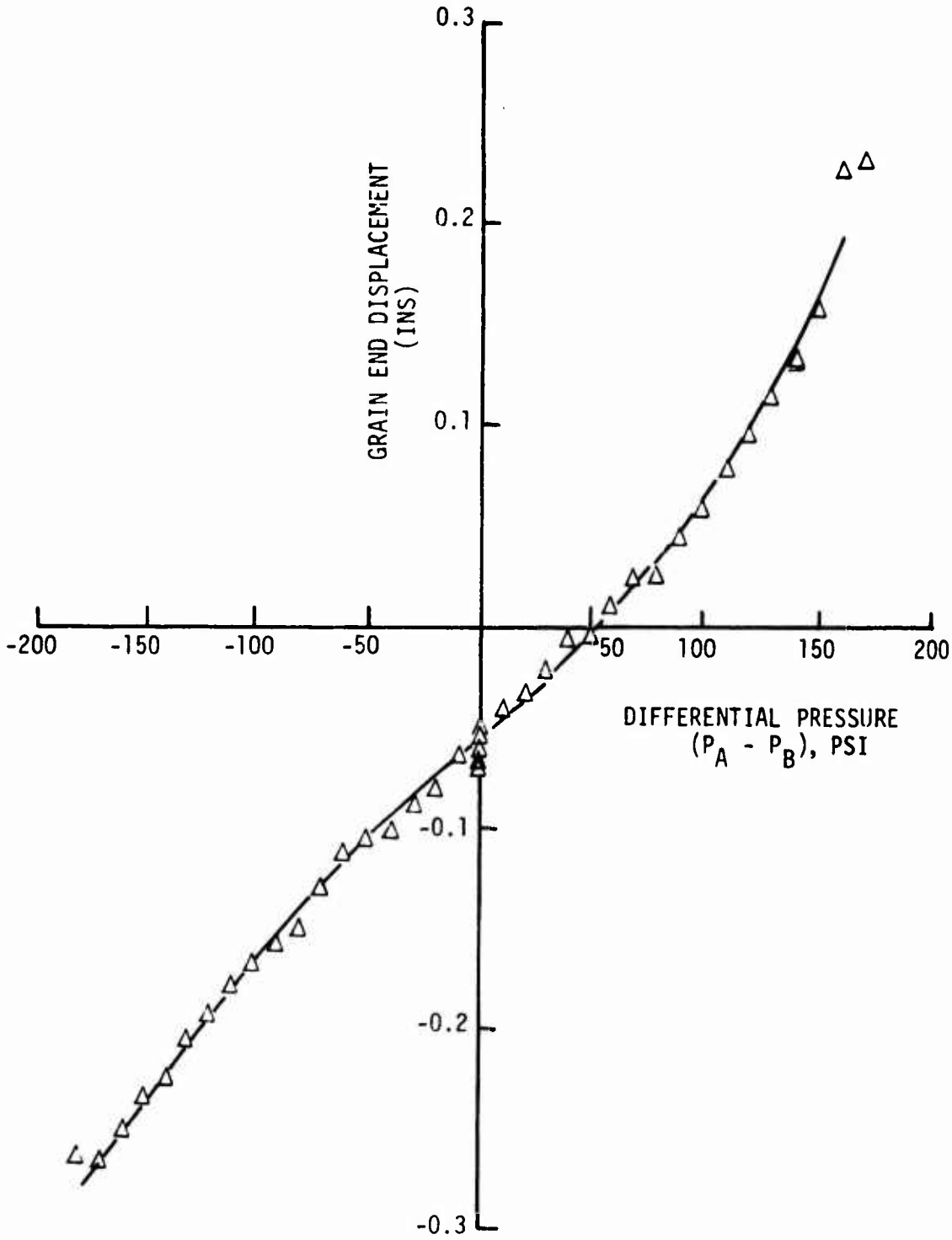

Figure 57. STV. No. 5. Failure Test. Linear Potentiometer A vs. Differential Pressure

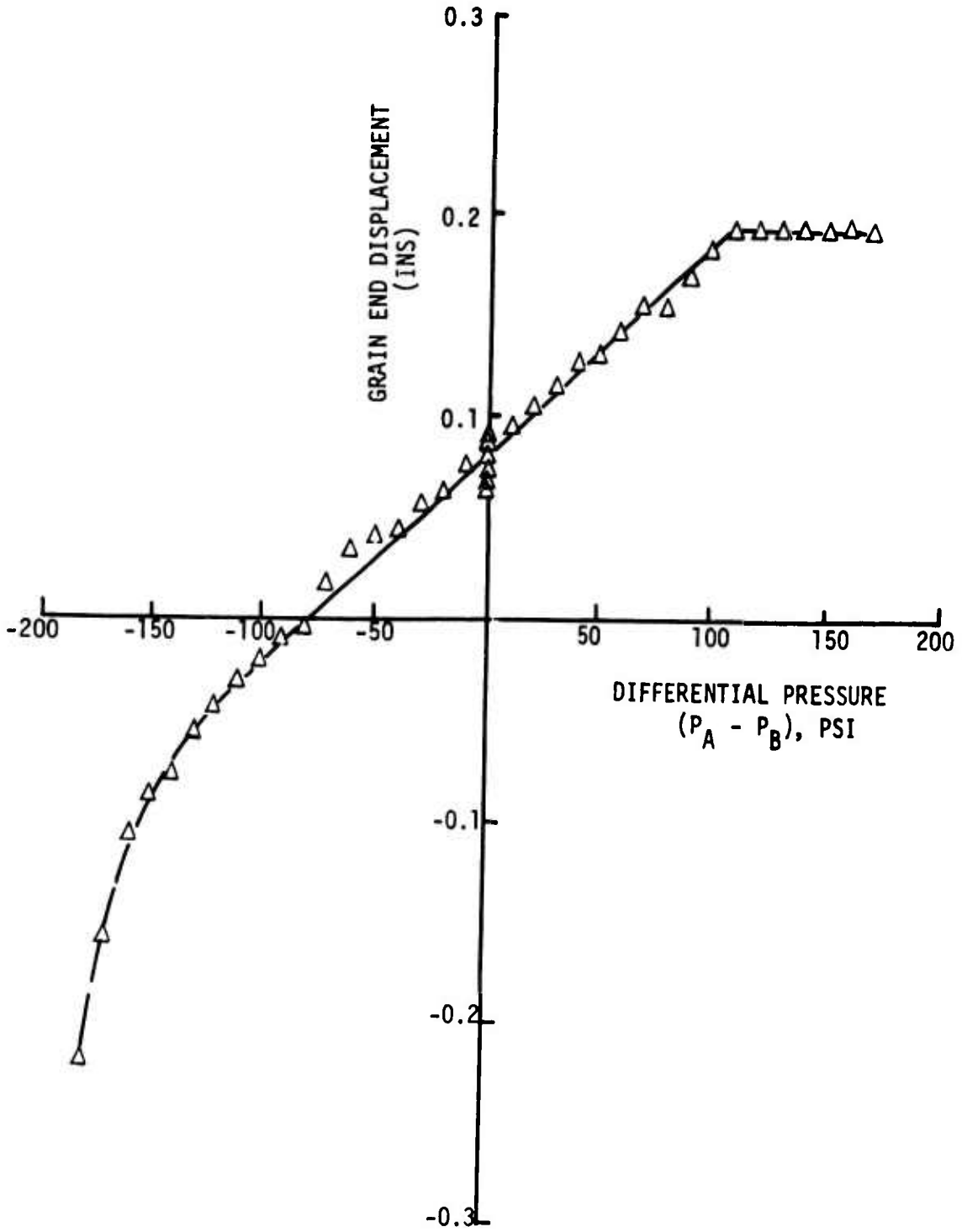

Figure 58. STV. No. 5. Failure Test. Linear Potentiometer B vs. Differential Pressure

REFERENCES

1. "Polaris A-3 First-Stage Chamber Preparation and Hydrotest for Structural Evaluation of Through-the-Forward-Head Instrumentation", Final Report, Aerojet Solid Propulsion Company, Report No. POL 71416, (12 March 1971).

2. "First Stage Polaris Model A-3P Alternative Forward-Head Repair Selection", Report POL 71439-1, (18 June 1971).

3. Leeming, H., et al, Final Report, Solid Propellant Structural Test Vehicle, Cumulative Damage and Systems Analyses, Technical Report No. AFRPL-TR-68-130, (October 1968).

4. Leeming, H., et al, Final Report, Solid Propellant Structural Test Vehicle and Systems Analysis, Technical Report No. AFRPL-TR-70-10, (March 1970).

5. Leeming, H., et al, Final Report, Solid Propellant Structural Test Vehicle Program, Report No. AFRPL-TR-72-29, (April 1972).

6. DePree, D. O., "Demonstration of a Sterilizable Solid Rocket Motor System", Technical Report No. NASA CR-111889, (January 1971).

APPENDIX A

NORMAL STRESS GAGES

DESCRIPTION AND PREPARATION

PROCEDURES

GENERAL DESCRIPTION

The normal stress gages used (Konigsberg Instruments P-14EB Series) were simply a form of a miniature load cell whereby active semi-conductor gages were bonded onto a thin machined diaphragm. The design is shown in Figure A-1. It is constructed as a "fluid" pressure transducer, with an internal pressure reference cavity, and four semi-conductor strain gages bonded to the integrally machined pressure sensing diaphragm. The transducer is only 0.060 in. thick, has a tapered frontal surface, and cables exiting from the rear. Measurement of residual transducer-induced perturbations are minimized by having the active portions of the strain gages extend to 50% of the diaphragm radius. Artifacts caused by propellant stress-induced bending of the transducer are minimized by internal stiffening members.

The transducer is calibrated as two independent half-bridges that follow the circuit shown in Figure A-2. Adjustments in the fixed resistors provide the required temperature compensations. The dual bridge circuits allow a direct comparison between the readings from two independent circuits subject to the same stress. This redundancy in the gage design was employed for the first time in the Flexible Case-Grain Interaction program.

To provide the sensitivity required for the less severe loadings and the range required for the very important pressurization loads, two types of diaphragm transducers were used on the program. One was the 150 psi full-scale gage that had been found to satisfactorily resolve stress changes on the order of 1 psi: the other, a 450 psi full-scale gage that is known to operate well above 500 psi pressure.

The following specifications refer to transducer performance measured under fluid pressure conditions in the laboratory.

1.	Pressure ranges	150 and 450 psia
2.	Maximum applied pressure (No damage)	200% of rated range
3.	Excitation voltage	28.0 Vdc
4.	Gage voltage (nominal) (Note: Higher gage voltages to 2.5 Vdc are acceptable in In-Situ calibration)	1.5 Vdc
5.	Output voltage, at 100% of pressure range	135 $\pm$ 15 mV
6.	Calibration temperature range (Note: Transducers can be compensated over the temperature range from -85 to +180°F, although temperature effects become markedly nonlinear below -65°F and above 150°F)	QC calib. +30 to +130°F TC calib. -65 to +150°F
7.	Non-Linearity, Hysteresis, and Repeatability Combined	$\pm$ 1.0% F.S., B.S.L.
8.	Zero temperature shift/100°F	$\pm$ 2.0% F.S., B.S.L.
9.	Sensitivity temperature shift/100°F (Note: Temperature shift specifications can be improved, depending on range)	$\pm$ 2.0% F.S., B.S.L.
10.	Output impedance - half bridges, R_1-R_4 and R_2-R_3 configuration, nominal	800 Ohms

PREPARATION

IBT-115 trowelable insulation was selected as the material to encapsulate the normal stress gages and to bond the gages to the case wall. A two-piece mold fixture to encapsulate the normal stress gages was designed and fabricated out of aluminum as shown in Figure A-2. The size of the fixture is 12 in. long and 1.5 inches wide. The diameter of the mold cavity is 3/4 inch and it is 1/2 inch deep. The fixture allows potting of nine gages at one time. To facilitate mold release, the mold was designed in two pieces (Figure A-3).

The IBT-115 was cast into the mold after pre-heating both for 20 minutes at 175°F. After casting the adhesive is cured at 175°F for 4 hours. This should yield a cured material with a Shore A hardness of 66 to 70 and 77°F.

CALIBRATIONS

After encapsulation, the normal stress gages were calibrated and temperature compensated over the range from 30° to 130°F.

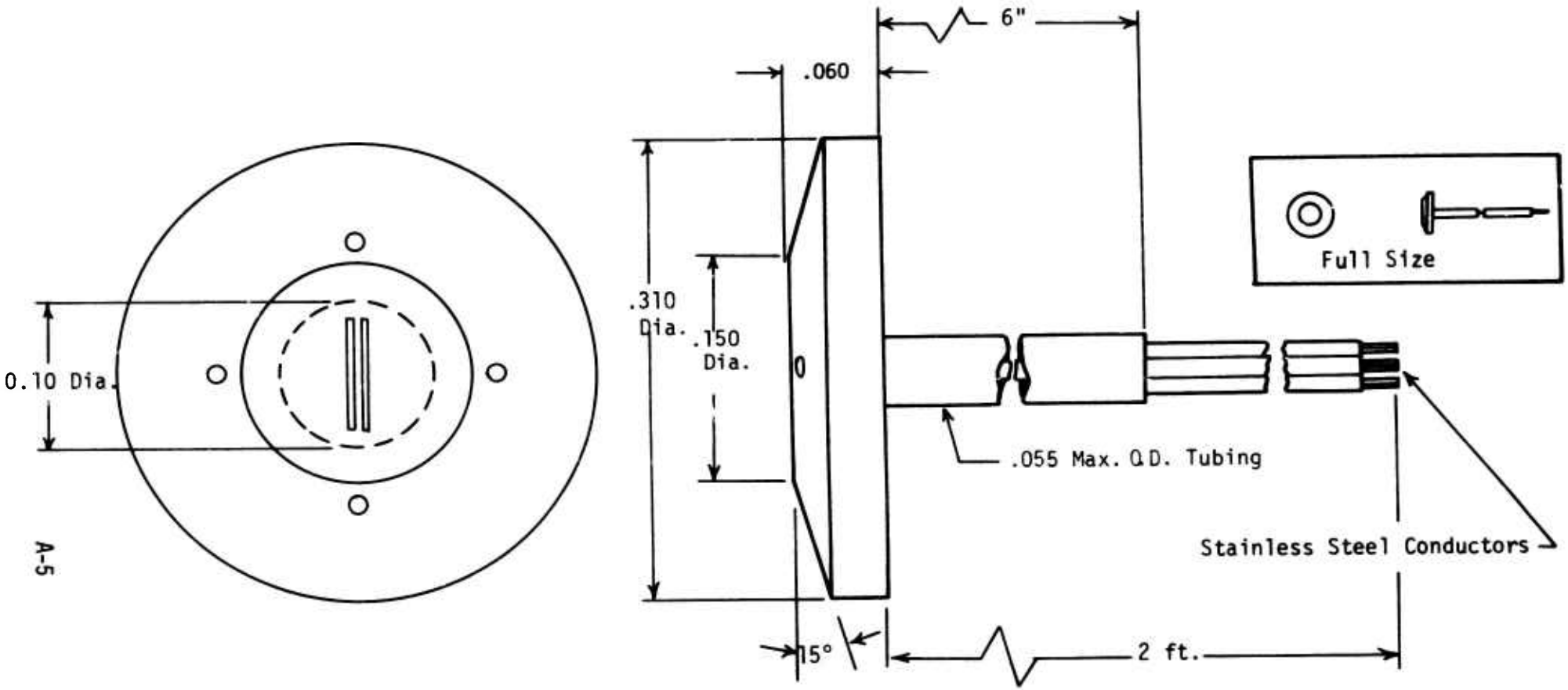

Figure A-1. Outline Drawing of Normal Stress Gage

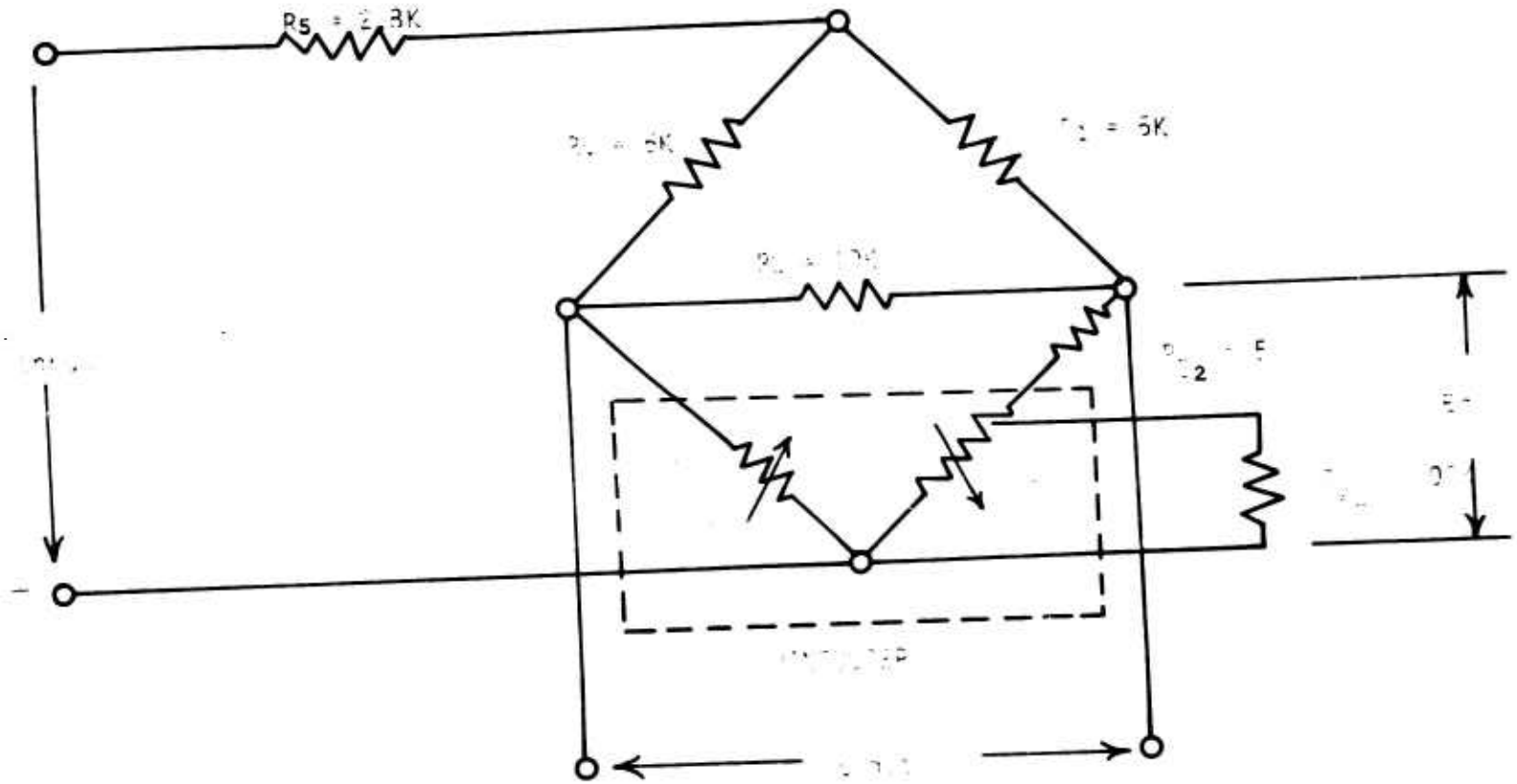

Figure A-2. Circuit Diagram for the Normal Stress Gage P14EB-SC-150 Serial No. 2
(Typical Half-Bridge)

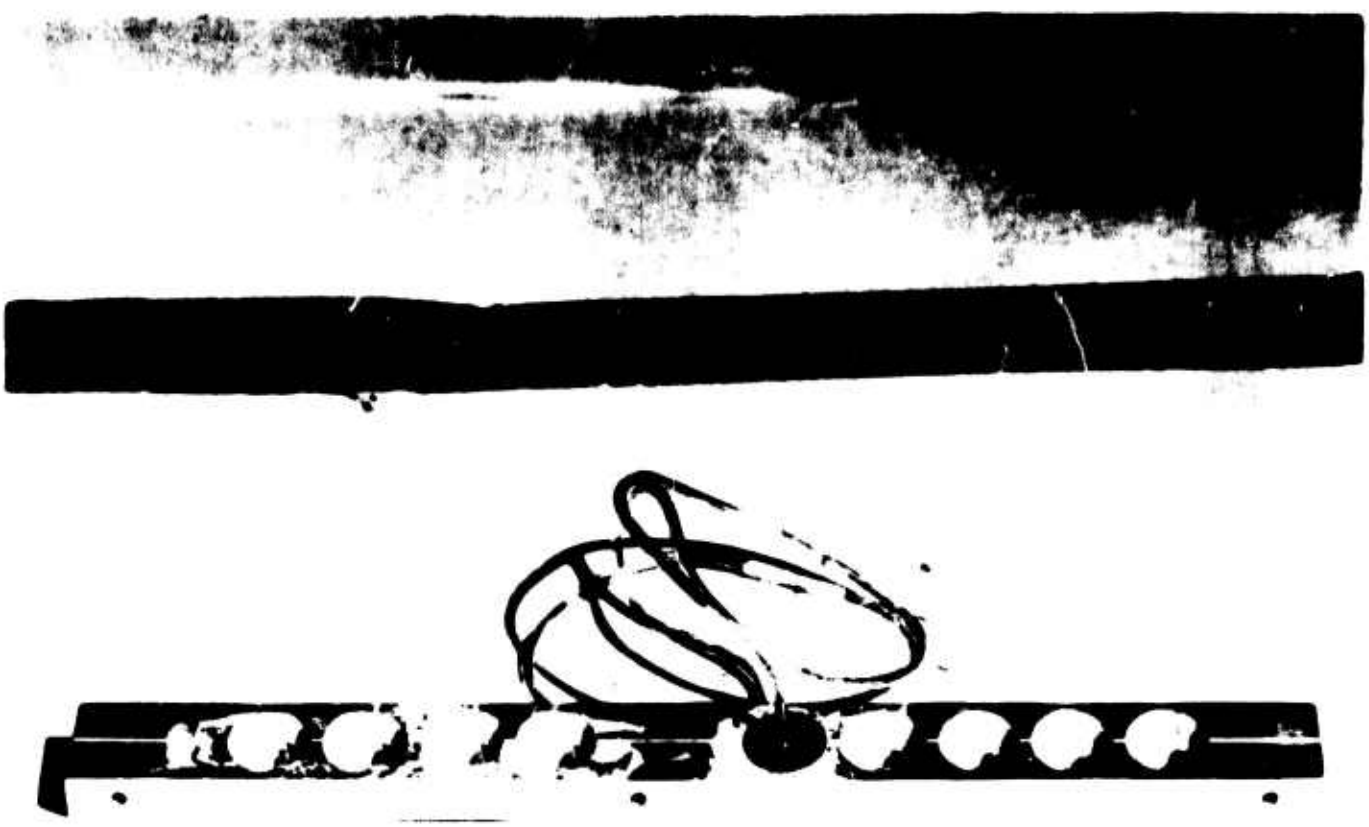

Figure A-3. Encapsulation Fixture for Normal Stress Gages

Figure A-4. Encapsulation Fixture Shown Separated for Easy Removal of Gages

APPENDIX B

SHEAR STRESS GAGES

(DESCRIPTION AND PREPARATION PROCEDURES)

GENERAL DESCRIPTION AND PREPARATION

The shear gages, or cubes, consisted basically of two semi-conductor strain gages mounted in a 45 degree plane of a transducer body, Figure B-1. The body of the transducers was molded from V-45 insulation material in the fixture shown in Figure B-2. The body was basically a triangle with a base of 1/2 inch, altitude of 1/4 inch, 1/2 inch thick, and base angles of 45 degrees.

After the semi-conductor strain gages were installed onto the basic triangular body, these assemblies were bonded to a strip of molded V-45 fabricated from the fixture shown on Figure B-3, which contained "cut-away" triangular slots to accommodate flush bonding of four basic triangular units. Two of these strips, with the basic triangular gage units bonded into place, were then bonded to pieces of wood to form the complete fixture for calibrating eight shear gages, Figure B-4. A completed shear cube is shown in Figure B-5.

CALIBRATION PROCEDURES

The transducers were calibrated as a simple bridge circuit that employed the schematic shown in Figure B-6.

For calibrating purposes, the completed shear calibration fixture, Figure B-4, was mounted in an Instron tensile tester. In general, the shear cubes were loaded to 120 to 150 lbs, which is equivalent to approximately 10 to 15 psi shear. The shear gage calibrations were performed at 30°, 80°, and 130°F by applying shear loads, first in one direction then reversing the direction so as to avoid accumulative zero shifts during testing. The load reversals were obtained by inverting the shear specimen in the test fixture.

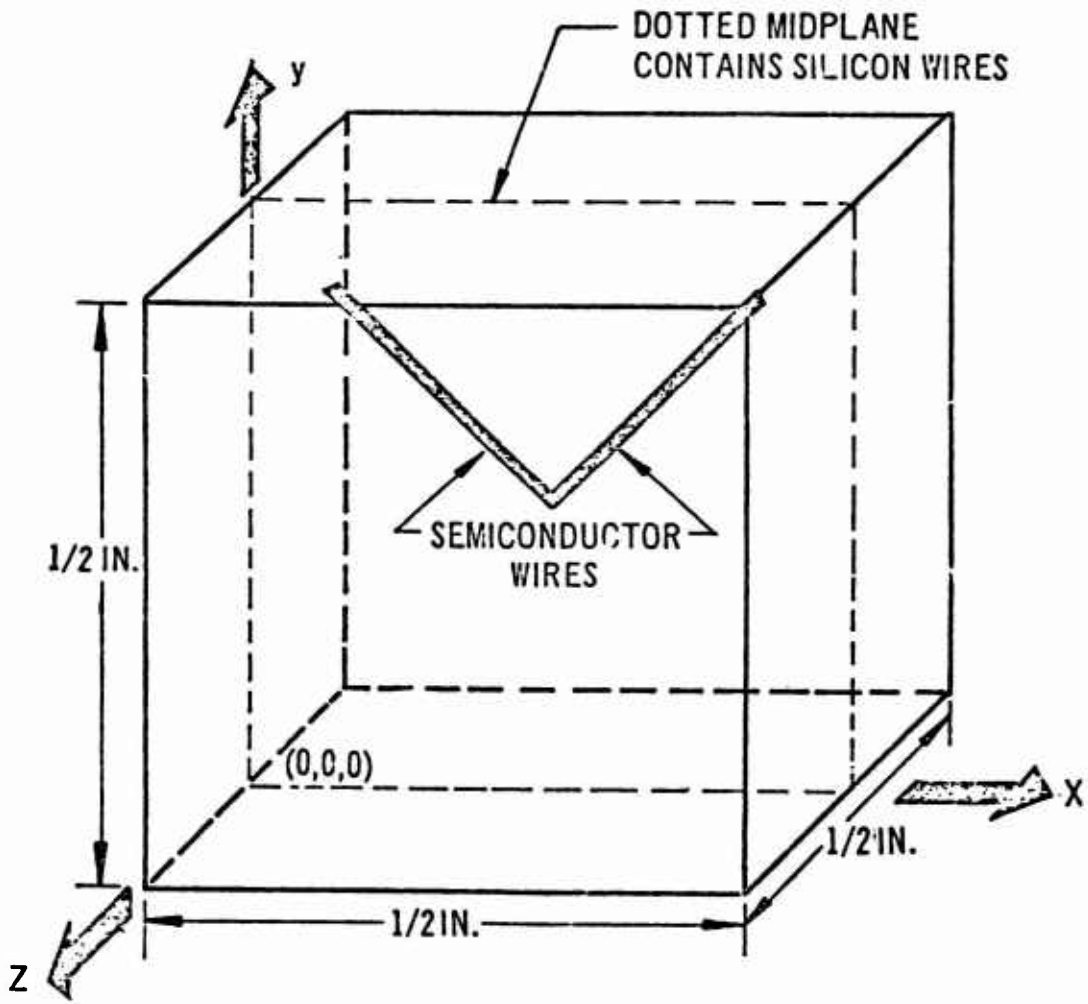

Figure B-1. Schematic of Shear Cube

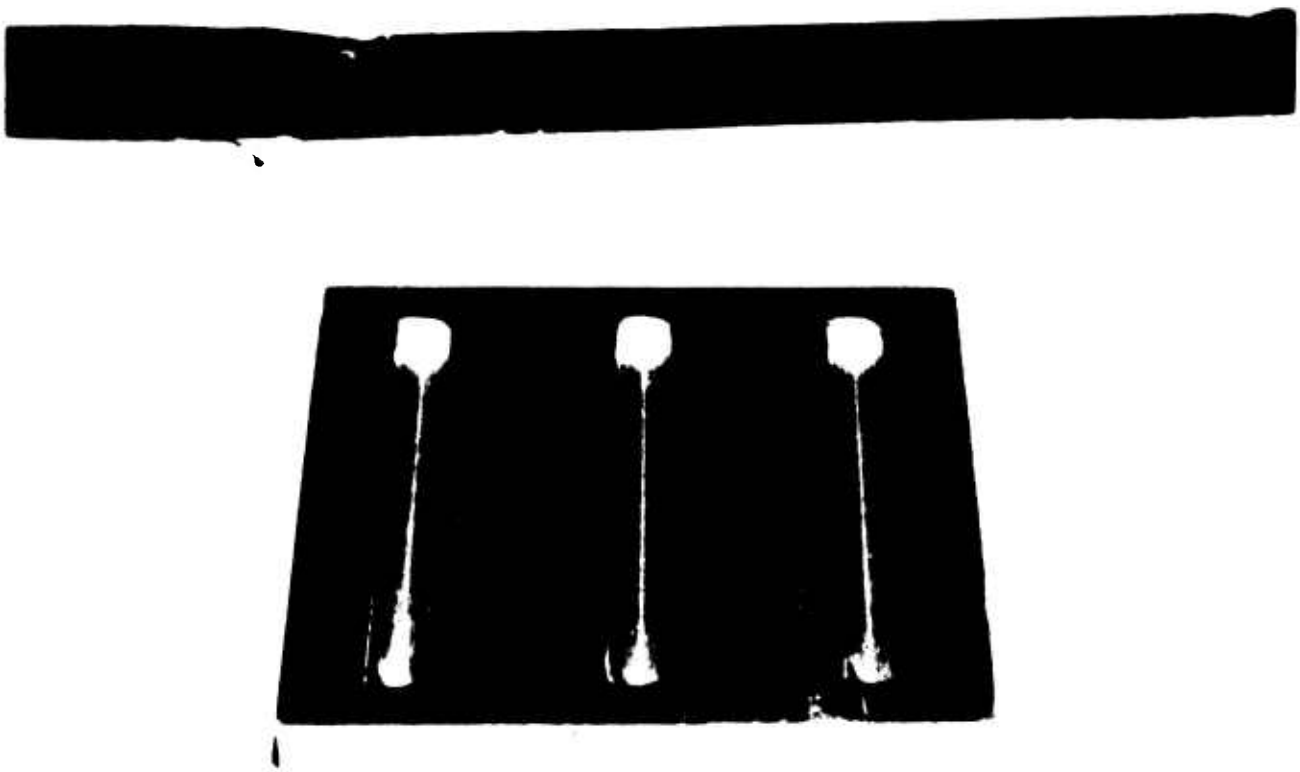

Figure B 2. Mold for Body of Shear Cube

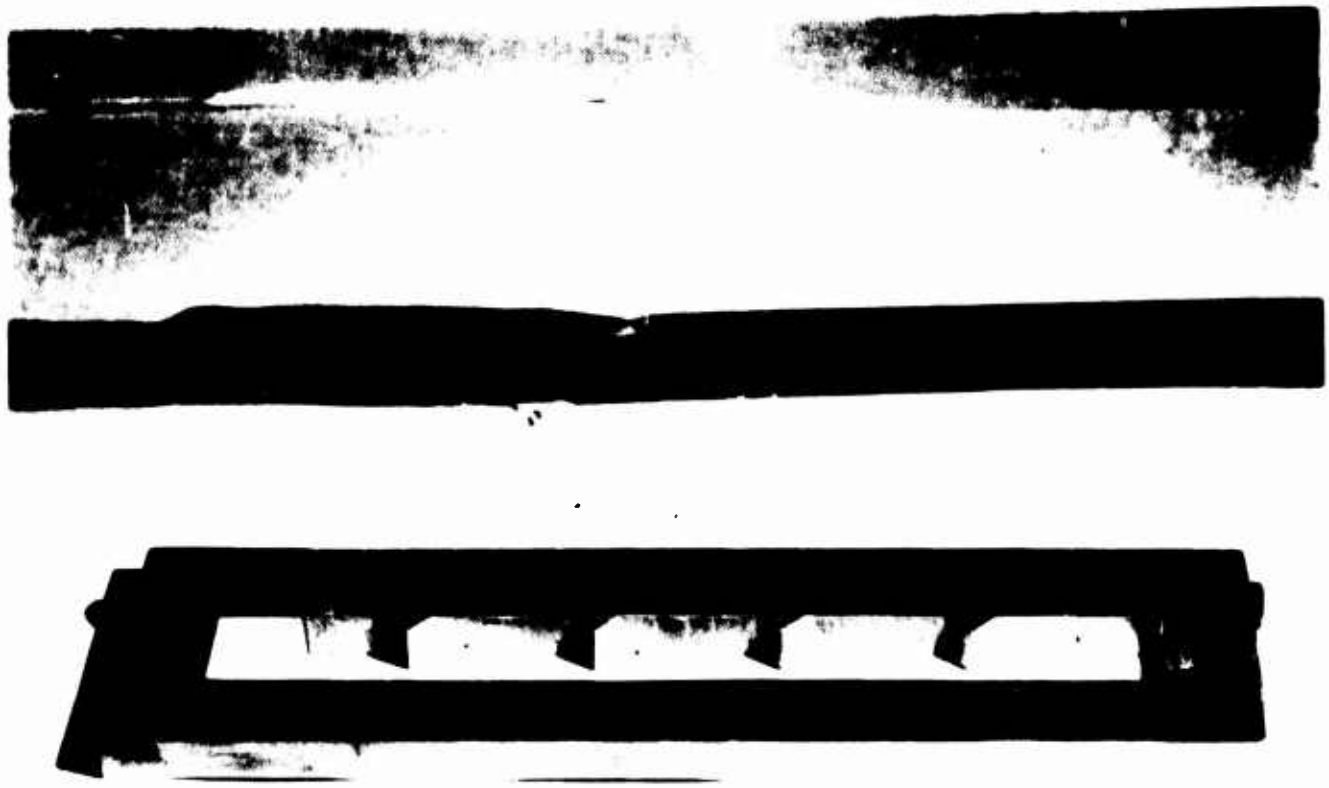

Figure B-3. Mold for V-45 Rubber Calibration Matrix

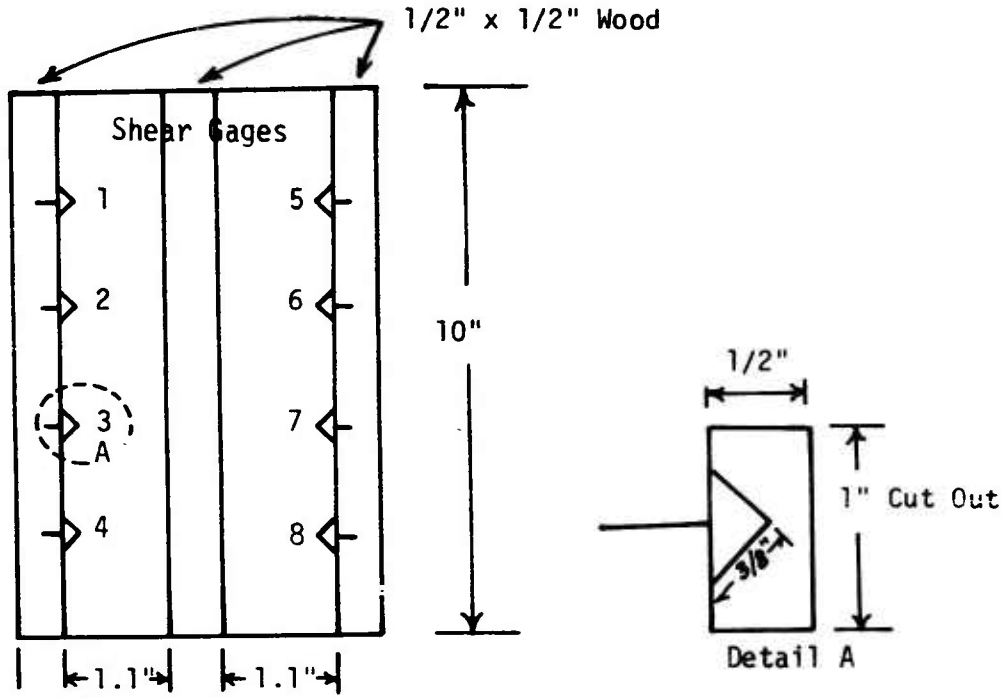

Figure B-4. Shear Calibration Fixture

Figure B-5. Photograph of Completed Shear Cube

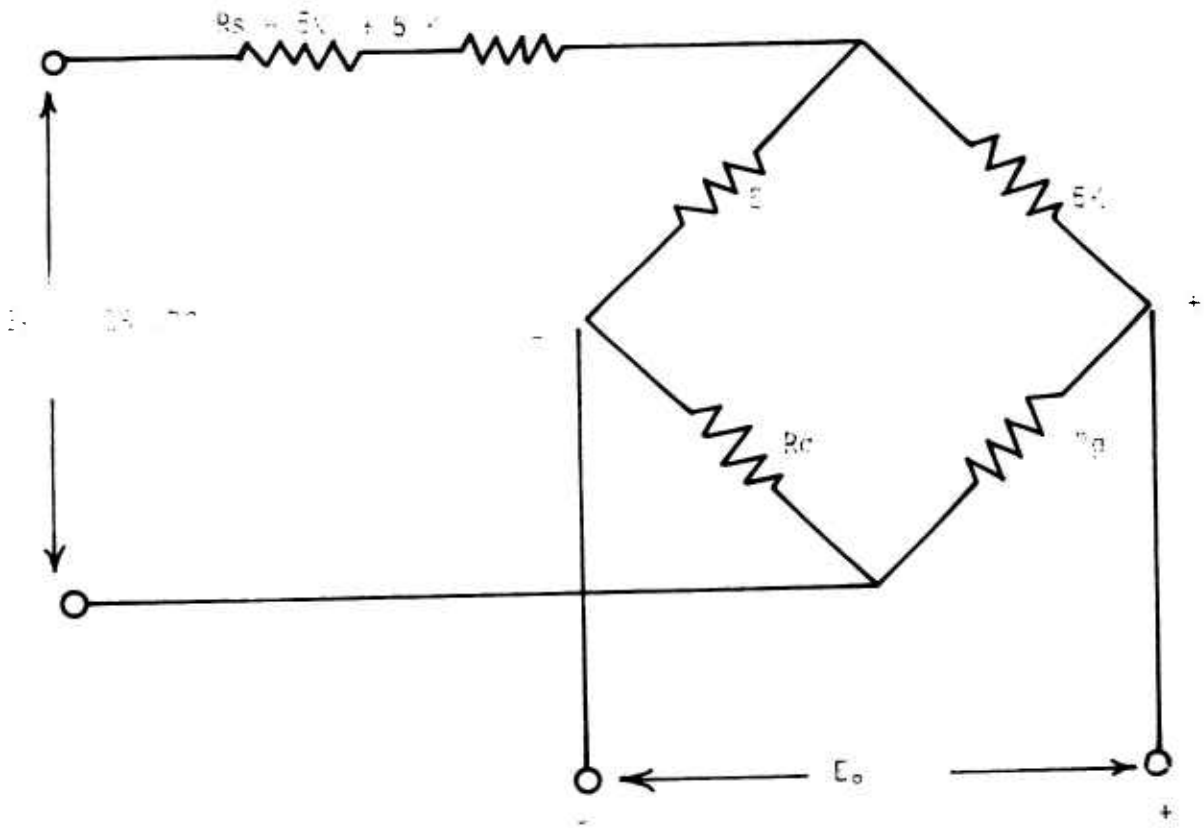

Figure B-6 Circuit Diagram for the Shear Gage H2A, Serial No. 2

APPENDIX C

STV NO. 2 GAGE CALIBRATION AND TEST DATA

RAW CALIBRATION DATA

The following calibration curves for the normal stress gages were obtained (before the grain was cast) with the units bonded in place in the STV. The motor was internally pressurized in 10 psi steps while the electrical output of the gages was monitored. The results are given in Figures C-1 to C-8 for test temperatures of 28°, 77° and 130°F. The finally accepted gage calibration data are summarized in Table C-1.

Additional shunt resistances were added to the circuits to reduce the output voltages at zero stress. All of the normal stress gages received these shunts after the 130°F calibrations, while gages 3-1, 3-2, and 4-2 received additional shunts after the calibrations at 28°F (the final temperature for the pressure calibration measurements). These shunts produced vertical shifts in the curves of Figures C-1 to C-8, but did not change the slopes of these lines. Therefore, it was only necessary to return the STV to each test temperature (28°, 70° and 130°F) and measure the new zero stress output voltages. These latter voltage measurements are also tabulated in Table C-1.

The shear gage sensitivity data, also summarized in Table C-1, were obtained at 34, 78, and 145°F. These test results are shown in Figures C-9 and C-10. The zero stress calibrations were obtained at 28, 70, and 130°F along with those taken on the normal stress gages.

After grain casting the STV was subjected to hydrostatic pressure and vacuum loadings on the grain at temperatures from 30 to 130°F. The gage output data are given in Figures C-11 to C-27.

CALIBRATION BEHAVIOR OF PROPELLANT POTTED NORMAL STRESS GAGES

The two normal stress gages, N-1 and N-2, were initially bonded in place within the STV and were then embedded within live propellant in the shape of a rough 1-inch diameter hemisphere. This is the calibration technique previously devised at Lockheed Propulsion Company.

Gage No. 1 behaved exactly as expected with no special problems. The gage sensitivities for the two half-bridge circuits are shown in Figures C-28 and C-29. Both half bridge circuits showed the same small loss in sensitivity when calibrated after potting the gage in-situ in the propellant (compared to the Konigsberg Instrument fluid calibration).

After casting and curing the propellant grain the gages were again subjected to hydrostatic pressure testing at 30°, 70° and 110°F using 10 psi pressure steps to 50 psig, and vacuum pressure testing to about 5.1 psia. Structural analyses of this grain showed that the nearly incompressible grain should only slightly attenuate the pressure (applied equally to both ends of the grain). That is, about 99.2% of the applied pressure should be observed at the gage.

Expressed mathematically, we can show that the gage sensitivity, b, may be obtained directly from a plot of voltage output, v, and the applied pressure, p,

$$\frac{dv}{dp} = -f_n b \qquad \text{(C-1)}$$

where f_n is the fraction of the hydrostatic pressure that reaches the gage.

We believe that the observed decrease in gage output is consistent with good gage performance and is due to attenuation in the propellant caused by its porosity. An estimated 5% stress decrease is believed attributable to this cause. The remaining differences are within 5% of the original gage calibration results, which is considered to be a reasonable error band for these gages.

Initially, gage N-2 behaved normally and showed only small losses in sensitivity after the potting operation, as shown in Figures C-30 and C-31. Also, subsequent pressure test data after the grain was cast showed no unexpected results. However, gage N2-1 evinced serious difficulties in the step vacuum test, which was applied to the cast and cured STV grain. This gage showed a very high response at 30°F when compared with the pressure test response at the same temperature. The cause of this excessive response to vacuum at 30°F is not known. A possible explanation is the presence of a void or unbond adjacent to the diaphragm of the gage.

Gage N2-2 did not read after the preliminary 70°F pressure test because of a broken connection. Thus, gage No. 2 was not used in any of the planned comparisons between gage pre-potting and potting in-place in the motor.

CALIBRATION BEHAVIOR OF THE PRE-POTTED NORMAL STRESS GAGES

Gages N-3 and N-4, both with redundant dual half-bridge circuits, were potted into a 3/4-inch diameter by 3/8-inch tall cylinder of IBT 115 trowelable insulation material, as described previously. The potting was performed by ASPC personnel at Konigsberg Instruments' Pasadena facility. Pressure calibration and thermal zero and span compensation were also performed on the pre-potted gages at Konigsberg's Pasadena facility.

Following calibration and temperature compensation the gages were shipped to ASPC and installed within recessed holes in the V45 insulation of STV No. 2 using the IBT-115 material as an adhesive.

The sensitivity data from gage N-3 were not as good as those from gage No. 4. Figures C-32 and C-33 contain the sensitivity versus temperature plots for Gages N3-1 and N3-2 respectively. It was noted that the ASPC pre-casting calibration of the potted gage embedded within the STV resulted in higher sensitivities than those obtained at Konigsberg Instruments. After the grain was cast the gage responses were much closer to the original calibration although they were still high at 110°F.

Examination of the raw data showed distinct curvature of the calibration curves, Figures C-11 to C-27. It is believed that the observed high sensitivity and non-linear behavior of gage N-3 were caused by air bubbles or voids in the potting compound near the gage. The void partially collapses under the pressures used in calibration, thus modifying the stresses seen by the gage diaphragm. (Note: The relative positions of the void and of the diaphragm may lead to stress-increasing or stress-decreasing effects upon the gage).

Clearly, in the potting or pre-potting of the normal stress transducers great care must be taken to exclude voids. This is, of course, true whether the potting material is an inert IBT-115 insulation material or a live propellant.

Gage N-4 behaved in an exemplary fashion throughout, from the initial calibration in the potting material at Konigsberg Instruments to the final pressure step check when embedded within the STV grain at ASPC. The gage sensitivity versus temperature curves for the two half-bridge circuits are shown in Figures C-34 and C-35. These curves show that

the initial calibration at Konigsberg Instruments and the later ASPC calibration with the gage bonded in place in the STV resulted in almost identical gage sensitivities at the three temperatures. As expected, the hydrostatic pressure and vacuum testing of the STV after the propellant grain was cast showed smaller, but acceptable (considering grain attenuation and a 5% error band) gage response.

TABLE C-1

SUMMARY OF STV NO. 2 GAGE CALIBRATION DATA

Gage Number	Gage Sensitivities*			Zero Stress Output (in STV)		
	28°F	77°F	130°F	28°F	70°F	130°F
N1-1	0.679 MV/psi	0.779	0.793	0.25 MV	0.104	0.042
N1-2	0.661	0.775	0.808	0.72	-0.800	0.933
N2-1	0.816	0.826	0.815	2.00	0.120	0.667
N2-2	0.818	0.829	0.815	1.90	0.247	0.198
N3-1	0.916	0.935	0.920	2.04	0.084	-2.451
N3-2	0.938	0.948	0.933	2.23	-0.416	-3.066
N4-1	0.819	0.845	0.841	1.84	0.587	-1.413
N4-2	0.787	0.810	0.803	-0.60	-0.147	0.016
	34°F	78°F	143°F			
SH-1	4.08 MV/psi	4.62	5.50	1.17	-2.480	-4.257
SH-2	-5.41	-6.25	-6.71	6.26	1.540	-3.228

* Sign convention for normal stress transducer sensitivity: output is positive for a pressure load (compressive stress).

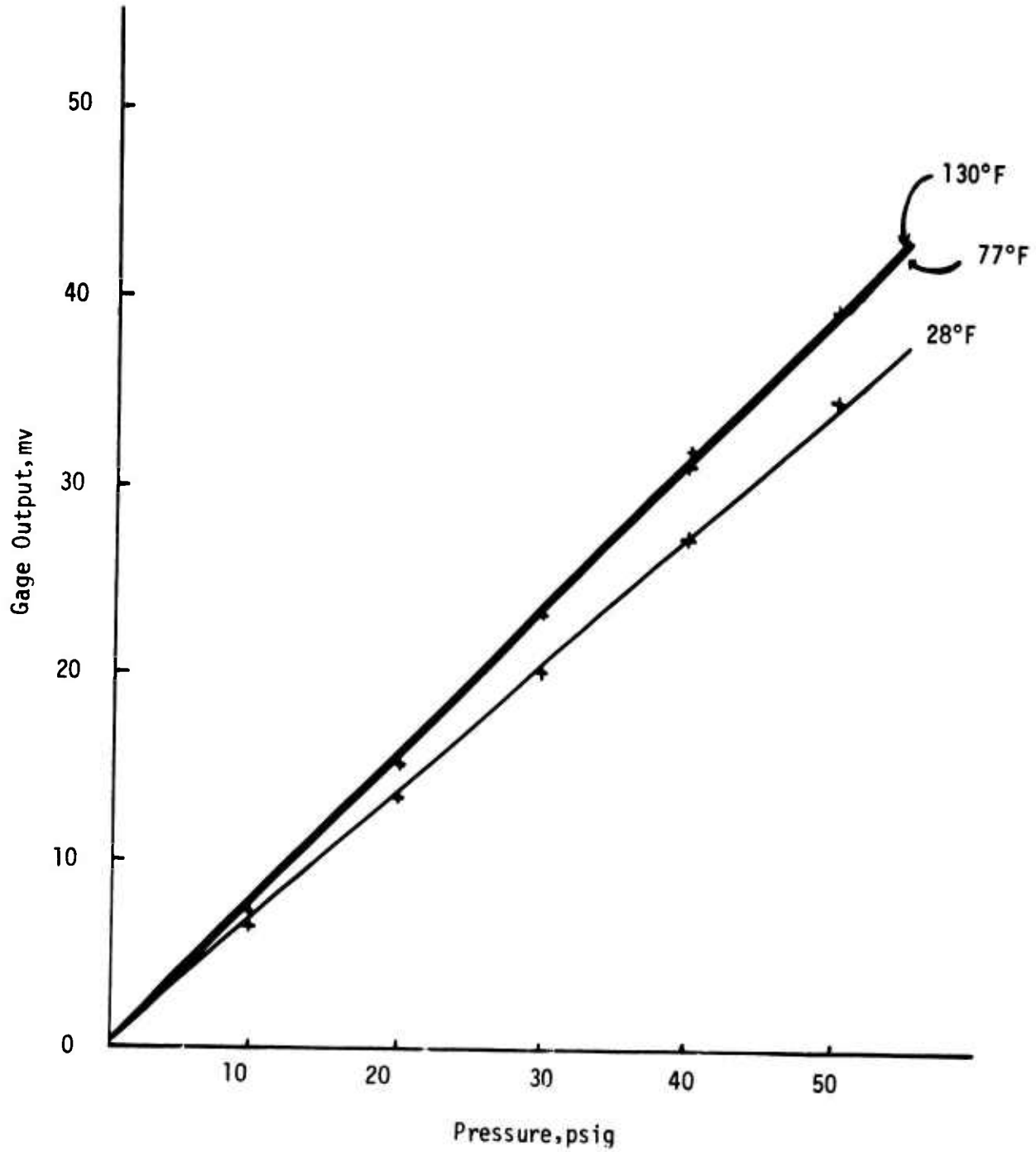

Figure C-1. STV No. 2 Normal Gage N1-1

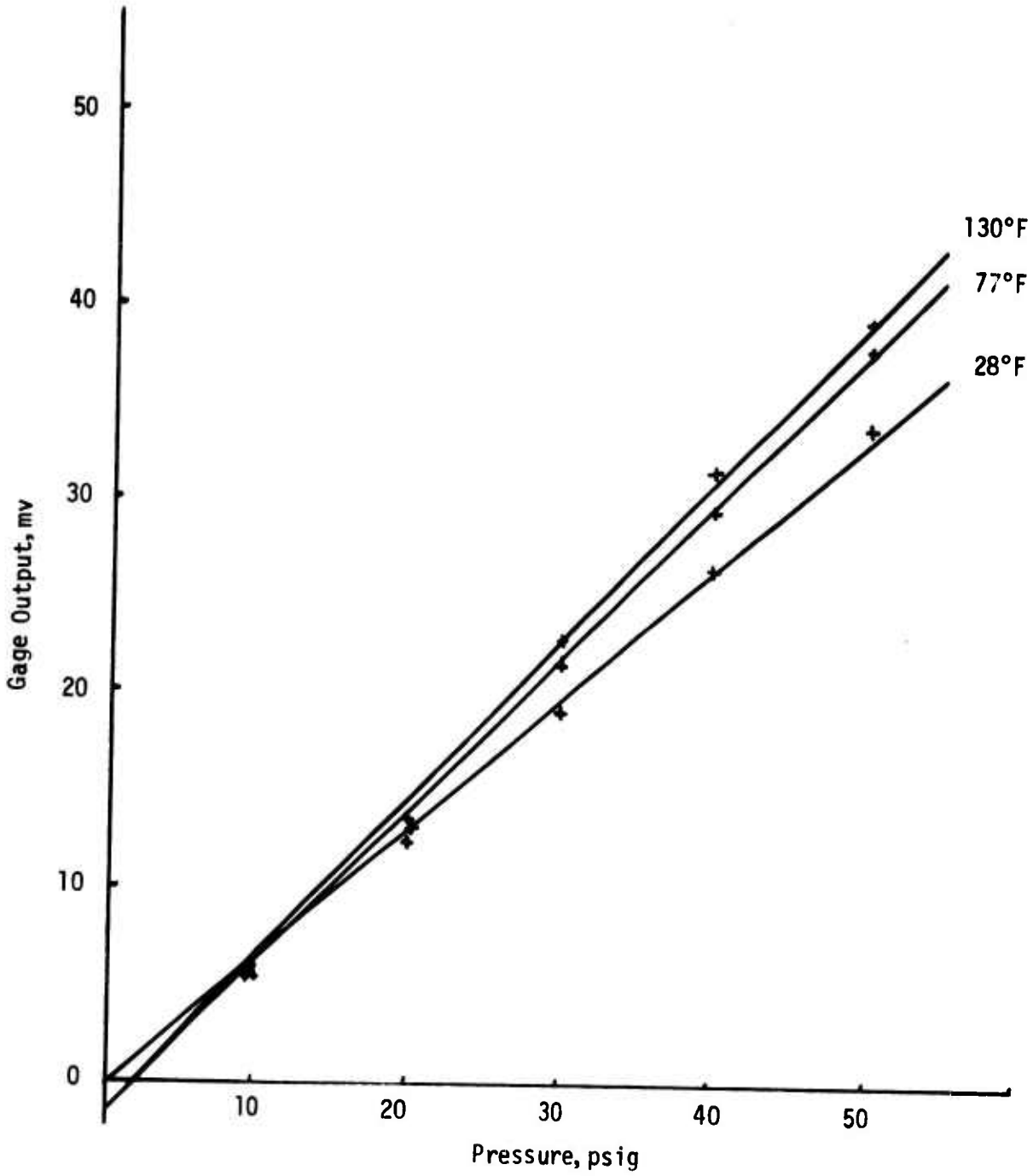

Figure C-2. STV No. 2 Normal Gage N1-2

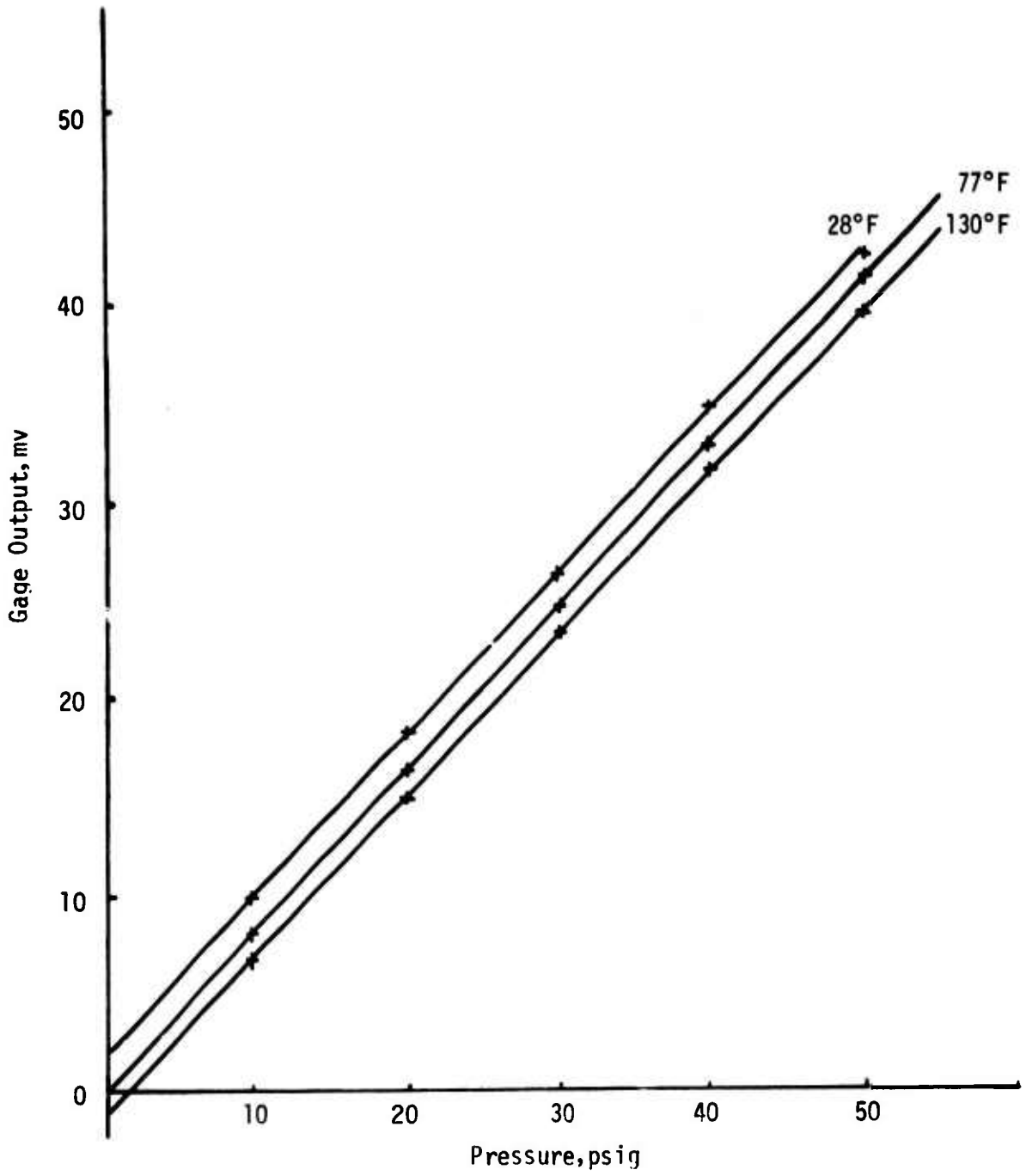

Figure C-3. STV No. 2 Normal Gage N2-1

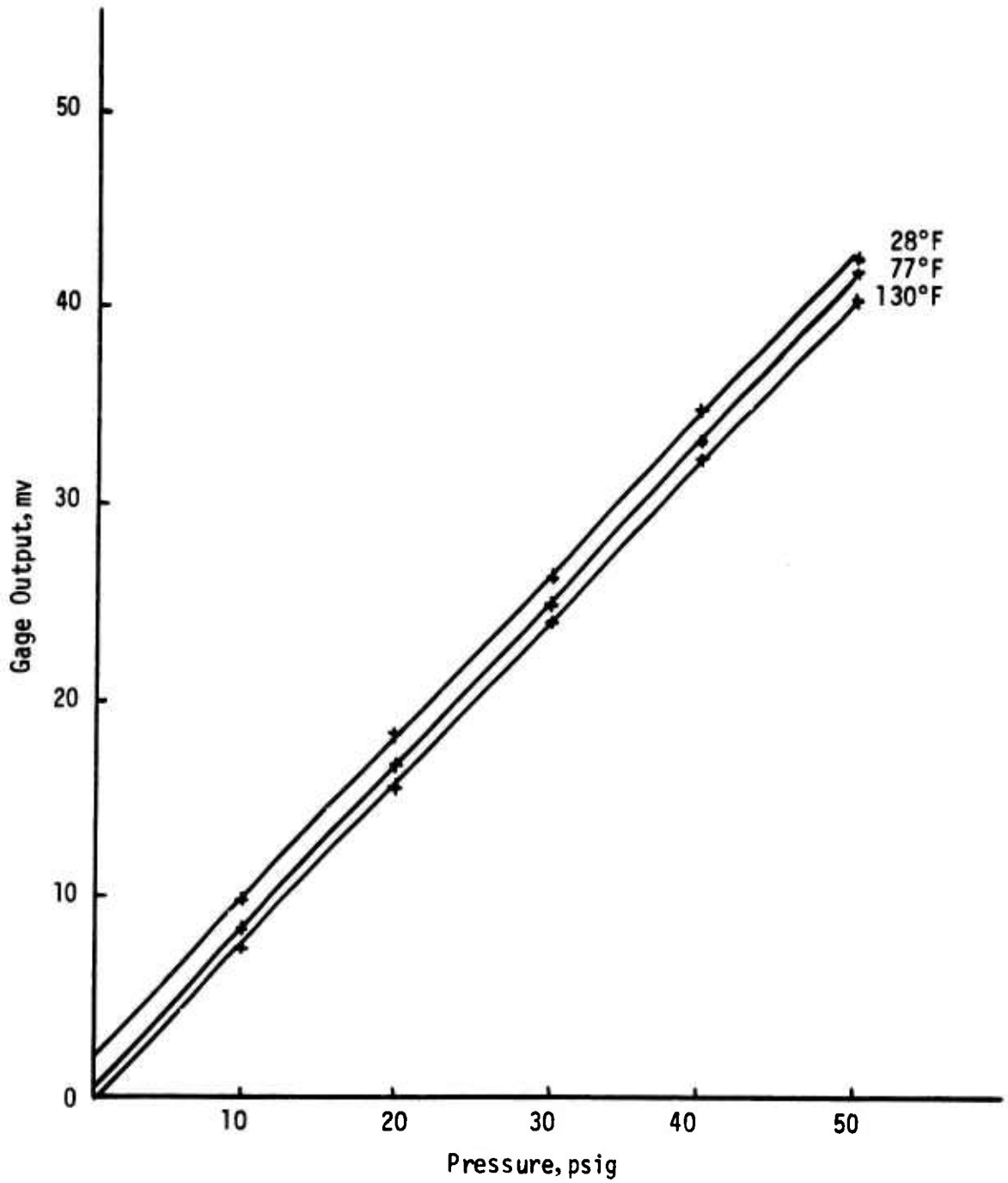

Figure C-4. STV No. 2 Normal Gage N2-2

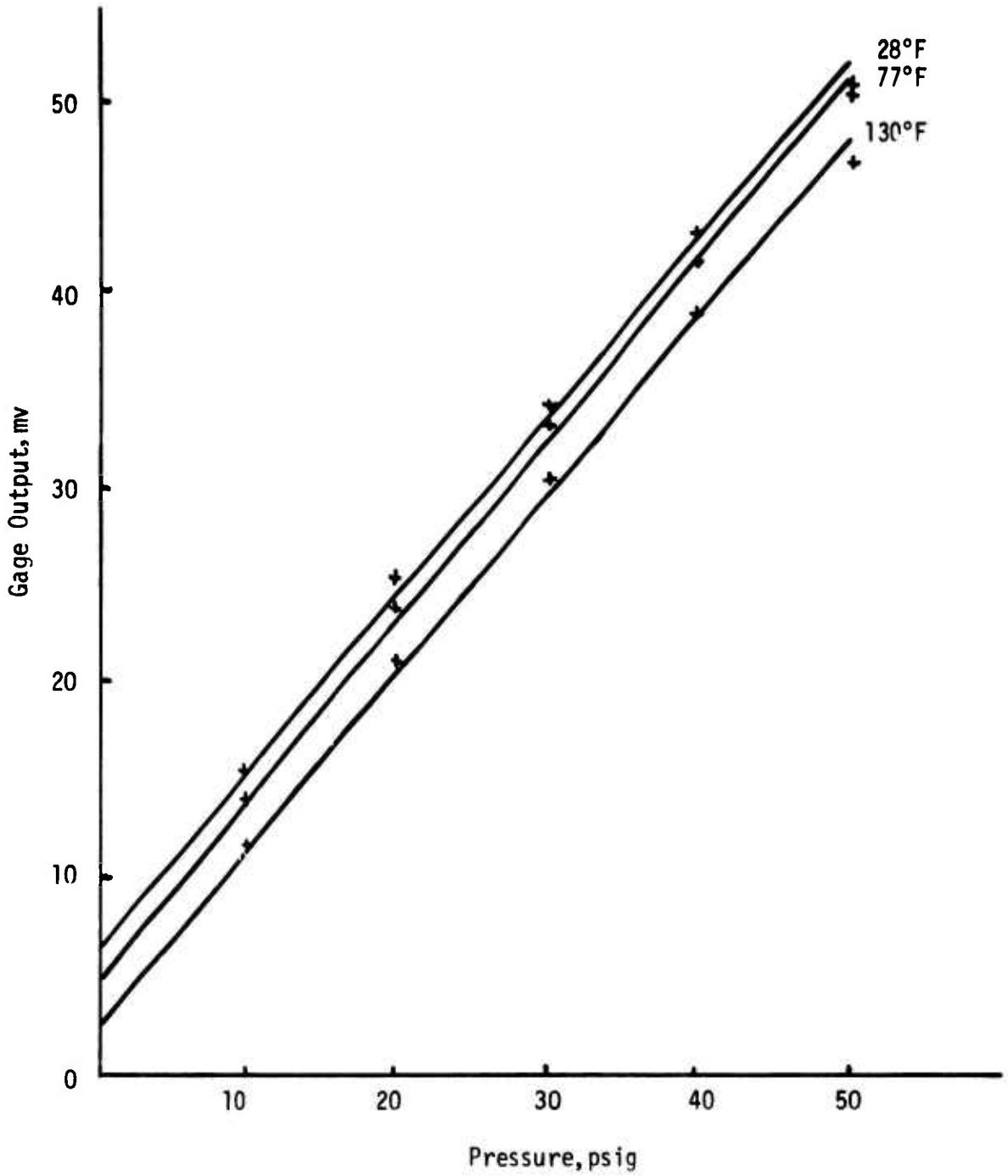

Figure C-5. STV No. 2 Normal Gage N3-1
(Best Linear Fit)

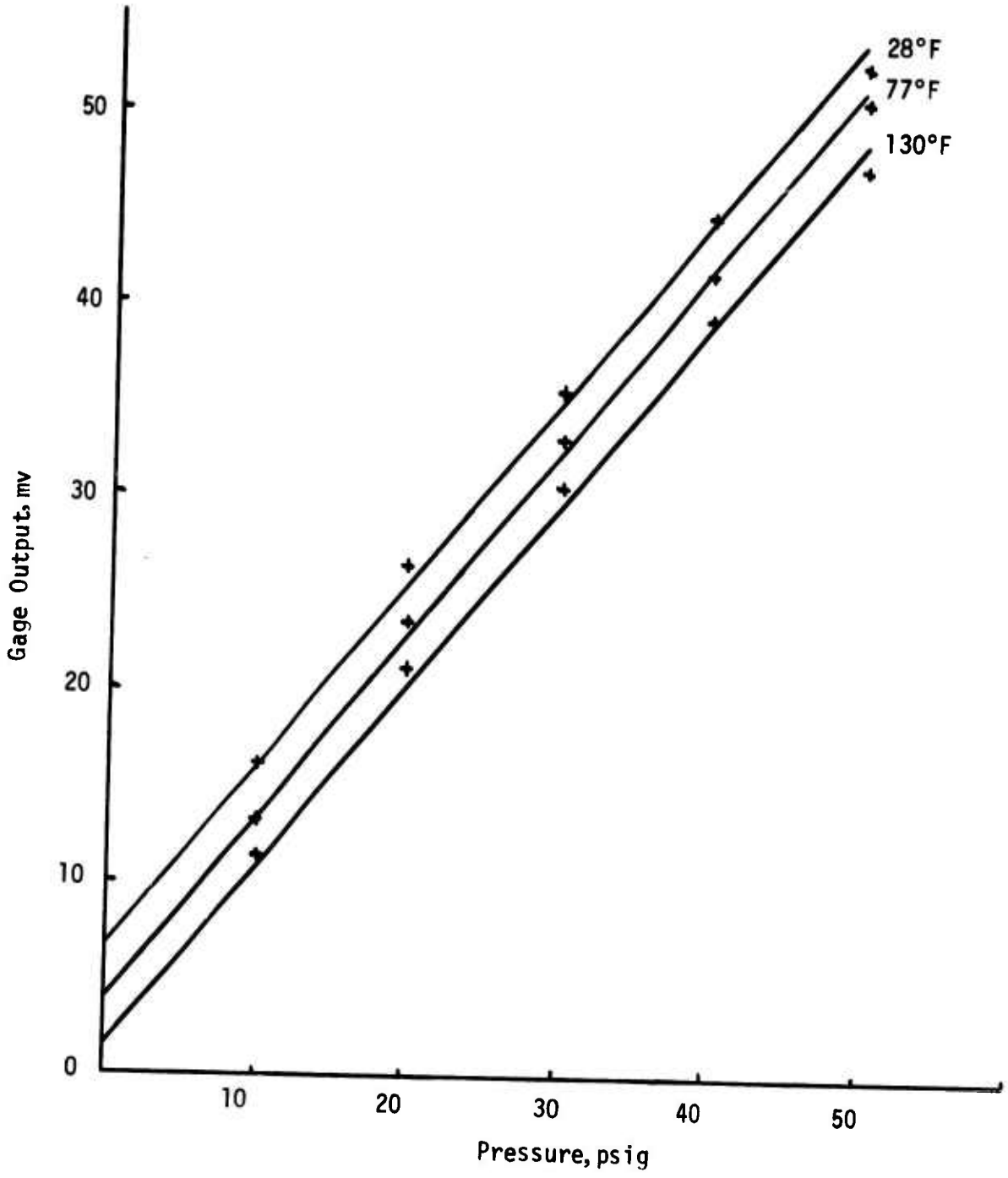

Figure C-6. STV No. 2 Normal Gage N3-2
(Best Linear Fit)

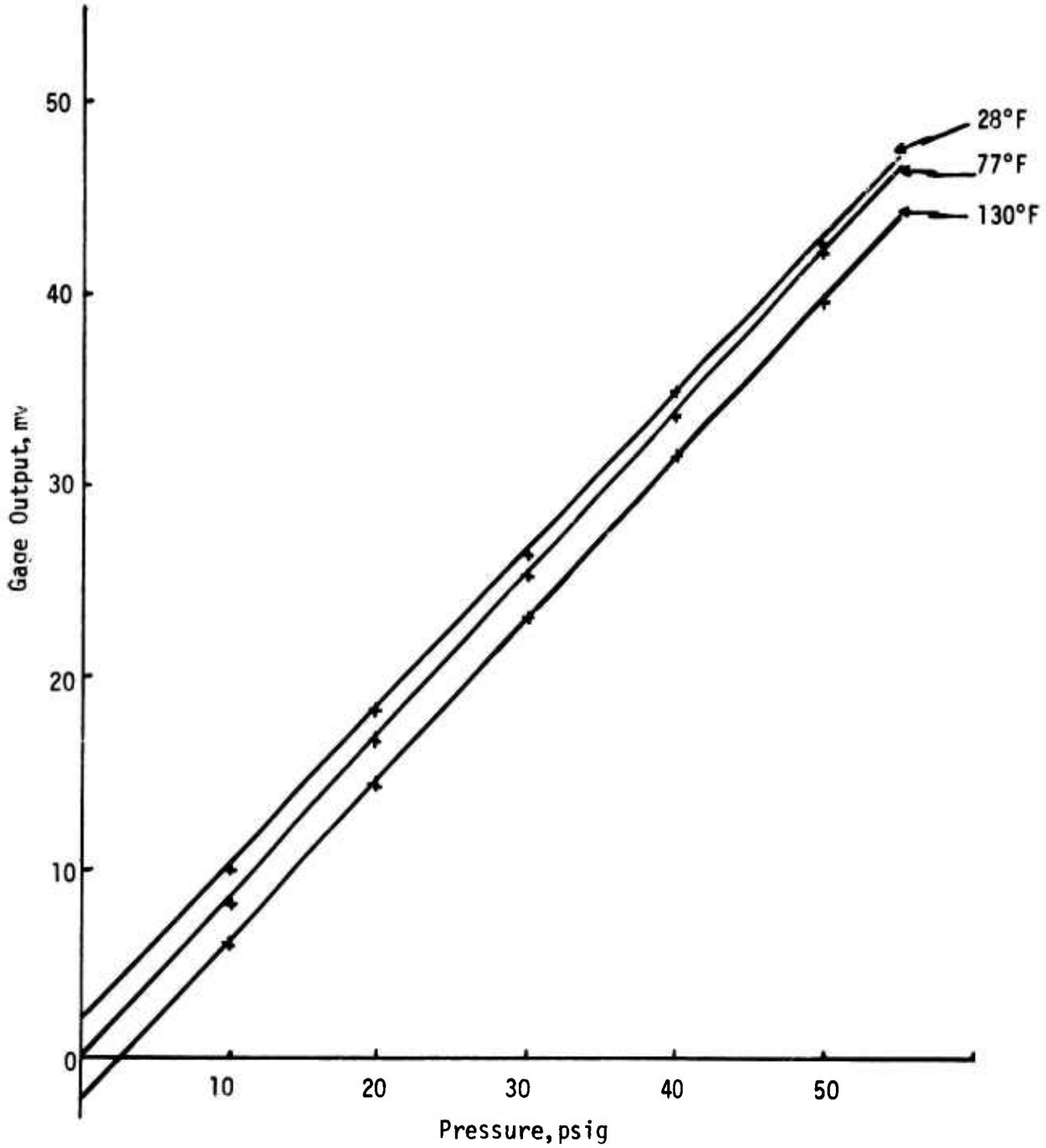

Figure C-7. STV No. 2 Normal Gage N4-1

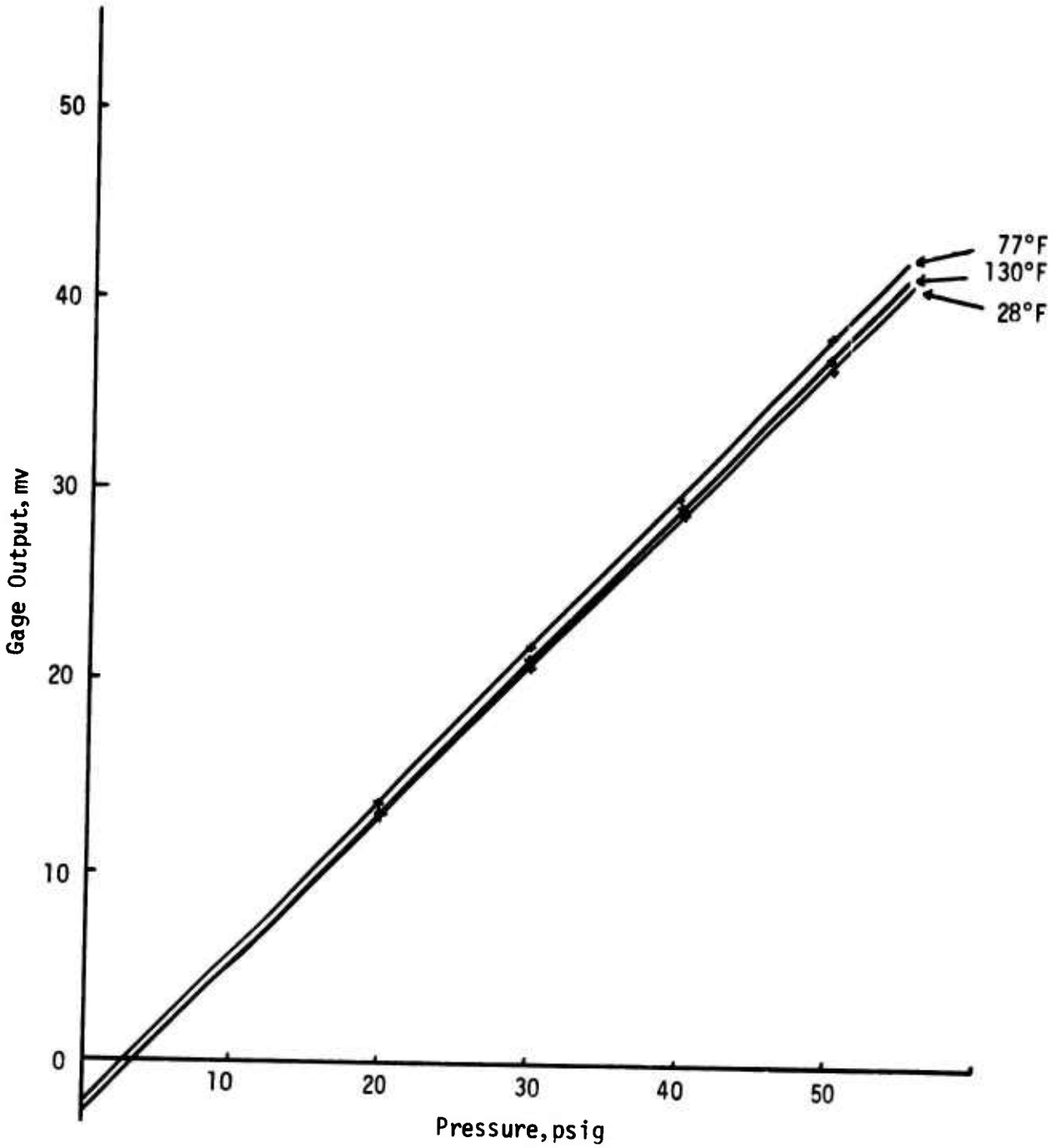

Figure C-8. STV No. 2 Normal Gage N4-2

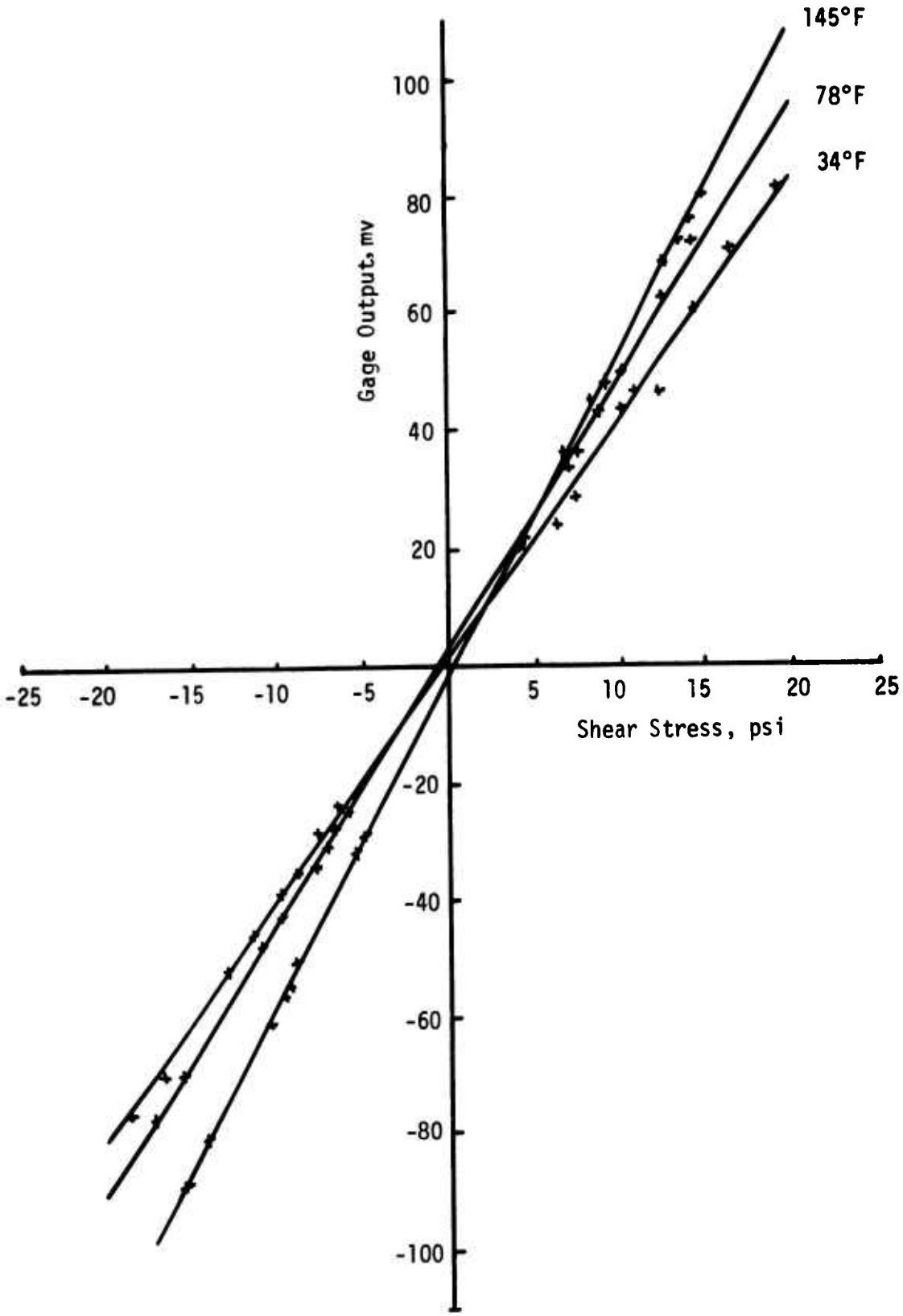

Figure C-9. STV No. 2 Shear Gage SH-1

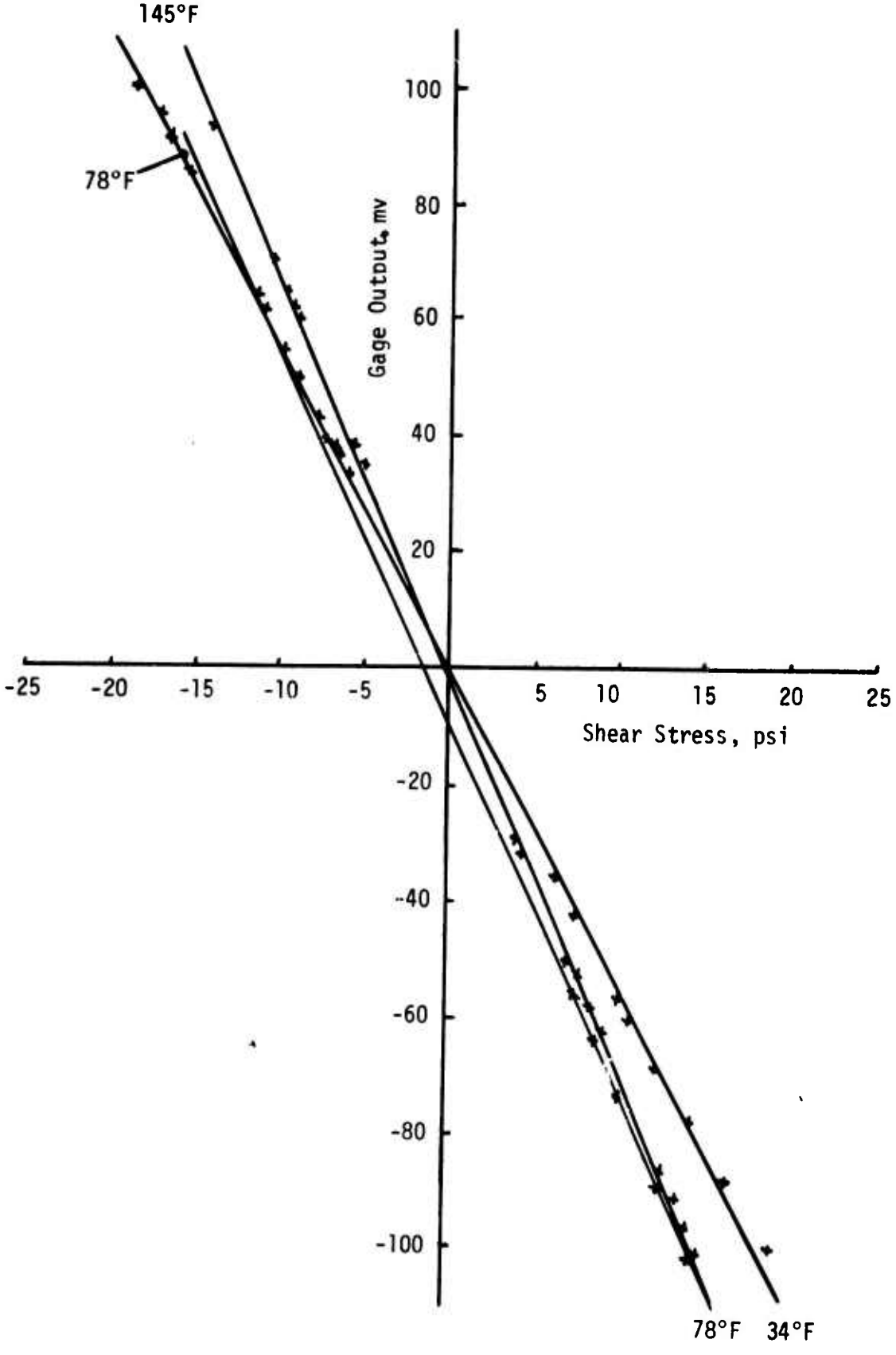

Figure C-10. STV No. 2 Shear Gage SH-2

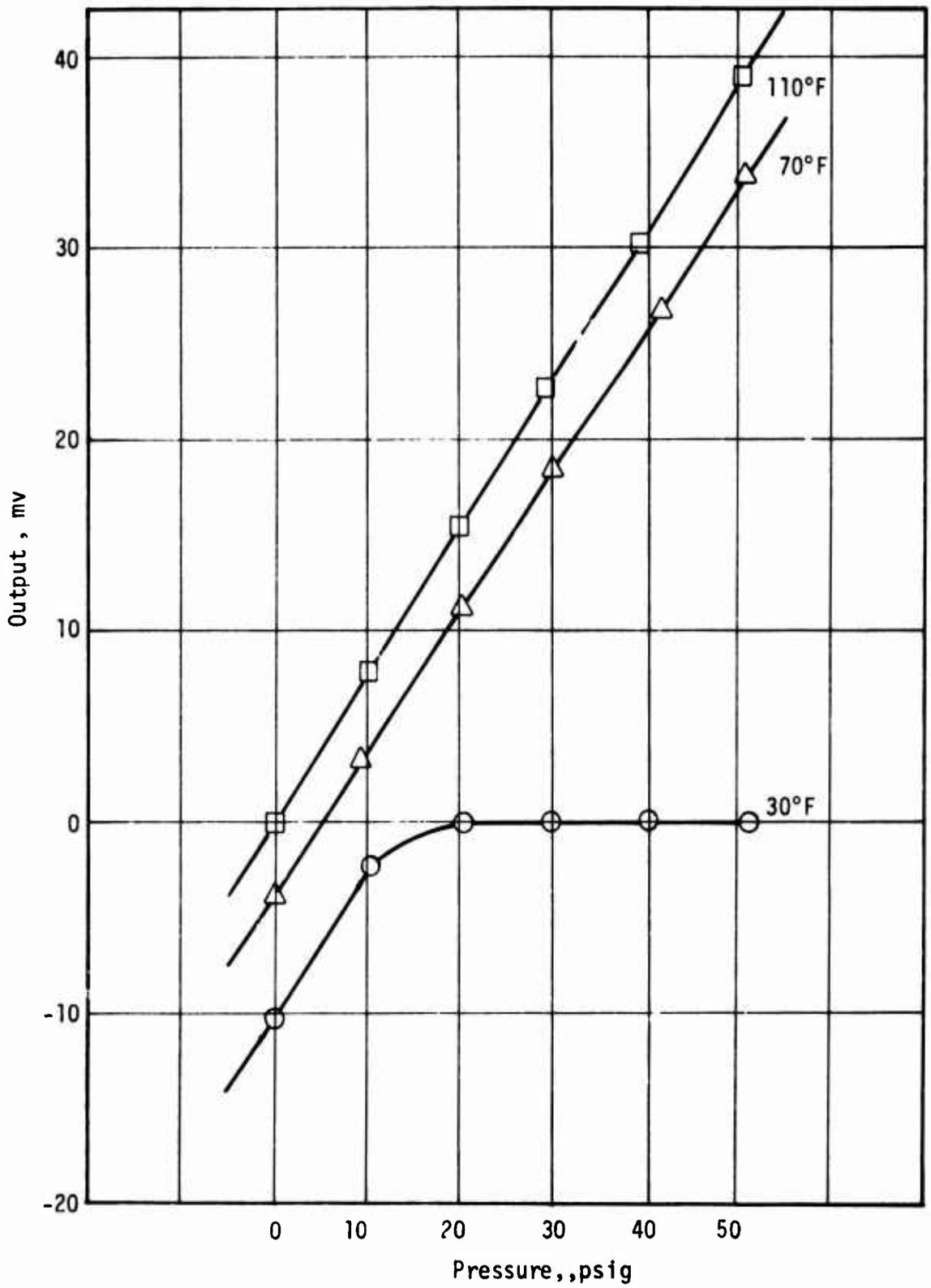

Figure C-11. Millivolt Output of Normal Stress Gage N1-1 During Hydrostatic Pressure Test of Propellant Grain STV-2

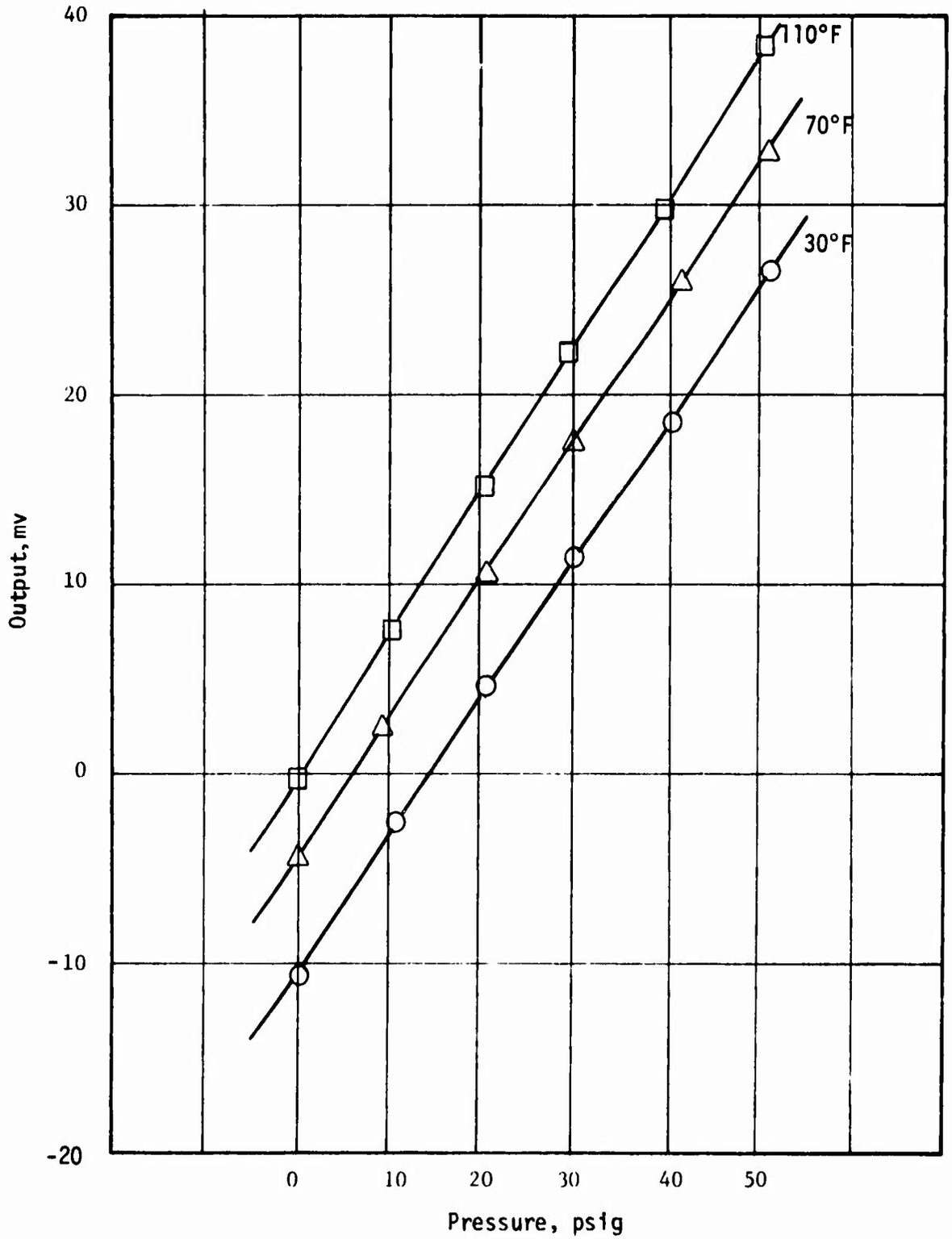

Figure C-12. Millivolt Output of Normal Stress Gage N1-2 During Hydrostatic Pressure Testing of Propellant Grain

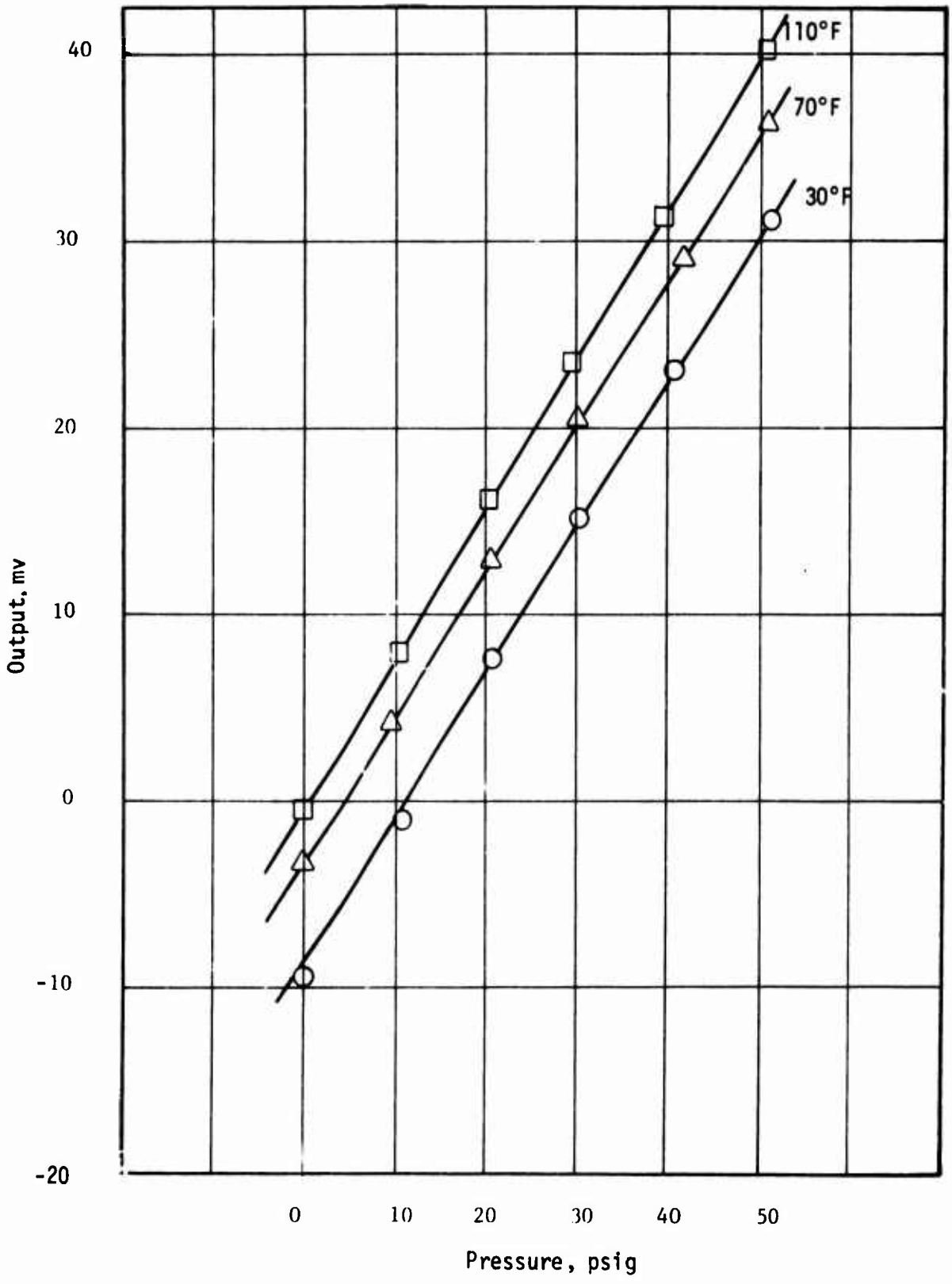

Figure C-13. Millivolt Output of Normal Stress Gage N2-1 During Hydrostatic Pressure Testing of Propellant Grain

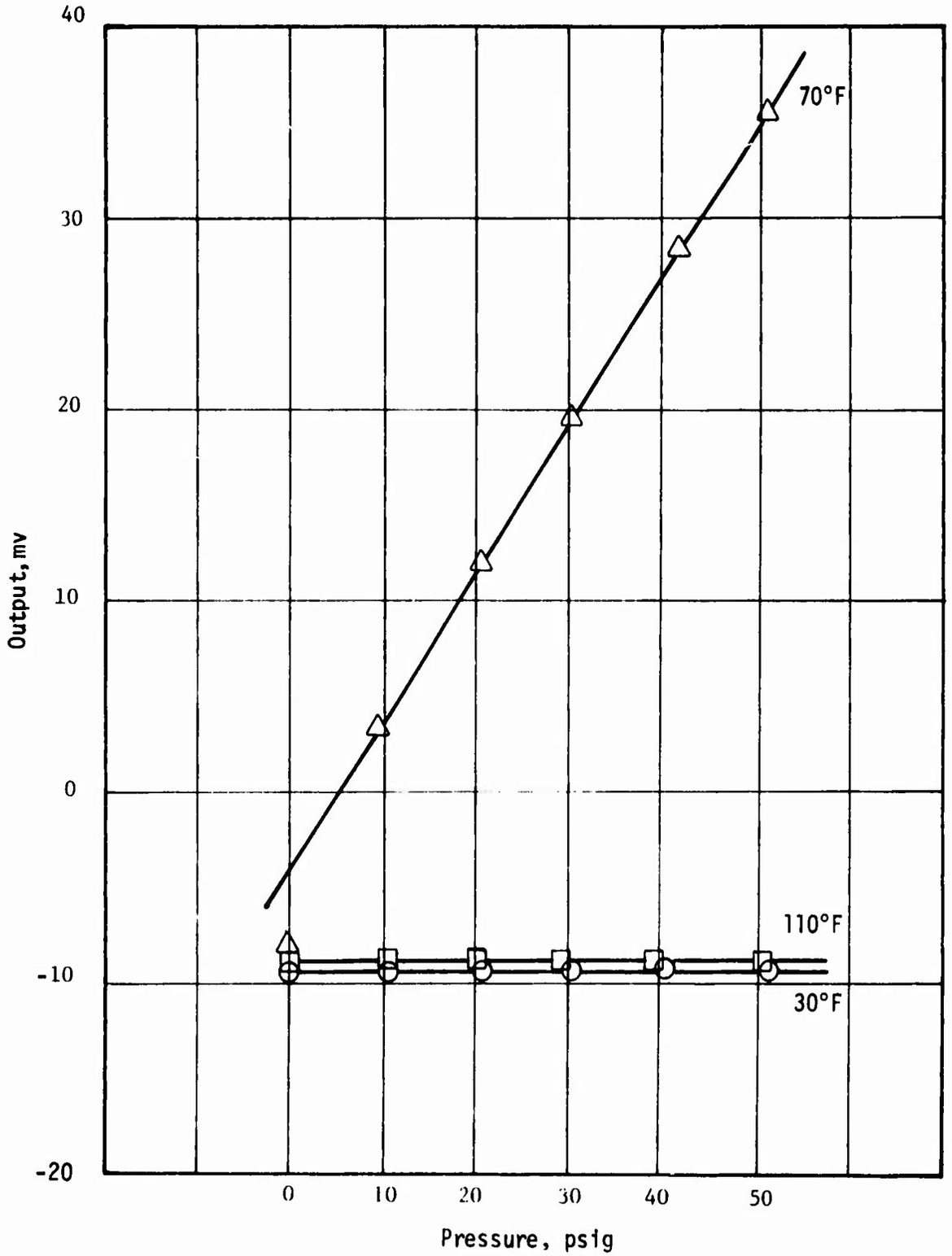

Figure C-14. Millivolt Output of Normal Stress Gage N2-2 During Hydrostatic Pressure Testing of Propellant Grain

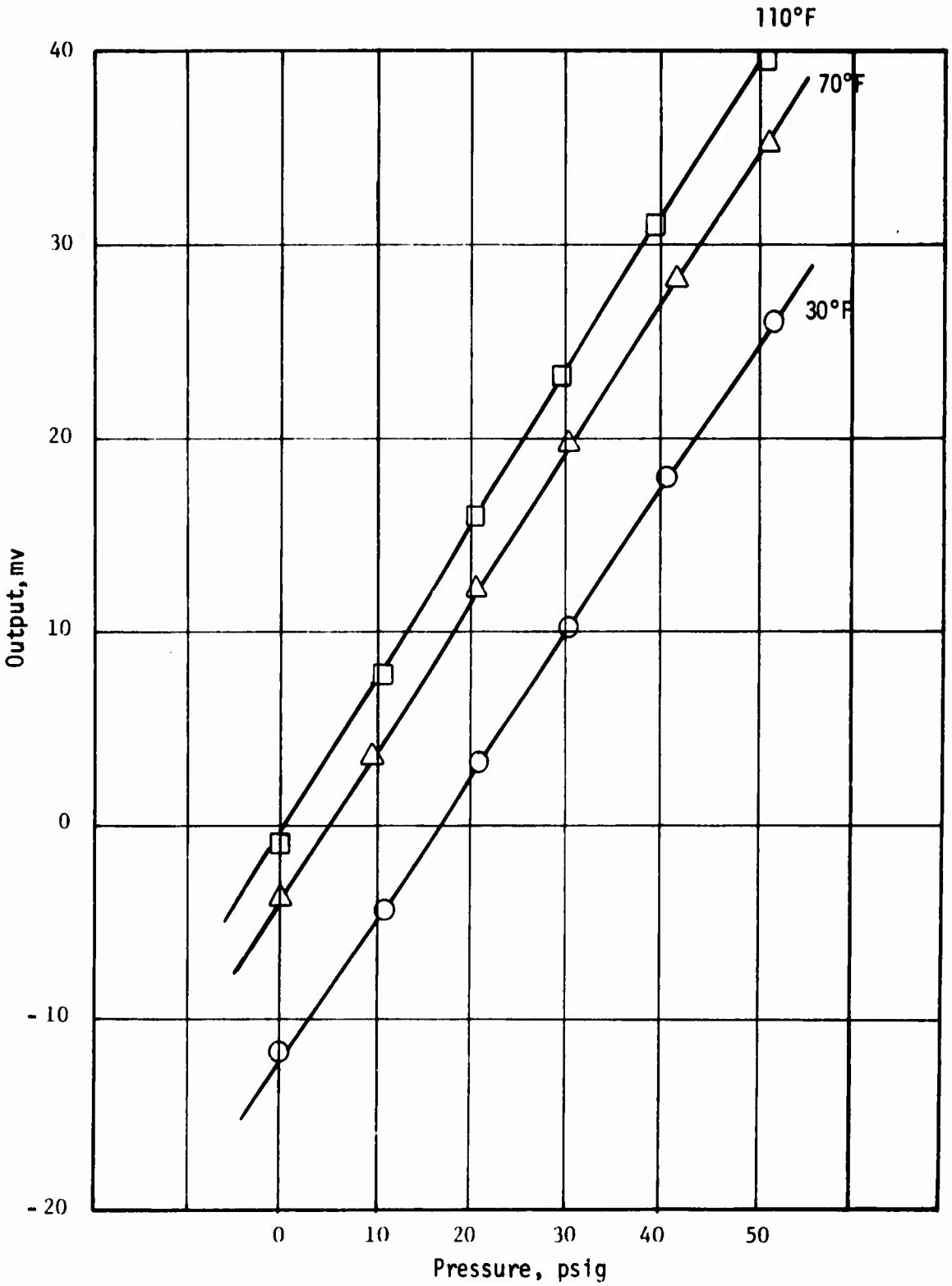

Figure C-15. Millivolt Output of Normal Stress Gage N3-1 During Hydrostatic Pressure Testing of Propellant Grain

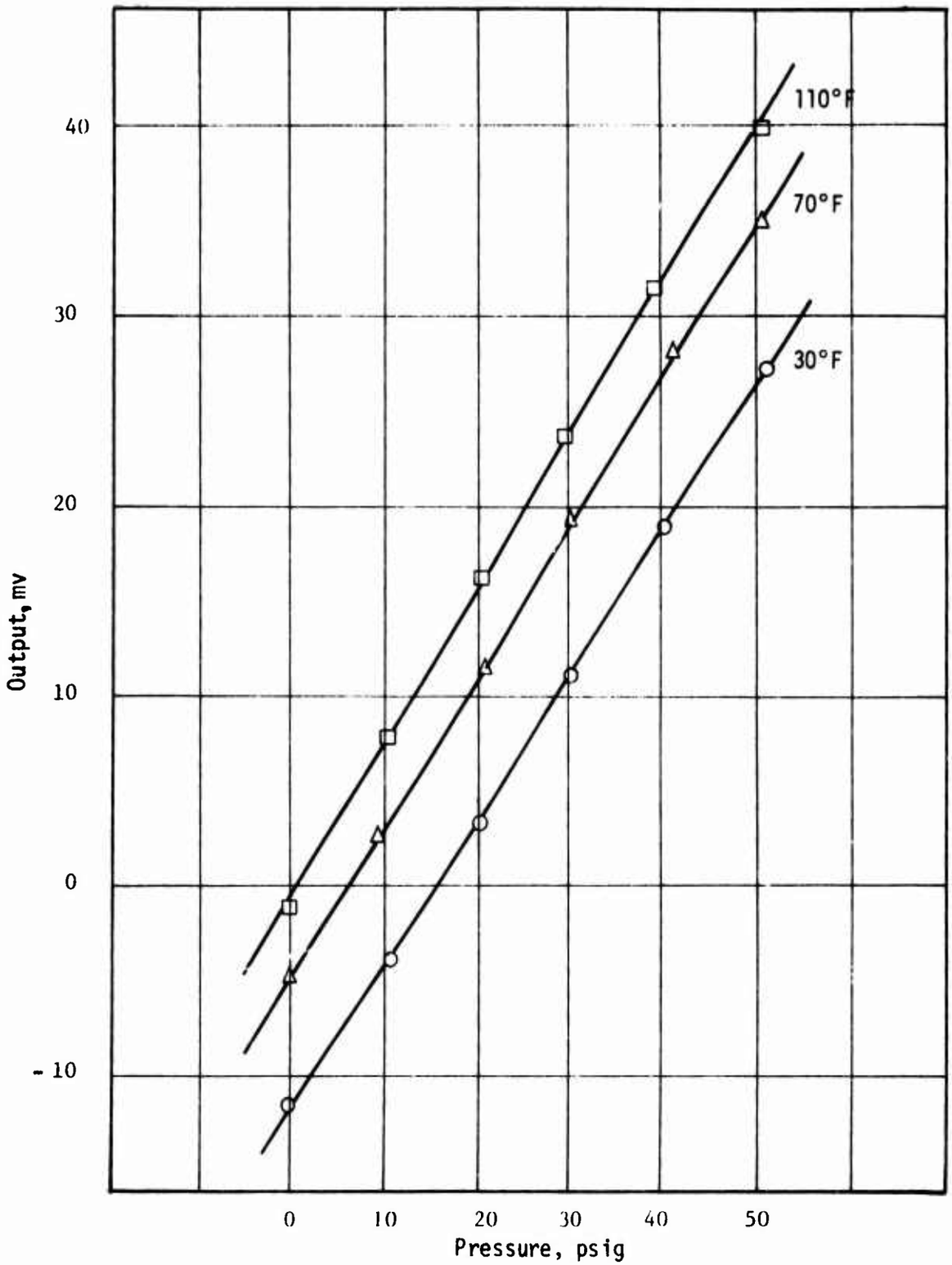

Figure C-16. Millivolt Output of Normal Stress Gage N3-2 During Hydrostatic Pressure Testing of Propellant Grain

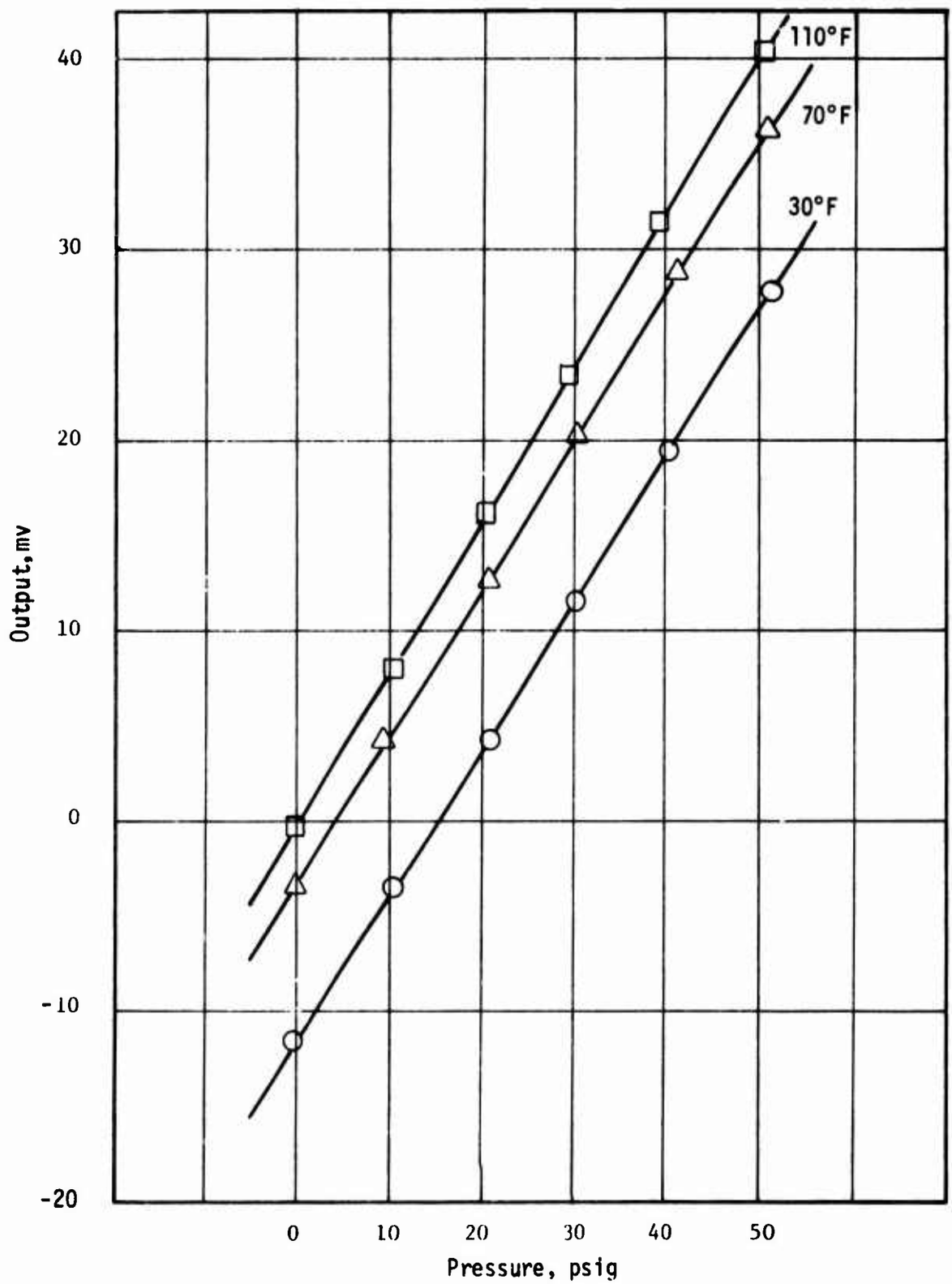

Figure C-17. Millivolt Output of Normal Stress Gage N4-1 During Hydrostatic Pressure Testing of Propellant Grain

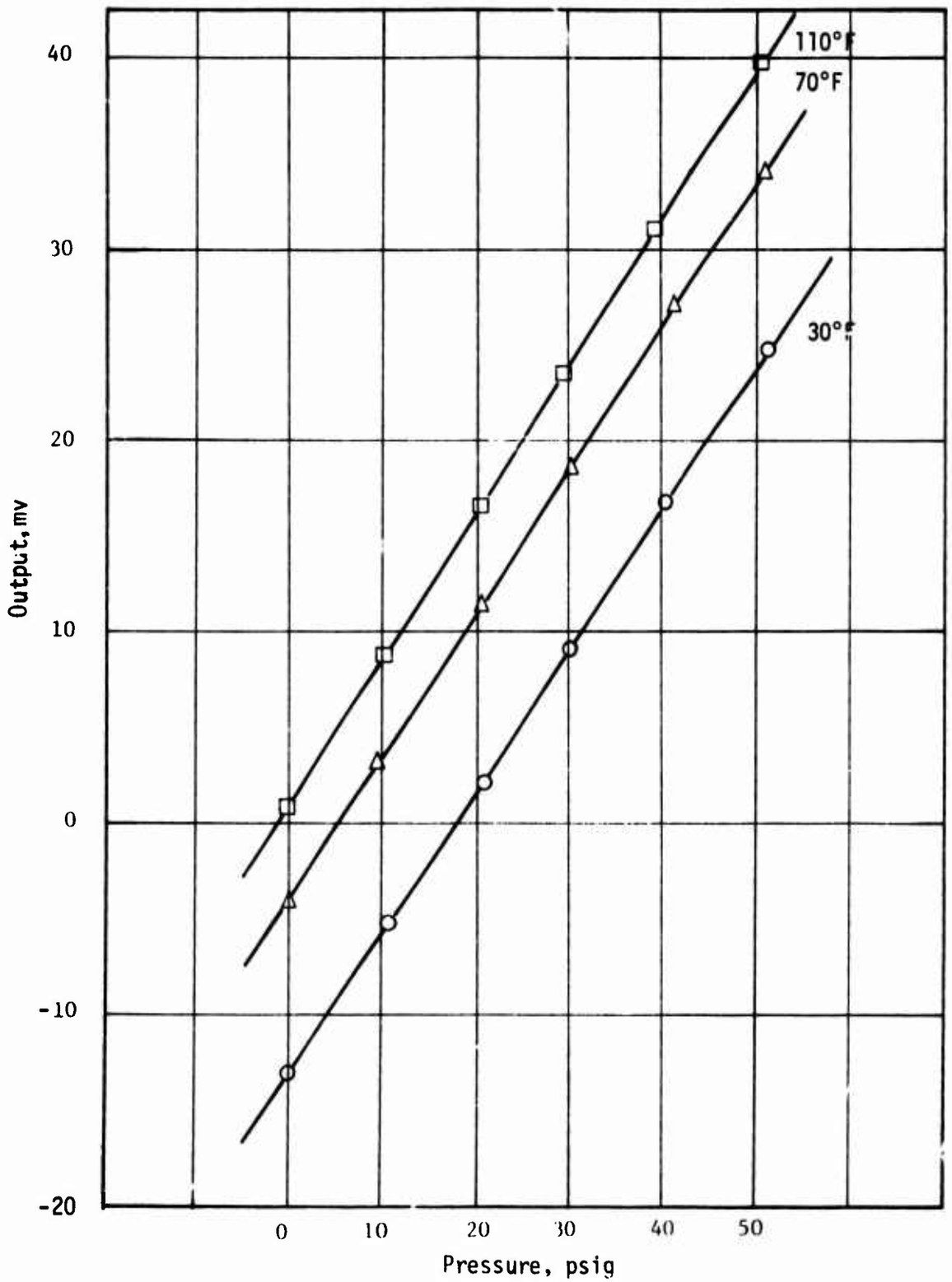

Figure C-18. Millivolt Output of Normal Stress Gage N4-2 During Hydrostatic Pressure Testing of Propellant Grain

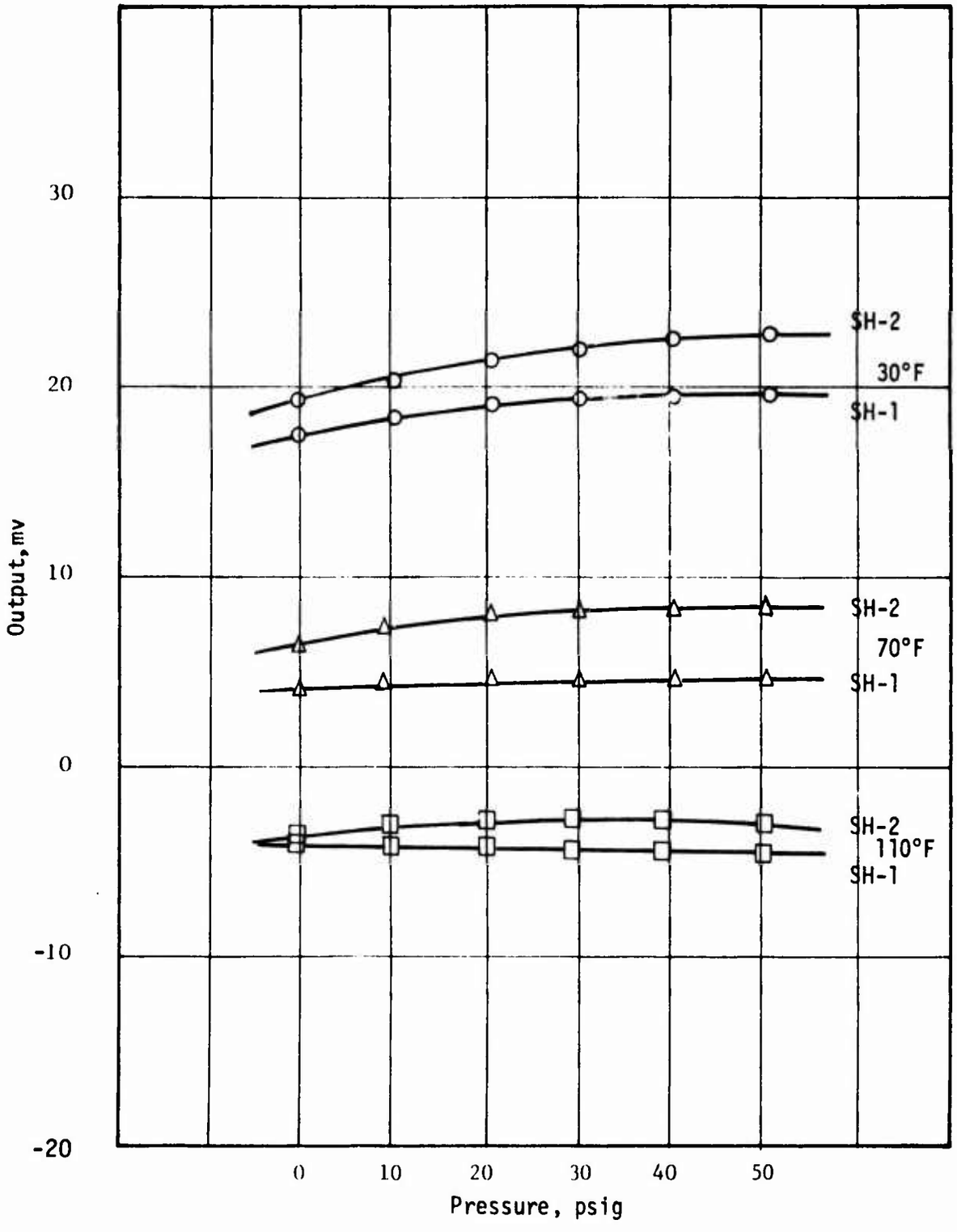

Figure C-19. Millivolt Output of Shear Stress Gages SH-1 and SH-2 During Vacuum Testing of Propellant Grain STV-2

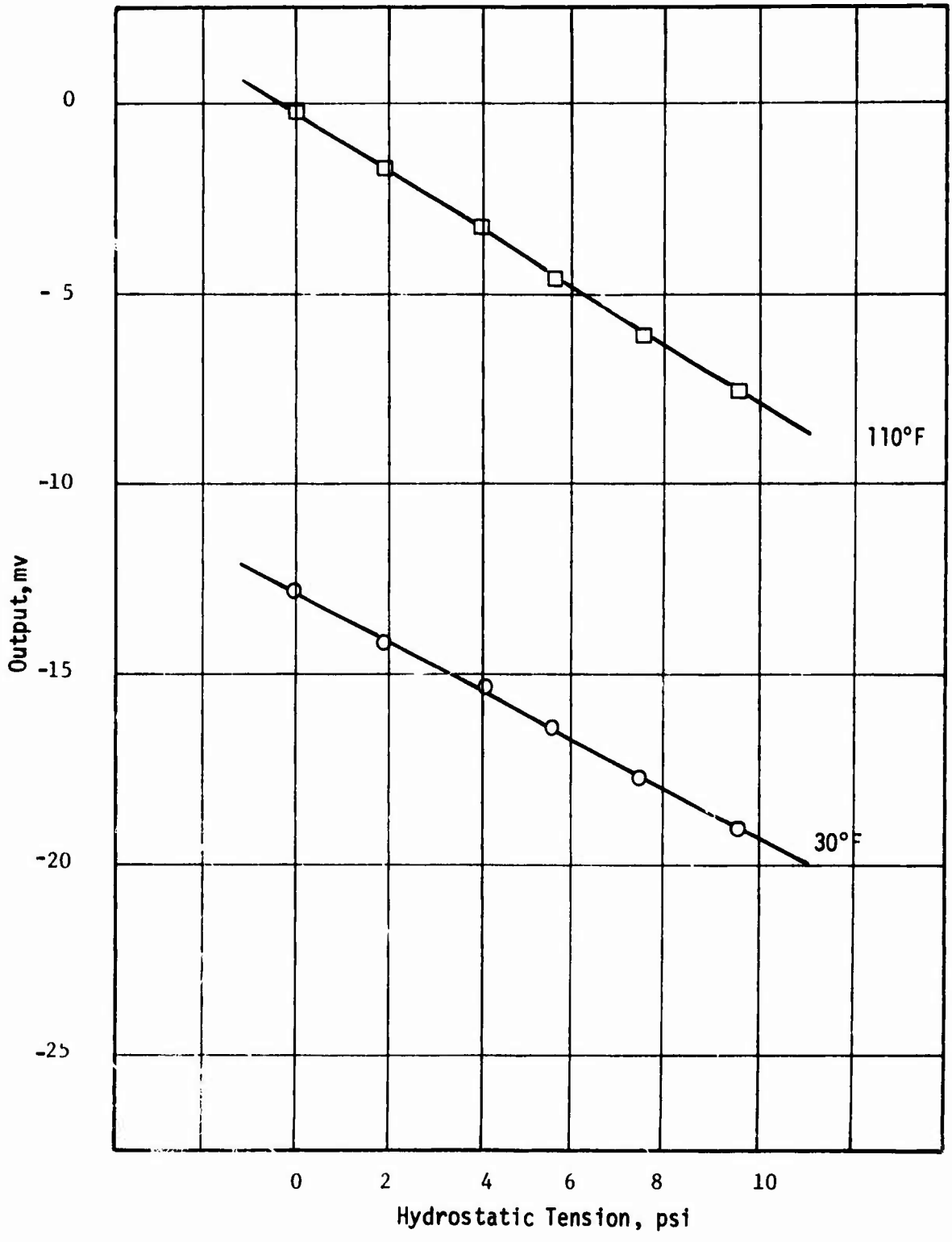

Figure C-20. Millivolt Output of Normal Stress Gage N1-1 During Vacuum Testing of Propellant Grain STV-2

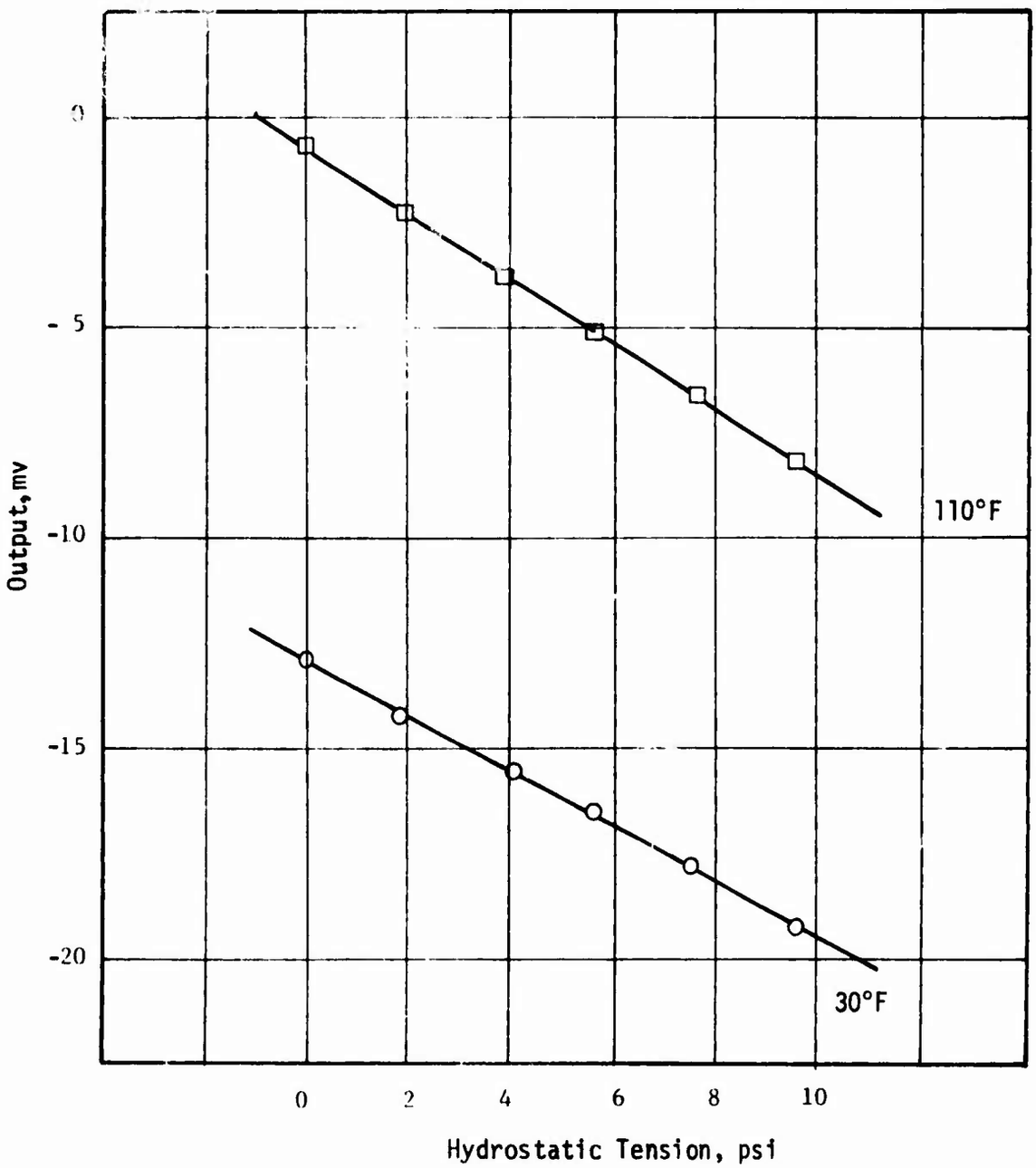

Figure C-21. Millivolt Output of Normal Stress Gage N1-2 During Vacuum Testing of Propellant Grain STV-2

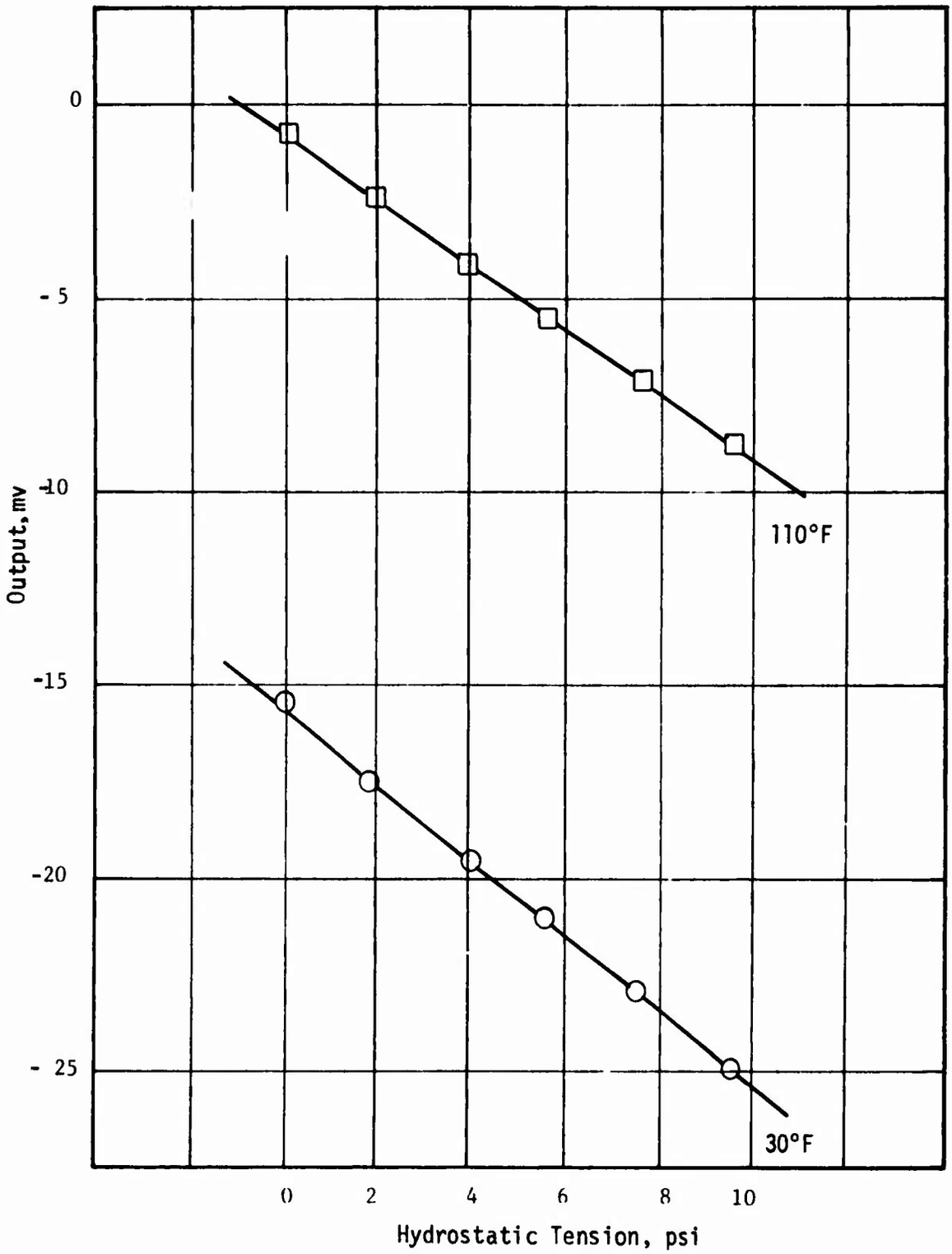

Figure C-22. Millivolt Output of Normal Stress Gage N2-1 During Vacuum Testing of Propellant Grain STV-2

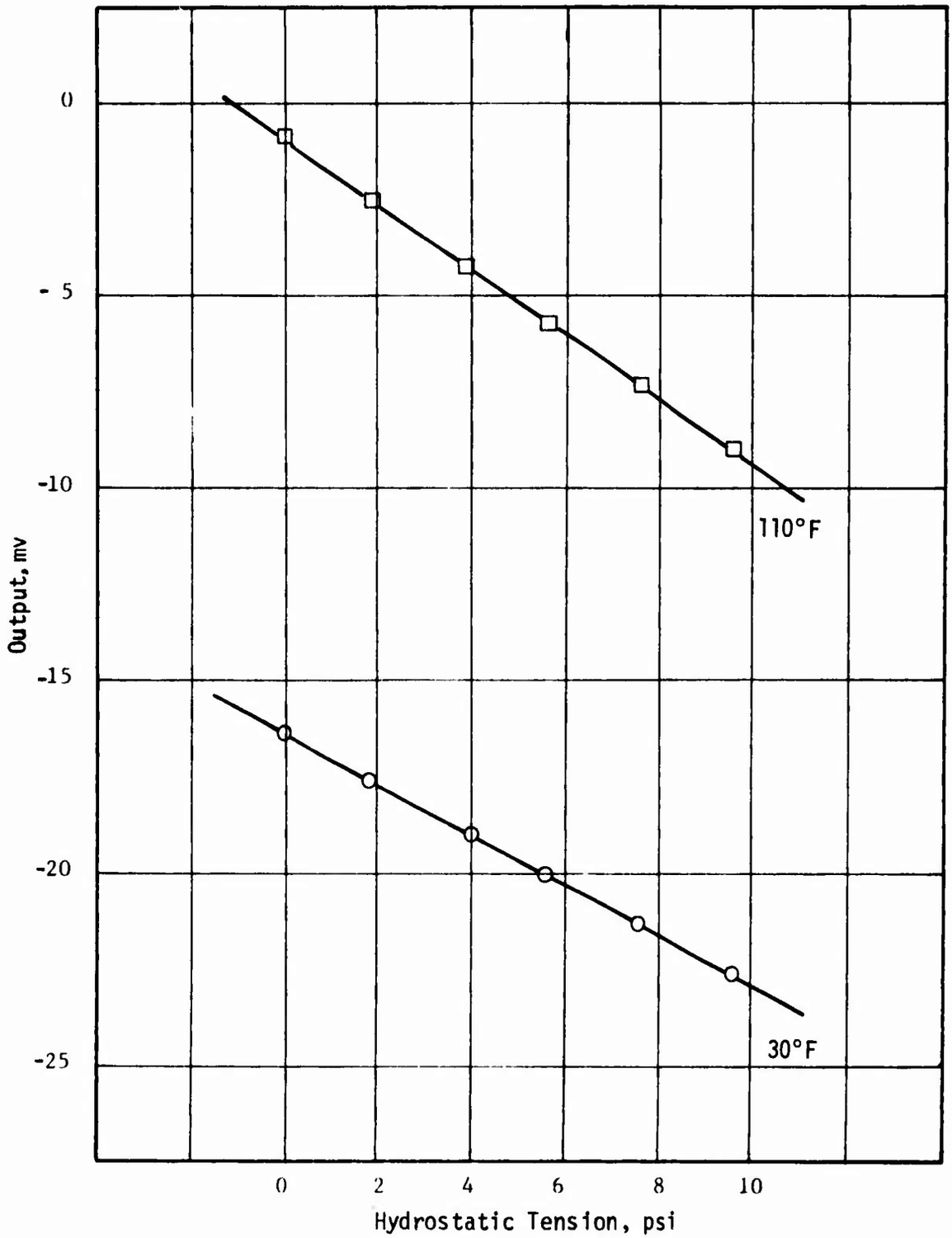

Figure C-23. Millivolt Output of Normal Stress Gage N3-1 During Vacuum Testing of Propellant Grain STV-2

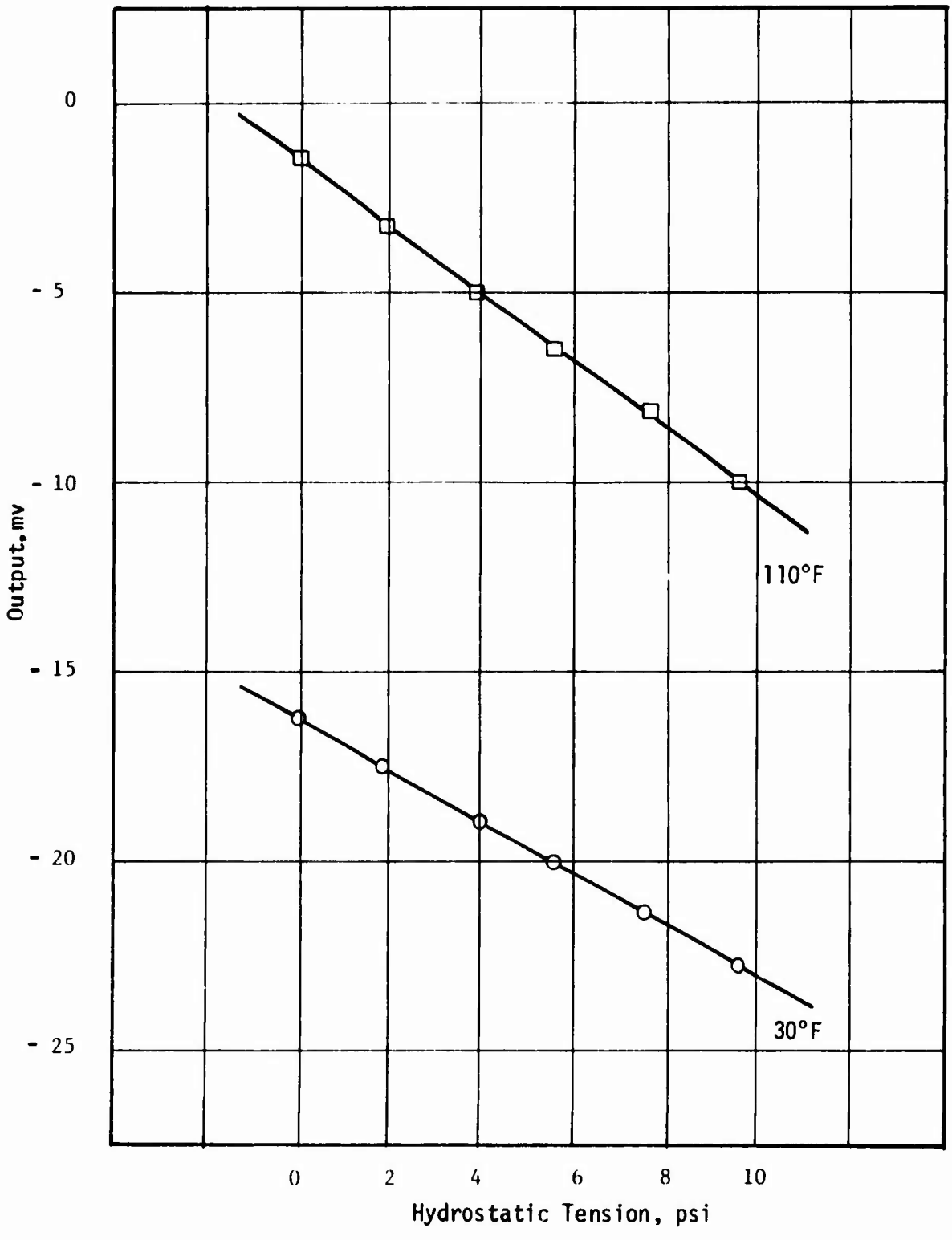

Figure C-24. Millivolt Output of Normal Stress Gage N3-2 During Vacuum Testing of Propellant Grain STV-2

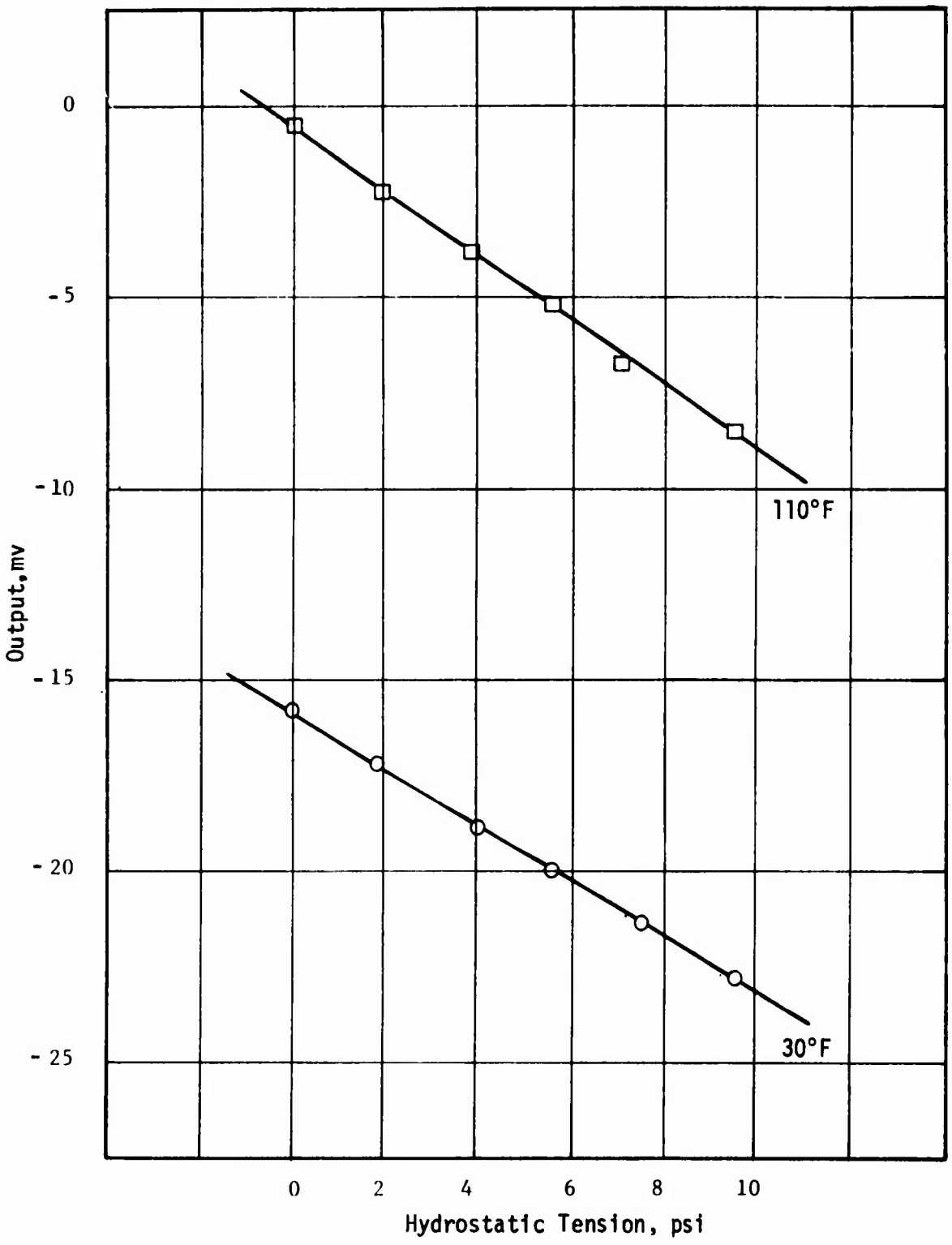

Figure C-25. Millivolt Output of Normal Stress Gage N4-1 During Vacuum Testing of Propellant Grain STV-2

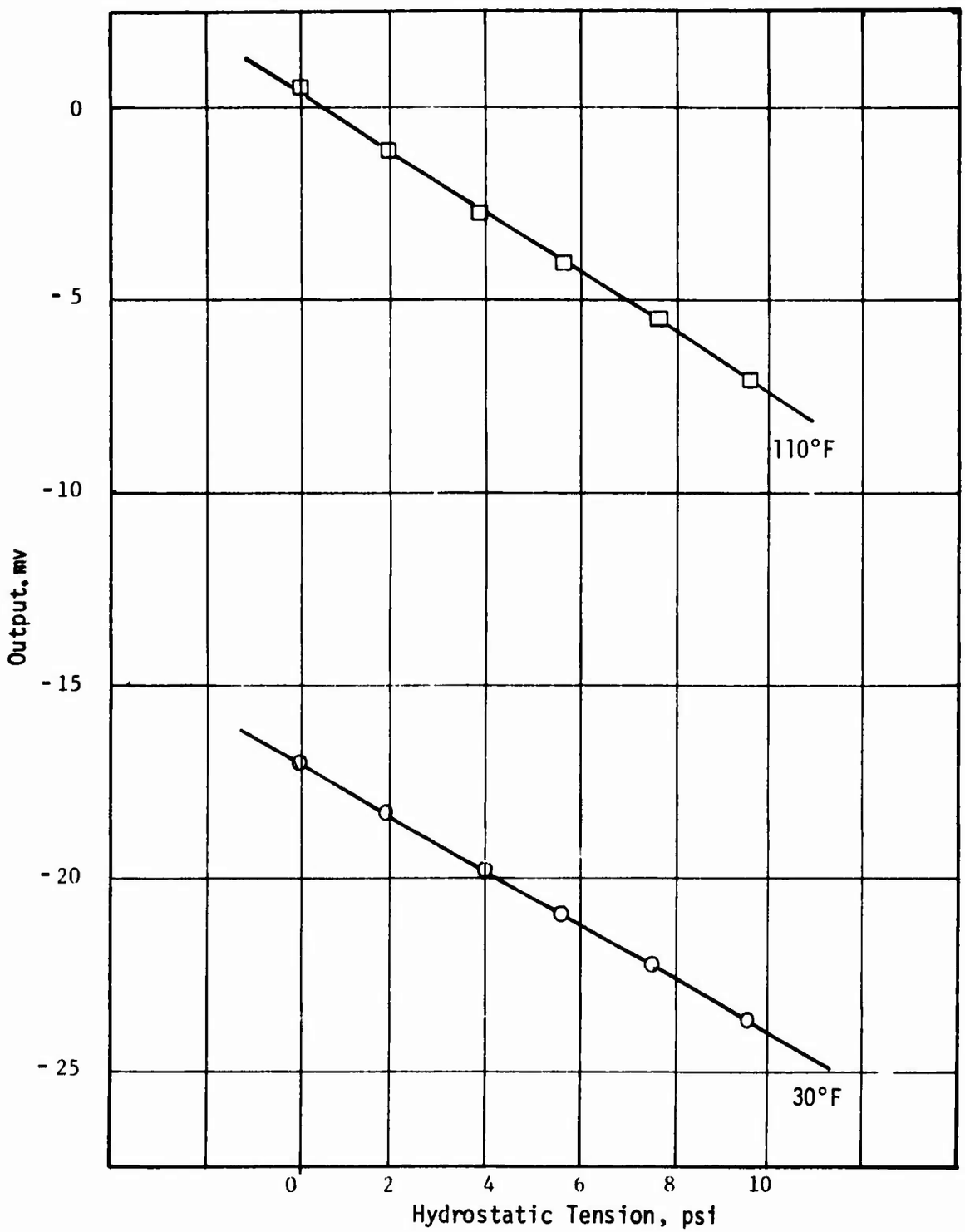

Figure C-26. Millivolt Output of Normal Stress Gage N4-2 During Vacuum Testing of Propellant Grain STV-2

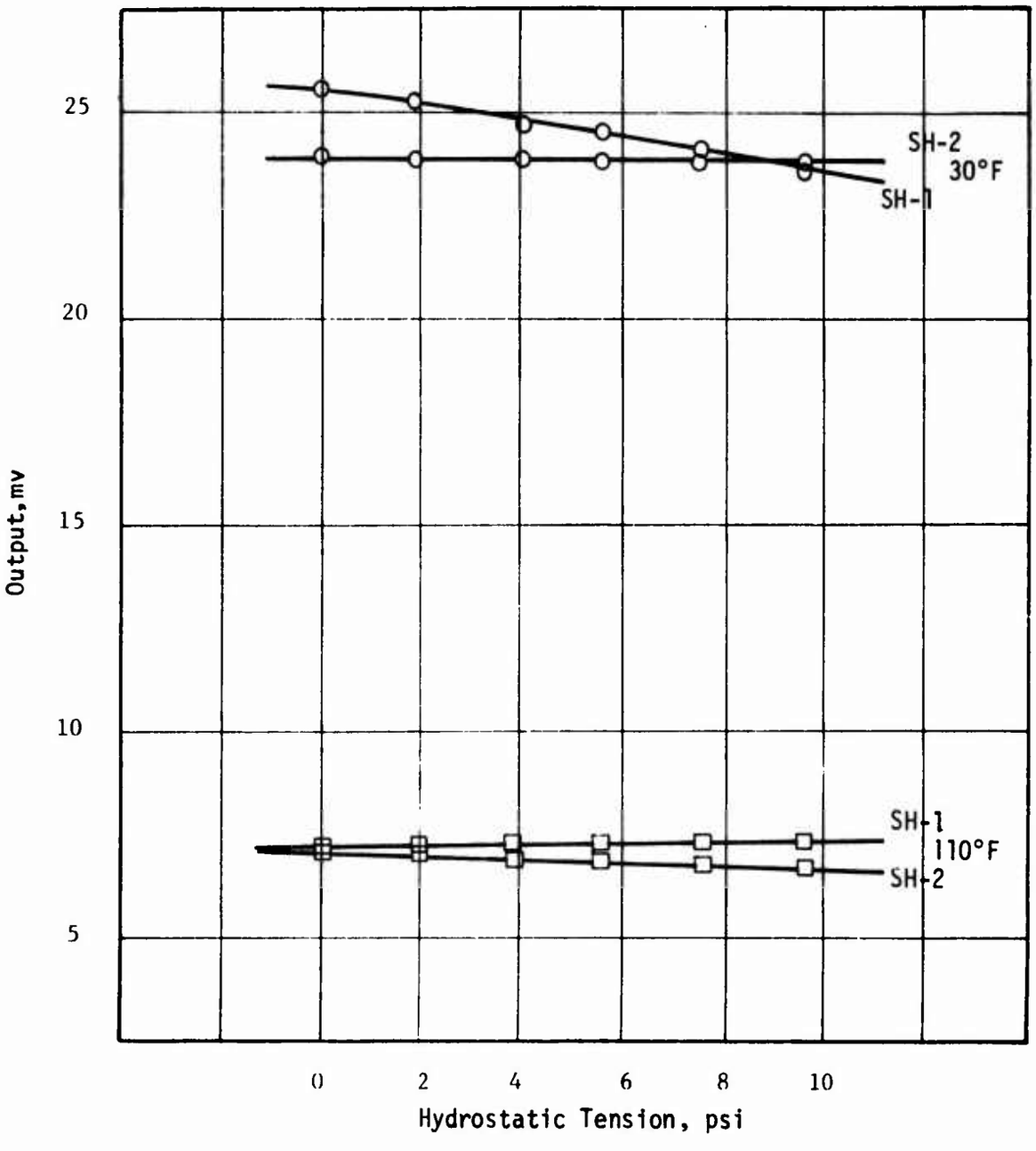

Figure C-27. Millivolt Output of Shear Stress Gages SH-1 and SH-2 During Vacuum Testing of Propellant Grain STV-2

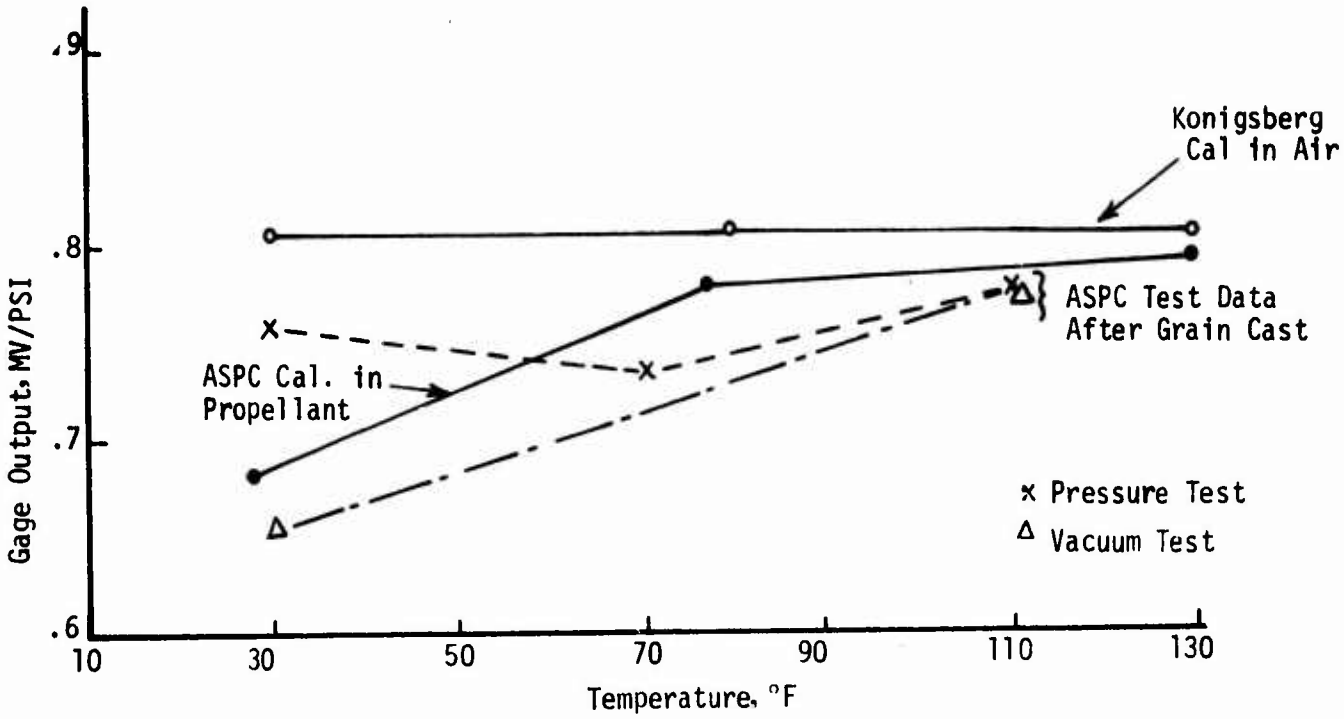

Figure C-28. Comparison of Calibration and Test Data for Gage N1-1

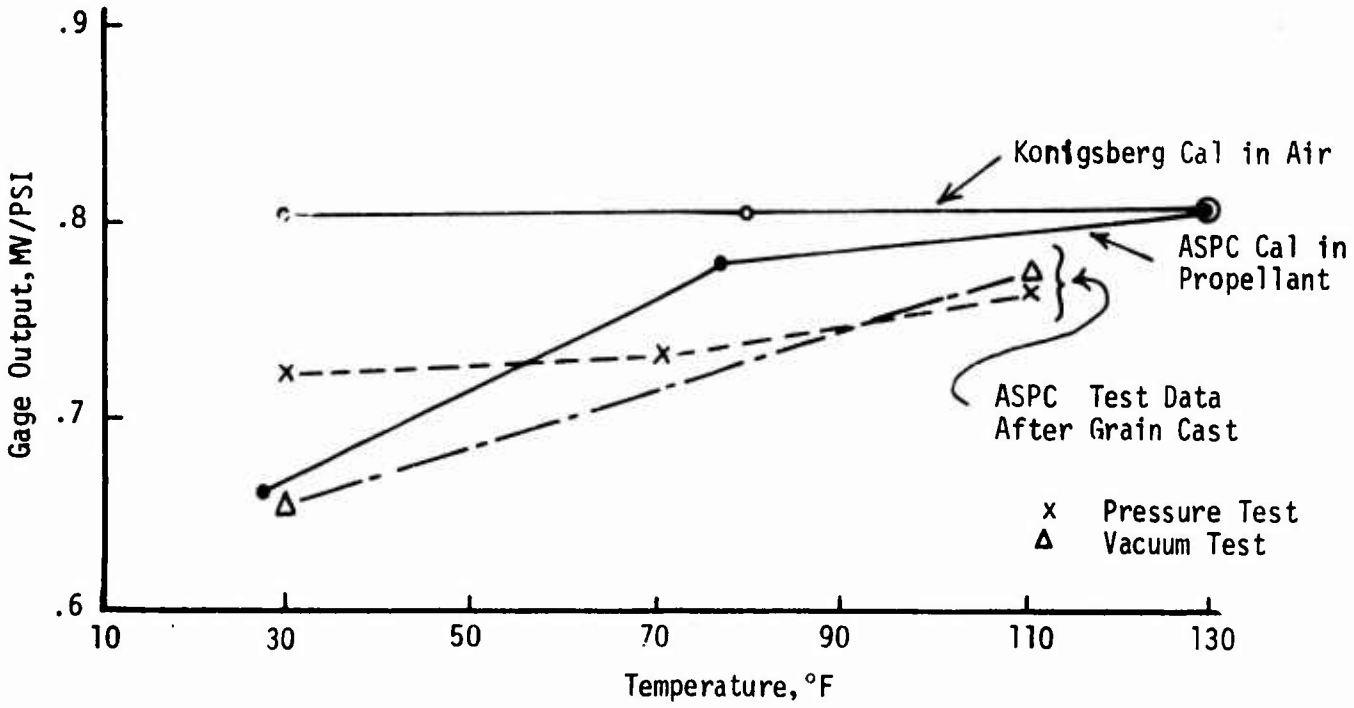

Figure C-29.Comparison of Calibration and Test Data for Gage N1-2

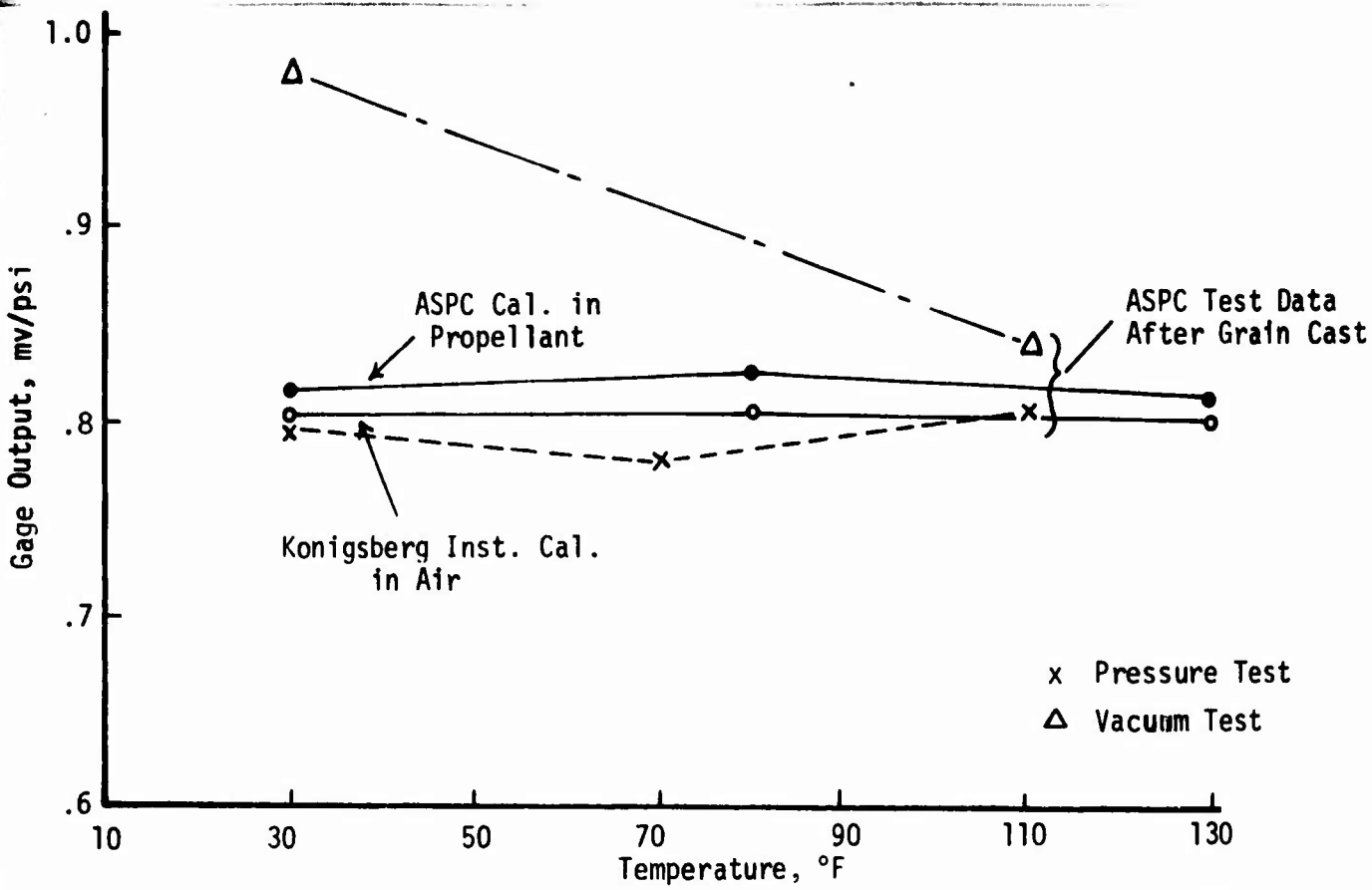

Figure C-30. Comparison of Calibration and Test Data for Gage N2-1

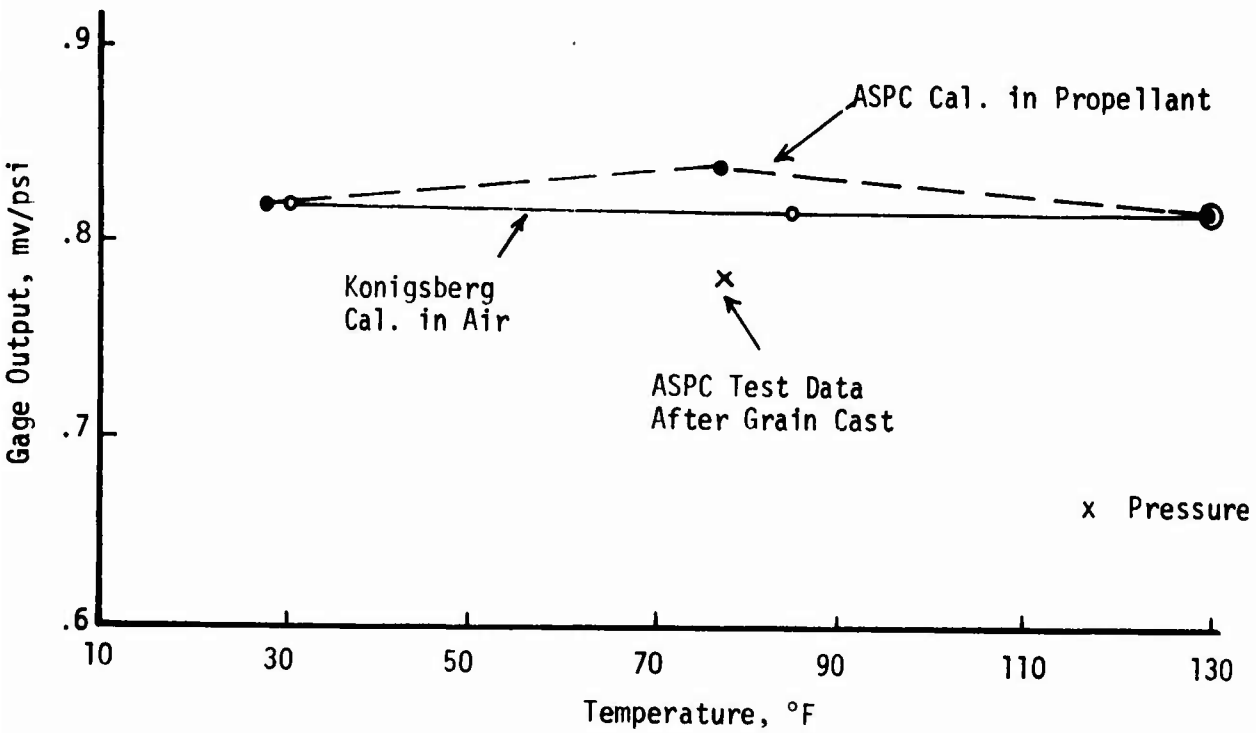

Figure C-31. Comparison of Calibration and Test Data for Gage N2-2

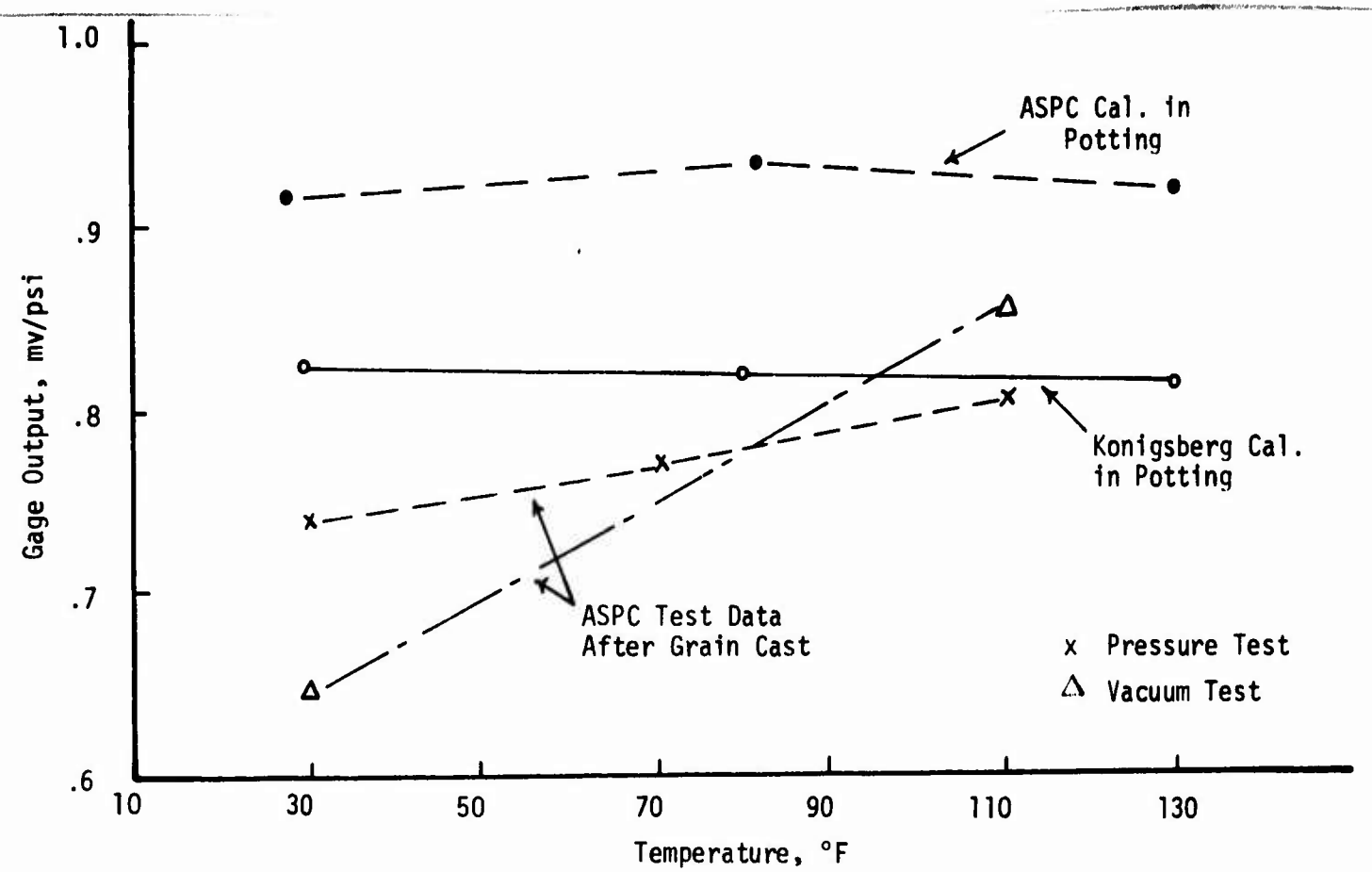

Figure C-32. Comparison of Calibration and Test Data for Gage N3-1

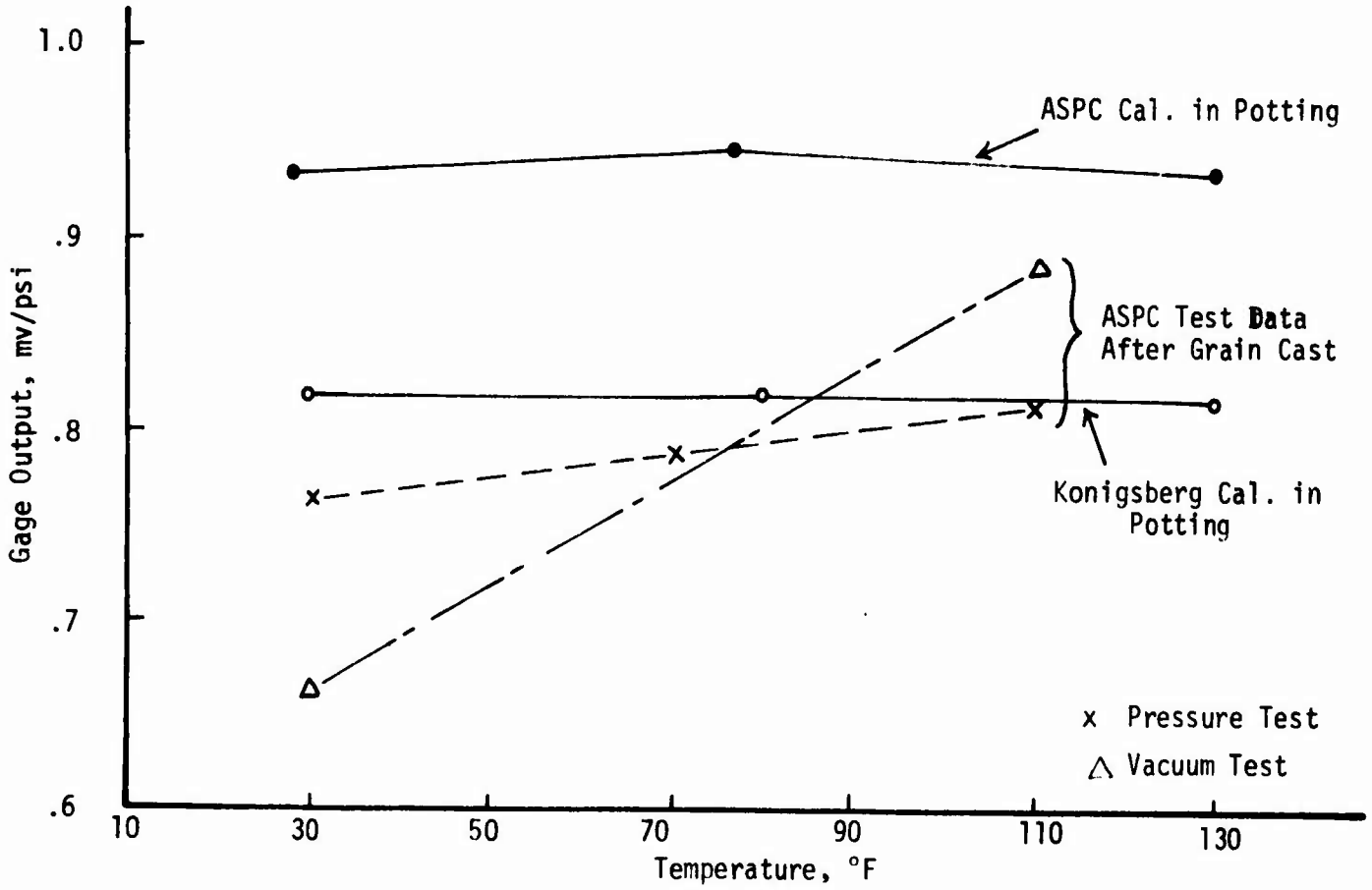

Figure C-33. Comparison of Calibration and Test Data for Gage N3-2

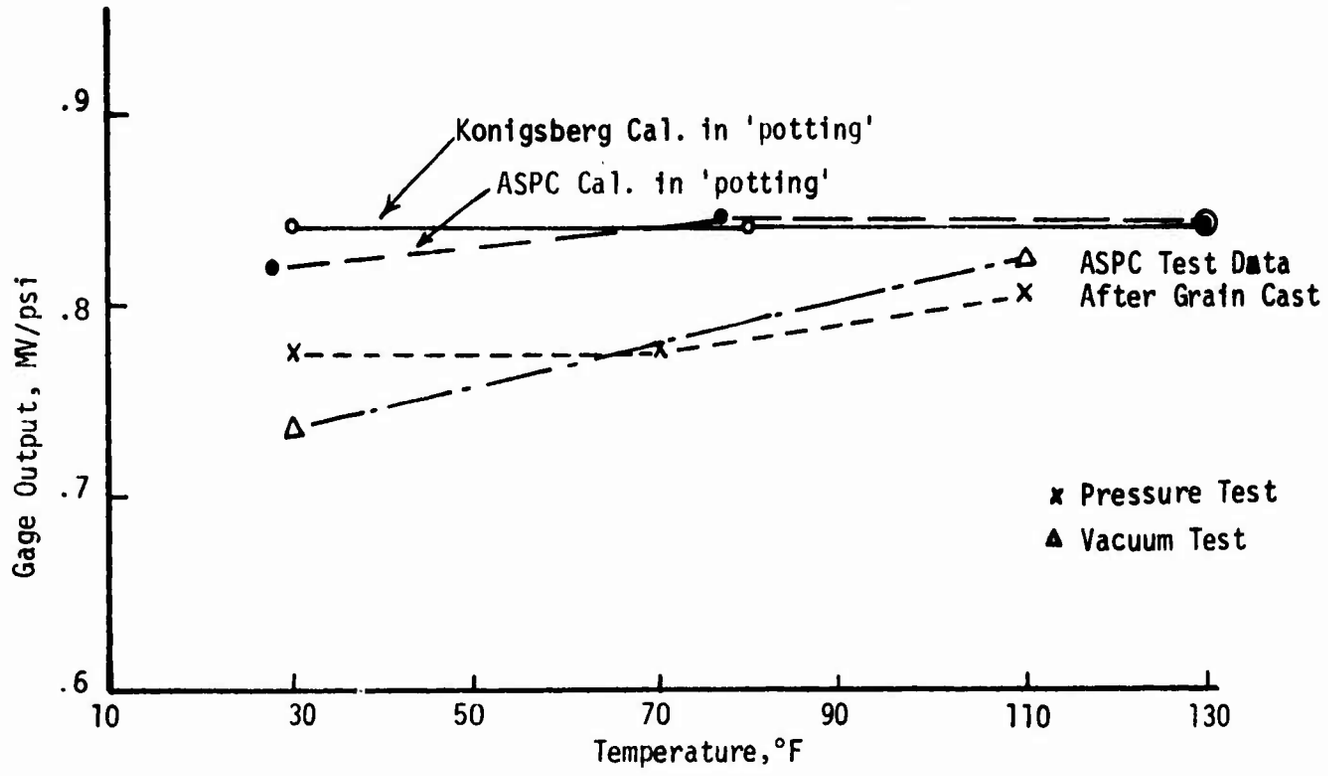

Figure C-34. Comparison of Calibration and Test Data for Gage N4-1

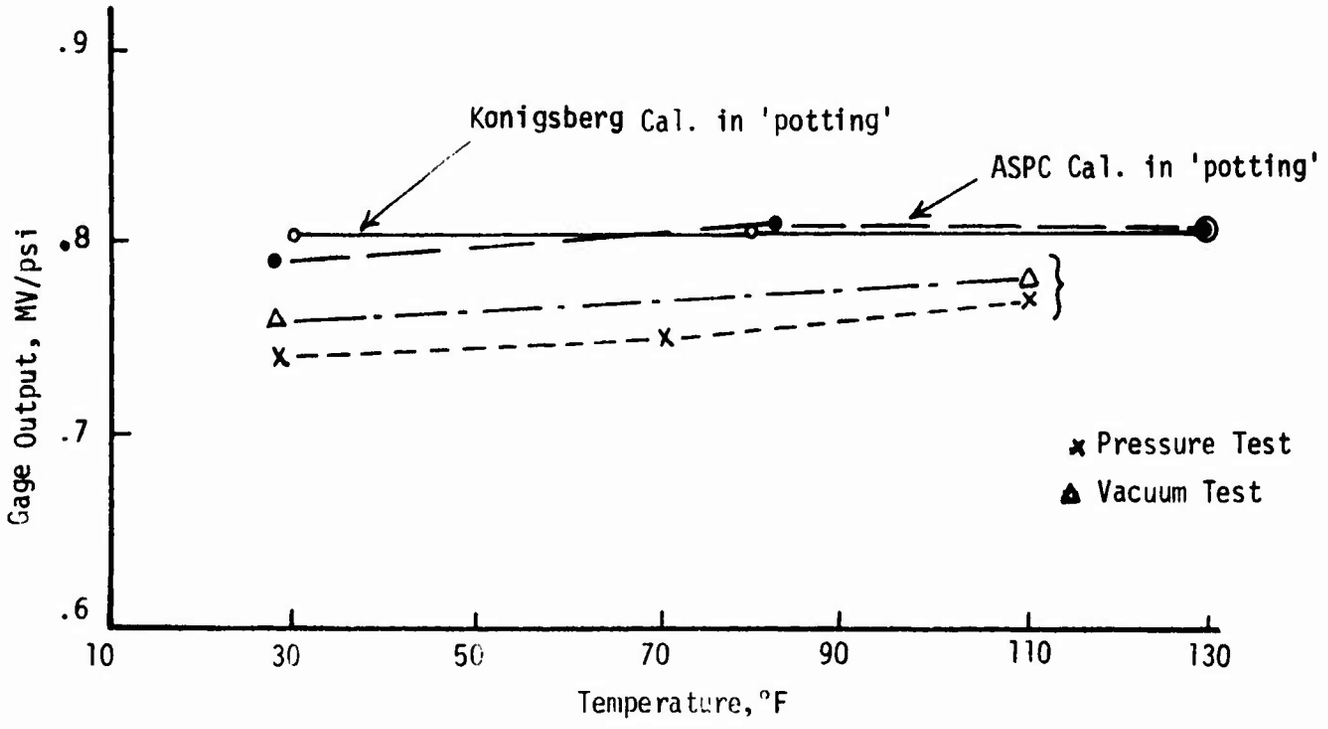

Figure C-35. Comparison of Calibration and Test Data for Gage N4-2

APPENDIX D

STV NO. 3 GAGE CALIBRATION DATA

TABLE D-1

SUMMARY OF STV NO. 3 GAGE CALIBRATION DATA

Gage Number	Gage Sensitivities		
	34°F	78°F	142°F
SH-5	-5.02 mv/psi	-6.69	-7.14
SH-6	-5.90	-8.24	-7.75

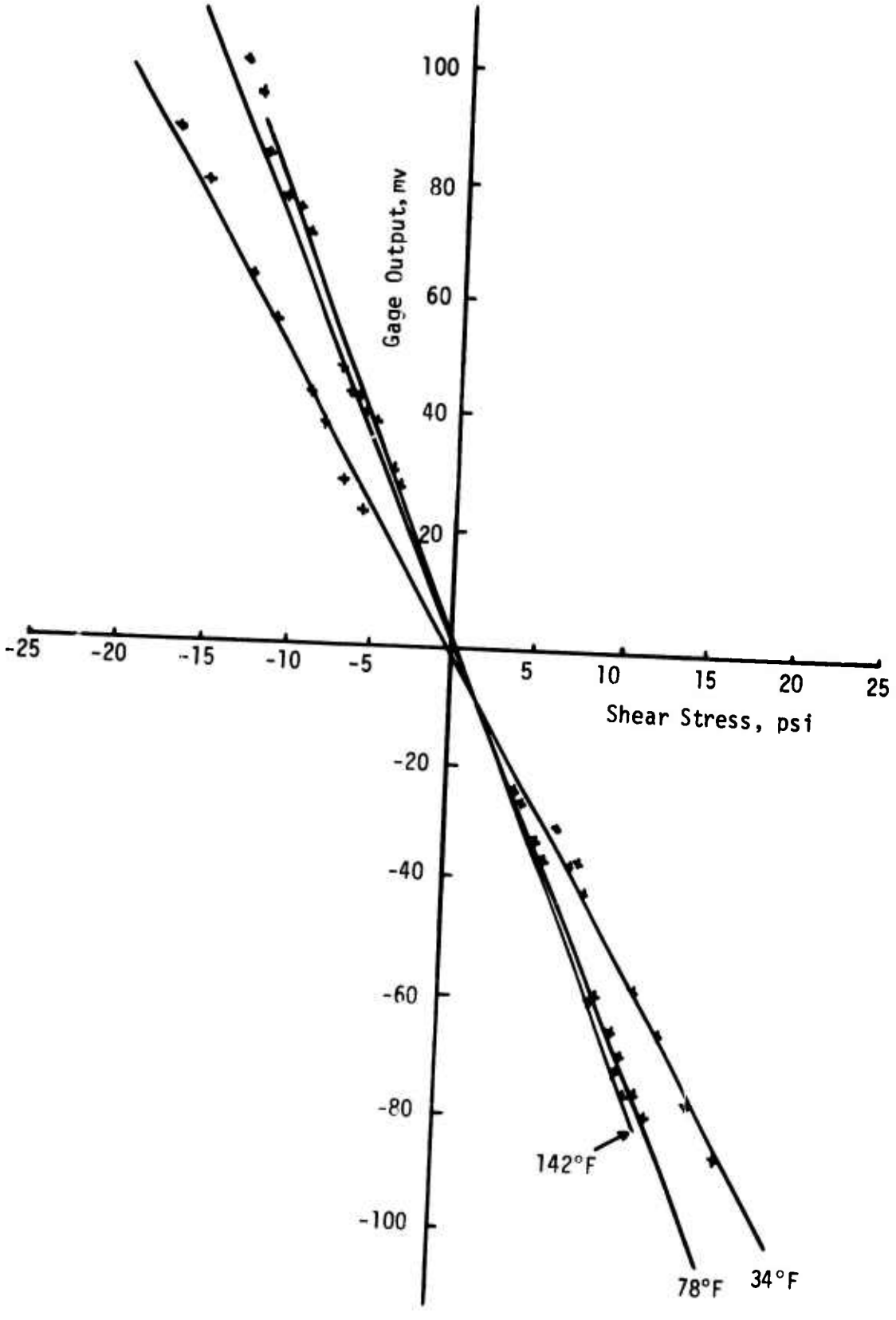

Figure D-1. STV No. 3 Shear Gage SH-5

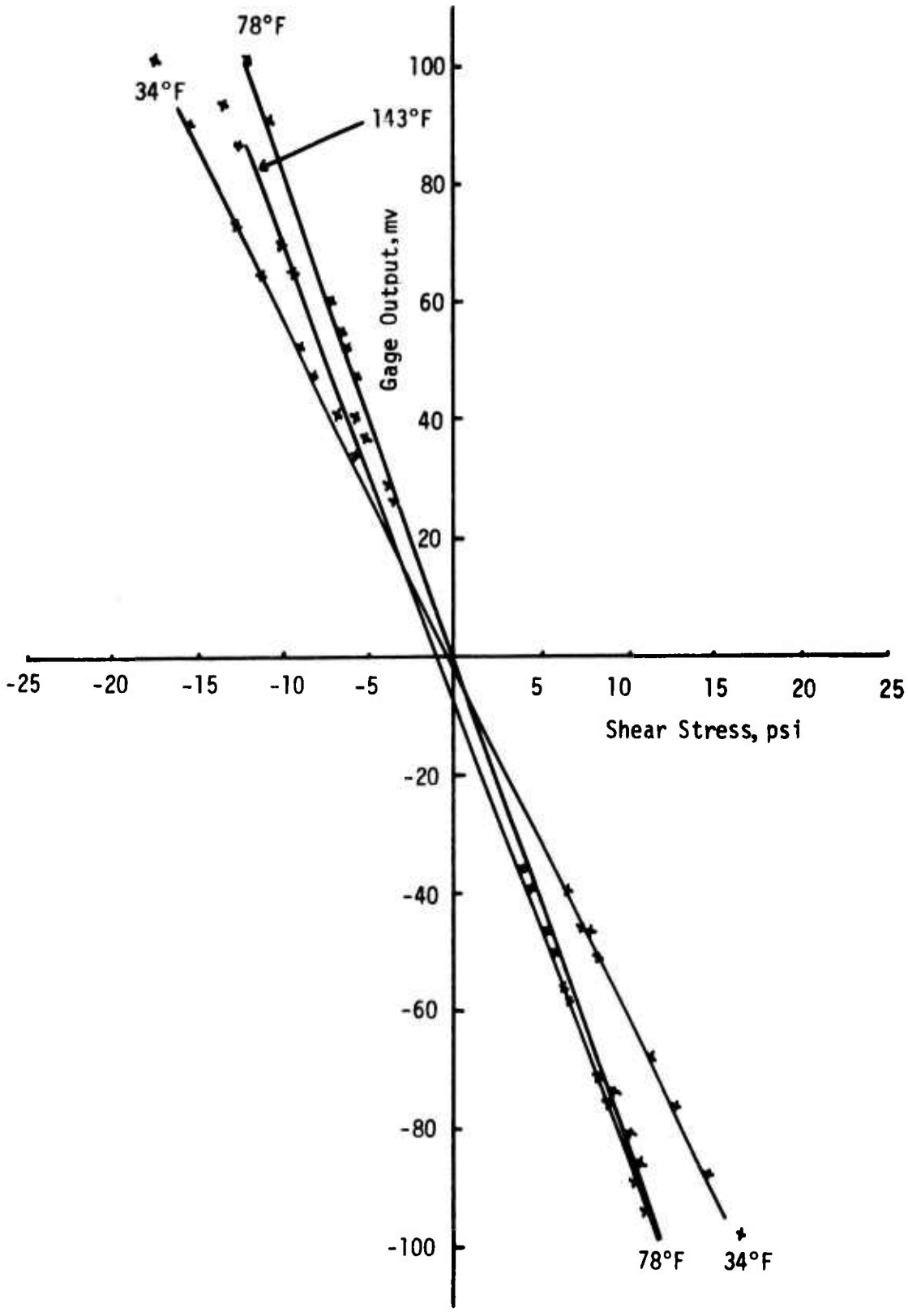

Figure D-2. STV No. 3 Shear Gage SH-6

APPENDIX E

STV NO. 4 CALIBRATION AND TEST DATA

RAW CALIBRATION DATA

The calibration curves (Figures E-1 and E-2) for the shear gages were obtained in laboratory test fixtures at 34, 78 and 142°F. But, the normal stress gage had to be calibrated after bonding it in place in the STV (before grain casting). The sensitivity values of the gages are summarized in Table E-1.

It was necessary to shunt the gages to reduce the zero stress readings (see Appendix C), so the new values were measured in the STV at 70, 88 and 110°F. They are also give in Table E-1.

Table E-2 contains a complete tabulation of the grain stress data taken on STV No. 4 after the grain was cast.

CURE AND COOLDOWN

Figures E-3 and E-4 show the normal stress and shear stress data measured during cure and cooldown of STV No. 4.

An examination of these figures shows that the normal and shear stress gages were functioning during the cure and cooldown of the grain. The two half-bridges of gage N-5 gave data close to each other (Figure E-3), generally within 1 psi. But, the shear data (Figure E-4) exhibited surprisingly large thermal stresses and the two gages differed from each other by about 1.5 psi.

TABLE E-1

SUMMARY OF STV NO. 4 GAGE CALIBRATION DATA

Gage Number	Gage Sensitivities*			Zero Stress Output (in STV)		
	34°F	78°F	142°F	70°F	88°F	110°F
SH3	4.73 mv/psi	5.82	6.10	+1.8 mv	+3.3	+5.0
SH4	4.06	5.30	5.56	+0.1	+3.0	+6.6
	30°F	77°F	130°F			
N5-1	.808	.808	.808	+4.2	+3.8	+3.3
N5-2	.807	.807	.807	+1.6	+1.3	+0.9
Grain Pot		4.0 V/in.				

* Sign convention for normal stress transducer sensitivity: output is positive for a pressure load (compressive stress).

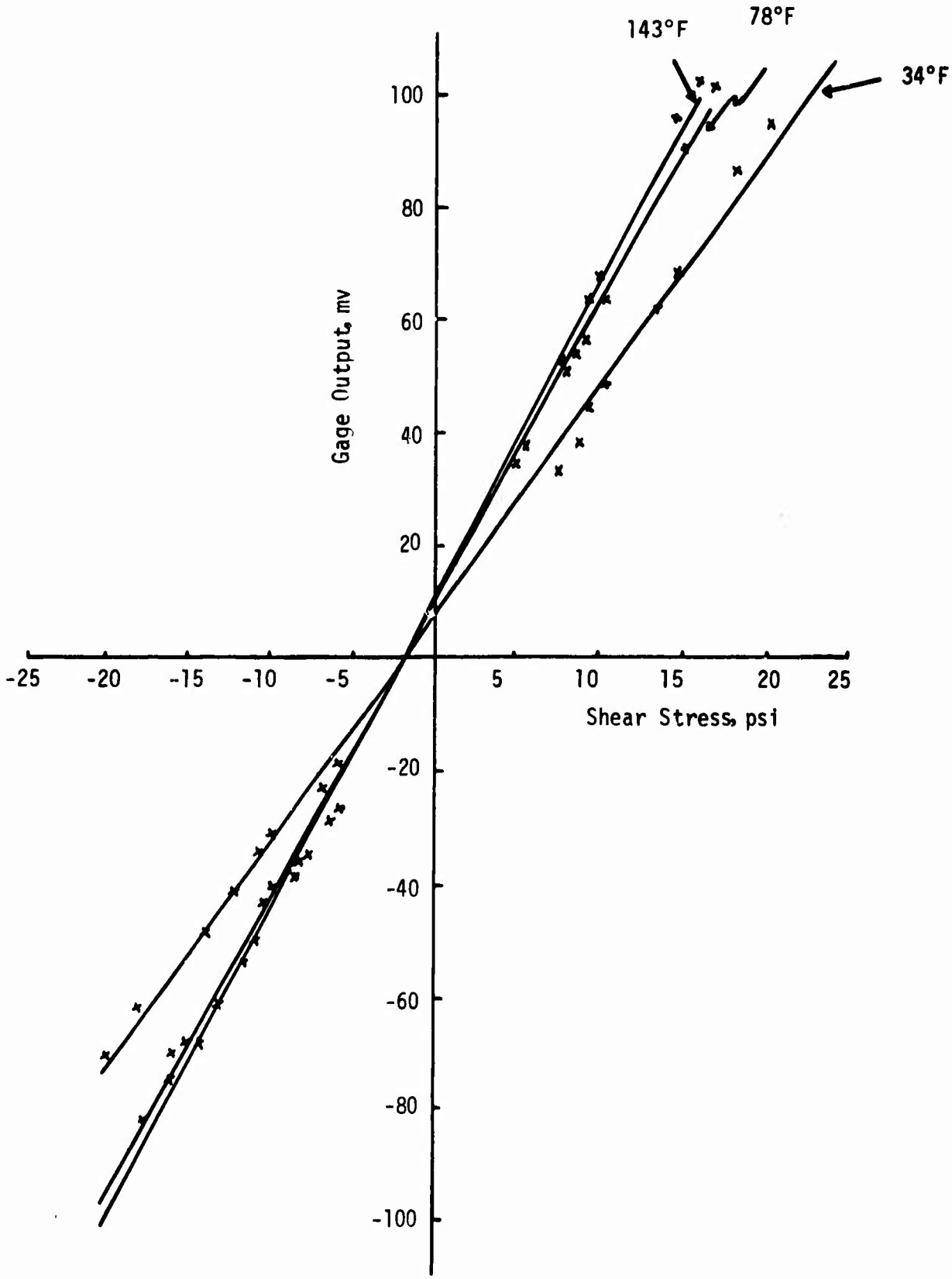

Figure E-1. STV No. 4 Shear Gage SH-4

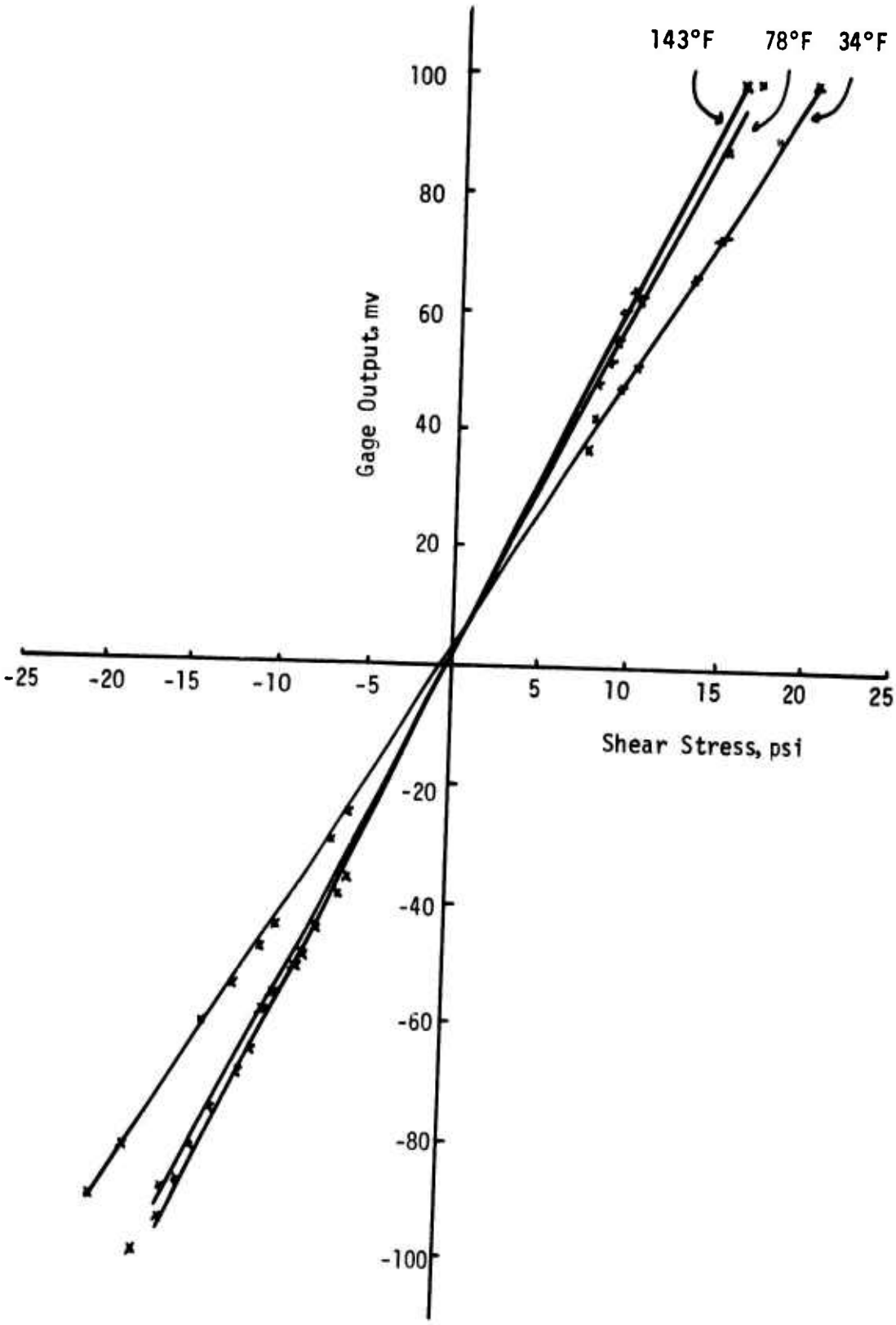

Figure E-2. STV No. 4 Shear Gage SH-3

Table E-2

Flexible Case STV No. 4 Calculated Data

Date	Hour	Temp, °F	Condition	SH-3 psi	SH-4 psi	N5-1 psi	N5-2 psi	Grain Pot in.
10 Aug. 1972	1800	88	Grain Cast	0.00	0.00	0.00	0.00	
11 "	930	110	Curing	0.00	0.00	0.00	0.00	
11 "	1030			0.00	0.02	0.21	0.22	
	1210			0.01	0.04	-0.12	0.04	
	1530			0.03	0.09	-0.21	0.01	
12 "				0.06	-0.04	-0.20	-0.31	
13 "				0.10	0.05	-0.31	-0.24	
14 "	745			0.25	-0.14	-0.03	-0.43	
15 "	740			0.35	-0.16	-0.07	-0.48	
16 "	745			0.46	-0.16	-0.31	-0.62	
17 "	740			0.43	-0.13	-0.47	-0.79	
18 "	750			0.47	-0.07	-0.57	-0.81	
21 "	1530			0.51	0.02	-1.14	-1.18	
22 "	930		Start	0.62	-0.02	-1.20	-1.34	
22 "	1030		Cool Down	1.00	-0.31	0.24	0.55	
22 "	1230			1.58	-0.64	1.56	0.63	
22 "	1430			1.75	-0.35	1.99	2.35	
22 "	1630			2.22	-1.38	3.69	3.81	
23 "	930	77		2.92	-2.11	3.99	5.86	
23 "	1650			2.92	-1.65	5.00	5.03	
24 "	1600			3.03	-2.15	4.12	6.03	
25 "	1300			2.93	-1.87	4.37	5.29	
28 "	745			2.95	-2.02	4.37	4.92	
30 "	745			2.45	-1.28	4.37	3.93	
31 "	945			2.45	-1.25	4.37	3.68	
1 Sept.				2.53	-1.38	4.49	3.80	
5 "				2.93	-2.04	4.37	4.92	
13 "				3.03	-2.41	3.87	5.42	
15 "				2.76	-1.95	4.74	4.30	
18 "				2.60	-1.76	4.74	3.80	
19 "				2.55	-1.77	4.74	3.80	
25 "				2.62	-1.74	4.62	3.43	
29 "				2.60	-1.74	4.37	3.43	

Table E-2 (Cont.)

Flexible Case STV No. 4 Calculated Data

Date	Hour	Temp, °F	Condition	SH-3 psi	SH-4 psi	N5-1 psi	N5-2 psi	Grain Pot in.
3 Oct. 1972		77		2.62	-1.74	4.37	3.43	
9 "				2.62	-1.73	4.25	3.18	
16 "				2.86	-2.02	2.27	4.92	
31 "				2.72	-1.97	3.87	2.94	
6 Nov.				2.72	-1.81	3.87	2.94	
16 "				2.79	-1.95	4.00	2.94	
28 "				2.63	-1.95	4.00	2.44	
21 Dec.				2.58	-1.69	2.88	2.07	
28 "				2.70	-1.68	2.88	1.45	
8 Jan. 1973				2.77	-1.74	3.38	1.33	
15 "				2.70	-1.63	3.01	1.33	
5 Feb.				2.74	-1.59	2.27	0.58	
23 "				2.74	-1.49	1.77	0.46	
13 Mar.				2.81	-1.61	1.89	0.09	
27 "				2.81	-1.54	1.77	0.09	
16 April				2.76	-1.41	1.28	-0.66	
14 May				2.45	-0.89	0.29	-1.52	
25 "				3.00	-1.38	0.53	-0.90	
4 June				2.74	-1.23	0.66	-1.28	
18 "				2.69	-1.17	0.16	-1.65	
27 "				2.69	-0.92	0.16	-1.65	
29 "								
6 Aug.	1258			2.13	-0.89	-0.46	-1.03	0.000
	+ 1 Min.		+67.5 psi	-9.81	-18.38	-34.49	-34.86	.080
	+ 300 sec.		End B	-9.81	-18.22	-34.49	-34.86	.094
	+ 1700 sec.			-9.81	-18.22	-34.00	-34.36	.105
	1358			-10.04	-18.38	-34.74	-35.23	.109
	1558			-10.21	-18.38	-34.49	-35.11	.119
7 "	745			-10.07	-18.38	-33.50	-34.11	.132
	1140			-10.50	-17.73	-34.74	-35.23	.132
8 "	740			-10.28	-15.79	-32.02	-33.87	.144

Table E-2 (Cont.)

Flexible Case STV No. 4 Calculated Data

Date	Hour	Temp, °F	Condition	SH-3 psi	SH-4 psi	N5-1 psi	N5-2 psi	Grain Pot in.
8 Aug. 1973	1107	77		-10.53	-15.10	-34.49	-34.98	.142
	1535			-10.59	-15.17	-34.74	-35.11	.152
9 "	930			-10.31	-15.50	-33.75	-34.11	.147
	1213			-10.52	-15.07	-34.74	-35.23	.147
	1400			-10.54	-15.07	-34.62	-35.23	.147
	1600			-10.52	-15.07	-34.49	-35.11	.147
10 "	1015			-10.42	-15.18	-34.49	-34.98	.149
	1205			-10.59	-14.94	-34.99	-35.48	.147
	1350			-10.62	-14.92	-35.11	-35.48	.149
13 "	1500			-10.71	-14.69	-34.86	-35.35	.152
14 "	1030			-10.71	-14.66	-35.36	-35.97	.152
	+ 1 Min.		Remove	1.70	-1.00	0.78	0.21	-.063
	+ 300 sec.		Pressure	1.81	-1.12	0.78	0.21	.056
	+ 1500 sec.			1.84	-1.17	1.15	0.33	.048
	+ 4000 sec.			1.86	-1.17	1.28	0.46	.042
	1446			1.88	-1.15	1.28	0.58	.033
	1800			1.91	-1.13	1.52	0.71	.030
16 "	1600			2.03	-0.97	0.78	-0.04	.021
16 "	1630			2.10	-0.97	1.40	0.58	.020
20 "	1010			2.24	-1.04	0.90	0.09	.018
21 "	800			2.41	-1.28	1.28	0.33	.018
22 "	745			2.50	-1.38	1.40	0.33	.019
23 "	800			2 60	-1.53	1.65	0.58	.020
24 "	745			2.58	-1.51	1.52	0.46	.020
27 "	740			2.60	-1.48	1.40	0.21	.019
28 "	740			2.67	-1.56	1.52	0.4[illegible]	.020
29 "	740			2.53	-1.38	1.40	0.33	.019
30 "	740			2.55	-1.40	1.40	0.21	.020
31 "	740			2.58	-1.41	1.28	0.21	.020
4 Sept.	740			2.43	-1.15	1.03	0.09	.018
5 "	740			2.60	-1.41	1.40	0.21	.018
10 "	740			2.74	-1.61	1.65	0.33	.019

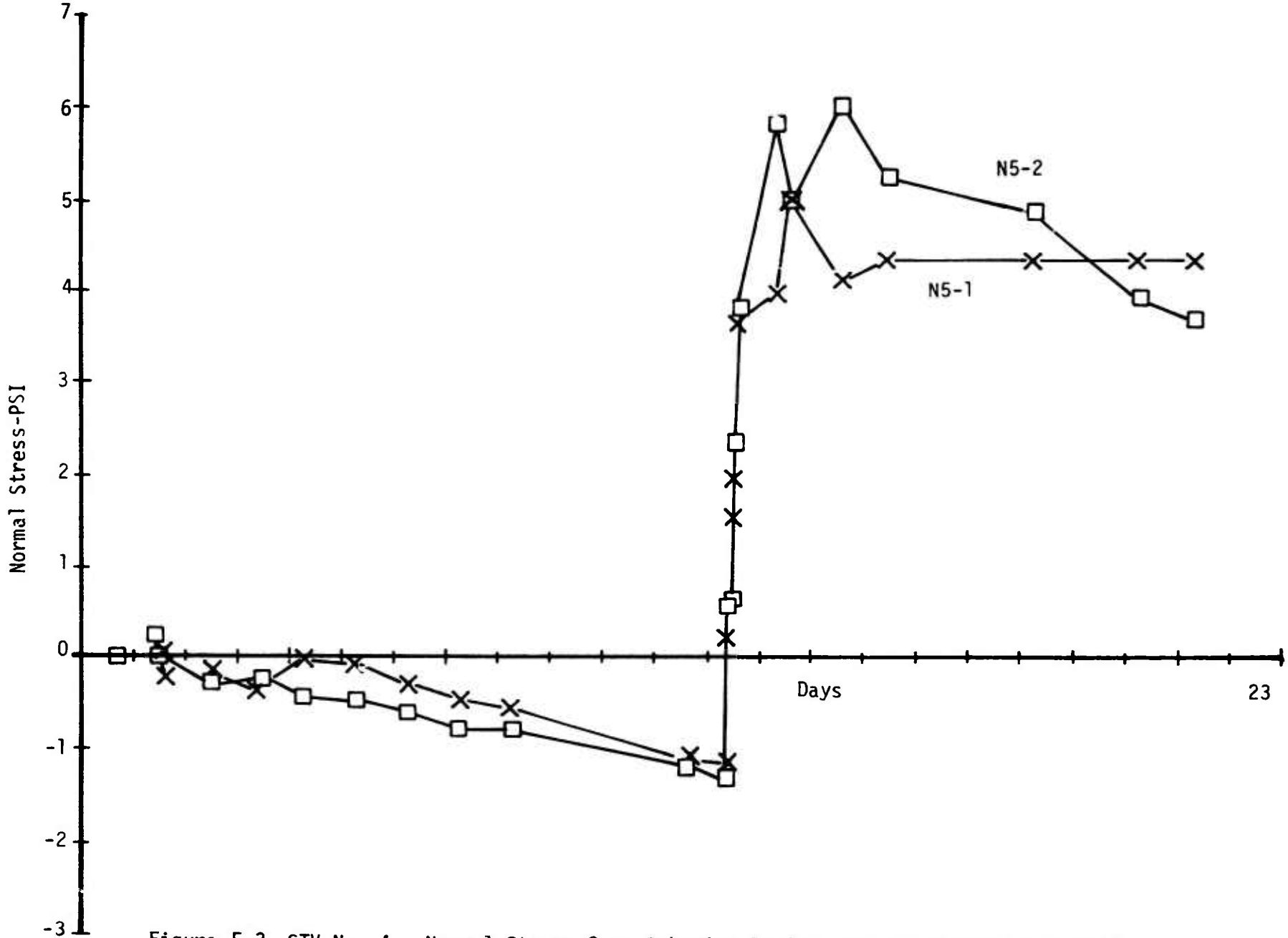

Figure E-3. STV No. 4 - Normal Stress Gage Behavior During Cure and Cooldown to 77°F

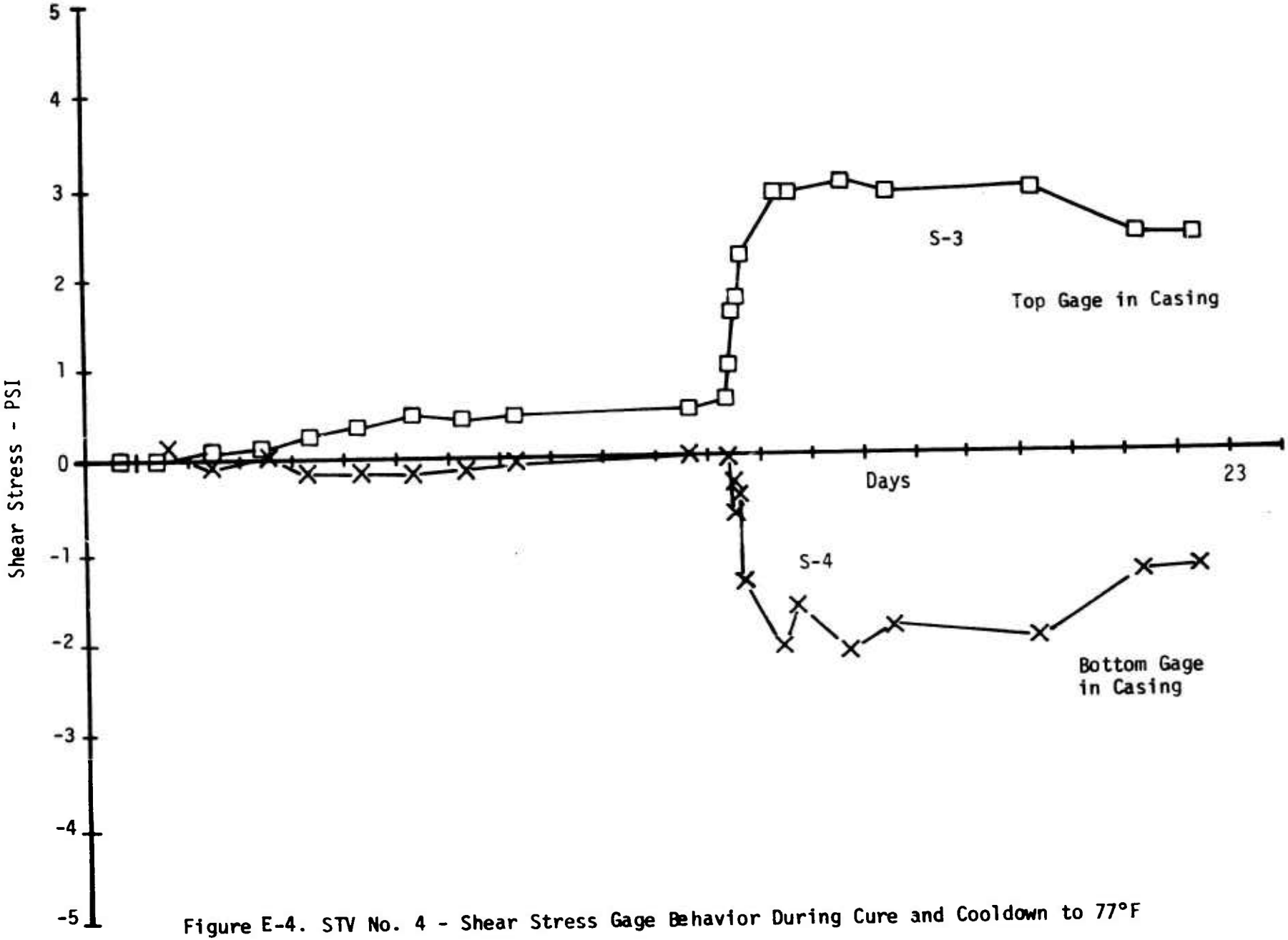

Figure E-4. STV No. 4 - Shear Stress Gage Behavior During Cure and Cooldown to 77°F

APPENDIX F

STV NO. 5 GAGE CALIBRATION AND TEST DATA

TABLE F-1

SUMMARY OF STV NO. 5 GAGE CALIBRATION DATA

Gage Number	Gage Sensitivities*, mv/psi			Zero Stress Output (in STV), mv		
	44°F	72°F	106°F	26°F	77°F	110°F
SH64	.53	.60	.55	-14.3	-5.3	+2.9
SH66	4.29	5.00	4.79	+ 8.8	+3.9	-1.8
	30°F	77°F	130°F			
SH100	2.09	2.14	2.70	+ 6.6	+6.2	+6.1
SH101	2.08	2.34	2.53	+ 8.7	+5.5	+2.4
SH102	1.48	1.60	1.91	+ 3.9	+5.0	+6.9
SH103	1.72	2.02	2.39	+ 6.8	+3.7	-0.8
SH39	2.87	3.26	3.68	+ 8.0	+5.8	+3.6
	0°F	80°F	150°F			
N34	.813	.809	.816	+ 7.2	+7.3	+7.1

* Sign convention for normal stress transducers sensitivity: output is positive for a pressure load (compressive stress).

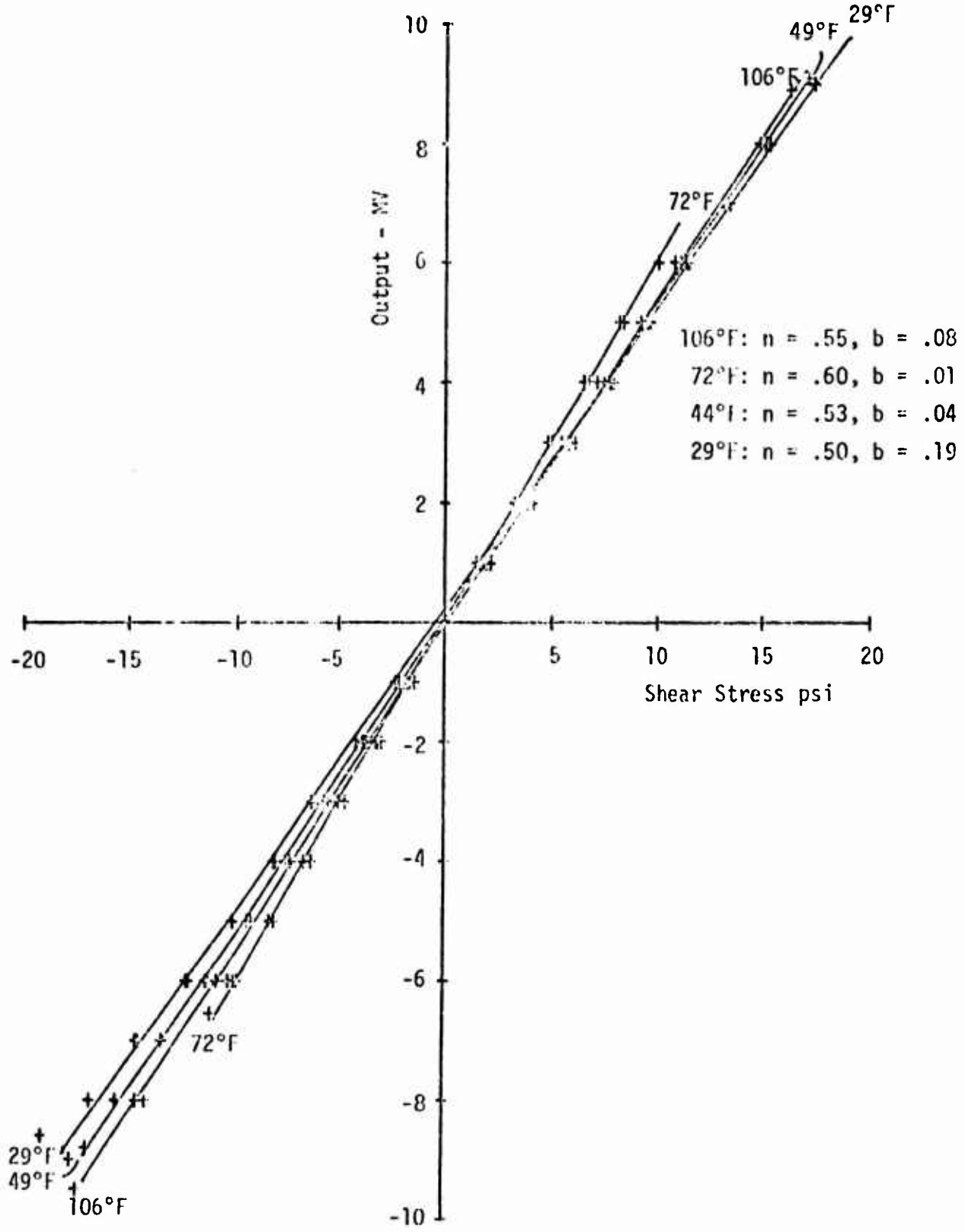

FIGURE F 1. SHEAR GAGE SH-64

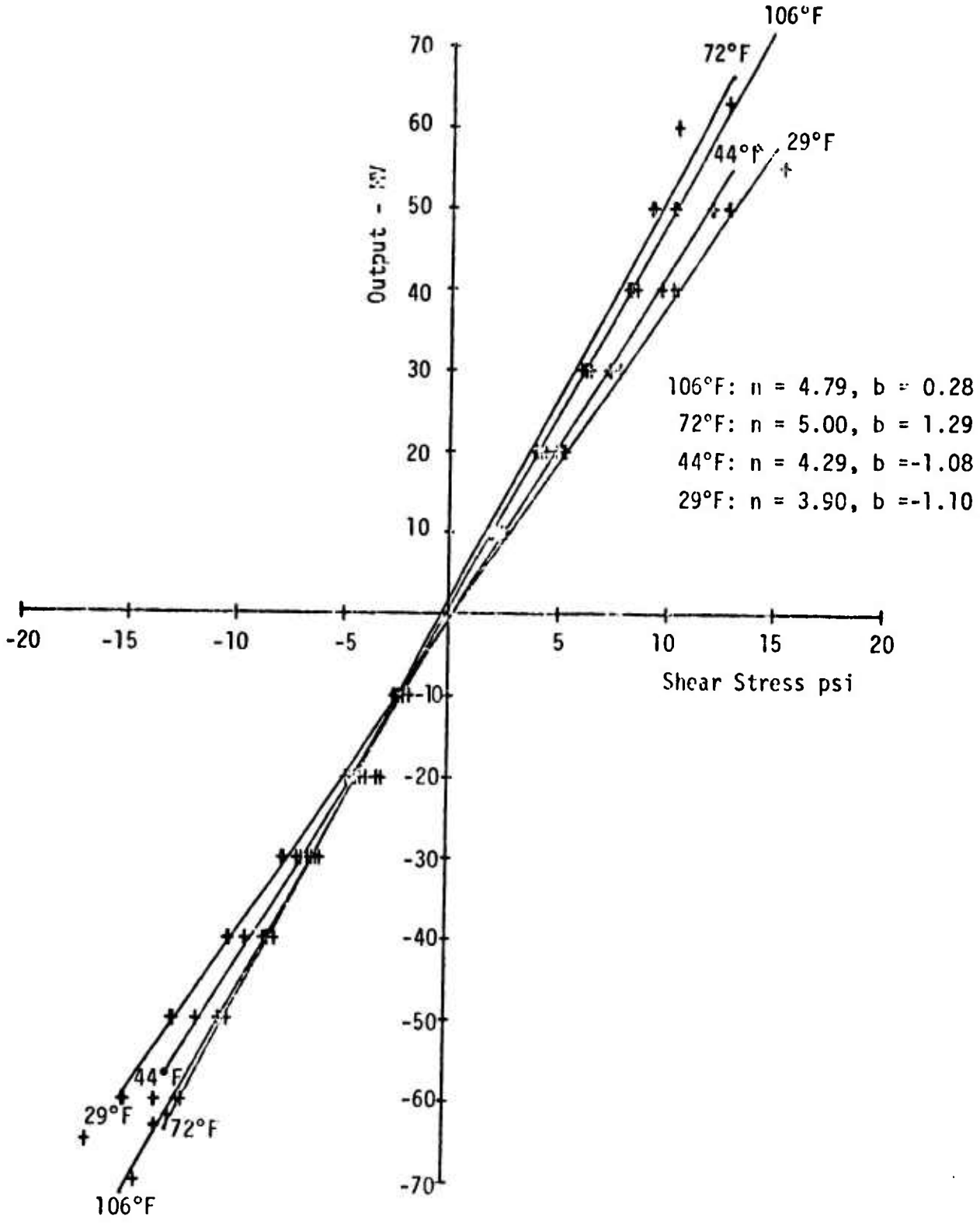

FIGURE F-2. SHEAR GAGE SH-66

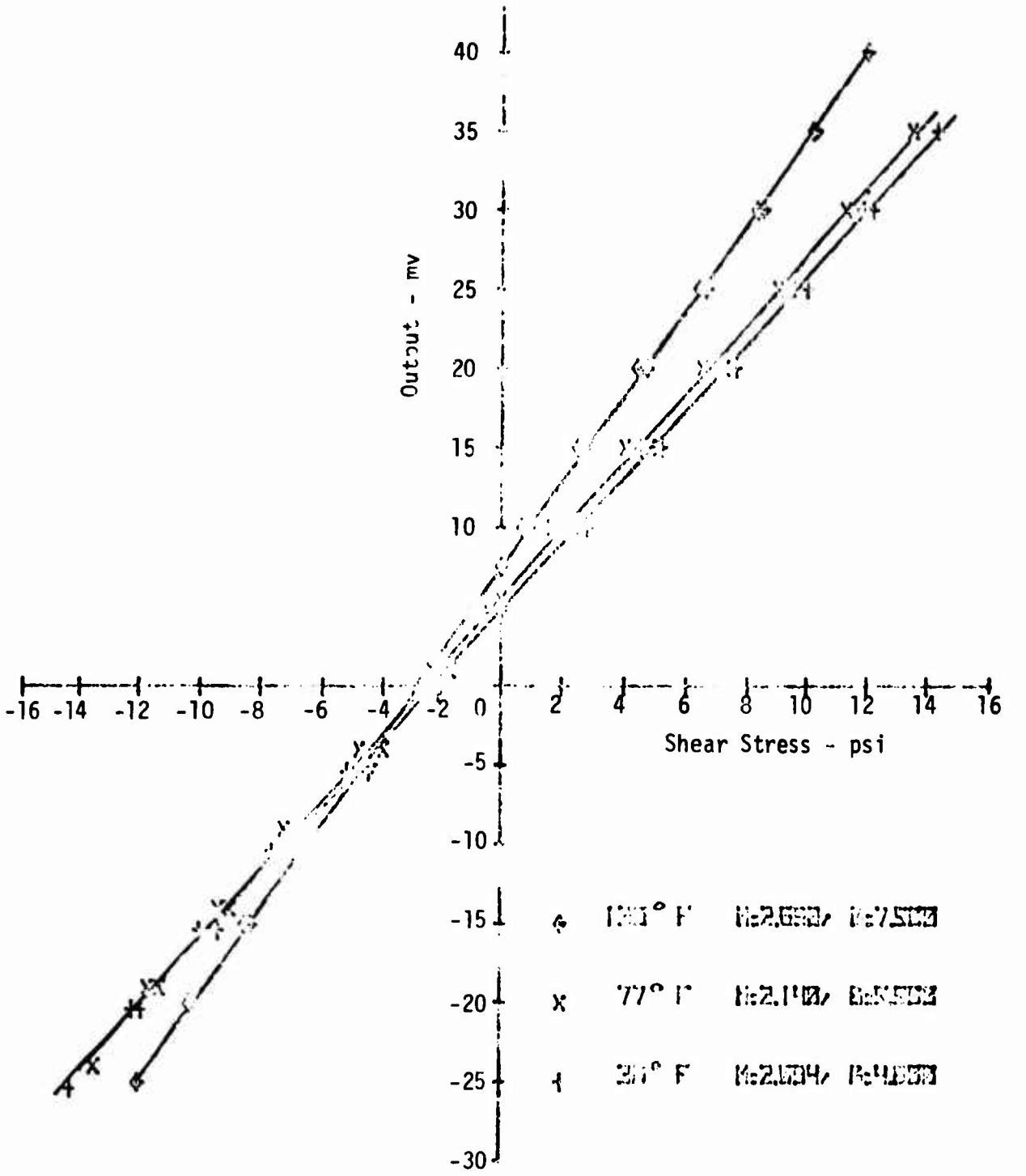

FIGURE F 3. SHEAR GAGE SH-100

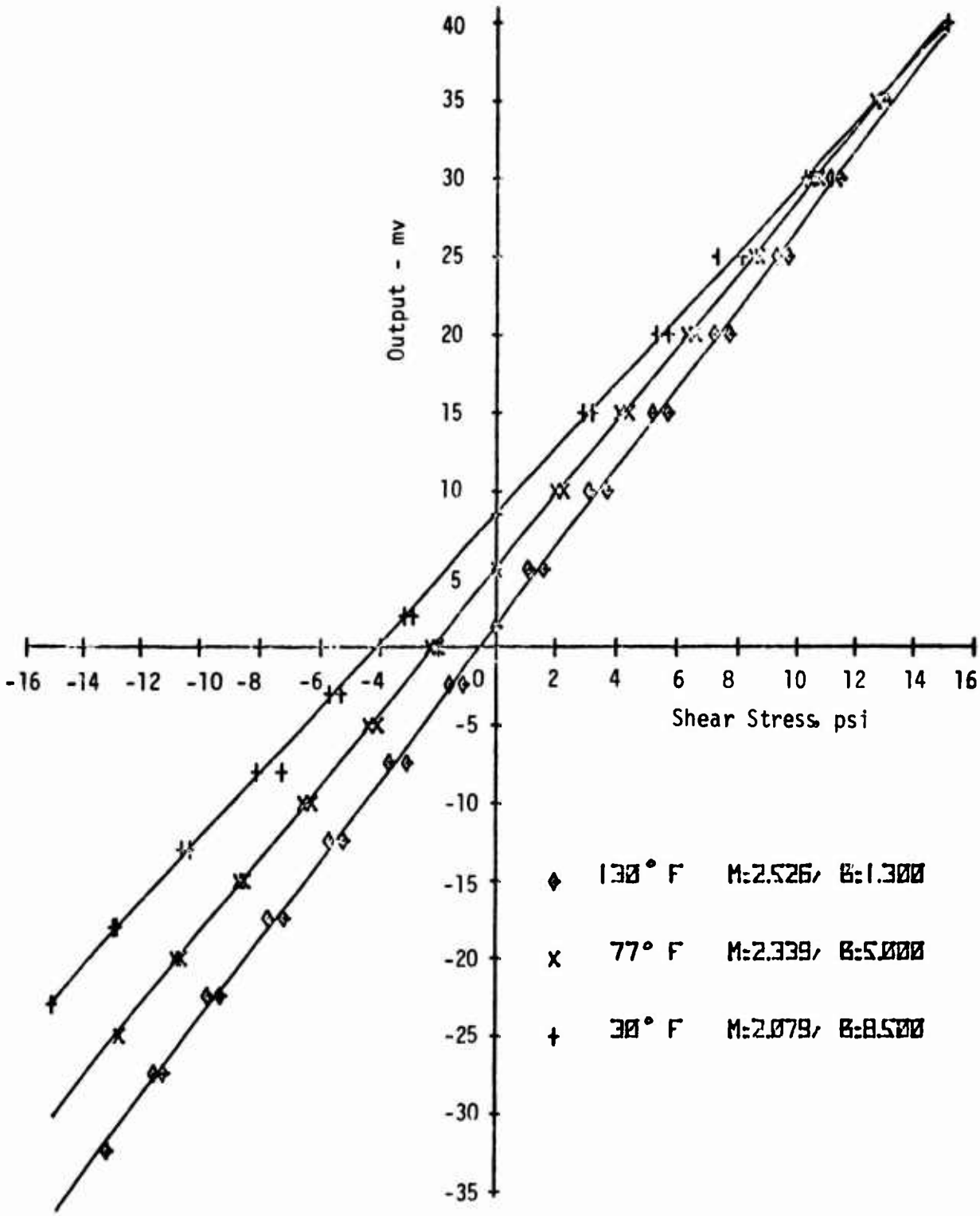

FIGURE F-4. SHEAR GAGE SH-101

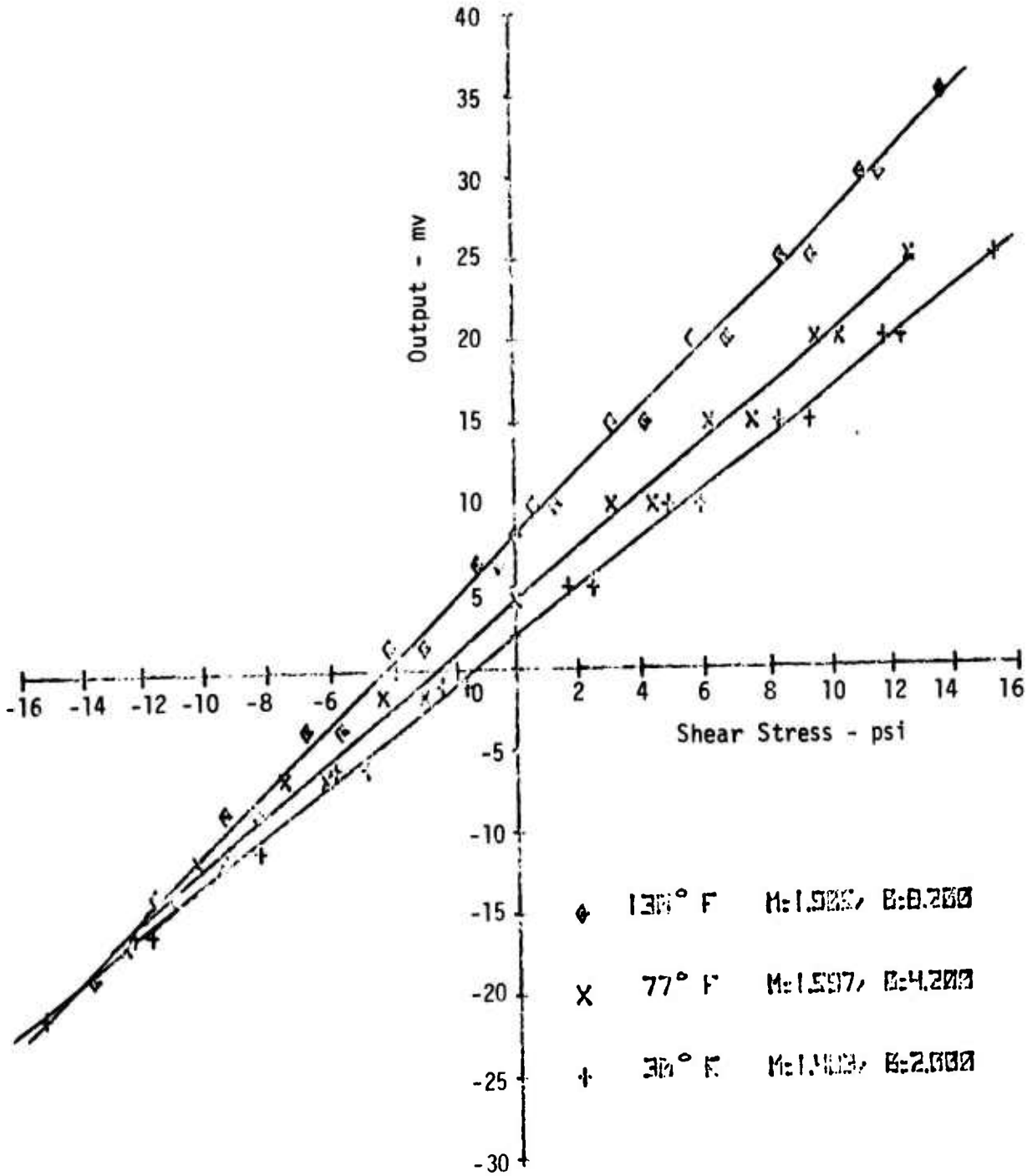

FIGURE F-5. SHEAR GAGE SH-102

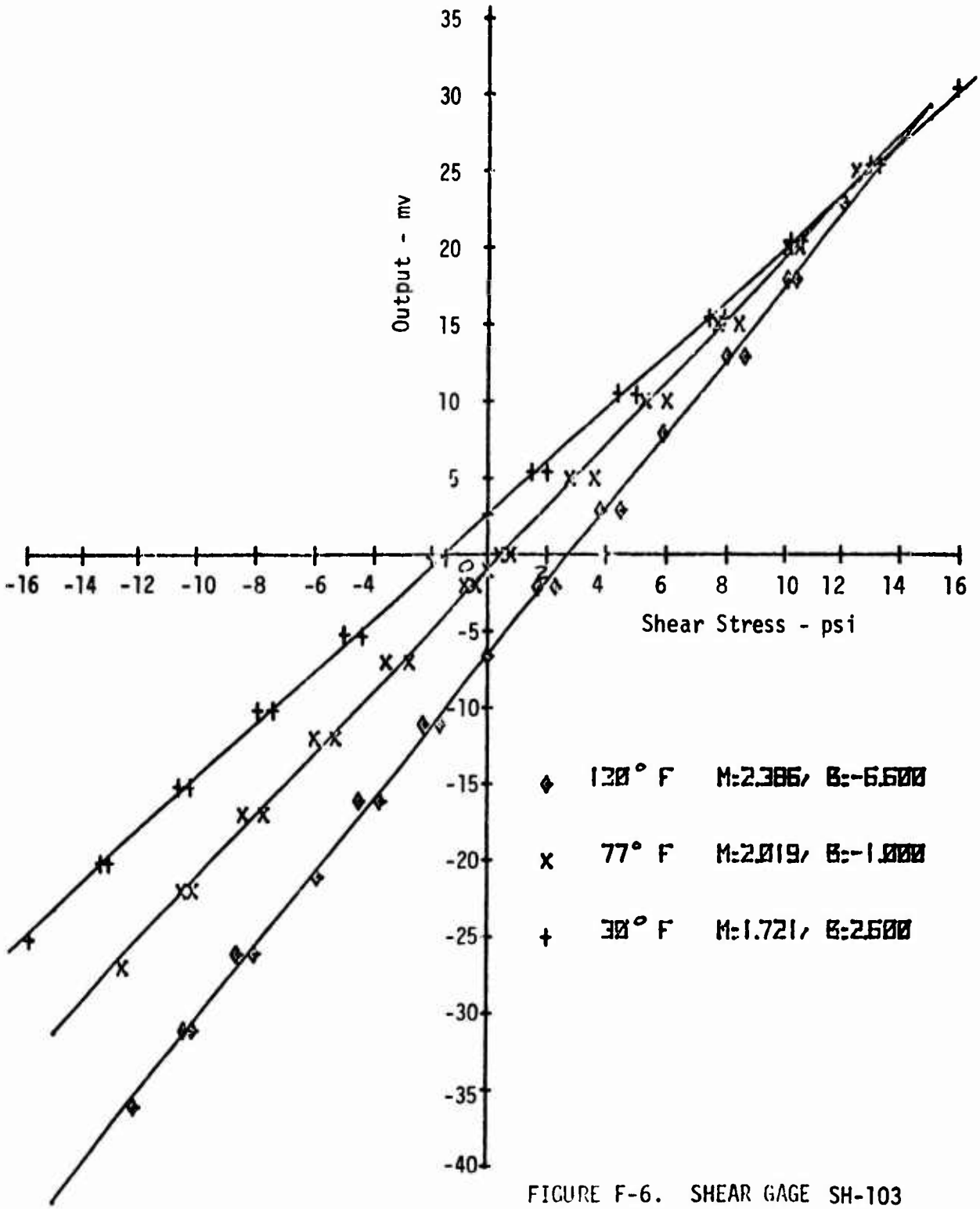

FIGURE F-6. SHEAR GAGE SH-103

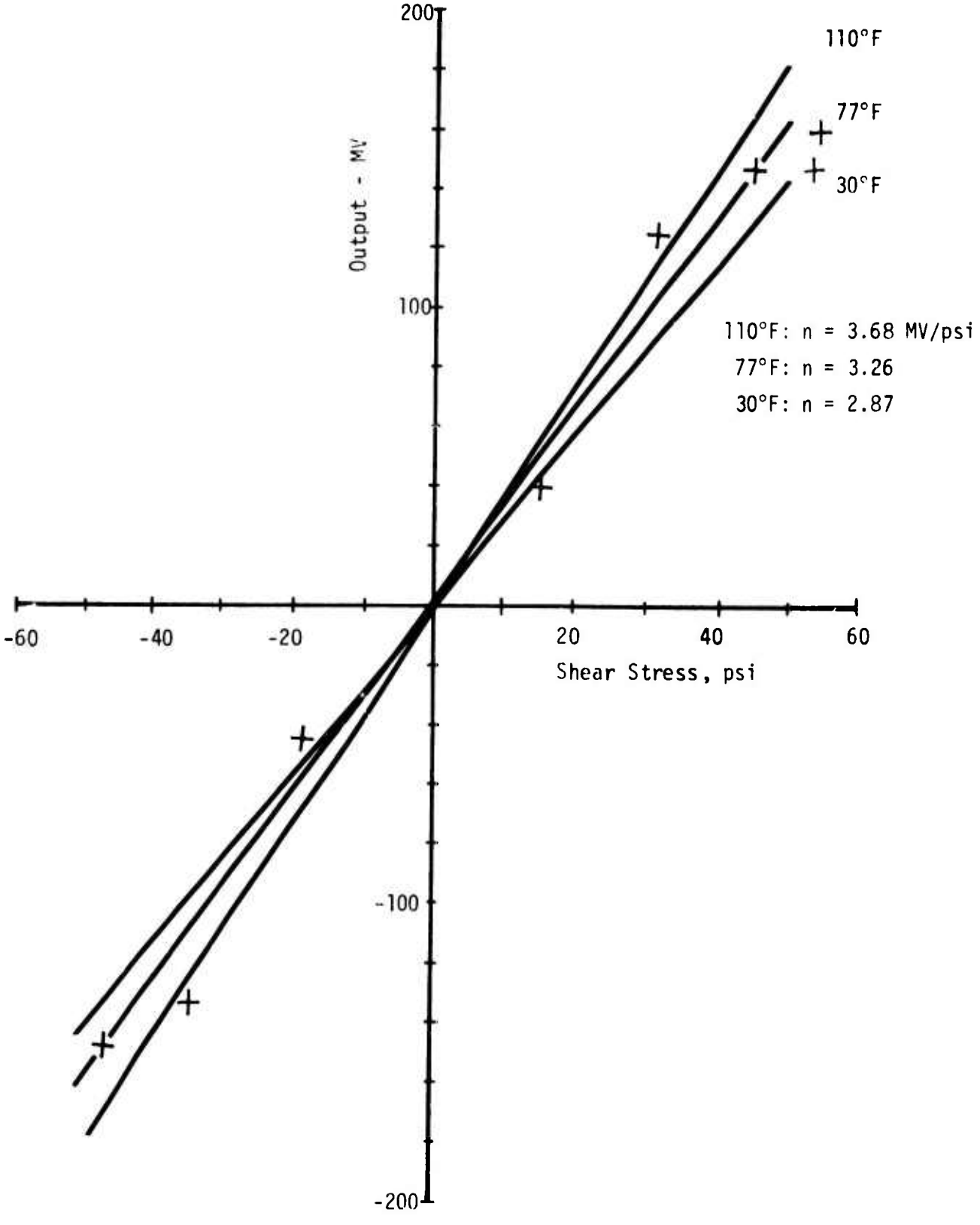

Figure F-7. Shear Gage SH-39

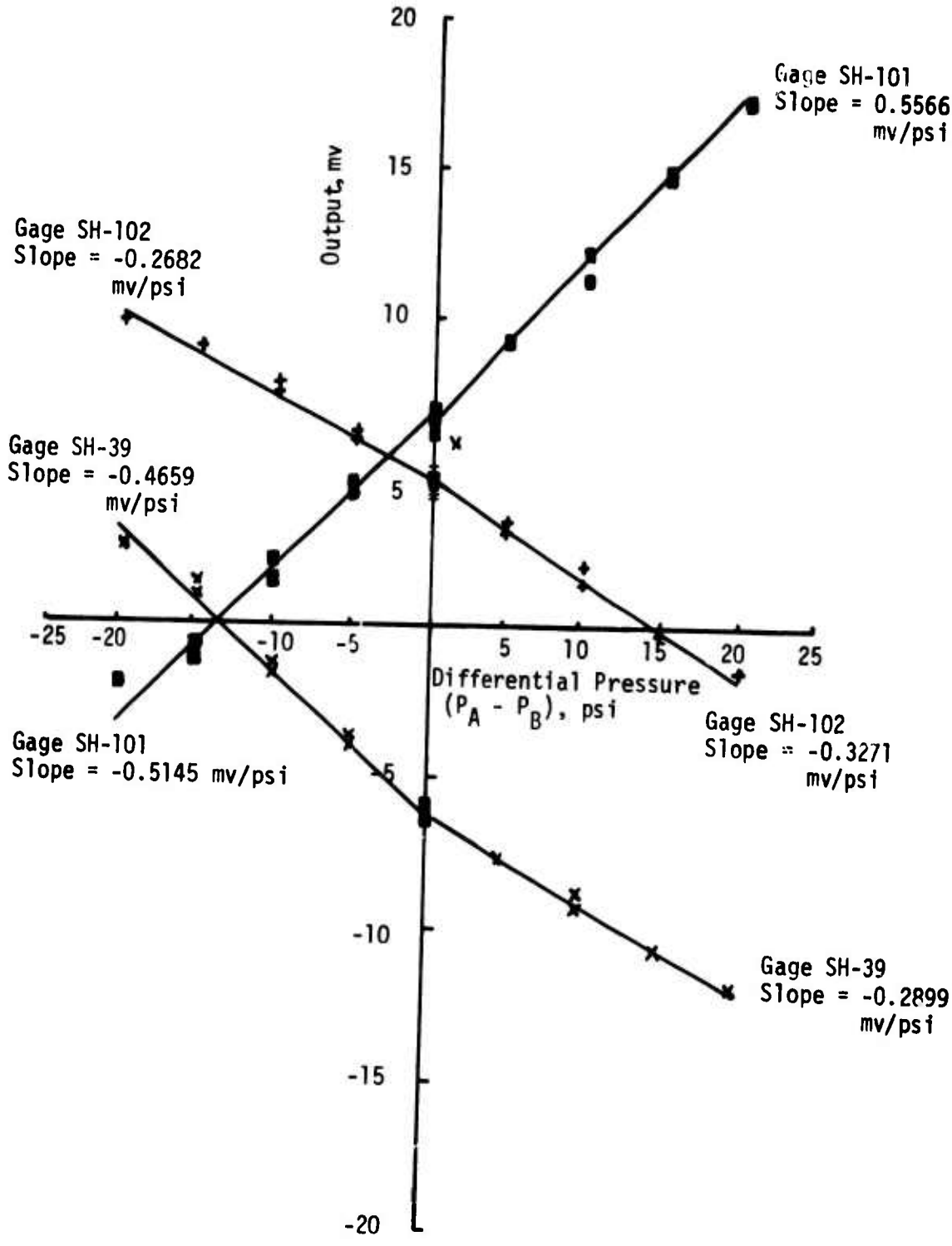

Figure F-8. STV No. 5 Mid-Plane Shear Gages: Output Versus Differential Pressure, T = 80°F, P_H = 0

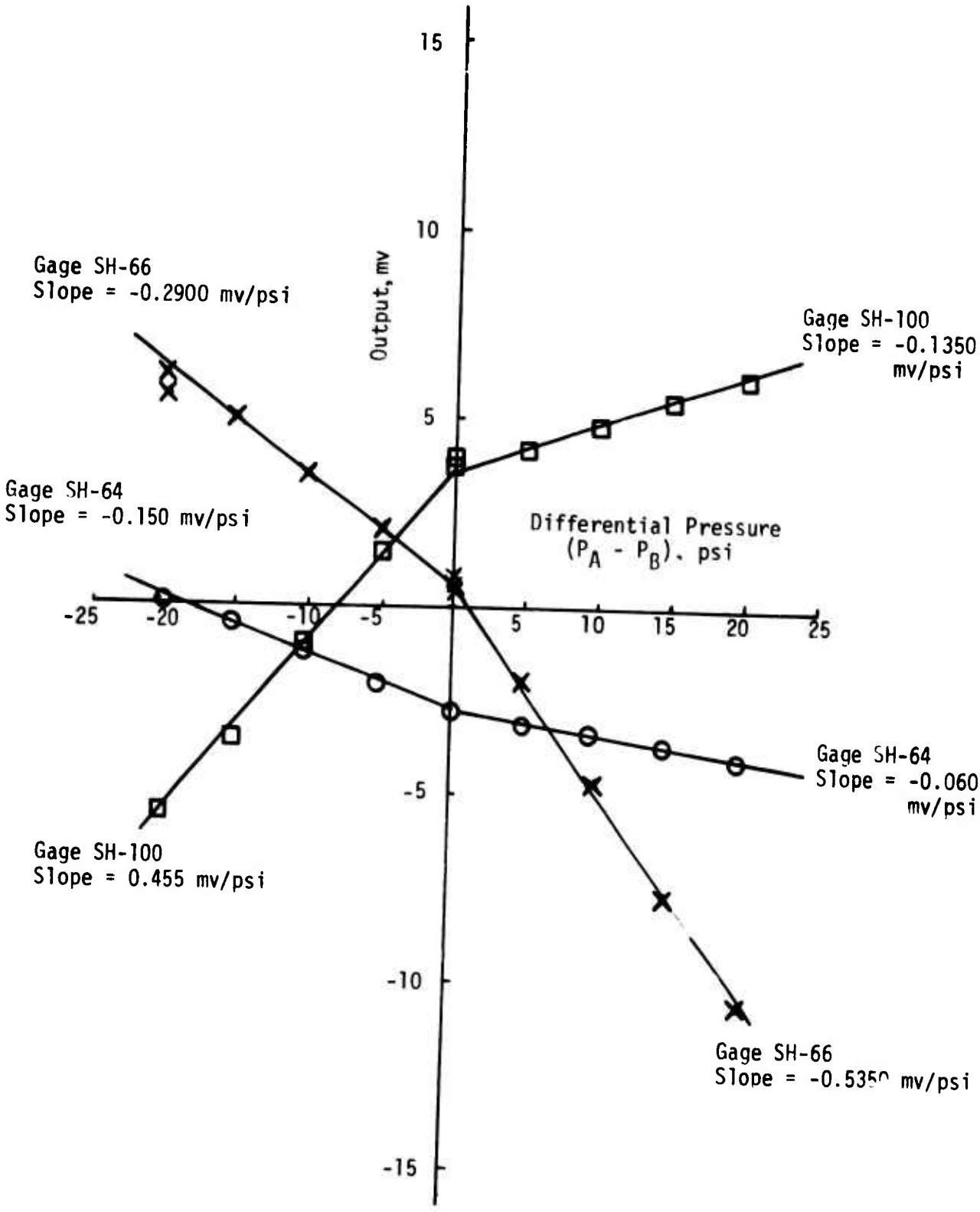

Figure F-9. STV No. 5 End Shear Gages; Output vs Differential Pressure, T = 80°F, P_H = 0

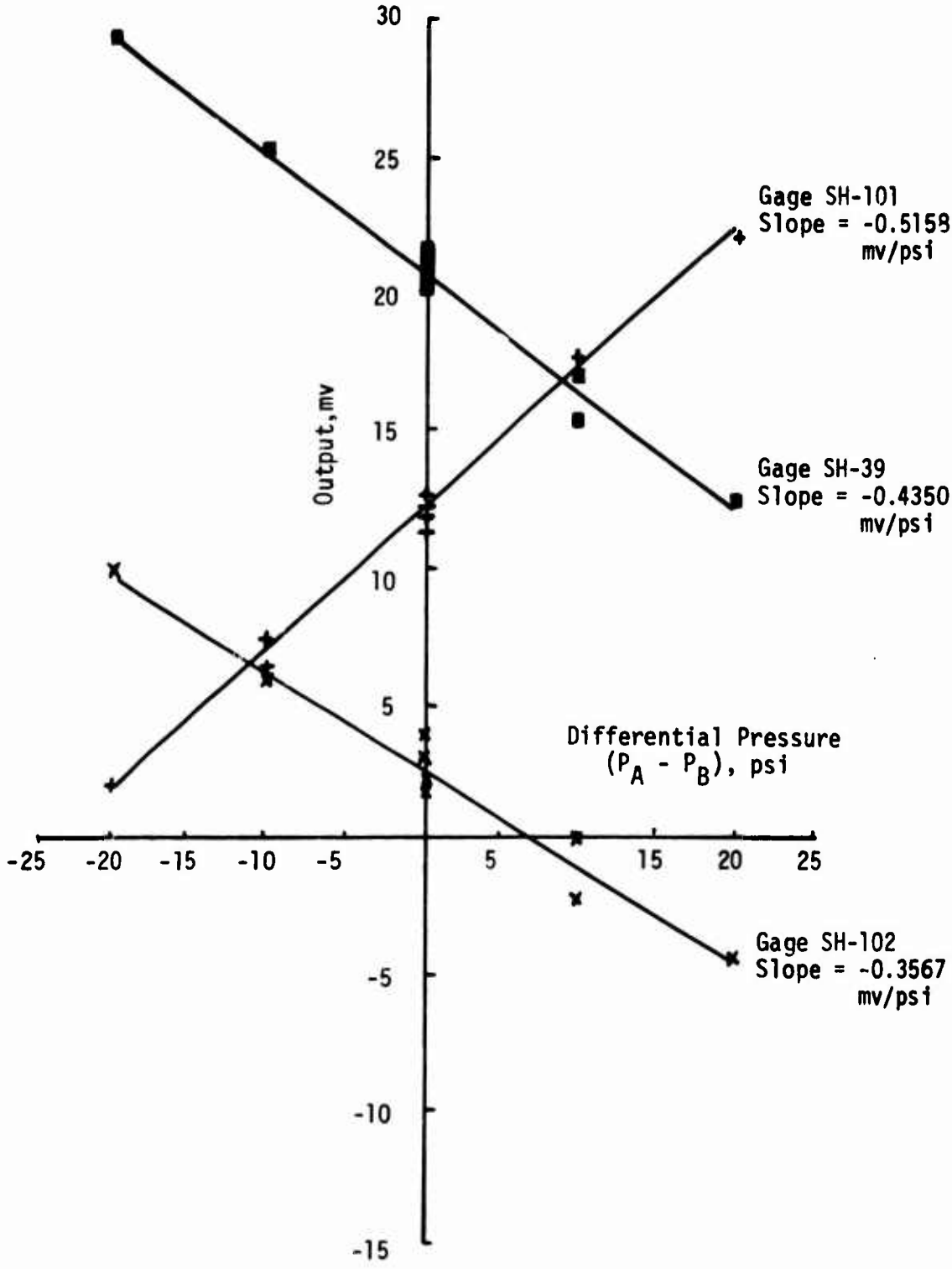

Figure F-10. STV No. 5 Mid-Plane Shear Gages; Output Versus Differential Pressure, T = 80°F, P_H = 200 psi

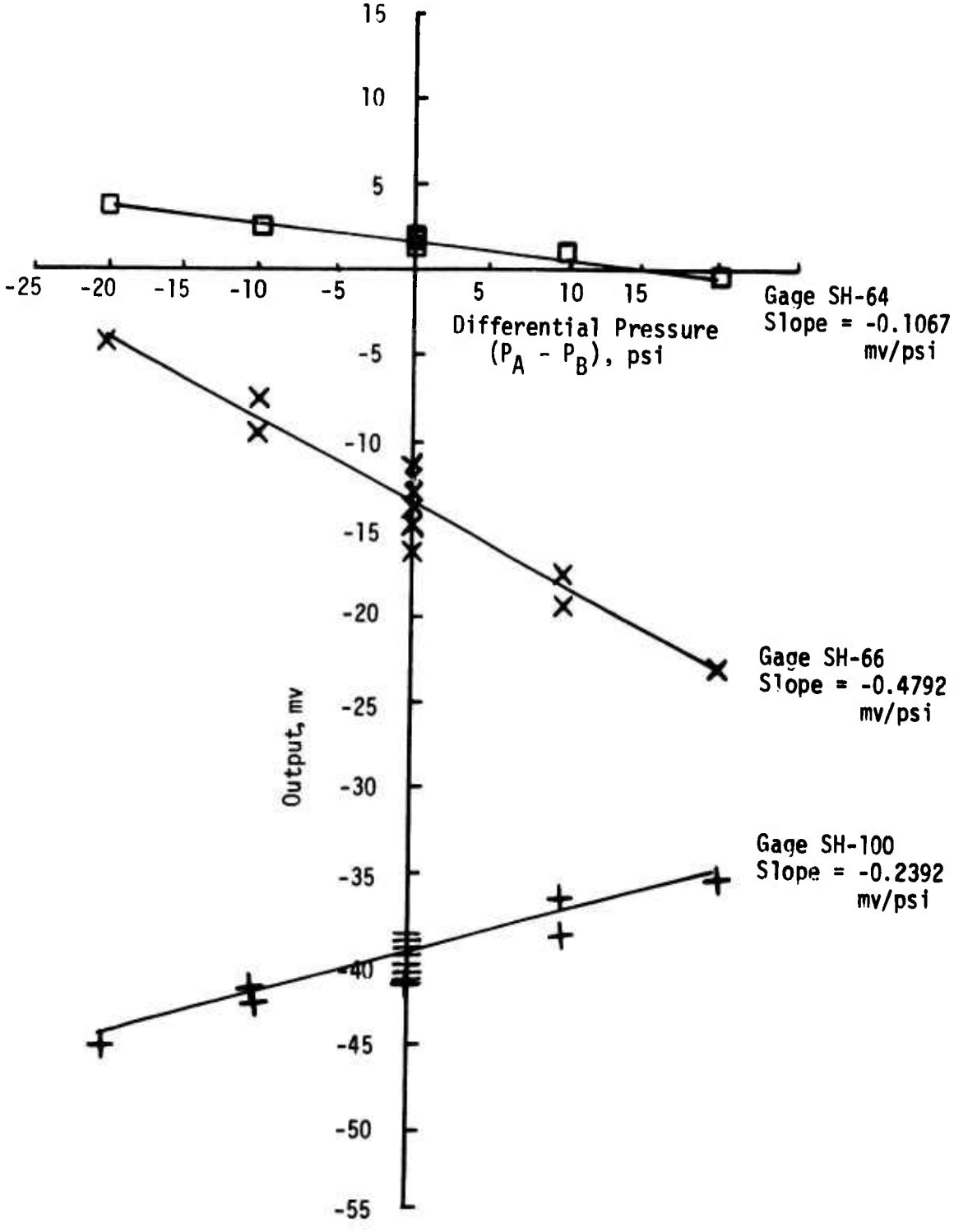

Figure F-11. STV No. 5 End Shear Gages; Output Versus Differential Pressure, T = 80°F, P_H = 200 psi

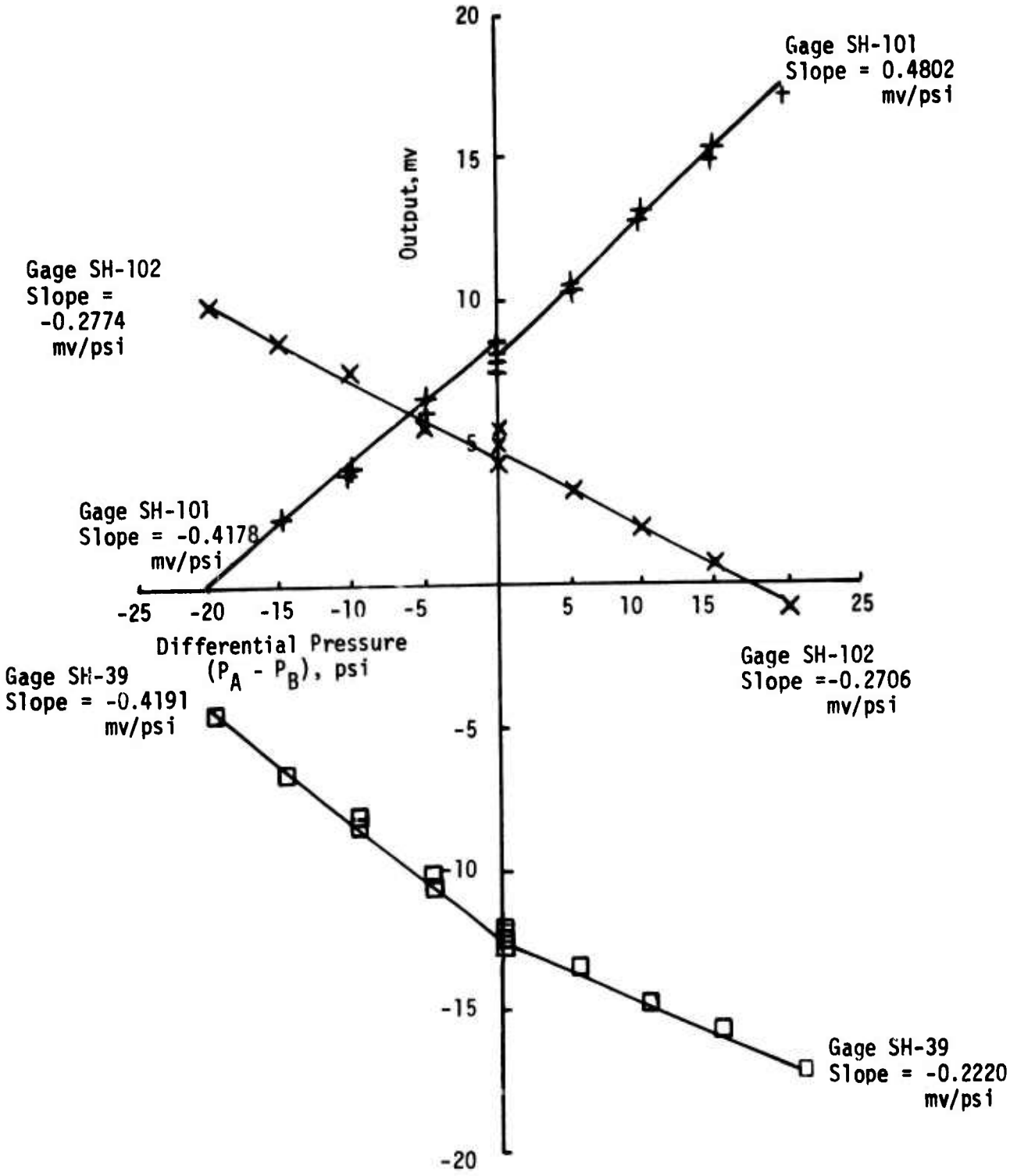

Figure F-12. STV No. 5 Mid-Plane Shear Gages; Output Versus Differential Pressure, T = 44°F, P_H = 0

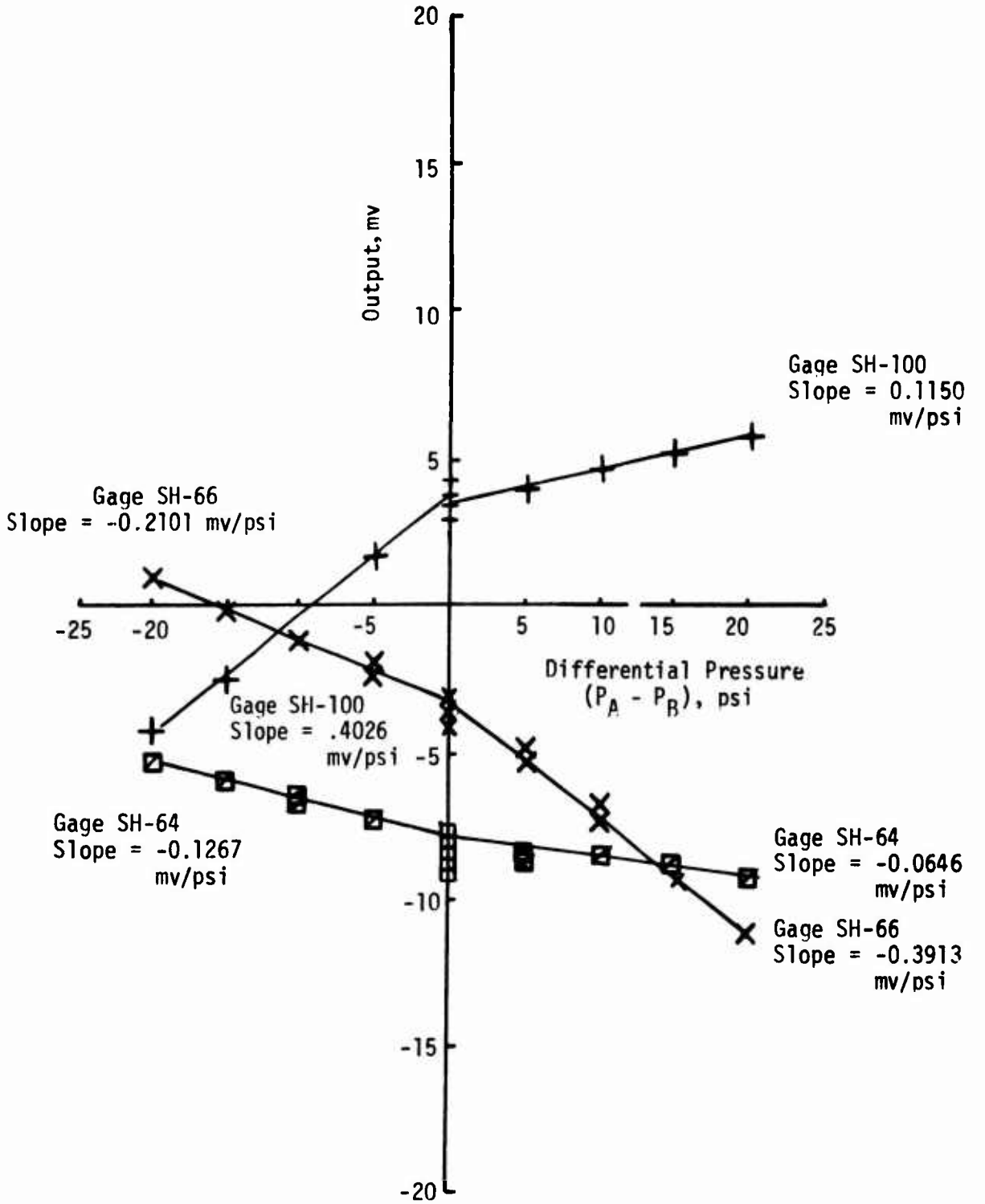

Figure F-13. STV No. 5 End Shear Gages; Output Versus Differential Pressure, T = 44°F, P_H = 0

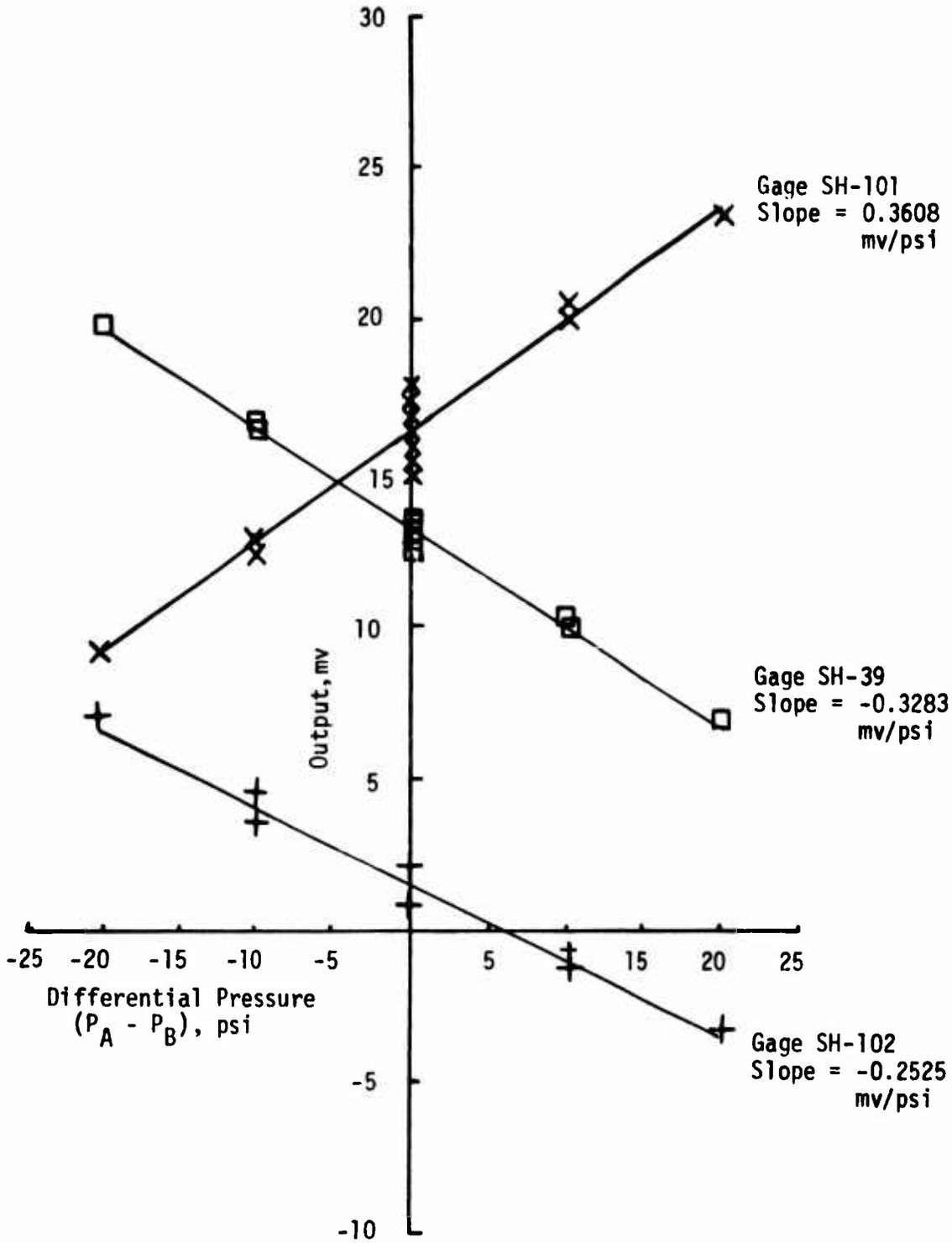

Figure F-14. STV No. 5 Mid-Plane Shear Gages; Output Versus Differential Pressure, T = 44°F, P_H = 200 psi

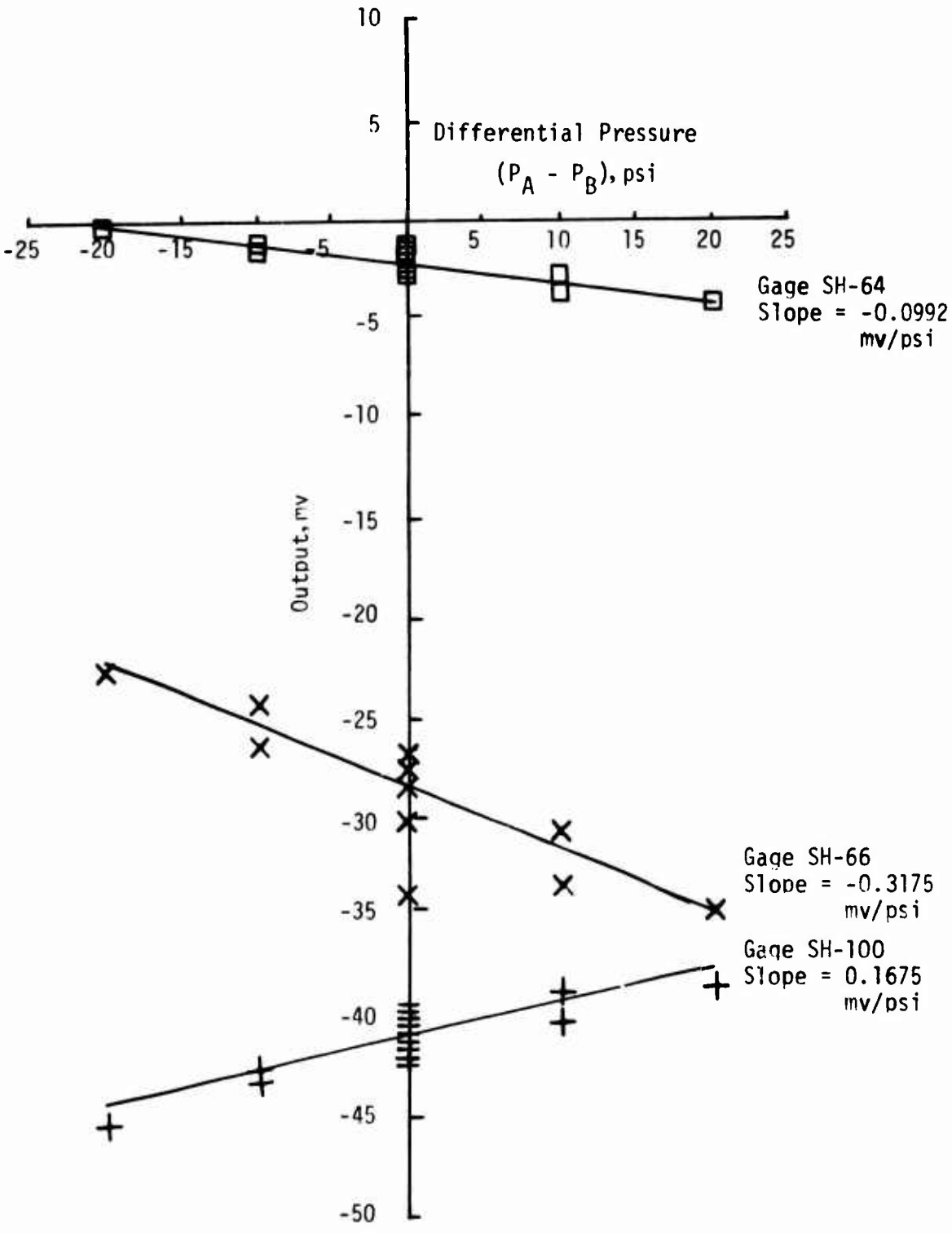

Figure F-15. STV No. 5 End Shear Gages; Output Versus Differential Pressure, T = 44°F, P_H = 200 psi

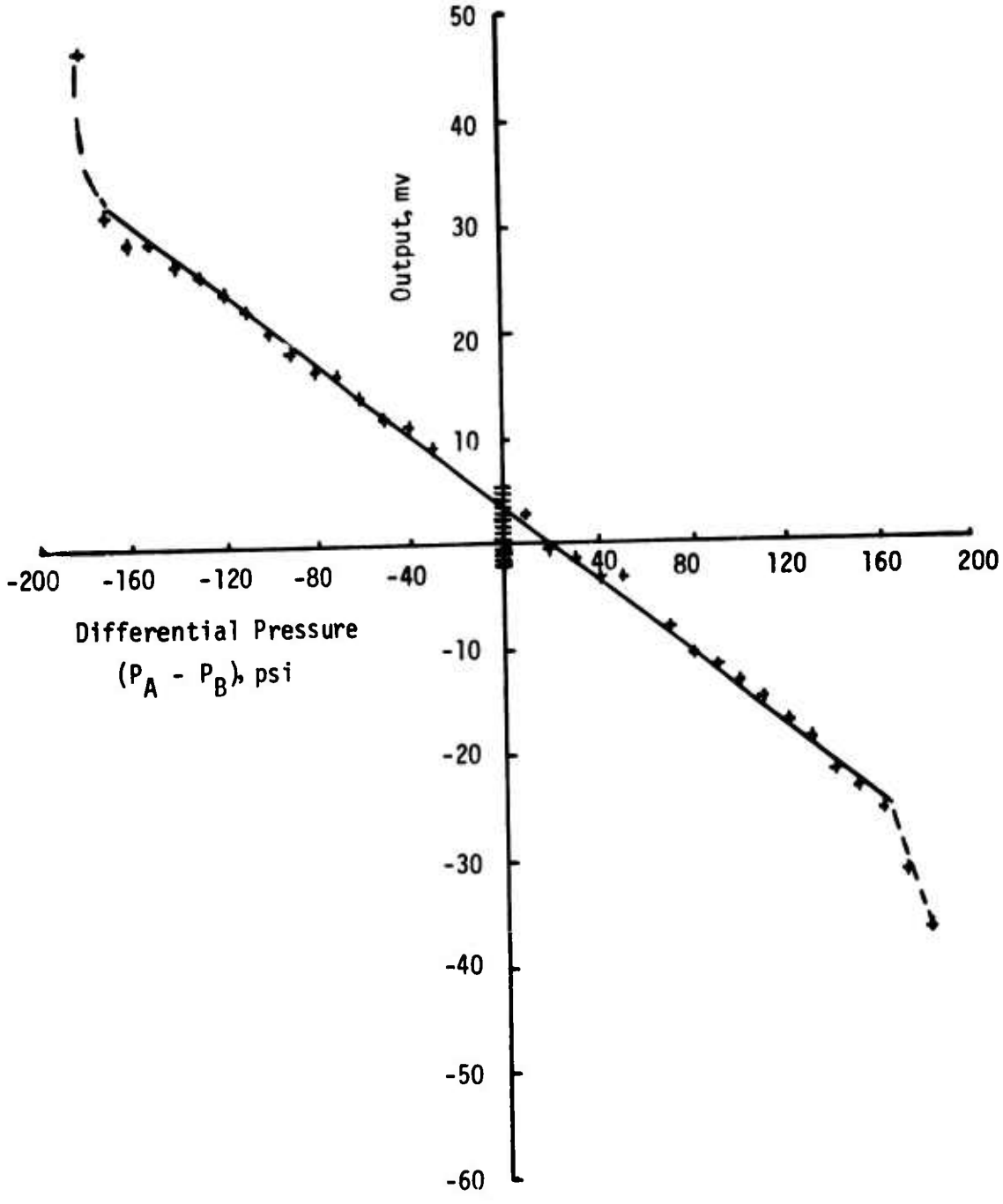

Figure F-16. STV No. 5 Failure Test - Shear Gage SH-64
Output Versus Differential Pressure

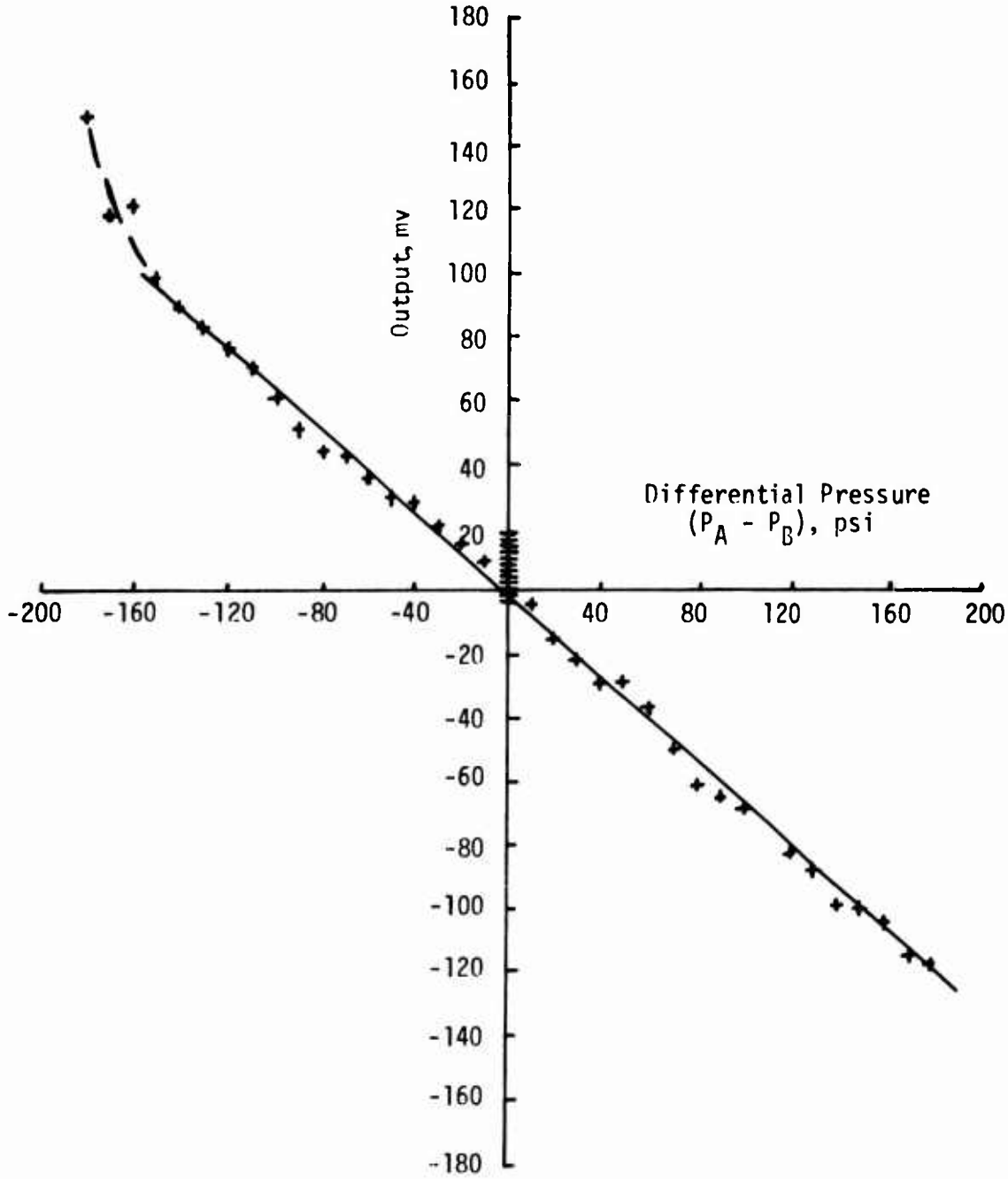

Figure F-17. STV No. 5 Failure Test - Shear Gage SH-66
Output Versus Differential Pressure

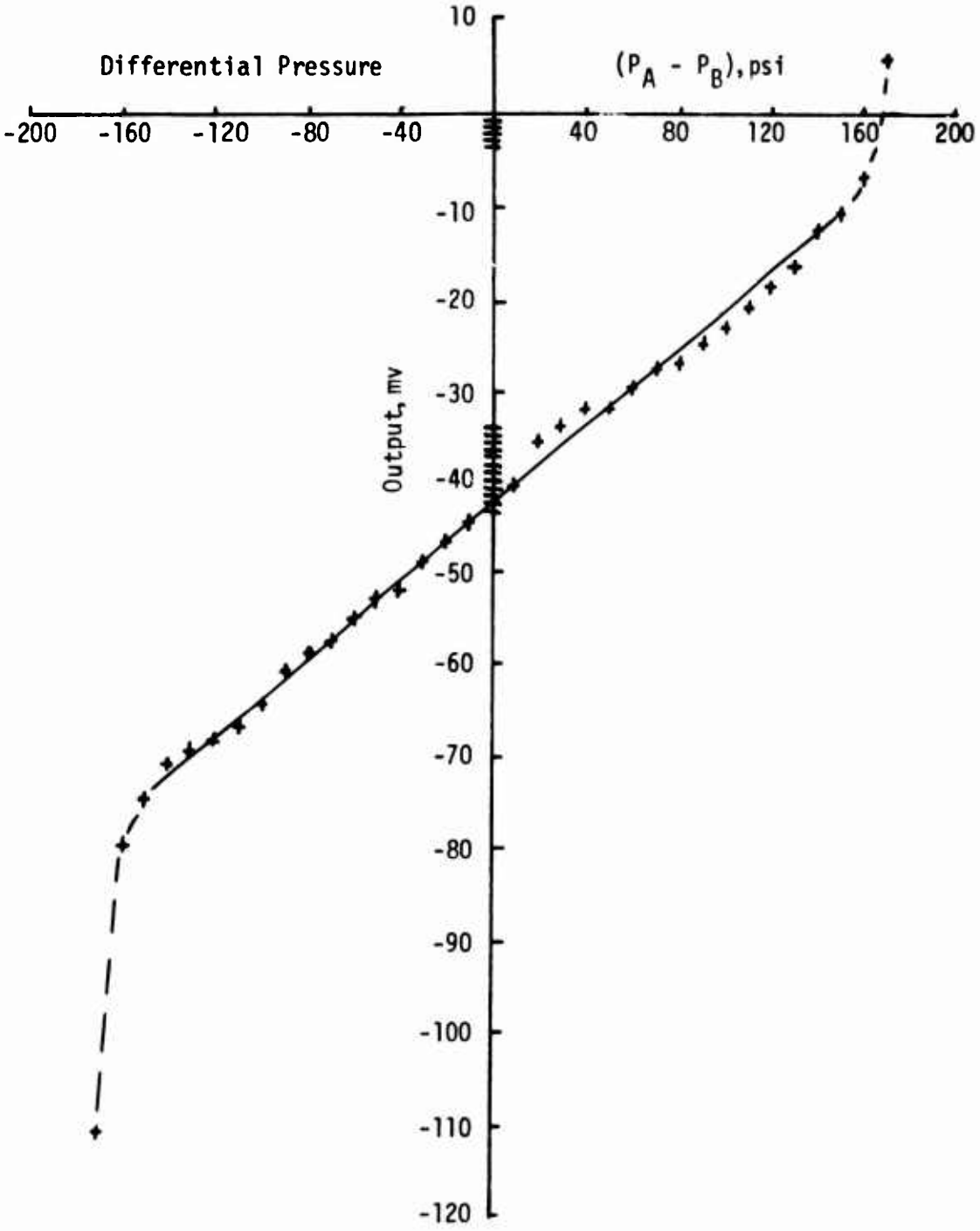

Figure F-18. STV No. 5 Failure Test - Shear Gage SH-100
Output Versus Differential Pressure

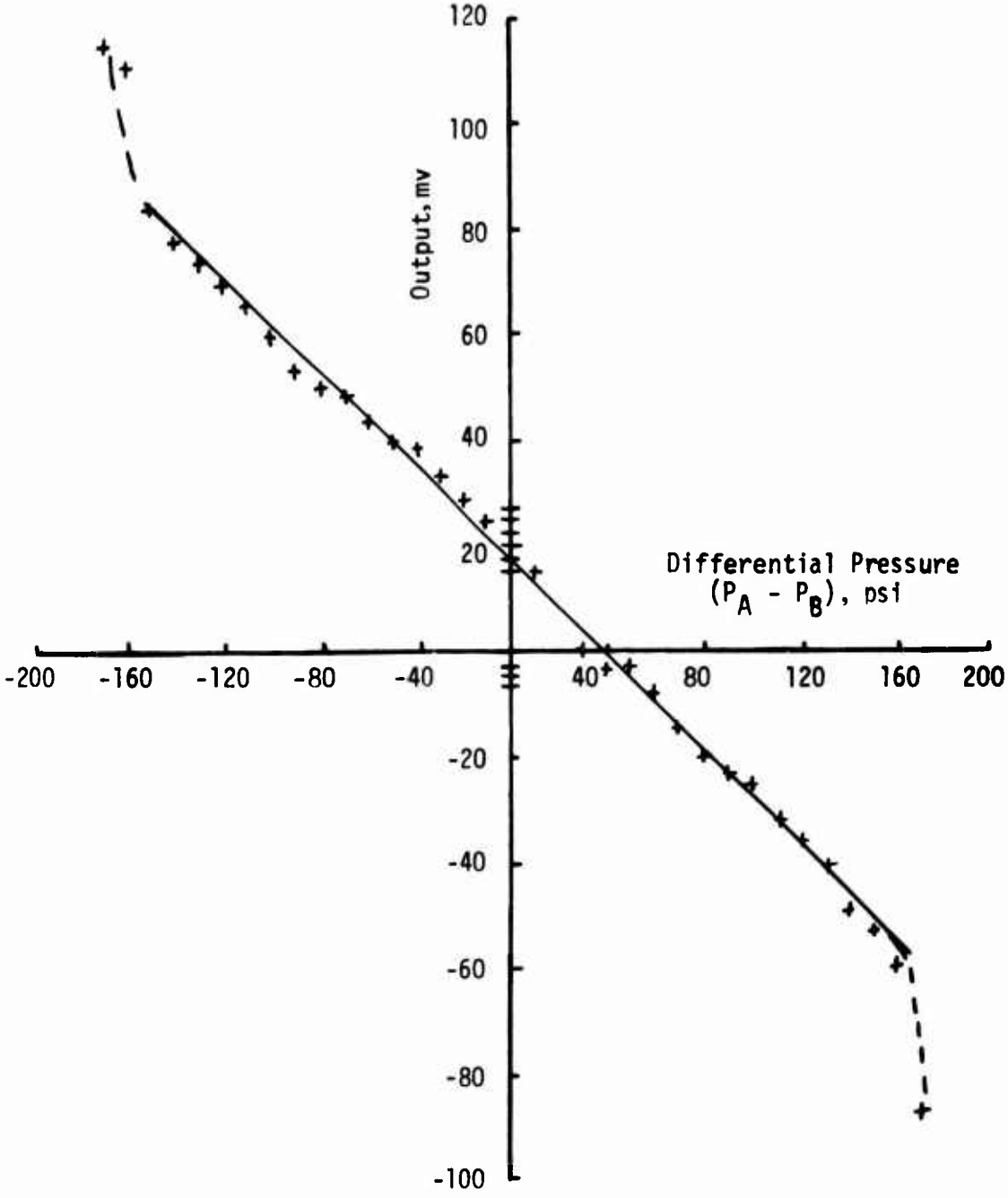

Figure F-19. STV No. 5 Failure Test - Shear Gage SH-103
Output Versus Differential Pressure